NANYANG TECHNOLOGICAL UNIVERSITY

COATING DEPOSITION IN COLD SPRAY PROCESS

KOH PAK KENG

School of Mechanical and Aerospace Engineering

A thesis submitted to the Nanyang Technological University in partial fulfillment of the requirement for the degree of Doctor of Philosophy

2016

ABSTRACT

Cold spray technology is an emerging spray coating process that uses high velocity (kinetic energy) impact instead of high temperature melting (as in thermal spray) for its coating mechanism. With its unique working principle, the coating produced has numerous advantages over conventional thermal spray processes such as high density, low oxide content and minimal or no change in microstructure of the coating. Its distinctiveness presents immense opportunity in providing a new platform to address wear, erosion, corrosion and environmental attack issues.

Preliminary study demonstrates the technical viability of the cold spray process as an alternate repair method to address corrosion issues for gas turbine engine fan cases. However, being a relatively new coating process, the effect of pre and post coating processes on the properties of the coatings needs to be better understood. The effect of grit blasting of the substrate on the mechanical properties and microstructures of the cold spray coatings was first investigated. The results showed that grit blasting may not enhance the microhardness or tensile adhesion strength of the cold spray coating and may be eliminated as a pre-coat process. The effect of post coating heat treatment was also evaluated. The results indicated that both stress relief and annealing processes reduce as well as homogenize the microhardness of the coatings while the tensile adhesion strength was unaffected by stress relief but improved significantly when subjected to annealing.

In addition, components that are cold sprayed usually come in complex shapes and sizes. It is difficult to ensure that the spray angle is consistently normal to the surface of the component.

As such, the effect of the spray angle on the microhardness, tensile adhesion strength, and microstructure was examined. Results indicated that the effect of off-normal spraying has minimal impact on tensile adhesion strength and a positive effect on the microhardness of the coating. Furthermore, the relative coating efficiency of the cold spray process at various spray angles was also evaluated. Significant detrimental impact on the relative coating deposition efficiency was observed for spray angles smaller than 60°.

The deposition phenomenon of the coating, during build-up on a stationary substrate, at different dwell times was also experimentally investigated. The mound-like built up was cross sectioned and viewed with microscopy and showed delamination from the substrate. The delamination phenomena were, however, absent in continuously sprayed coatings. The study postulated that the built-up of compressive residual stresses on the coating have resulted in the contraction of the coating and subsequent delamination from the substrate.

The scope of the study has the intent of establishing optimum and preferential conditions for cold spray processes in general. This will pave the way for the industrial application of such a technology in a cost effective and efficient manner.

ACKNOWLEDGEMENTS

It's been a long and challenging journey, this project took 8 years and in between, 3 different jobs, 3 children and 2 supervisors. I am aware that this would not have been possible without the love and support of the following people, all of whom I am eternally grateful for:

- Evina, Ethan, Elijah and Elise. Thank you my beloved wife and 3 lovely children for the constant encouragement and support. You are all my source of motivation and I shall always remember your assurance and sacrifices.
- Assoc Prof Ng Heong Wah for the help and support. I am thankful for all the encouragement you have given me. I am deeply aware that there is no way I can complete this PhD without your guidance and help, for that I am extremely thankful.
- Assoc Prof Philip Cheang, a mentor and great friend. Thank you for the enlightenment and encouragement all these years.
- Mr Kelvin Loke, a fellow researcher and great friend. Thank you for all the support and help you have given me.
- My family members who have supported me all these years without fail.
- Colleagues in SIM University, especially Ann, Stephen, Prof Tsui Kai Cheong, Prof Cheong Hee Kiat and many others whom have offered their encouragement all these years. And especially to Chui Ping for proof-reading my thesis.
- Assoc Prof Simon Yu for all your encouragement and support.
- Many others whom have helped me in one way or another to complete this work. Please know that you are always in my heart.
- Lastly but most importantly, to God whom I draw my strength from and has given me the rest and encouragement when I was weary.

TABLE OF CONTENT

LIST OF FIGURES

LIST OF TABLES

LIST OF SYMBOLS

Symbol	Nomenclature
A_t	Throat area of convergent-divergent nozzle
A_e	Exit area of convergent-divergent nozzle
D_p	Average particle diameter
HV_{100}	Vickers Pyramid Number using a 100 gf load
P	Pressure of gas flow at any given point in convergent-divergent nozzle
P_a	Ambient pressure
P_e	Exit gas pressure of convergent-divergent nozzle
P_i	Intake pressure of convergent-divergent nozzle
P_t	Pressure at throat of convergent-divergent nozzle
R	Gas constant
R_a	Arithmetic average of absolute surface roughness values
T_g	Temperature of gas flow at any given point in convergent-divergent nozzle
T_{gi}	Gas temperature at nozzle intake
T_i	Initial temperature of powder
T_m	Melting temperature
U_g	Velocity of gas flow at any given point
V_{cr}	Critical velocity of cold spray particle
V_n	Normal component of cold spray particle velocity
V_p	Velocity of cold spray particle
V_t	Tangential component of cold spray particle velocity
d_e	Splat diameter
d_x	Diameter of elliptical splat in the x-axis
d_y	Diameter of elliptical splat in the y-axis
m	Mass flow rate of process gas in convergent-divergent nozzle
t	Thickness of splat
v_i	Specific volume of gas in convergent-divergent nozzle

Greek Symbol	**Nomenclature**
ε	Flattening ratio
θ	Spray angle
κ	Gas specific heat ratio
ρ	Bulk density of powder
σ_u	Ultimate strength
ψ	Aspect ratio of splat

CHAPTER 1

INTRODUCTION

1.1 Background

Cold gas dynamic spraying (more commonly known as cold spray) is a comparatively new coating process [Alkhimov *et al*., 1994]. It falls under the broad family of thermal spray processes but is unique in that it can produce a coating at relatively low temperatures. Essentially, cold spray process uses high pressure carrier gases to accelerate particles to high enough velocities such that upon impact, the particles plastically deform and bond to the surface of the substrate, thus forming a dense coating or structural deposit. On subsequent passes, the particles bond to the previously deposited layer, forming a thick coating.

Many damaging effects associated with high temperature reactions in conventional thermal spray processes are either avoided or minimised in cold spray as it is a solid state process that uses high velocity instead of high temperature to produce coatings. Distinctive benefits of coatings produced by the cold spray process include high density and oxide-free coatings, compressive rather than tensile stresses and coatings with a wrought-like microstructure. In addition, the cold spray beam has a very narrow footprint (about 20 mm). The high density particle beam facilitates high growth rate of coating thickness and offer great control over the shape of the coating, usually without the need for masking [McCune *et al*., 1995].

Due to the various advantages, the use of cold spray as an alternate surface coating process is fast gaining popularity [Gartner *et al*., 2006]. Its distinctiveness from conventional thermal spray coating processes presents opportunity in providing a new platform to address wear, erosion, corrosion and environmental attack issues for the coating industry. One of the intents of this research work is to identify and evaluate possible applications of the cold spray technology, specifically, in the area of repair of aerospace components. To start-off, an experimental study was carried out to evaluate the coating capability of the cold spray technology using single metallic powder. The choice for the powder and substrate was made with an industrial application in mind.

1.2 Industry Application for Cold Spray Technology

Corrosion in the form of pitting is common on the fan cases of gas turbine engines due to the retention of water during and after flight operations. This is particularly pronounced between the four o'clock and eight o'clock region where stagnant water usually resides (Figure 1.1). The existing repair procedure allows the pits to be manually polished to a certain depth. However, beyond certain blending limits, the wall thickness of the fan cases falls below the structurally acceptable margins, deeming the fan cases unserviceable.

Current repair methods allow a variety of techniques such as plasma spray, high velocity oxygen fuel (HVOF) and epoxy bonds for the dimensional restoration of these aluminium fan cases. However, these repairs offer no structural advantage when applied to the affected area. Although the cases may be restored dimensionally, these repair methods do not redeem the strength of the underlying structure and violate minimum

dimension conditions. Fusion welding processes, while capable of producing structural repairs, often result in unacceptable distortion due to the thermal stresses the fan cases are subjected to. In addition, the high temperature that fusion welding generates has a detrimental effect on the material properties of the fan cases.

Cold spray is a process that can produce coatings at temperatures very much lower than the melting temperatures of the raw materials. This ensures that the input powder materials do not experience any grain growth, oxidation or phase changes when formed into coatings. This ability of cold spray has been proven by research that showed that the process can produce coatings retaining nano-sized and sub-micron particles [Ang *et al*., 2011]. It is this property of cold spray that makes it attractive as a coating method while retaining their unique material properties.

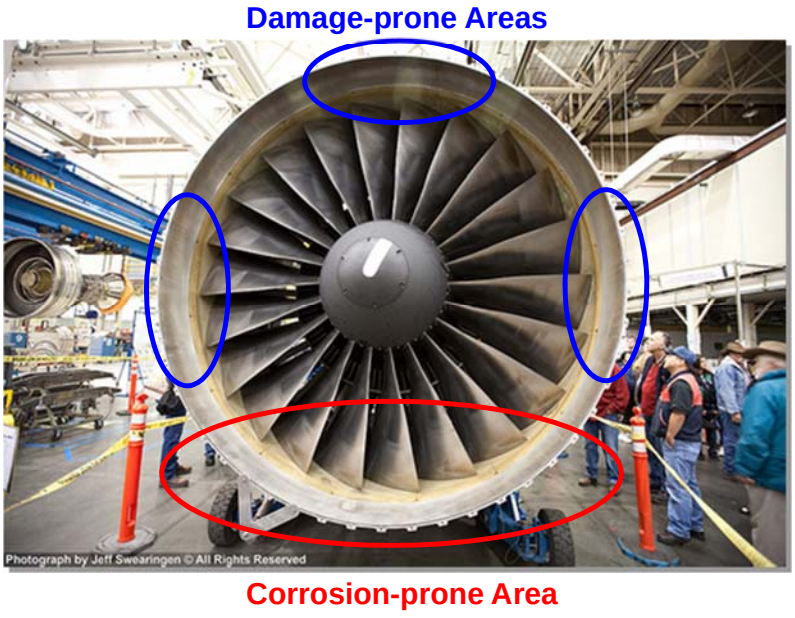

Figure 1.1: Area on fan case which is prone to corrosion due to retention of water.

1.2.1 Preliminary studies

The cold spray technology presents opportunity in providing a new platform to address corrosion issues for the gas turbine engine fan case. The following studies were carried out to explore the use of cold spray technology as a viable alternative repair method. The present study will focus on the evaluation of the mechanical properties of cold sprayed aluminium Al-6061 coating, such as the microhardness, tensile bond strength and as well as the microstructural features [Koh *et al*., 2012].

Gas atomized Al-6061 powder used for the study was obtained commercially from Valimet, Inc. (California, USA). The scanning electron microscope (SEM) images of the Al-6061 feedstock powder are shown in Figure 1.2. The SEM micrographs indicate that the particles are spherical in shape and range in size from 5 μm to 50 μm. The chemical composition of the powder analysed using inductively coupled plasma atomic emission spectroscopy (ICP-AES) is shown in Table 1.1. The mechanical properties of the Al-6061 bulk material is shown in Table 1.2.

Al-6061 is widely used in the aviation industry. Aside from gas turbine fan cases, Al-6061 is typically used in the aircraft fuselage, cowling and cold section structural components of aircraft engines.

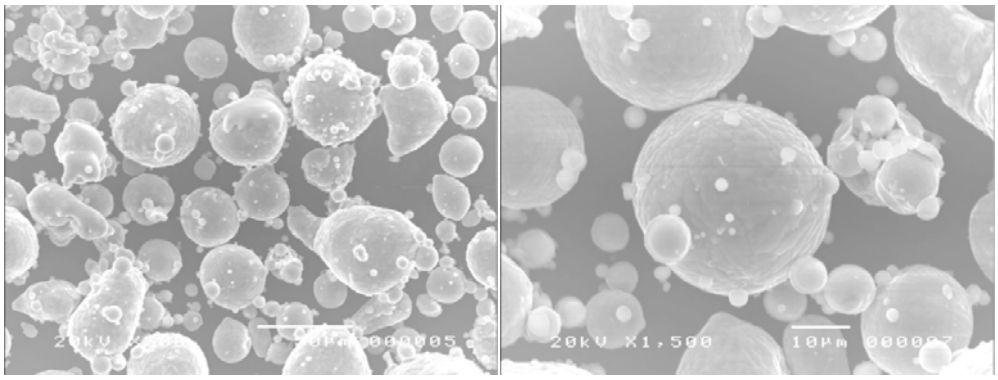

(a) (b)

Figure 1.2: SEM images of the Al-6061 feedstock powder at (a) 500X and (b) 1500X.

Table 1.1: Chemical composition of Al-6061 feedstock powder (source: Valimet, Inc.).

Element	Percentage (%)
Al	Balance
Cr	0.08
Cu	0.27
Fe	0.25
Mg	0.93
Mn	0.03
Si	0.57
Ti	<0.01
Zn	0.03

Table 1.2: Mechanical properties of Al-6061 bulk material (source: ASM Material Data Sheet).

Properties	**Value**
Density	2.7 g/cc
Hardness, Vickers	107
Ultimate Tensile Strength	310 MPa
Tensile Yield Strength	276 MPa
Elongation at Break	12 %
Modulus of Elasticity	68.9 GPa
Poisson Ratio	0.33
Fatigue Strength	96.5 MPa
Shear Modulus	26 GPa
Shear Strength	207 MPa

1.2.2 Cold Spray Parameters

Aluminium alloy Al-6061 substrates were cleaned with acetone prior to spraying. Helium set at 200 °C and 10 bars was used as the carrier gas. The standoff distance was set at 15 mm from the cold spray nozzle exit and the traverse speed of the nozzle relative to the substrate was 80 mms^{-1}. The powder feed rate is 180 $gmin^{-1}$ and the substrate temperature was at room temperature (25 °C). The footprint of the cold spray coating is about 20 mm.

1.2.3 Mechanical Properties Evaluation

A total of five microhardness measurements were obtained from the Al-6061 cold spray coating. An average microhardness value of 104.7 HV_{100g} was obtained, with the root mean square value calculated as 104.9 HV_{100g}. This is in comparison to the 103.8 HV_{100g} mean value obtained for the base Al-6061 material. The identical microhardness of the coating is likely to be the result of a gradual compaction due to the constant and repeated impact of the cold sprayed impinging particles. The lack of porosity in the

underlying layers observed by SEM in the deposited material as shown in Figure 1.3 is evidence of the coating coherency.

The tensile adhesion bond strength of the Al-6061 coatings was evaluated using the ASTM C633-01 [ASTM International, 2013] test. A total of three coating samples were tested and the results are shown in Table 1.3. The coatings failed at an average of 34 ± 6 MPa, partly in the coating-substrate interface and partly in glue-pull off bar interface. Comparatively, the bond strength results for plasma sprayed coatings performed under identical standards yielded much lower average adhesion strength of 20 MPa, indicating significantly stronger tensile bond strength for the cold sprayed Al-6061 coatings.

Table 1.3 Tensile adhesion bond strength test results for Al-6061 coatings.

Description	**Sample 1**	**Sample 2**	**Sample 3**
Area (mm^2)	495.60	496.78	496.39
Max. Load (N)	16006	19608	13829
Bond Strength (MPa)	32	40	28
Failure Mode	Coating/Base Metal Interface		

1.2.4 Microstructure Evaluation

Scanning electron microscopy pictures of the Al-6061 coating at different magnification are shown in Figure 1.3. The coating thickness was between 500 and 600 micrometers. The images demonstrated that there is low porosity in the coating, consistent with typical coating obtained using a low temperature cold spray process. This result indicates the ability of the cold spray system to produce a high density

coating. The well-defined interface between the coating and substrate also suggested good adhesion of the coating to the base material.

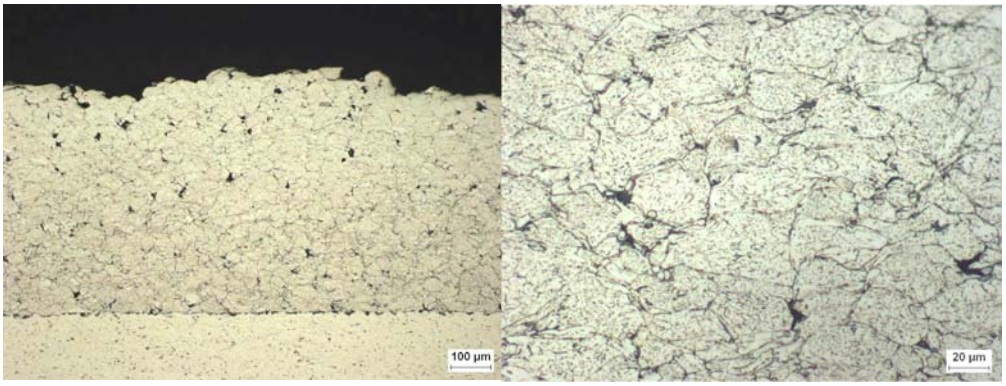

(a) **(b)**

Figure 1.3: SEM micrographs of a cross-section of the Al6061 coating at (a) 100x magnification and (b) 500x magnification.

Figure 1.4 shows the XRD patterns for the Al-6061 powders together with the coating obtained using helium as the carrier gas. The coatings deposited were about 0.5mm thick. The results show minimal differences in crystal structure as shown by the identical 2 Theta readings between the starting powder and the coatings, implying that no microstructural changes took place during the spraying process. Thus, verifying the ability of the cold spray process to retain the feedstock properties in the coating.

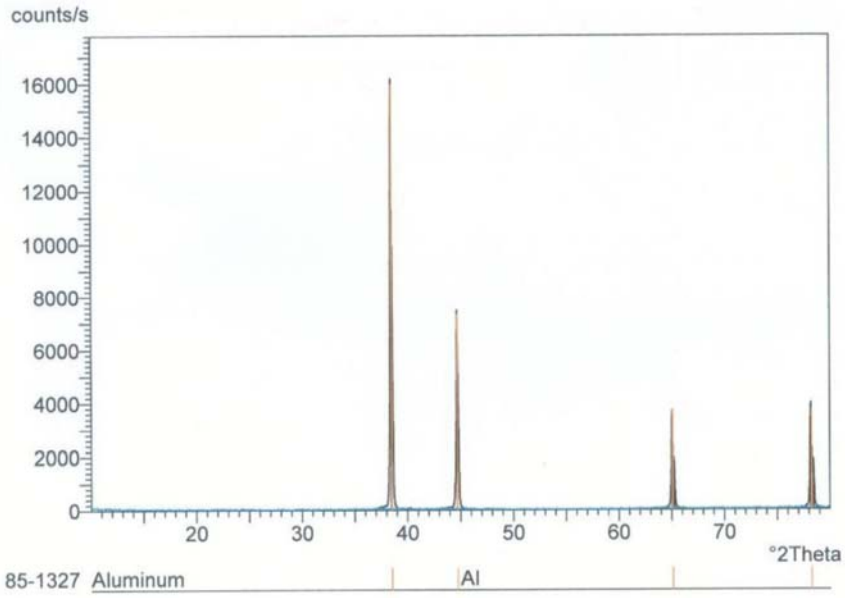

(a)

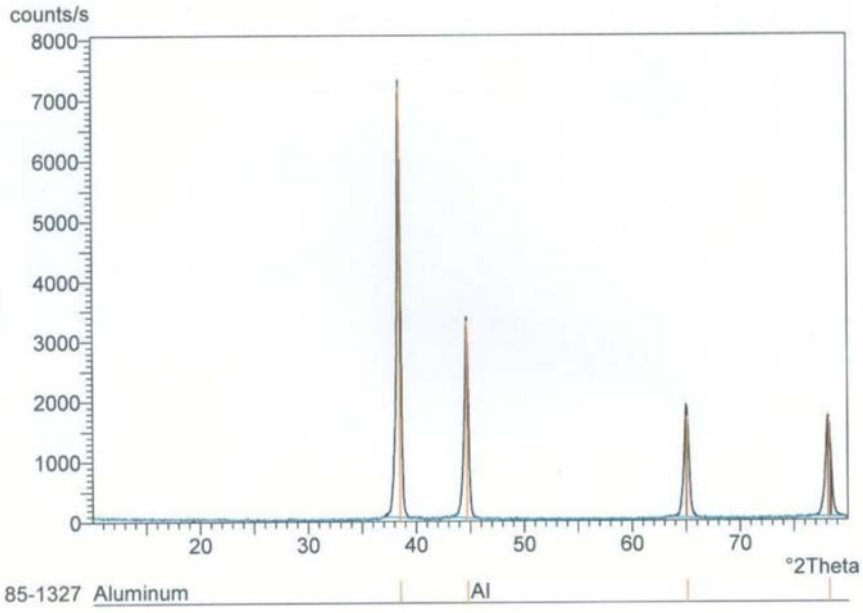

(b)

Figure 1.4: XRD diffraction patterns for (a) Al-6061 powder and (b) coatings produced using Helium gas as carrier gases.

1.2.5 Conclusion

Aluminium (Al-6061) powder was deposited on aluminium Al-6061 substrates using cold spray parameters of 10 bars under helium gas and 200 °C. The coatings were subjected to tensile bond strength measurement and Vicker's microhardness tests as well as microstructure evaluation. The results indicated that the cold sprayed Al-6061 coatings were almost identical in content from the feedstock powder, exhibiting no oxidation and low porosity. They also exhibited superior adhesion strength and microhardness properties similar to the base material. These results demonstrate the technical viability of the cold spray process as an alternate repair method to address degradation issues for gas turbine engine fan case.

However, being a relatively new coating process, the understanding on the effect of pre and post spraying conditions on the properties of the coatings is still in its infancy. An in-depth study of the pre-coating substrate surface roughening and post-coating heat treatment on the quality of the coating will have direct impact on the viability of the application of the cold spray technology.

In addition, components that are cold sprayed usually come in complex shapes. It is difficult to ensure that the spray angle is consistently perpendicular to the surface of the components, especially when coating complex geometrical parts or the internal diameter of components. In a typical coating situation, thousands of particles ejected from the cold spray nozzle will impact the three-dimensional surface at a multitude of angles. As such, the effect of varying spray angle of incidence on the coating properties needs to be further evaluated.

One of the greatest challenges of the cold spray process is controlling the parameters to obtain optimal coating effectiveness and efficiency. Traditionally, the way to determine the effect of each spray parameter on the coating properties and microstructures is to adjust the individual parameter and examine the outcomes [Gilmore *et al*., 1999, Champagne *et al*., 2005]. This process however, has proven to be time consuming as repetitive effort is needed to prepare the coating for property evaluations and microstructural analysis. Furthermore, the relationship between each spray parameter and the coating property is usually not straightforward. Other uncontrollable contributing factors such as the wear state of the nozzle will further affect the uncertain relationship between the control parameters and the coating properties [Alkhimov *et al*., 2001].

1.3 Objectives and Scope

The objectives and scope of this study is as follows:

- To establish the optimum spraying condition for the Russian Academy of Science cold spray system. An experimental study is first carried out to evaluate the in-flight velocity profile of cold sprayed aluminium powder at varying temperature, pressure and powder feed rate. Data is collected at eight downstream locations from the nozzle exit, starting from 5 mm to 40 mm at 5 mm intervals using the Spraywatch-2i in-flight diagnostics system.

- To quantify the impact of grit blasting on the cold spray coating microhardness, tensile adhesion strength and microstructure. An experimental study on the impact of grit blasting on the cold spray coating microhardness, tensile adhesion

strength and microstructure is carried out. Al-6061 coatings are first obtained by cold spraying Al-6061 powders on both grit blasted (using alumina grits) and non-grit blasted Al-6061 substrates. Evaluation on the relative coating microhardness, tensile adhesion strength and microstructure is subsequently performed.

- To quantify the effect of stress relief and full annealing on the coating mechanical properties. An experimental study to evaluate the effect of stress relief and full annealing on the coating mechanical properties is also carried out. Cold sprayed Al-6061 coatings on Al-6061 substrates are subjected to stress relief (150 °C for 2 hours and air-cooled to room temperature) and full annealing (535 °C for 2 hours followed by 177 °C for 8 hours before air-cooled to room temperature) before they are evaluated for their coating microhardness, tensile adhesion strength and microstructure.

- To quantify the effect of the spray angle of the cold spray nozzle (θ) on the microhardness, tensile adhesion strength and microstructure of the coating. An experimental study to evaluate the effect of the spray angle of the cold spray nozzle (θ) on the microhardness, tensile adhesion strength and microstructure of the coating is also evaluated. Coatings are obtained by cold spraying Al-6061 powder onto Al-6061 substrates positioned at spray angles θ= 90° (normal to substrate), 80°, 70°, 60°, 50° and 40° respectively. The microstructural evaluation of single splats formed at various angles is initially performed. The coatings are subsequently evaluated for their relative microhardness, tensile

adhesion strength and microstructure. The impact of the spray angle on the relative coating effectiveness is also evaluated.

- To evaluate qualitatively the effectiveness and built-up of cold spray coating by holding the nozzle at a localized position. An experimental study to evaluate the effect of stationary nozzle deposition is carried out. Al-6061 powder is first cold sprayed onto Al-6061 substrate while holding the nozzle stationary at dwell times of one to five seconds at one second intervals. The microstructure of the coating build-up is subsequently evaluated.

The scope of the thesis is as follows:

Chapter 3: The use of optical diagnostic devices to monitor and control in-flight data such as particle diameter, temperature and velocity has been used in the thermal spray process [Ma *et al*., 2005]. The intent of studying the particle in-flight velocity is to predict the sprayed coating properties and to determine the optimal parameter settings to achieve the desired coatings. The objective of the research is to monitor the in-flight particle velocity using SprayWatch-2i diagnostic system (Oseir Ltd, Tampere, Finland) and establish the optimal settings of the cold spray parameters. Specifically, aluminium powders are cold sprayed at varying cold spray temperature, pressure and powder feed rate and the velocity data at different downstream locations from the nozzle exit is captured and analysed in detail.

Chapter 4: In conventional thermal spray processes, one of the key factors in ensuring the quality of the coating is in the execution of the pre-coating processes. Pre-coating

processes such as masking, cleaning and surface roughening are crucial steps that ensure that the coating properties are enhanced. Specifically, surface roughening, usually in the form of grit blasting, prepares the substrate surface to accept the sprayed materials. An appropriately roughened substrate surface will provide the crucial interface for the first layer of impacting coating particles by considerably increasing the surface area for particle-to-substrate contact. This will significantly improve the atomic interaction. Consequently, the tensile adhesion strength of the coating to the substrate would be significantly enhanced. It is generally believed that surface roughening of substrates would have similar benefits for the cold spray process. However, unlike conventional thermal spray processes, cold spray is a solid state process and the influence of grit blasting of the substrate on the coating properties is not well studied or understood. It is the intent of this study to investigate the effect of grit blasting of the substrate on the mechanical properties and microstructures of the cold spray coatings. Specifically, Al-6061 powders are cold sprayed on both grit blasted and non-grit blasted Al-6061 substrates and the coatings subjected to the tensile adhesion strength test, microhardness assessment and microstructure evaluation. The detailed experimental procedures and the comparative results are documented and discussed.

In addition, coatings are usually treated after the thermal spray processes to improve or enhance various properties. One of the most common post-coating processes is heat treatment that is typically performed to eradicate some of the detrimental effects of conventional thermal spray processes. This is particularly pertinent as the high temperature thermal spray processes usually result in coatings that have, among other undesirable characteristics, elevated oxide and porosity which inevitably affect coating quality. As such, heat treatment is usually a crucial post-coating process to prepare the

thermal spray coatings for service. However, in the cold spray process, coatings are formed with the feedstock powders in the solid state and many of the damaging effects of conventional thermal spray processes are prevented. Under this context, the extent to which heat treatment could enhance the coating quality needs to be further investigated.

It is also the intent of this study to examine the effect of heat treatment on the mechanical properties and microstructures of the cold spray coatings. Specifically, Al-6061 coatings that are cold sprayed on Al-6061 substrates are subjected to stress relief and full annealing and assessed for tensile adhesion strength and microhardness. The microstructure of the coatings are also evaluated and their comparative results presented and discussed in detail.

Chapter 5: When particles are cold sprayed at off-normal angles relative to the substrate surface, the particles will impact the substrate with both normal and tangential components. The normal component of the particle velocity will be lower compared to that of a particle hitting perpendicular to the substrate and the magnitude of decrease is directly related to the angle at which the particle impacts. As the deformation of the impacting particle depends on both the normal and tangential impact velocities, the angle at which the particle is cold sprayed will have a direct impact on the coating properties. Specifically, Al-6061 powder are cold sprayed at various cold spray angles onto Al-6061 substrates and the effect of the spray angle on the coating microhardness, tensile adhesion strength, microstructure are evaluated. In addition, to better understand the coating mechanism in off-normal angle spray condition, microstructure evaluation of single splats were also studied. Furthermore, the relative coating efficiency of the

cold spray process at various spray angles are also evaluated. The experimental procedure and results of off-normal angle cold spray are discussed.

Chapter 6: Cold spray is a relatively low temperature process compared to conventional thermal spray. Thus, the build-up of thermal residual stress is comparative lower. This presents the possibility of building-up a cold spray coating quickly in a local position by holding the cold spray nozzle stationary. However, the effect of this operational procedure on the coating quality is not well understood. An experimental study to observe the coating as it is built-up with the cold spray nozzle held stationary at various dwell times is carried out. Specifically, Al-6061 powder is cold sprayed on Al-6061 substrates with a nozzle held stationary at dwell times of one to five seconds and the microstructures of the coatings evaluated. To better understand the phenomenon as the coating builds up with the stationary cold spray nozzle, a finite element analysis to examine the internal residual stresses of the coating is performed. The experimental procedures results together with the outcome of the finite element analysis are documented.

Chapter 7: An in-depth discussion of all the findings from the various experimental and numerical studies is carried out with recommendations for optimum and preferential processes for cold spray process. The study concludes with suggestions on future works that can be carried out to enhance our understanding of the cold spray process.

With the establishment of the capability and potential of the cold spray system residing at the Singapore Technologies Kinetics-NTU Cold Spray Research Centre, the objectives of this research will focus on the processes involved in obtaining high quality cold spray coatings for industrial applications. The scope of the study has the intent of establishing optimum and preferential processes for cold spray technology in general. This is to pave the way for the industrial application of such a technology in a cost effective and efficient manner.

CHAPTER 2

LITERATURE REVIEW

2.1 Introduction

The literature review conducted in this study can be broadly catergorised into three distinct parts. Firstly, as cold spray is classified as a newly developed method under the thermal spray coating family, a review to identify the various conventional thermal spray processes as well as their advantages and disadvantages is carried out in the first part.

In the second part, a detailed review of the research that has been performed on the cold spray process is carried out. The areas covered include its bonding mechanism, numerical modelling and computational analysis, advantages and limitations, previous materials coated and its industrial application.

In the third part, similar research within the scope of this current study is reviewed. Areas covered include the in-flight characteristics studied previously on thermal spray processes, the research on effects of pre and post coating processes on cold spray coating properties and the effect on spray angles on the coating properties. The intent is to identify the areas that are not well covered and determine the gaps which this study intents to fill so that the knowledge generated will benefit the thermal spray industry.

2.2 Thermal Spray Process

Thermal spray is a common term to describe a cluster of coating processes for applying ceramic, cermet, metallic and in some cases, polymeric coatings for various applications. In general, the process, with the exception of cold spray, involves the heating of the feedstock materials, in powder, rod or wire form, to a semi-molten or molten state before being propelled towards the substrate. Upon impact, the particles flow into thin lamellae called splats and cool. A bond is subsequently formed between the substrate surface and the impacting particles, creating a coating. A thick layer is formed when succeeding particles continue to deposit onto the initial layer on consecutive passes. Coating thickness can differ from a few micrometers to a few centimeters though most applications use thickness in the range of 50 to 500 μm [Tucker, 2013].

2.2.1 Thermal Spray Process Classification

A conventional way of categorising thermal spray processes is by the mode in which the feedstock powder, rod or wire is coated onto the substrate. The two broad categories used are temperature and velocity based methods:

1. Temperature-based methods: a heating element such as arc, plasma or a flame gun is usually deployed to heat up the feedstock material to either a semi-molten or molten state before it is deposited onto the substrate surface. The method by which the extreme heat is introduced differentiates one process from another. Examples of such methods include flame spray, electric arc spray, plasma spray and detonation gun (also called D-gun^{TM}) deposition.

2. Velocity-based methods: feedstock materials are usually propelled towards the substrate surface at high velocity with the use of kinetic energy. Although in some cases, the feedstock materials are still partially melted, these coating methods depend less on the temperature of the feedstock and more on its velocity. Thus, a shorter transient time and lower temperature are usually required. Examples of such method include high velocity oxygen fuel (HVOF) and cold spray.

Another way of classifying the thermal spray coating processes is by grouping them under the sources of their energy, be it thermal or kinetic. Figure 2.1 illustrates the four major thermal spray processes – combustion, electric wire/arc, plasma, and cold spray - and their subsets.

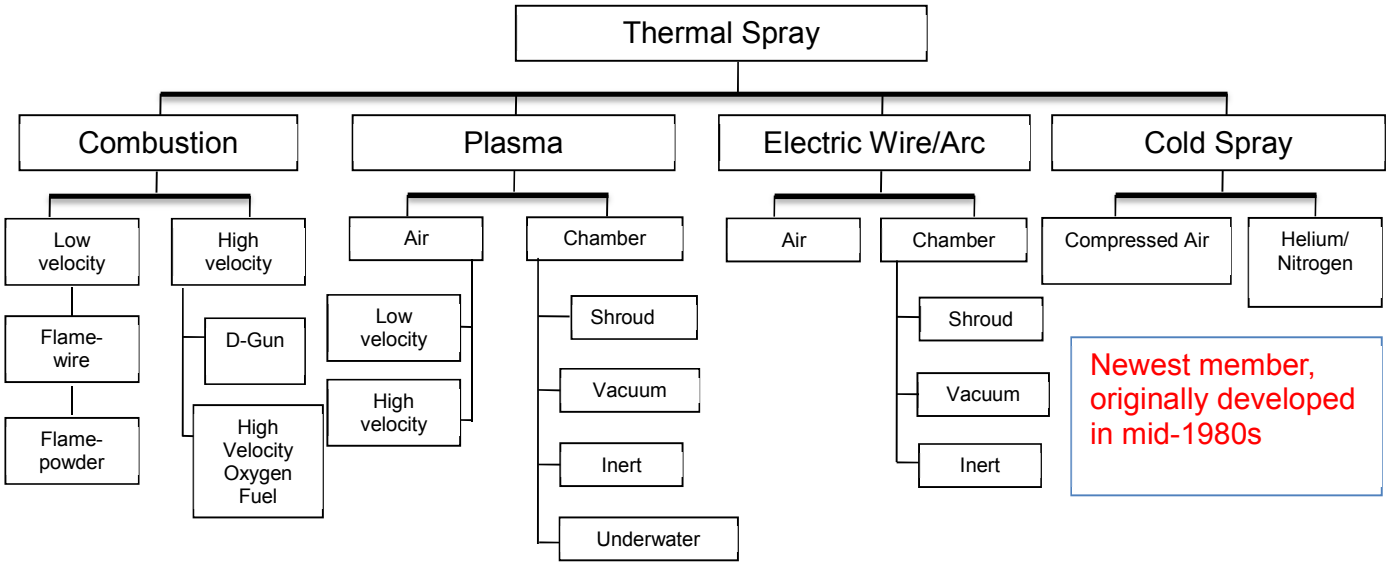

Figure 2.1: Classification of thermal spray processes [Tucker, 2013].

2.2.2 Conventional Thermal Spray Processes

There are five main types of conventional spray process.

- Flame Spray
- Electric Arc Spray
- Plasma Spray
- High Velocity Oxygen Fuel (HVOF) spraying
- Detonation Gun (D-gun^{TM}) spraying

In all these processes, the feedstock material, either in powder, rod or wire form, is first heated before being thrust towards the substrate. The major differences between the five processes and the coatings produced are the different forms of heat source and temperature, as well as the range of the powder velocities just before impact on the substrate material. The individual process will be described in greater detail in the following section.

Flame Spray

Despite being the first thermal spray process developed, conventional flame spray is still widely used in the thermal spray industry. In flame spray, the heat source to melt the feedstock material is derived from the chemical energy of combusting fuel gases. Acetylene is usually used as the sole fuel in combustion with oxygen in oxyacetylene torches. The feedstock materials which are introduced axially into the combustion flame through the back of the nozzle are melted and pushed towards the substrate surface by the expanding gas flow and air jet. A coating is formed as the feedstock material cools. Key advantage of the flame spray process is its ability to deposit a wide range of

materials, including metals, metal alloys, polymers and oxide ceramics. However, because of the heat source, coatings produced usually have high oxide content (2 to 15% porosity) and are relatively less dense (85 to 90% dense) [Crawmer, 2013]. Figure 2.2 illustrates a typical powder flame spray gun.

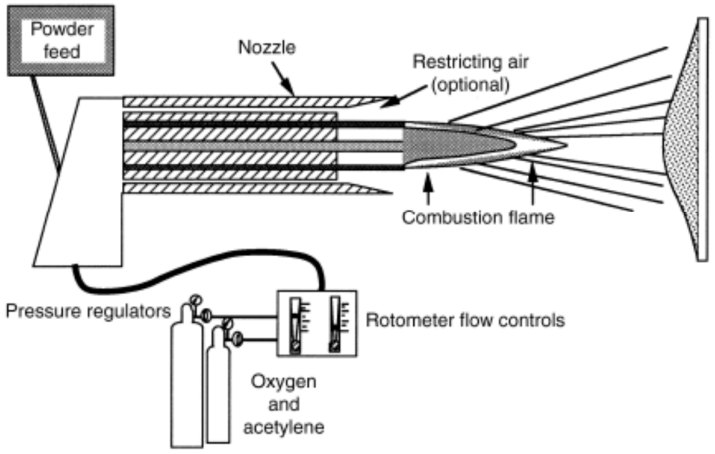

Figure 2.2: Powder flame spray system [Tucker, 2013].

Arc spray

In an arc spray process, a direct current (dc) electric arc is used to effect the melting of two feedstock electrode wire. This is unlike the other thermal spray processes in which heated gas jets are usually used to heat the feedstock indirectly. As the two feedstock wires are constantly fed together, an electric arc is formed in the gap between the wire tips. The molten feedstock is then atomized by the compressed air and thrust towards the substrate where they impact, deform and solidify to form a coating. The relative thermal efficiency of electric arc spray process is significantly higher when compared to other thermal spray processes as the feedstock wires are directly melted by the electric arc. In

addition, arc spray coatings are denser and have better adhesion strength than normal combustion spray coatings. Furthermore, it is relatively cheaper to operate and has higher production efficiency compared to other thermal spray processes. Other advantages include the ability to coat on low-melting point substrates such as polymers due to the lack of substrate heating and the high rate of deposition [Fauchais *et al*, 2014]. One of the key disadvantages of arc spray is its limited ability to coat a wide range of materials. This is due to the fact that the arc spray system can only coat electrically conductive materials which can be made into a wire. However, development in recent years has made it possible to arc spray certain materials which cannot be made into a wire. This is done by integrating them into the hollow core of conductive wires, commonly termed cored wire. Ceramics, such as carbides, have been effectively deposited with electric arc spray using the cored wire method. [Fauchais et al, 2014]. One other disadvantage of arc spray is that a separate heat source may also be required if pre-heating of the substrate is necessary. Figure 2.3 illustrates a typical arc spray gun.

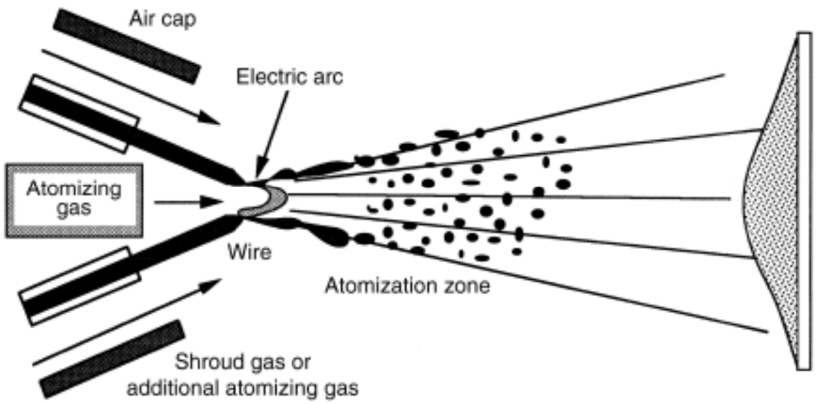

Figure 2.3: Electric arc spray system [Tucker, 2013].

Plasma spray

Plasma is usually created when energy is transferred into a gas until the energy level is high enough to ionize it. In such a state, plasma, often called the fourth state of matter, consists of neutral atoms, positive ions and free electrons which are allowed to act freely from each other. When placed under an electric field, the free electrons moved through the ionized gas, sustaining a current. Heat and light energy are released when the energy input is removed and the electrons and positive ions re-combined.

In the case of plasma spray, a DC electric arc high voltage discharge from a copper anode and tungsten cathode is utilized to form a high temperature plasma gas from either argon, hydrogen, helium or nitrogen. As a result, a plasma flame is formed at the anode nozzle exit as the resistance heating causes the inert gas to expand and ionize. The plasma flame rapidly heats up the feedstock powder which is fed into the flame and accelerated onto the substrate. A cleaner (<1% porosity), denser (99% density) and high bond strength (> 34 MPa) coating [Crawmer, 2013] is usually obtained in plasma spray process.

With temperature generated exceeding 20,000 °C, one of the key advantages of plasma spray is its versatility in coating a diverse and wide range of materials, including those with very high melting point such as tungsten and zirconia. The main disadvantages of the process are its complexity and relative high operating cost. Figure 2.4 illustrates a common plasma spray gun.

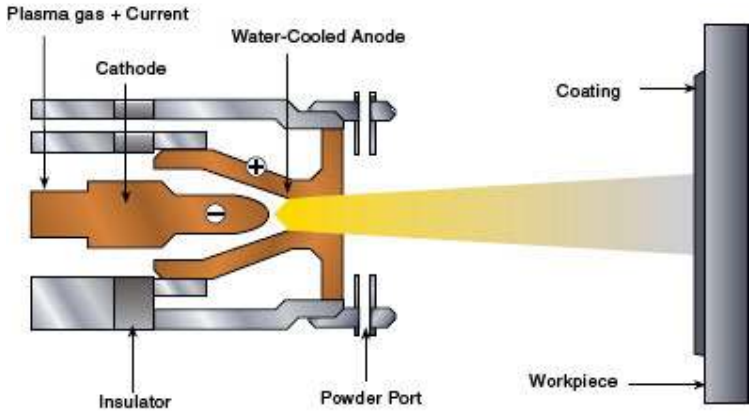

Figure 2.4: Plasma spray system (Courtesy of Sulzer Metco).

High Velocity Oxygen Fuel (HVOF) spray

In HVOF spray, oxygen is mixed with either a liquid fuel (kerosene or propylene) or gas (hydrogen or acetylene) and ignited in a water-cooled, high pressure combustion chamber. As a result, a supersonic velocity jet is created due to the heated and expanded combustion mixture. Feedstock powder is then fed axially into this jet that propels it towards the substrate. The molten particles become entrained into the confined, high-pressure flame and form a coating upon impacting onto the substrate.

One of the key advantages of HVOF spray is its ability to produce very dense coatings with low porosity and excellent bond strength. However, due to its relatively lower temperature and high velocity of the particles which translates to low residence time, only powders of certain sizes (5 to 60 um) can be sprayed. Figure 2.5 illustrates a typical HVOF gun.

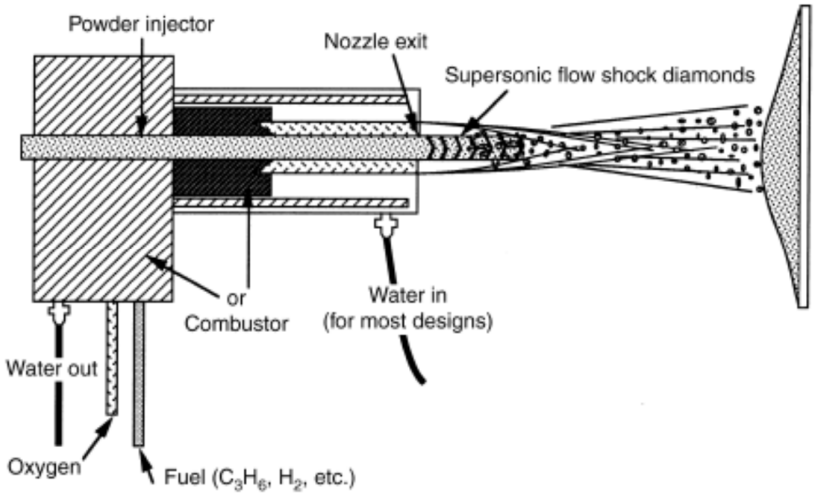

Figure 2.5: High-velocity oxygen fuel spray system [Tucker, 2013].

Detonation Gun (D-gun^{TM}) spraying

The detonation gun spraying process works on the principle of generating a detonation-pressure wave by igniting a mixture of fuel, oxygen and powder in a long (about 1 m) barrel (typical inside diameter of 2.5 cm) with a spark plug. This detonation-pressure wave then heats and pushes the entrained feedstock powders towards the substrate surface at a supersonic velocity. The remaining hot powder is subsequently flushed out of the barrel with nitrogen to prevent any unwanted detonation and shock wave. To obtain the required coating thickness, the detonation process is repeated.

The key advantage of the detonation gun spraying process is its ability to produce high quality, dense and hard coatings which are excellent for wear resistant. However, as the system contains several mechanical components, the reliability and safety of the gun mechanisms and valves can be a concern. The high level of noise created by the system

is also an environmental and health concern. As such, the process is usually carried out only in an enclosed sound insulated chamber. Figure 2.6 illustrates a typical D-gun™.

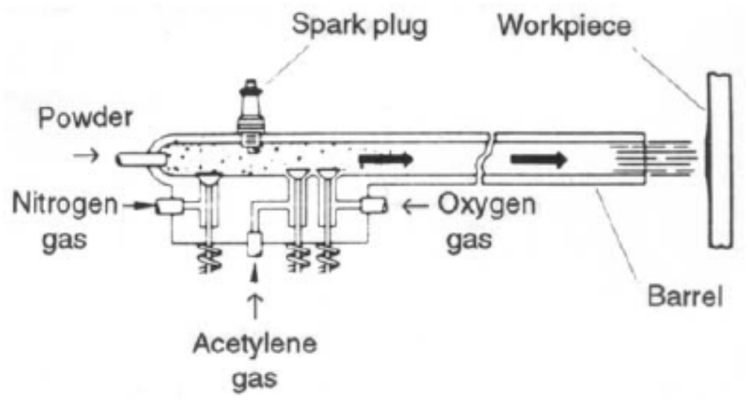

Figure 2.6: Detonation gun system (Courtesy of Praxair Surface Technologies).

2.2.3 Advantages and Limitations of Thermal Spray Processes

Properly applied thermal spray coatings have many applications and numerous advantages [Tucker, 1994]:

Versatility: a wide range of materials including metals, metal alloys, oxide and non-oxide ceramics, plastics, cermets and composite structures made up of metals, ceramics and plastics can be deposited as coatings. Essentially, thermal spray processes can be used for any material which can be melted without decomposing.

Wide range of coating thickness: coating thickness from as thin as 25 μm to 6.5 mm are achievable for typical current application. Thicker coatings are possible using electric arc spray, vacuum plasma spray and cold spray processes.

Low processing costs: Due to the rapid spray rates and high deposition efficiencies, the processing costs for thermal spray processes are generally relatively lower compared to chemical vapour deposition and physical vapour deposition processes. Deposition rates of 1 to 45 kg per hour are achievable with some thermal spray processes such as electric arc spray compared to 2 to 7 kg per hour for chemical vapour deposition and physical vapour deposition processes [Crawmer, 2013].

Minimal thermal degradation of substrates: In terms of substrate interaction, thermal spraying is a relatively cold process with substrate temperature usually kept below 65 °C. There is little risk of thermal degradation of the substrate during coating. As a result, there is very little impact on the properties and thermal distortion of the coated components even when high melting point materials such as tungsten are applied. This applies to components which are finely machined and fully heat treated as well.

However, as with all coating technologies, thermal spray has its limitations. Some of these are listed below.

Porosity: Thermal spray coatings generally exhibit some porosity, ranging from up to 20% for arc spray to 15% for flame spray and up to 5% for HVOF, D-gun™ and air plasma spray [Crawmer, 2013]. The porosity allows the passage of gases and/or liquids through to the coating and substrate interface. Mechanical properties of the coating may also be adversely affected. Specifically, porosity makes thermal spray coatings poor at withstanding concentrated forces such as point and line loads, and will usually collapse, resulting in permanent surface deformation.

Line-of-sight process: thermal spray can coat only the surfaces that the torch can "see". For simple geometrical configurations, the deposition process is straightforward. However, for complex geometries, the process would require automated, robotically-controlled manipulation of the gun and/or substrate for effective adhesion of the coatings. For parts with small and deep cavities, it will not be possible to coat if the torch is not able to fit into the space. Off-angled thermal spraying is possible but usually at the expense of the coating quality.

Low bond strength: the tensile bond strength achieved via conventional thermal spray process is relatively lower than other coating processes. Using ASTM Standard C 633 as a comparative test, tensile adhesion of thermal spray coatings typically measures between 41 and 83 MPa whereas that for plating, welding and vapour deposition processes usually has a minimal value of 103 MPa.

Anisotropic properties: thermal spray coatings are anisotropic. They are likely to have up to 10 times the tensile strength in the longitudinal direction than in the direction parallel to the spray. As a result, they are generally more brittle than corresponding wrought or cast materials and do not resist impact loading unless heat treated after deposition.

2.3 Cold Spray Process

Cold spray is a material deposition process that uses a high pressure and velocity gas jet to impart the kinetic energy for the coating particles and subsequently developing a coating on an appropriate substrate by an impaction process. It belongs to the broader thermal spray coating processes and is widely regarded as one of the newer members of the coating technology, together with suspension and solution precursor plasma spray and very low pressure plasma spray. Its origins dates back to the early 1980s when it was accidentally discovered as an alternate coating process at the Institute of Theoretical and Applied Mechanics of the Siberian Branch of the Russian Academy of Science [Alkhimov *et al*., 1994]. While attempting to understand the effect of supersonic two-phase flow on models in a wind tunnel, it was discovered that particles adhere to the model instead of eroding it when they reach above a certain minimum particle velocity. A coating was formed on the model.

When compared to conventional thermal spray processes, the distinctive feature of cold spray process is its ability to produce coatings at gas pre-heated from 0 to 1000 degrees Celsius. This range is usually much lower than the melting point of the particle materials (thus the term “cold” spray). In reality, the temperature experienced by the feedstock particles is even lower as the temperature at the nozzle exit is significantly lower than the pre-heat gas temperature. Table 2.1 illustrates the comparative gas and particle velocity and temperature between cold spray and the other more typical thermal spray processes.

Table 2.1: Comparative gas and particle velocity and temperature among typical thermal spray processes [Crawmer, 2013].

Process	Gas Velocity (m/s)	Particle Velocity (m/s)	Gas Temperature (K)
High Velocity Oxygen Fuel (HVOF)	500-1,200	200-1,000	5,500
Arc Spray	50-100	50-100	>25,000
Air Plasma Spray (APS)	300-1,000	200-800	15,000
Vacuum Plasma Spray (VPS)	200-600	200-600	12,000
Cold Spray	300-1,200	300-1,200	1,000

Instead of high temperature, cold spray uses high velocity as the working principle behind its coating process. The coating process involves accelerating un-melted powder particles, of sizes in the range of 1 to 50 μm in diameter, to supersonic speeds of between 300-1200 m/s by either compressed air, nitrogen or helium carrier gas. A coating is formed by an impact process as the particles hit an appropriate substrate surface. Typically a De-Laval type converging diverging nozzle is used to bring the powders to high velocities as shown in Figure 2.7. There are currently two main types of cold spray systems: high pressure cold spray in which particles are injected prior to the spray nozzle throat from a high pressure gas supply; and low pressure cold spray in which powders are injected in the diverging section of the spray nozzle from a low pressure gas supply [Moridi *et al*., 2014]. Consequently, cold spray is also known as "kinetic energy metallisation", "high-velocity powder deposition", "kinetic spraying" or "cold gas-dynamic spray method".

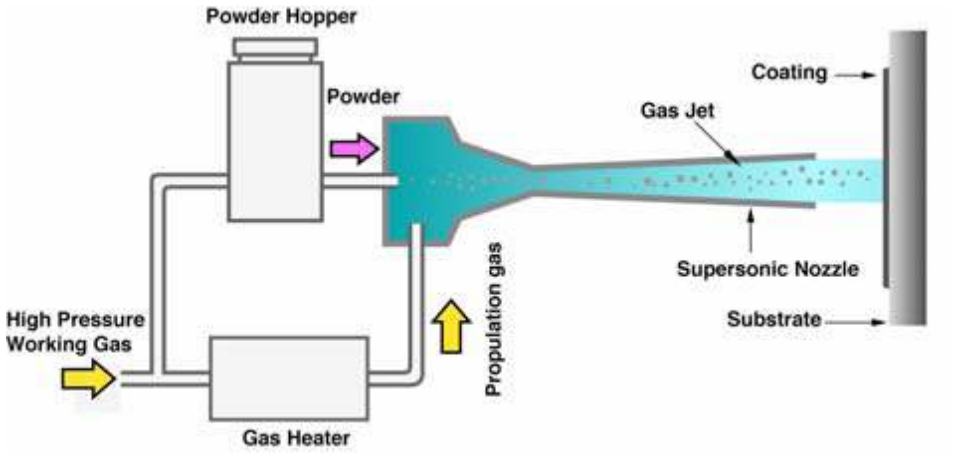

Figure 2.7: Schematic of a typical cold spray system set-up.

Depending on the particle velocity (V_p), three different phenomena can occur when a particle impinges on a substrate. In the first instance, the particle just bounces off the substrate surface when its velocity, V_p is low. As the particle velocity V_p increases to moderate values, erosion by the solid particle on the substrate occurs. When the particle velocity V_p increases further and exceeds a critical value, V_c, the particle plastically deforms and adheres to the substrate or on one another to form an overlay deposit as shown in Figure 2.8b [Karthikeyan, 2004].

Generally, for every material, as the velocity of the particle increases, there exists a critical velocity in which the particle transition from eroding the substrate to adhering to it. A coating is formed only when particles with velocity greater than this critical value lands onto the substrate. Figure 2.9 shows the influence of impact velocity and particle size on the impact phenomena [Klinko *et al*., 2005]. Details of the various area shown on the figure are defined on the referenced article.

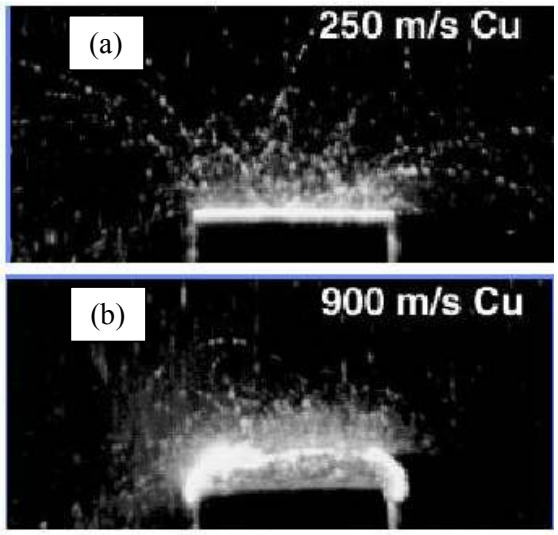

Figure 2.8: (a) Particle velocity (V_p) < critical velocity (V_c) solid particle erosion of surface. (b) Particle velocity (V_p) > critical velocity (V_c) particles plastically deform and adhere to the substrate [Karthikeyan, 2004].

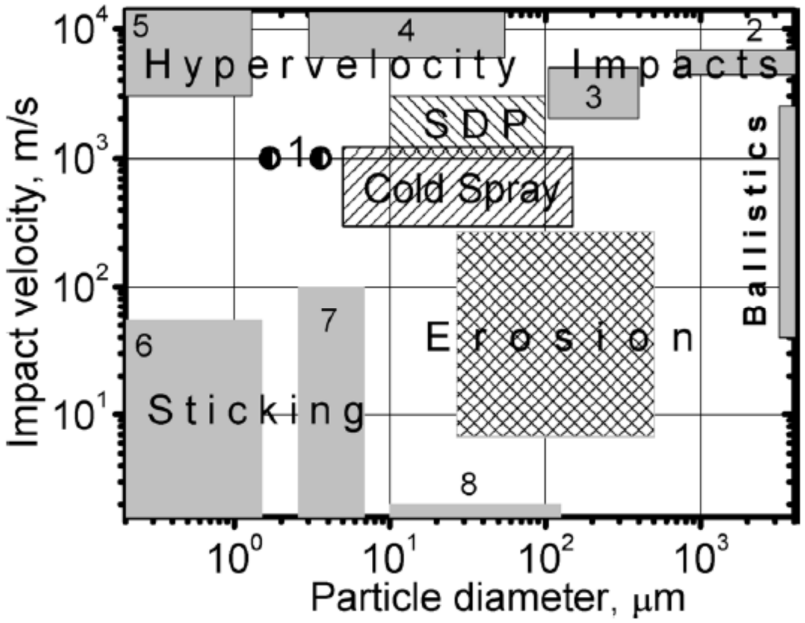

Figure 2.9: Influence of impact velocity and particle size on features of the interaction [Klinko *et al*., 2005].

Investigators have predicted critical velocities through numerical modelling of the deformation phenomena in cold spray [Schmidt et al., 2006, Klassen et al., 2006]. Based on the material properties, the effects on the critical velocity are summarised into expression 2.1 [Assadi et al., 2003]:

$$V_{cr} = 667 - 14\rho + 0.08T_m + 0.1\sigma_u - 0.4T_i$$

Eq 2.1

where

V_{cr} : critical velocity (m/sec)

ρ: bulk density of powder (g/cm^3)

T_m: melting temperature (°C)

σ_u: ultimate strength (MPa)

T_i: initial particle temperature in °C

It is generally believed that the momentarily high interfacial pressure and temperature is the mechanism that causes the impinging solid state particles to deform and bond with the substrate and among themselves. During the high velocity impact process, the atomic structures of the particle and the substrate surfaces are pressed into intimate contact with one another, disrupting their oxide films. The bond created at the interface level is a result of the hydrodynamic flow instability between the impinging particle and the surface of the substrate. This concept is similar to explosive welding process except that it happens on a micro-scale.

Though the preheated gas temperature for the cold spray process is in the range of 0 to 700 °C, the temperature as the gas exits the nozzle is actually lower. The lower

temperature arises because as the high pressure carrier gas flows into the converging portion of the De Laval type nozzle, it speeds up to sonic velocity in the throat region of the nozzle. The velocity of the carrier gas increases to supersonic (Mach number between 2 to 4) as it expands in the diverging portion of the nozzle. Cooling takes place as the carrier gas further expands in the nozzle, often resulting in it exiting the nozzle at a temperature below ambient. The comparative particle velocity and gas temperature ranges for the conventional thermal spray processes and cold spray are shown in Figure 2.10 [McCune *et al*., 1995]. The cold spray process, with its distinctively low process temperatures and relatively high particle velocities, positions itself as a unique coating process when compared to the other thermal spray processes.

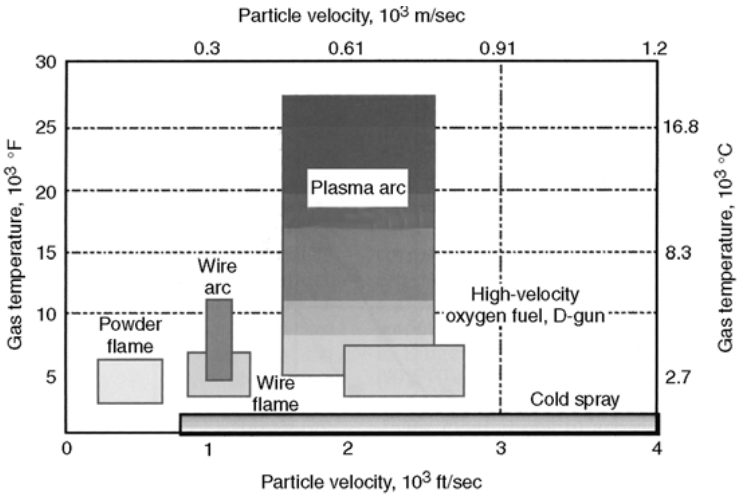

Figure 2.10: Gas temperature and particle velocity regimes for common thermal spray processes compared to cold spray technology [McCune *et al*., 1995].

2.3.1 Bond Mechanism

There has been extensive study into the bonding mechanism between the cold sprayed particles and the substrate. However, the actual mechanism by which the cold sprayed

particles deformed and bond to the substrate is not fully understood. What is well accepted is that during impact of the feedstock powder onto the substrate, the deposited particle undergoes extensive localized deformation. It is believed that the adhesion between the particle and the substrate occurs at atomic length-scale level and is enhanced by two favourable conditions, clean surfaces and high contact pressures to force the two surfaces to mutually conform. As a result, the magnitude of the bond is dependent on the attraction or repulsion character of the atomic interactions. This in terms is dependent on the atomic electron orbital localization/delocalization tendencies and also by the orientation and crystallographic specifics of the contact surfaces. This implies that complete mutual solubility of two metals in the solid state would indicate a weak repulsive or attractive atomic interactions.

A computational analysis done by Grijicic *et al*. [2003] suggests that clean surfaces and great contact pressures are the two key characteristics for effective bonding to occur at the particle and substrate contact surface when the high velocity particle impact the surface. The required cleanliness between the particle and contact surface of the substrate is enhanced by the adiabatic shear instability and the associated localization of the plastic flow into the interfacial jets. In addition, the high contact pressure between the particle and substrate is achieved by the high impact velocities of the particles.

Thus, the size of the particle and substrate contact surface area have a big impact on the strength of the resultant particle-substrate adhesion bond. In cases where the substrate interface surfaces are wavy and contain vortex-like features, a stronger bond was observed.

2.3.2 Modelling of Gas Flow and Particle Velocity

The cold spray process is alike conventional thermal spray processes in many aspects. Pressurised carrier gas is heated and forced through a converging-diverging nozzle to create a supersonic gas jet that propels the feedstock powders to the substrate. However, unlike conventional thermal spray processes, heat is introduced in the carrier gas not as a means to melt the feedstock powder. Rather, the intent for heating the carrier gas is primarily to accelerate its sonic velocity as it flows through the converging-diverging nozzle and in the process, generates a higher flow velocity without increasing carrier gas usage. This can be easily illustrated by the modelling of the carrier gas within the nozzle [Sakaki, 2007].

Assuming the process gas flow within the nozzle is the quasi-one-dimensional isentropic flow of semi-perfect gas and the gas flow in the convergent-divergent nozzle is supersonic, the ratio of the throat pressure P_t to the nozzle intake pressure, P_i is given as:

$$\frac{P_t}{P_i} = \left(\frac{2}{\kappa + 1}\right)^{\frac{\kappa}{\kappa - 1}}$$

Eq. 2.2

where κ is the gas specific heat ratio of the carrier gas to the atmospheric air.

For sonic conditions to be maintained at the nozzle throat, the throat pressure P_t must be above ambient. An optimal nozzle throat area A_t where gas flow is sonic can be calculated as:

$$A_t = \frac{m}{\sqrt{\kappa \left(\frac{2}{\kappa+1}\right)^{\frac{(\kappa+1)}{(\kappa-1)}} \frac{P_i}{v_i}}}$$

Eq. 2.3

where m is the mass flow rate of the process gas and v_i is the specific volume of the gas and is given as:

$$v_i = \frac{RT_{gi}}{P_i}$$

Eq. 2.4

where R is the gas constant and T_{gi} is the gas temperature at the nozzle intake.

The nozzle exit area A_e can be expressed as:

$$\frac{A_t}{A_e} = \left(\frac{\kappa+1}{2}\right)^{\frac{1}{(\kappa-1)}} \left(\frac{P_e}{P_i}\right)^{\frac{1}{\kappa}} \sqrt{\frac{\kappa+1}{\kappa-1}\left[1 - \left(\frac{P_e}{P_i}\right)^{\frac{(\kappa-1)}{\kappa}}\right]}$$

Eq. 2.5

Optimal exit area A_e is obtained when the nozzle exit gas pressure P_e is equal to the ambient pressure P_a.

The pressure, P, temperature T_g and velocity U_g of the gas flow can be calculated from the ratio of the nozzle cross-sectional area A at a given point to the nozzle throat area A_t by:

$$\frac{A}{A_t} = \sqrt{\frac{\left(\frac{\kappa-1}{2}\right)\left(\frac{2}{\kappa+1}\right)^{\frac{(\kappa+1)}{(\kappa-1)}}}{\left[\left(\frac{P}{P_i}\right)^{\frac{2}{\kappa}} - \left(\frac{P}{P_i}\right)^{\frac{(\kappa+1)}{\kappa}}\right]}}$$

Eq. 2.6

$$T_g = T_{gi}\left(\frac{P}{P_i}\right)^{\frac{(\kappa-1)}{\kappa}}$$

Eq. 2.7

$$U_g = \sqrt{2\frac{\kappa}{\kappa-1}P_i v_i\left[1-\left(\frac{P}{P_i}\right)^{\frac{(\kappa-1)}{\kappa}}\right]+U_{gi}^2}$$

Eq. 2.8

$$U_g = \sqrt{2\frac{\kappa}{\kappa-1}RT_i\left[1-\left(\frac{P}{P_i}\right)^{\frac{(\kappa-1)}{\kappa}}\right]+U_{gi}^2}$$

Eq. 2.9

Due to the rapid cooling of the carrier gas as it expands in the diverging section of the nozzle, it usually exits the cold spray nozzle at a significantly lower temperature. In some cases, the carrier gas was at temperatures lower than ambient, hence the term cold spray.

2.3.3 Computational Analysis

Numerical studies on the cold spray process have been conducted to better understand the process. In the study performed by Jen *et al.* [2005], a numerical simulation is carried out for the gas-particle two phase flow with copper (Cu) and platinum (Pt) particles. The particles, ranging from 100 nm to 50 μm in diameter, are accelerated by carrier gases helium or nitrogen in a supersonic De-Laval type nozzle. As shown in Figure 2.11, three distinct features were observed in the area between the nozzle exit and the substrate surface. Firstly, a Mach disk is formed close to the nozzle exit. This

is followed by a weaker Mach disk near to the substrate and subsequently, a bow shock on the substrate itself. The pressure across the bow shock undergoes a steep increase and the study indicates that the bow shock actually prevents smaller size particles (less than 0.5 μm) from penetrating, leading to poor or no coating on the substrate.

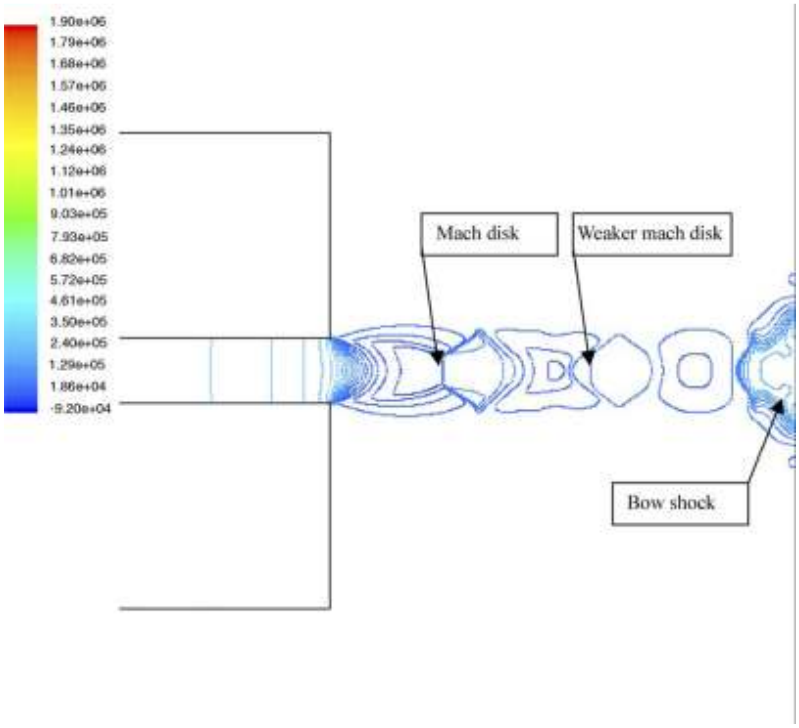

Figure 2.11 Pressure contour of N_2 between the nozzle and substrate [Jen *et al.* 2005].

The existence of a high pressure bow shock region near the substrate was subsequently validated by Samareh *et al.* [2007]. Using a three-dimensional numerical analysis approach, the study shows the formation of a strong bow shock formed on the substrate with a high stagnation point created near the plate as shown in Figure 2.12. The existence of this high pressure region results in the slowing down of the cold sprayed

particles and in some cases, impacting the substrate at an off-normal angle. The effect can be so drastic that the trajectories of some particles may be deviated from the centreline and are washed away by the gas flow without impacting the substrate. Additionally, those particles that hit the substrate with such a low-normal impact velocity do not have adequate kinetic energy to create a bond to the substrate. These two phenomena are attributed as the key factors for directly reducing the cold spray process deposition efficiency.

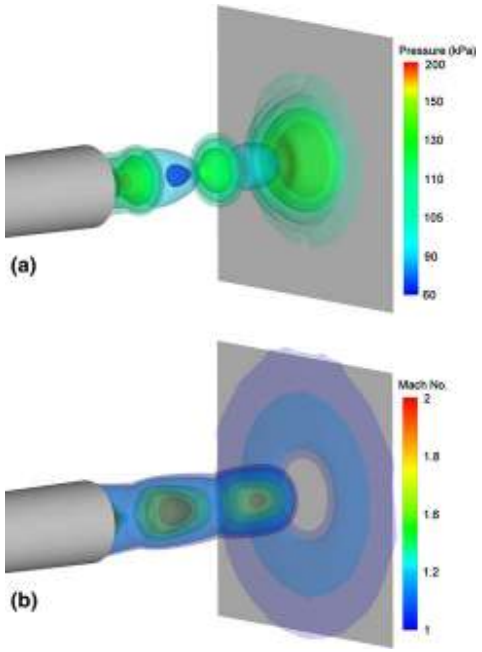

Figure 2.12 (a) Pressure iso-surface for a flat substrate located at a standoff distance of 20mm. (b) Mach number iso-surface for the same substrate [Samareh *et al.*, 2007].

A recent in-depth study examined impact conditions of the cold sprayed particles using modelling and computational methods [Schmidt *et al.*, 2009]. The intent was to evaluate the bonding mechanisms of the particles on the substrate and to predict the particle

temperatures and velocities at the time of impact on the substrate as a function of gas temperature, pressure and nozzle design. The results of the simulation indicate that the strong plastic shear deformation between the particle and substrate surface interfaces at impact contributes to the formation of the bond. Deformation was calculated to happen within 50 nano-seconds such that there is insufficient time for the heat produced to dissipate, resulting in the formation of highly localized adiabatic shear instabilities. In addition, the temperatures in the interface area can rise to near melting point of the material and further promotes bonding.

The cold spray is a good candidate for numerical modelling due to its relative simplicity. As the carrier gas is only pre-heated electrically, modelling does not have to consider combustion or heat transfer and expansion of various gases in electrical discharges. In addition, the particles are in the solid state and are hardly oxidized as they impact the substrate, so the modelling of particle collision has to deal only with plastic deformation. Furthermore, complicated effect such as solidification and corresponding shrinkage associated with conventional thermal spray processes as well as in-flight and post-impact oxidation of the sprayed coating can be ignored. As a result, highly accurate modelling results on impact conditions and particle bonding of cold spraying can be obtained.

Computational analysis of adiabatic shear localization of the particle-substrate interaction upon impact has also been performed by Grujicic *et al*. [2003]. The study shows how a crater forms in the substrate as the particle penetrates it. The depth and diameter of this crater increase as the particle-substrate contact time decreases while the height-to-width aspect ratio of the particle decreases. The plastic deformation in

both the particle and substrate is concentrated in a narrow region surrounding the particle-substrate interface. An interfacial jet composed of the highly deformed material is formed as a result. As the particle impact velocity increases, the thickness of the interfacial jet decreases, indicating an increased level of plastic strain localization in the interfacial region.

2.3.4 Advantages of Cold Spray Process

Due to the absence of a high-temperature heat source prevalent in a conventional thermal spray process (electric arc spray, plasma spray, HVOF etc), the cold spray process offers a number of advantages in the area of coating deposition and formation. Among the more significant ones are [Smith, 2007]:

a) Unlike conventional thermal spray processes, there is an absence of splashing with the solid state cold spray deposition process. Furthermore, the peening effect of impinging high velocity solid particles compacts previously deposited materials and closes any small pores in the underlying material. As a result, a high density coating with minimal or no change in microstructure is achievable as the amount of heating on the particle is relatively small.

b) The presence of oxides in most conventional thermal spray coatings can have a detrimental effect on the electrical, mechanical and thermal properties of the coatings. Deposition of thermal and oxygen sensitive materials such as titanium and copper by cold spray can be achieved with little significant material degradation due to the minimal in-flight oxidation and other chemical reactions characteristic of conventional thermal spray processes.

c) Multiple-elements metal alloys may undergo chemical changes in conventional thermal spray deposition. This is due to the preferential vaporization of more volatile elements in the high temperature deposition processes. In addition, the melting and solidification process can severely modify the phase composition and crystal structure of the sprayed coating material compared to the feedstock material. In the cold spray process, the solid spray particles experience little heating, implying that there is no modification in the chemistry of a compound alloy and the initial phase composition and crystal structure are preserved. Coatings produced are of low oxide content, with low shrinkage stresses and have reduced material loss due to vaporization and reduced grain growth, minimal or no phase composition change and recrystallisation.

d) In conventional thermal spray processes, temperatures as high as 20,000 °C can be used and small particles have a tendency to vaporise in the process as a result. In cold spray, comparatively smaller particles, ranging in size from 1 to 60 μm can be used as the feedstocks. This usually has a positive impact on the efficiency of the deposition process.

e) In the cold spray process, the small size nozzle (5–20 mm) coupled with short spray distance (10-50 mm) equate to a small spray beam. This allows better and more accurate control on the area of deposition. This presents the possibility for cold spray to be used on a localised area without masking operations which can save costs compared to traditional thermal spray processes.

f) The "peening" effect of the impacting particles results in compressive residual stresses. This is contrary to the highly unfavourable tensile residual stresses created as a result of solidification shrinkage in a traditional thermal spray process. This implies that thick coatings in the range of 5 to 50 m can be obtained without bonding failure due to the absence of tensile residual stresses which facilitate the opening or extension of cracks in the coating.

2.3.5 Limitations of Cold Spray Process

Although the cold spray process has important advantages over conventional thermal spray processes, it also has its own inherent limitations. Among the more noteworthy ones are:

a) The range of materials and compatible substrates which cold spray can be utilized is limited. This is due to the fact that the process does not involve the melting of particles, unlike conventional thermal spray processes which have the versatility to coat a wide range of materials on similarly wide range of substrates. The materials which cold spray can be utilized to deposit are limited to ductile metals on ceramic, metal or fairly hard substrates, though in recent years, metal-metal matrix composite such as titania has been successfully cold sprayed as well [Moridi *et al*., 2014].

b) As the cold spray process depends largely on the process gas to carry the powder particles, it requires larger amount of process gas than traditional thermal spray processes. In certain applications, helium may be used as the primary cold spray

process gas to achieve the necessary impact velocities and coating qualities, the process cost may increase significantly in such cases.

c) As the spray trail for the cold spray process is relatively small (typically less than 1 cm in diameter), it may not be well suited for coating large surfaces. This is unlike some of the traditional thermal spray process such as electric wire arc spray in which the foot print is significantly larger and usually deployed for marine and oil and gas applications.

d) Being a relatively new process, the amount of published data on the cold spray coating performance and properties in industrial applications is fairly limited. This implies that new application of cold spray technology would require additional evaluation.

Due to the limitation in terms of the types of materials and substrates for which cold spray can be used, as well as the other reasons stated, it will not completely substitute conventional thermal spray processes. However, cold spray represents a new process capability that may replace certain conventional thermal spray processes in specific applications. Examples will be provided in Section 2.37 of this chapter.

2.3.6 Materials Coated Using Cold Spray Process

A wide variety of materials such as aluminum [Van Steenkiste *et al*., 2002 & Morgan *et al*., 2004], aluminum alloys [Ajdelsztajn et al., 2005], copper [Borchers *et al*., 2003] , nickel alloys [Sansoucy *et al*., 2004], WC-Co [Lima *et al*., 2002], zinc [Li *et al*., 2004] and titanium [Li *et al.*, 2003] among others have been successfully cold sprayed. This

is noteworthy as unlike conventional thermal spray processes, there is a limitation on the types of materials which cold spray can deposit. Among the dominant theories, intense local plastic deformation has been cited as the sole reason for the coating to form. [Dykhuizen *et al*., 1999, Assadi *et al*., 2003, Alkhimov *et al*., 2000], although some researchers have theoretically shown that localized melting is possible [Schmidt *et al*., 2006].

One of the distinctive features of cold spray process is its ability to produce nanocrystalline coatings by simply using nanocrystalline feedstock [Richer *et al*., 2004]. This is due to the absence of severe heating and the associated grain growth mechanism in cold spray. The attractiveness of nanocrystalline coatings is its enhanced mechanical properties due to its ability to inhibit dislocation motion with its increased number of atoms located at grain boundaries [Gaffet *et al*., 1993]. Even though plasma and HVOF spray has previously demonstrated its ability to produce coating with fine grain structures (80 to 200 nm) [Ajdelsztajn *et al*., 2005], with the much higher operating temperatures, it is inevitable that they will cause grain growth and some degree of oxidation. Cold spray is a feasible alternative in obtaining nanocrystalline coatings.

In a recent study on cold spraying stainless steel 316L powder having two different morphologies and almost the same size distribution, angular particles were found to reach higher velocity than spherical ones which and translated to better deposition efficiency [Fukanuma *et al*., 2006]. This runs against the trend of conventional thermal spray processes in which spherically shaped powders are preferred as they are easier to transport during the powder feeding process and are more uniformly melted during the heating process, resulting in a more uniform coating. The principle behind angular

particle achieving faster velocity in supersonic gas flow is an area of interest and worthy of further investigation as it could result in a totally different approach towards coating powder preparation for the cold spray process.

2.3.7 Application of Cold Spray

Historically, the advancement in thermal spray technology has been driven by the need to fulfill a demand in the aerospace industry. Rapid growth in revenue for the thermal spray industry was observed during the period between 1960 and 1990s when the application of the technology for aircraft engines grew (Figure 2.13). The key contributors of this growth were the commercial introduction of plasma spray, the detonation gun and high velocity oxygen fuel (HVOF) spray, new and improved process control equipment and materials. All these coincided with the thermal spray application for advanced gas turbine engine components such as compressor blades, cases, stator vanes, bearing housings and labyrinth seals. Many of these applications were subsequently leveraged onto the other industries such as the marine, oil and gas, medical and nuclear energy. It is no surprise that the application of cold spray in the aerospace industry is keenly watched by many thermal spray practitioners.

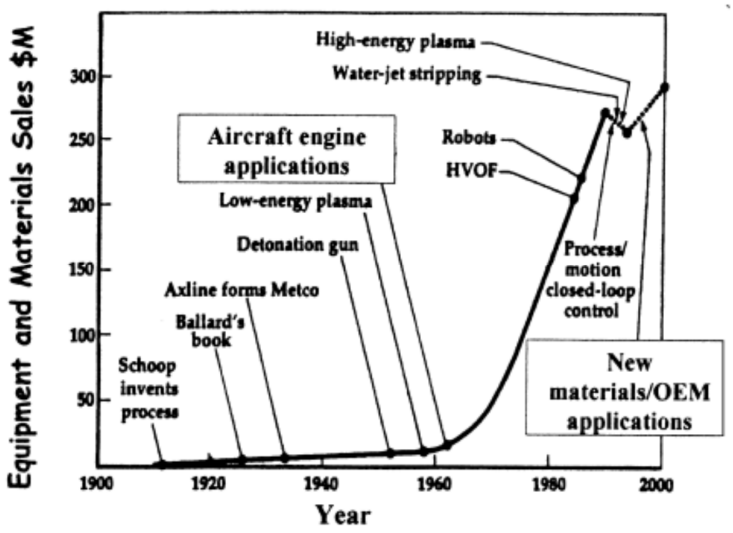

Figure 2.13: Timeline of significant developments during the growth of the thermal spray industry. Source: R. Smith, ASM Notes.

With its unique ability to produce well-defined and high particle density spray footprint, the cold spray process has been used in many industries for specific applications. Broadly, cold spray application can be classified into four main categories: (1) repair and restoration, (2) corrosion resistance, (3) wear resistance and (4) electrical application. Examples of the various applications are captured in the following section.

2.3.7.1 Repair and Restoration

The use of cold spray as a possible coating option to restore damaged and corroded magnesium helicopter components back to serviceable condition in rotorcraft was first explored by the US Army Research Laboratory [Champagne *et al*., 2002]. Magnesium alloys are currently used for helicopter transmission gearboxes as they are widely available and easily machined. In addition, they have low density and excellent stiffness and damping capacity as well as thermal conductivity. The only major disadvantage is that they are prone to galvanic corrosion. This is because magnesium is one of the most

electrochemically active structural metals. Restoration work carried out by Champagne [2008] demonstrated the ability of using cold sprayed commercially pure (CP) aluminium and Al-6061 aluminium alloy to restore the damaged gearbox dimensionally as shown in Figure 2.14.

Figure 2.14: Magnesium helicopter transmission gearbox restored by cold spray using CP aluminium and Al-6061 aluminium alloy powders [Champagne, 2008].

In a similar project, a severely corroded magnesium main rotor transmission housing from a Sikorsky UH-60 Black Hawk helicopter was also cold sprayed repaired using CP aluminium and Al-6061 aluminium powder by Champagne *et al*. [2012] as shown in Figure 2.15.

Figure 2.15: Restoration work on UH-60 main rotor transmission housing using cold sprayed CP Aluminium and Al-6061 Aluminium powders [Champagne *et al.*, 2012]

In another application, the Moog Aircraft Group [2012] successfully repaired a corroded Boeing 737 nose wheel steering actuator using cold sprayed nickel alloy coatings. Nose wheel steering actuator barrels of aircraft landing gears are commonly made of high strength nickel alloys (Inconel). These components, which are located on the front of the aircraft, are usually subjected to high thermal and mechanical stresses during flight. In addition, due to their location on the aircraft, they are regularly subjected to moisture and dirt that ingresses into the joints when the landing gears are engaged, causing them to corrode. The restoration process involves firstly removing the corroded area by pre-machining the barrel. The barrel is subsequently built-up by cold spraying it with nickel metallic powder before machining it back to its original part dimensions. Figure 2.16 shows the before and after photos of the restoration work.

Figure 2.16: Before and after photos of cold sprayed repaired B737 nose wheel steering actuator barrel [MOOG Aircraft Group, 2012].

The successful application of cold spray in landing gears was also demonstrated by the work done by Birtch et al. [2008]. The application of Ion Vapour Deposited aluminium (IVD aluminium) coating as an alternative to cadmium plating for high strength steel landing gears has been more widespread in recent years. The IVD aluminium coatings however are susceptible to corrosion once they are damaged during flight operation. Cold sprayed aluminium process was established as a repair procedure to address the corrosion issue and the coating has shown to be non-embrittling to the high strength steel and capable of meeting the MIL-DTL-83488D [Military Specification, 1999] specifications.

In a demonstration of cold spray application in the automobile industry, McCune et al. [2008] used cold spray as a technique for repairing car wheel rims that were damaged after an accident.

2.3.7.2 Corrosion Resistance

Aside from providing dimensional restoration, cold spraying CP aluminium has been shown to provide corrosion protection to magnesium components. As the addition of aluminium to magnesium promotes the formation of better passive films than unalloyed magnesium, cold spraying CP aluminium or Al-6061 onto magnesium seemed to inhibit corrosion and this was demonstrated by Zhang et al. [2006].

In another study conducted using cold sprayed amorphous aluminium coating, [Koh *et al.* 2012], the ability of the Al-Ni-Ce coating to prevent corrosion of exposed or cut surfaces of aluminium alloys substrate was demonstrated. XRD analysis also verified cold spray's ability to preserve the coating's amorphous nature while providing a relatively better adhesion strength compared to Al-6061 cold sprayed coatings.

2.3.7.3 Wear Resistance

The use of cold spray as a process to apply a wear resistant coating was explored by Walia [2006]. Self-lubricating composite coatings of nickel and molybdenum disulphide (Ni and MoS_2) were cold sprayed on Ti-6Al-4V dovetail contact areas of turbine blades as a fretting wear protective layer. Cold spray was used for the deposition because the MoS_2 particles tended to oxidise at high temperatures. The thin lubricant film of MoS_2 was shown to improve the ability of the turbine blades to withstand wear and significantly reduce the amount of friction on the coated surfaces of the dovetail joints.

MCrAlY coating was also successfully applied on nickel-based turbine blades using cold spray [William *et al*., 2005]. The coating was shown to be effective as a thermal barrier coating.

2.3.7.4 Electrical Application

The use of conventional thermal spray processes in the electrical/electronic industry is limited due to the high temperature and porosity associated with the application of the coating. However, cold spray offers a possible alternative due to its significantly lower temperature and highly dense coatings. In one of the first applications in the electronics industry, copper was successfully cold spray deposited onto an aluminium heat sink as a base layer for a subsequent soldering process [Grasme, 2003]. The advantage of cold spraying a layer of copper is that it removes the natural aluminium oxide film on the heat sink and provides a copper-plated solderable surface for the electronic component.

In 2006, van Steenkiste *et al*. [2006] from Delphi Technologies, Inc. patented the process of using cold spray to apply electrical contacts such as tin on conductive substrates (copper, aluminium, brass, stainless steel and tungsten). The main advantage of using cold spray in this application is its ability to apply a coating well beyond the 5 μm thickness that the existing electroplating process can achieve. In the same year, Morelli *et al*. [2006] also from Delphi Technologies, Inc. patented the process of using cold spray to apply a metal matrix composite heat sink laminate. This is for the thermal management of high power density electrical components such as silicon chips. The process involves cold spray coating a layer of a dielectric material (alumina, aluminium nitride or beryllium oxide) followed by a particle mixture (copper, tin, steel, diamond, silicon carbide or aluminium nitride) before attaching the metal matrix composite heat

sink laminate onto a silicon chip. In a third patent filed in the same year, van Steenkiste *et al*. [2006] proposed the use of cold spray as an alternative process to electroplating electrical connection points or a solderable pad of plastic covered ribbon type wiring in computers, automobiles and other electrical systems. The advantage of using cold spray is the elimination of the removal process for the plastic covering and thus minimising manufacturing footprints and time.

2.4 In-flight Characteristics Study

One of the greatest challenges of the cold spray process is controlling the parameters to obtain optimal coating effectiveness and efficiency. Traditionally, the most direct way to examine the impact of various spraying parameters on the properties and microstructure of the cold sprayed coating is to adjust the individual parameter while leaving the rest constant and to compare the resultant coating properties and microstructure [Gilmore *et al*., 1999 & Champagne *et al*., 2005]. This process is time consuming because a repetitive effort has to be put in for metallurgical preparation of the coating for the microstructure and other properties analysis. It was also found that there is usually no direct correlation between the individual spray parameter and the resultant coating properties. In addition, the uncertainty of the relationship is further aggravated by the numerous uncontrollable conditions such as the wear state of the nozzle inner diameter [Alkhimov *et al*., 2001].

The use of various optical diagnostic devices to study in-flight characteristics of thermal spray processes started as early as the 1980s. The Laser-Doppler method was one of the first methods used to diagnose a plasma jet [Saffman, *et al*., 1984, Lesinki *et al*., 1988] Optical diagnostic device usage has picked up in recent years [Fincke *et al*., 2001]. The

increase in the use of such optical diagnostic devices is driven by the desire to better predict thermal spray coating properties and establish optimal parameter settings for achieving desired coatings.

The Phase Doppler Anemometry (PDA) is one of the optical diagnostic devices which has proven its effectiveness in obtaining accurate and reliable velocity and size measurements simultaneously [Bauchhage *et al*., 1986, Qiu *et al*., 1992, Naqwi *et al*., 1992]. Originally developed as a method for measuring gas turbine atomization, air-fuel interaction, and liquid fuel combustion; PDA has evolved to become a standard diagnostic technique for characterization of the size and velocity of sprayed droplets and other spherical particles in a wide range of applications. Nevertheless, PDA technique was used to study thermal spray solid particles only in recent years [Cetegen *et al*., 1999], and the literature describing the deployment of PDA in the thermal spraying conditions is relatively uncommon [Ma *et al*., 2004].

However, the fact that most of the thermal sprayed (including cold spray) powder materials are non-transparent present PDA with an obvious advantage in measuring the particles. Essentially, possible measurement errors such as Gaussian effect and slit effect related to the PDA for transparent droplets will be avoided. In addition, with non-transparent particles, the mixing of different scattering modes of light can be prevented. Under these conditions, particle morphology and density are the two main considerations for utilizing PDA for thermal spray processes.

Particle velocity measurements based on the Laser Doppler technique are relatively mature and have been widely recognized as an accurate method. Unfortunately, particle

velocity information of the in-flight thermal sprayed powders has no direct relationship with the resulting coating properties [Friis *et al*. 2001, Planche *et al*., 2001, Kucuk *et al*., 2001, Bisson *et al*., 2003]. Higher particle velocity might lead to coatings with poorer quality and lower deposition efficiency. Particle temperature at impact is believed to be the most important parameter in determining the coating properties. However, measurements of particle temperature have always been subjected to great uncertainty [Mishin *et al*., 1987, Gougeon *et al*., 1993]. Thus, how the in-flight particle parameters change would influence the coating properties and the corresponding optimal settings of the spray parameters remained vague.

2.5 Effect of Substrate Surface Roughness on Coating Properties

The positive effect of substrate surface roughness on conventional thermal spray processes has been extensively researched and validated. For example, Staia *et al*. [2000] showed that the adhesive strength of HVOF coated WC-17%Co coatings on AISI 1020 steel substrates increases with increasing roughness of the substrate surface. In a separate study, Wang *et al*. [2005] showed that the adhesive strength of HVOF sprayed coatings are significantly higher on roughened mild steel substrate. This is the case for both fully melted NiCrBSi coating and a solid-liquid, two-phase WC-Co coating.

The effect of substrate surface roughness on the mechanical properties of cold sprayed coating is, however, not as well established. The impact of substrate surface roughness on coating bond strength was examined by Wu et al. [2006]. Using cold sprayed Al-Si coating coated over a range of particle velocities on mild steel, the study evaluated the relative coating bond strength achieved. The experimental results show that the adhesive bond strength of roughened specimen is close to or slightly better than the as-polished one when the impact velocity of the coated particles is near the critical velocity of the feedstock material. However, as the impact velocity increases, the bond strength of the grit blasted specimen becomes less than that of the as-polished one. Using micrographs at high magnification, the authors identified micro-pores and defects at the interface of the coating and roughen substrate surface that they attributed to causing the lower bond strength in the grit blasted specimen. Based on these observations, the authors concluded that the effect of surface roughness on the interface bonding is minimal.

In a separate study, Richer *et al.* [2006] investigated the impact of substrate roughness on cold spray coating efficiency. Nanocrystalline Al-Mg powder was cold spray deposited on aluminium substrates that are roughened by coarse silica grit (to roughness of 316 ± 57 μm) and fine glass bead grit (to roughness of 134 ± 20 μm). Marginally better coating efficiency was observed for the rougher substrate. The authors explained that deposition efficiency is enhanced by greater substrate surface roughness which promotes more deposited mass. The authors attributed this to the greater surface area of the rougher substrate that allows larger number of particles to come into direct contact with the substrate during the spraying of the initial layer. The effect on coating adhesion strength was not investigated.

In a study conducted by Kumar et al. [2009] to shed more light on the effect of roughened substrates on cold spray coating properties, copper powder was deposited onto smooth and grit blasted copper and aluminium substrates and evaluated. By evaluating the flattening ratio (defined as the ratio of the diameter of the bonded particle to that of a spherical particle of the same volume), individual particle deposition characterization done in the study indicates that substrate roughness whose crest size is the same as the particle size and the trough size is the half particle size creates better bonding as shown in Figure 2.17.

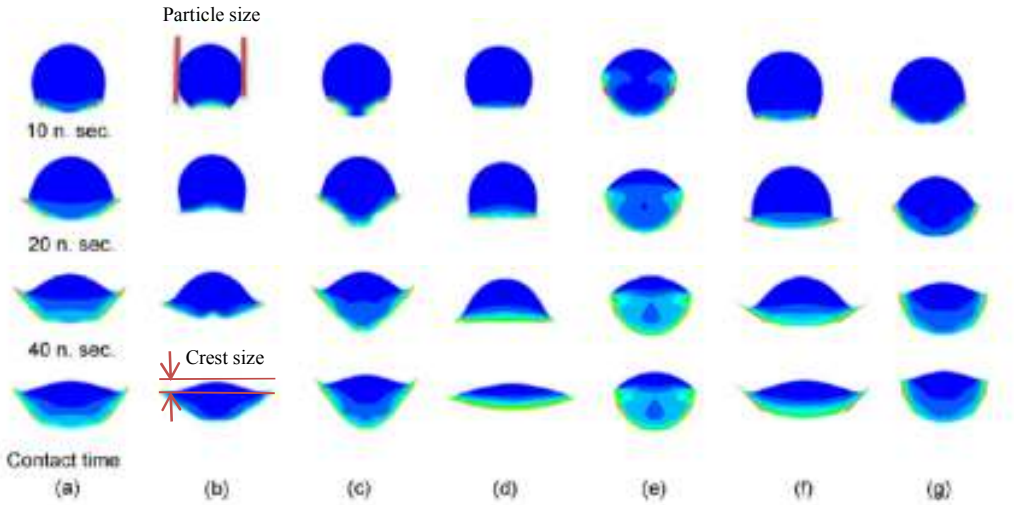

Figure 2.17: Numerical simulation results for impact behavior of particles on different substrates (a) planar, (b) crest size half of particle size, (c) trough size half of particle size, (d) crest size same as particle size, (e) trough size same as particle size, (f) crest size twice of particle size, (g) trough size twice of particle size [Kumar *et al*. 2009].

Though the authors suggested that grit blasting of the substrate enhances the bond strength of the coating, the results are inconclusive. Higher adhesion strength was measured for roughened substrates at lower impact velocities (<570 m/sec) but at higher impact velocities (600 m/sec), the bond strength of the copper coating on both smooth and roughened copper and aluminium substrates are almost identical as shown in Figure 2.18.

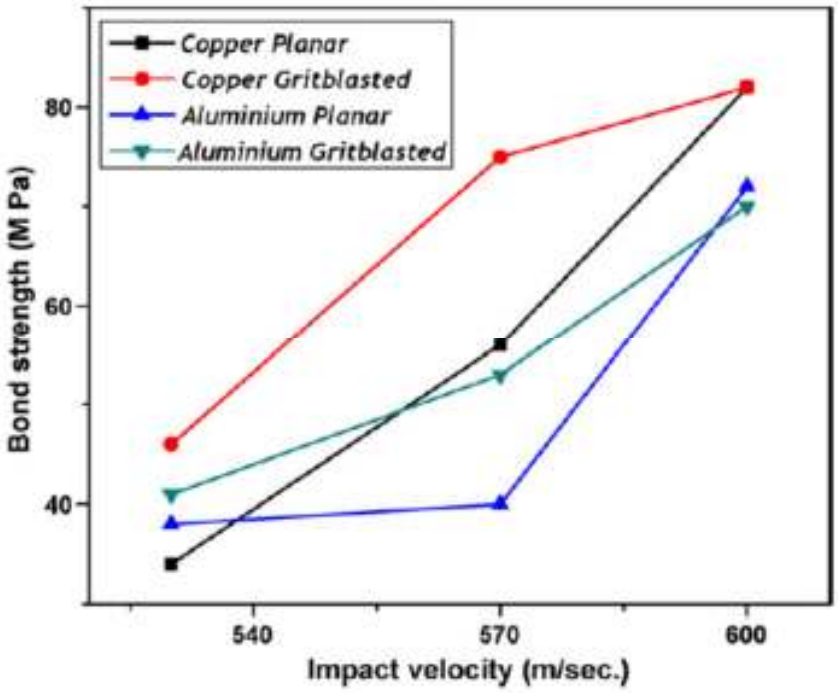

Figure 2.18: Coating bond strength as a function of impact velocity [Kumar *et al.* 2009].

2.6 Effect of Post Coating Heat Treatment on Coating Properties

In conventional thermal spray processes, a post coating operation in the form of heat treatment is usually performed to enhance certain material properties such as metallurgical bonding, ductility and fracture toughness of the coating [Longo, 2004]. As cold spray is a solid-state coating process that takes place in a relatively lower temperature, the equivalent benefits of post coating heat treatment need to be evaluated.

In a study done by Hall *et al*. [2006], cold sprayed aluminium specimens were annealed (300 °C, 22 hours air) and tested for its ultimate tensile strength. The experimental results show that the anneal samples demonstrated a decrease in ultimate strength and

significant increase in ductility (up to 10% elongation) when compared to as-sprayed samples. Recrystallisation within the cold sprayed splats and a reduction in dislocation density in the aluminium crystals are believed to be the reasons for the alteration in the mechanical properties.

Li *et al*. [2006] in a study on cold sprayed copper coatings, looked into the effect of annealing treatment on the microstructure, electrical resistivity and microhardness of the coatings. The study presented evidence of significant microstructure changes when the copper coatings were subjected to 350 °C and 650 °C heat treatment for various durations. The experimental results also showed that the microhardness of the cold sprayed copper coating decreased with increasing annealing temperature and at elevated annealing temperature, longer duration of annealing (12 hours) will bring the microhardness of the coating to that of annealed bulk copper. The authors also suggested that the anisotropy microstructure of the cold spray coatings can be eliminated through annealing treatment but did not provide quantitative microhardness data to support the claim.

In a similar study on cold sprayed copper coatings, Cella *et al.* [2006] obtained two sets of copper coatings sprayed at 298 and 523 K respectively using helium as the carrier gas. The experiment demonstrated a reduction of microhardness of the coating when subjected to annealing treatment at various temperatures. In addition, the specimen obtained at lower temperature exhibited recrystallisation at annealing temperature as low as 373 K with a corresponding reduction in microhardness. However, for the specimen coated at higher temperature, recrystallisation occurred at a much higher annealing temperature of 773 K. The study proposed that the specimen obtained at 523

K shows a higher dislocation density microstructurally and the low stacking fault energy of copper prevents recovery during annealing and, thus, changes in microstructure and microhardness values during annealing only start when recrystallisation begins.

Sundararajan *et al.* [2013] found that the elastic modulus of cold sprayed coatings of a wide variety of metallic materials (Cu, Ag, Zn, Nb, Ta, Ti and 316L stainless steel) are significantly lower than the values reported for bulk cast samples. The reduction in elastic modulus of the cold sprayed coatings was related to the extent of the inter-splat boundary cracking. However, the study also found that the elastic modulus of the coatings increases significantly after undergoing heat treatment processes. The authors attributed this observation to the decrease in the number of inter-splat cracking and porosity after the heat treatment process.

Similar findings were reported by Al-Mangour *et al.* [2014] who found that heat treatment was able to reduce porosity and improve inter-particle bonding of cold sprayed 316L stainless steel coating. The study also found increase in the ultimate tensile strength and ductility of the nitrogen-sprayed coatings after annealing. The report also showed that the microhardness of the coatings transitions four distinct stages associated with the corresponding presence (or absence) of recovery and recrystallisation of the coating microstructure.

2.7 Effect of Spray Angle on Coating Properties

The effect of spray angle on conventional thermal spray processes has been extensively studied [Montavon *et al*. 1997, Leigh *et al*. 1997 and Fukanuma *et al*. 2000]. In particular, Kang *et al.* [2006] studies the effect of oblique impact of plasma sprayed yttria-stabilized zirconia coating droplets on substrates and characterized the splat morphology and spreading behavior. As cold spray is a solid state deposition process, the effect of spray angle on mechanical properties and splat characterization is expected to differ from conventional thermal spray process.

In a study done by Li *et al.* [2003], the relative deposition efficiency of cold sprayed copper and titanium powder with changing spray angle was investigated. The experimental results show that the relationship between deposition efficiency and spray angle can be broadly categorized into three ranges: maximum deposition range, transient angle range and no deposition range.

In a more recent study, Yin *et al.* [2014] studied the effect of spray angle on the particle deposition behavior of titanium particles on a copper substrate. The experimental results showed that coating thickness decreases while coating porosity increases with reducing spray angle.

In the above studies, the focus has been heavily weighted on the impact of spray angle on the deposition efficiency. No quantitative investigation was performed to shed light on the effect of spray angle on mechanical properties such as tensile adhesion strength and microhardness of the coatings. From the industrial application perspective, this is critical information for optimizing the cold spray operation process.

2.8 Conclusion

This chapter provided a background to the thermal spray processes and identified the common thermal spray processes as well as their respective advantages and disadvantages. This chapter also reported the research that has been performed on the cold spray process to better understand the bonding mechanism, numerical modelling, and advantages and limitations of the cold spray process. Insights on the materials coated by cold spray as well as its industrial application were also presented.

In the last section, particular attention was given on the research work that has been reported on the pre and post coating process for cold spray, specifically surface roughening of the substrate and heat treatment after cold spray. The review found that though studies have been carried out in these areas, quantitative results of their effect on coating mechanical properties such as adhesion bond strength and coating microhardness is lacking. In addition, quantitative studies on the impact of spray angle on the cold spray coating mechanical properties is also missing. It is the intent of this research work to fill in these gaps. Experimental study will be carried out to achieve the following objectives:

1. To quantify the impact of grit blasting on the cold spray coating microhardness, tensile adhesion strength and microstructure.
2. To quantify the effect of stress relief and full annealing on the coating mechanical properties.
3. To quantify the effect of the spray angle of the cold spray nozzle (θ) on the microhardness, tensile adhesion strength and microstructure of the coating.

4. To evaluate qualitatively the effectiveness and built-up of cold spray coating by holding the nozzle at a localized position.

CHAPTER 3

IN-FLIGHT VELOCITY OF COLD SPRAYED ALUMINIUM POWDER

3.1 Introduction

An experimental study was carried out to evaluate the in-flight behaviour of cold spray powder particles under varying temperature, pressure and powder feeding conditions to better understand the particle behaviour of the cold spray process. This study examined the velocity data of the powders from the nozzle exit and subsequently established the optimum spray conditions. Data was collected at eight downstream locations from the nozzle exit, starting from 5 mm to 40 mm at 5 mm intervals. Compressed air was used as the carrier gas.

3.2 Experimental Equipment

This section documents the facilities and equipment used to conduct the various experimental studies. The two cold spray systems, together with their auxiliary equipment as well as the in-flight diagnostic system are described in the following sections.

3.2.1 Cold Spray Systems

Two separate cold spray systems were used during the course of the research work. The work carried out in Section 1.2.1 and this chapter was performed using the first system from the Russian Academy of Science. It was used primarily as a proof-of-concept study. The second cold spray system was subsequently brought in from Plasma Giken, Japan with funding secured through a grant from the Civil Aviation Authority of Singapore (CAAS). The newer Plasma Giken cold spray system was used for experimental work carried out in Chapters 4, 5 and 6 of this thesis. The results will be more relevant to the industrial project which will be use the newer cold spray system.

3.2.1.1 Russian Academy of Science Cold Spray System

The first cold spray system is currently residing at the Singapore Technologies Kinetics-NTU Cold Spray Research Centre at Singapore Technologies Kinetics (16 Tuas Avenue 7 Singapore 639271). It was purchased from the Khristianovich Institute of Theoretical and Applied Mechanics, Siberian Department of Russian Academy of Science (Siberia, Russia). This system is believed to be the first of its kind in the South-east Asia region when it was commissioned in 2007. Figures 3.1a and 3.1b show the spray booth built for the system as well as the spray room which houses the system.

Figure 3.1a: Singapore Technologies Kinetics-NTU Cold Spray Research Centre.

Figure 3.1b: Spray room of STK-NTU Cold Spray Research Centre.

The main components of the cold spray system are the spray unit which consists of a powder feeder, gas heater, supersonic nozzle and pre-chamber/mixing chamber. Other components include the compressor, spray chamber, a 6-axis robotic motion system, spray booth and a control panel for controlling and monitoring the spray parameters. Figure 3.2 shows the schematic of the main components of the cold spray system.

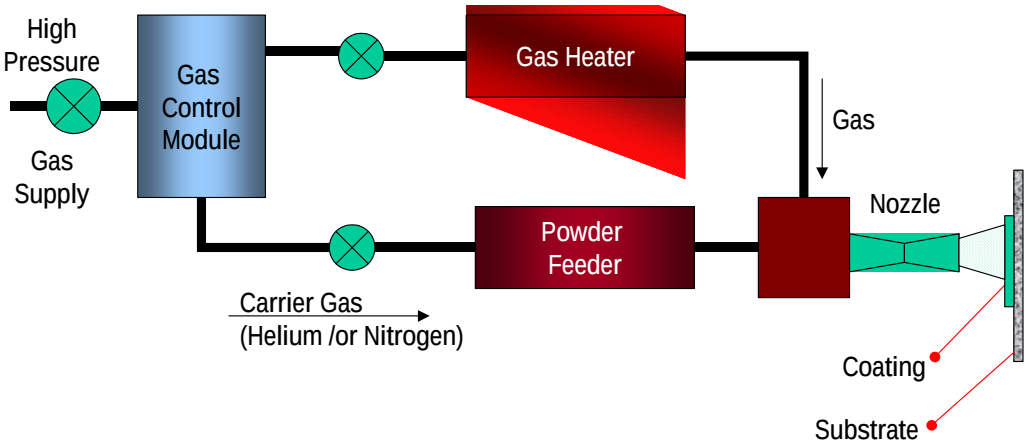

Figure 3.2: Schematic of main components of cold spray system.

3.2.1.2 Supersonic Nozzle

One of the most important components of the cold spray system is the De Laval type nozzle shown in Figure 3.3. The nozzle has an internal converging (length = 20.7 mm) and diverging (length = 98.6 mm) section that accelerates the flow of the carrier gas to supersonic speed. The cross section of the nozzle is circular, with the smallest diameter at 3.8 mm and the diameter at the nozzle exit at 6 mm, and it produces a conical spray profile. It is made of steel and developed for cold spray processes at elevated temperature of 500 °C.

Figure 3.3: De Laval type nozzle of the cold spray system.

3.2.1.3 Powder Feeder

The powder feeder is a key equipment for the cold spray system. Its function is to deliver a consistent and regulated supply of feedstock powder into the pre-chamber of the supersonic nozzle at pressures as high as 20 bars. A drum type powder feeder shown in Figure 3.4 was developed with this cold spray system. The powder is first poured into a chamber and falls onto the rotating feeder drum that is driven by an electric drive. The electric drive is provided by a dc motor that allows the regulation of the revolution rate of the feeder drum (0.03 to 0.1 rounds per second) and the corresponding change in powder feed rate. The powder is subsequently carried along by the serrated surface on the cylindrical surface of the feeder drum and drops into the mixing chamber. This is where it is mixed with the carrier gas (compressed air, nitrogen or helium) and further

transported into the outlet branch pipe before being pushed into the supersonic nozzle. Powders that are caught by the drum grooves are removed by the gas passing through the inlet branch pipe to the mixing chamber. The pressure difference between the powder chamber and the casing is equalised by the bypass pipe. The pressure readings are captured on the manometer located on the control panel.

Testing of the powder feeder revealed that there was no significant variation in particle concentration in the jet stream at relatively low pressure of 5 bars. Such reliability is crucial since it allows the use of only a small amount of powder (50 to 100 g) in the powder feeder.

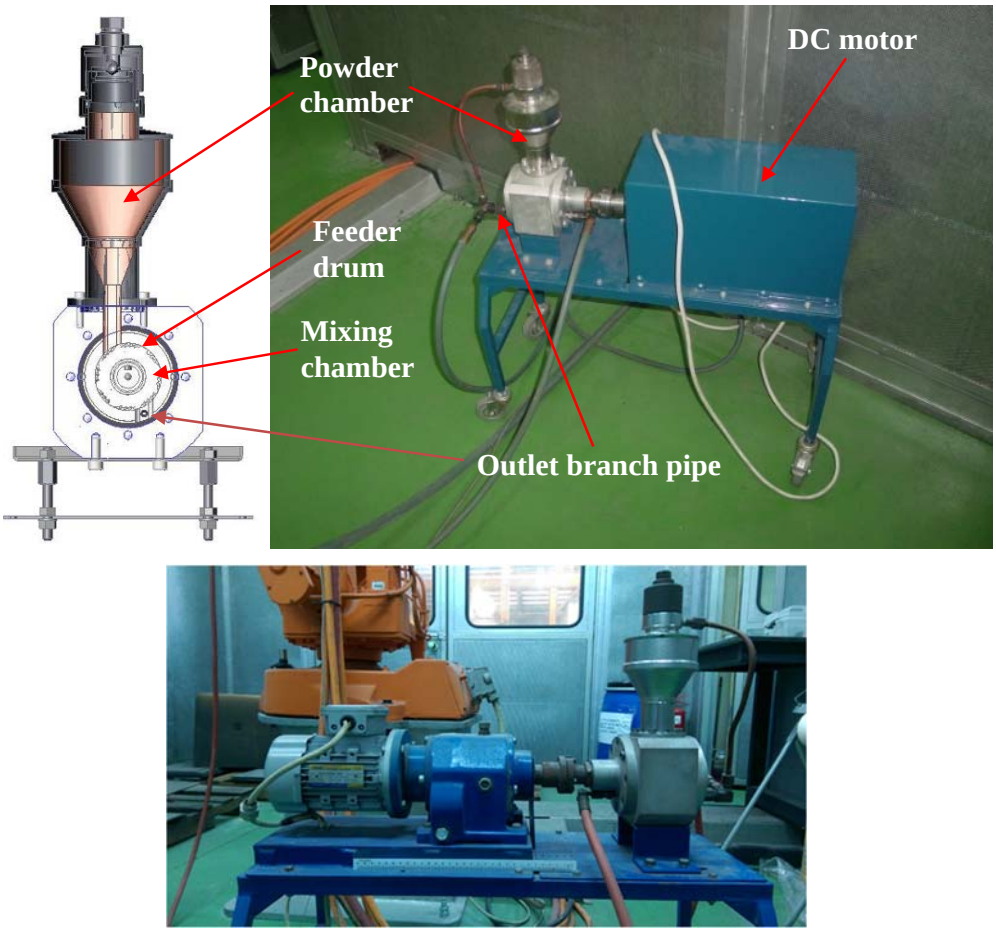

Figure 3.4: Drum type powder feeder.

3.2.1.4 Cold Spray Gun Device

The cold spray gun device consists of the heater for the carrier gas, thermocouples, a pre-chamber and the supersonic nozzle. The gas heater warms the flowing carrier gas to a pre-determined temperature. This reduces the effect of adiabatic cooling of the carrier gas as it passes through the converging-diverging nozzle. Clogging of the powder due to condensation is likely in the absence of heating. As shown in Figure 3.5, a simple yet reliable single tube heater coil is used with the carrier gas passing through the tubes. The nichrome tubes are heated by an electric current and are attached parallel in a sealed casing and connected in series into an electric circuit. This arrangement facilitates the heating of the gas stream by the ohmic (Ω) resistance of the heater coil when a current is applied to the coil. Though the heating coil is rated to withstand pressure of up to 25 bars, the operating pressure of the compressed air has been limited to 20 bars for safety consideration. Although the gas heater is bulky and weighs close to 8 kg, it can easily provide reliable heating of the carrier gas up to 600 °C.

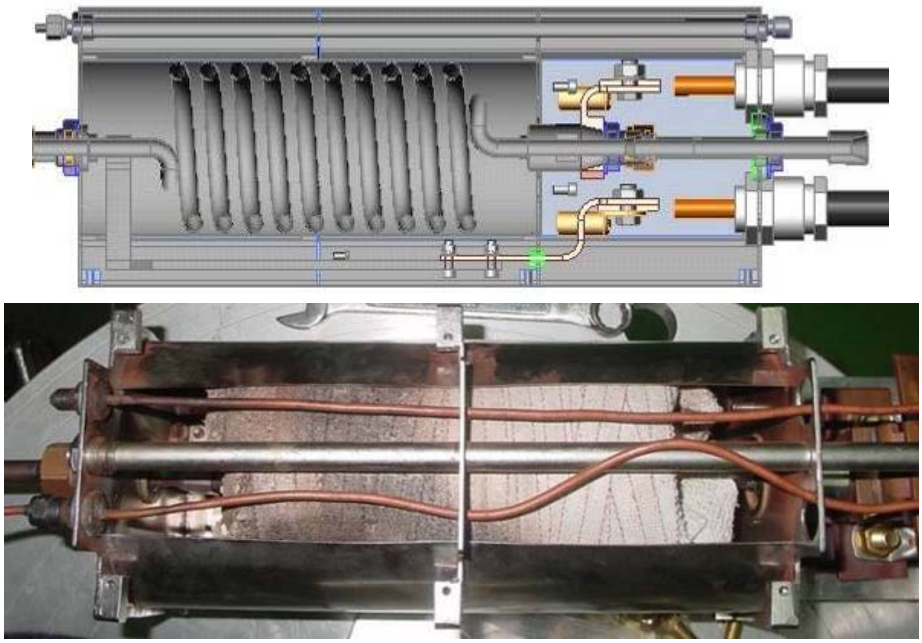

Figure 3.5: Gas heating device.

3.2.1.5 Feeder Gas System

The cold spray system requires a gas source for both the powder feeder to bring the powder to the pre-chamber/mixing chamber and also for the main propulsion of the powders in the gun device. Compressed air, nitrogen and helium are all possible options of carrier gas for the cold spray system. Compressed air is supplied by an external compressor while nitrogen and helium are supplied from liquid gas tank. Due to safety consideration and the capability of the system, the gas source was pre-set to not exceed 20 bars when using compressed air and 15 bars when using nitrogen or helium gas.

3.2.1.6 Control Panel

The control panel provides the interface between the cold spray system and the user. It consists of the manometer for controlling the pressure in the supplying pipes, ball shut-off valve, toggle switch for power supply of control apparatus and the valve for controlling the pressure inside the pre-chamber of the nozzle unit. In addition, there is a manometer indicating the pressure in the pre-chamber of the nozzle unit, valve for regulating pressure inside the powder feeder, manometer indicating the pressure inside the powder feeder, digital device for control of the temperature, regulator of frequency of rotation of motor-inducer to the powder feeder and the toggle switch for powder supply of motor-reducer of the powder feeder. Figure 3.6 shows the control panel of the cold spray system.

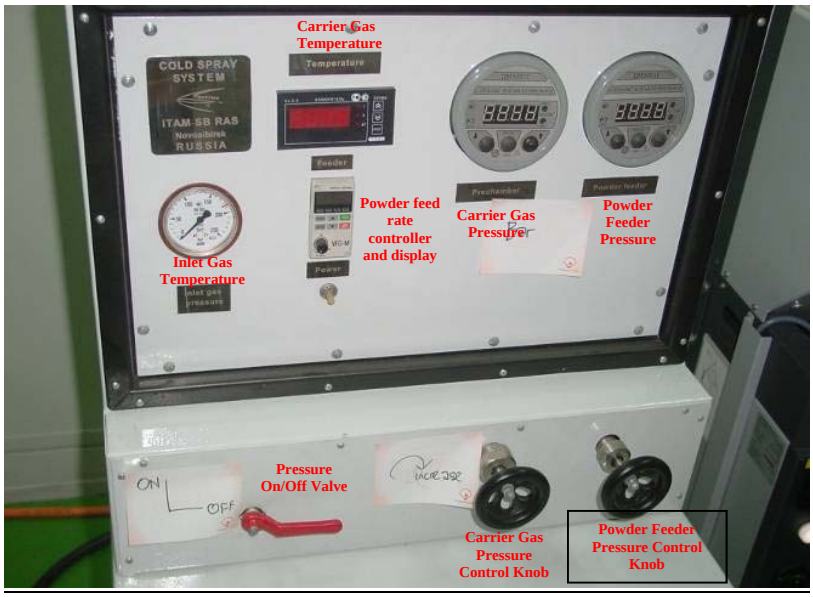

Figure 3.6: Cold spray system control panel.

3.2.1.7 Robotic Arm

The cold spray gun device is mounted on an ABB IRB 2400 (Zurich, Switzerland) 6-axis robot as shown in Figure 3.7. The robot arm has a reach of up to 1.5 metres and a working dimension of 1.2 metres by 1.2 metres and can travel up to 150° per second on all 6–axes or a maximum of 2000 mm per second in a linear motion. The technical capability of the robotic arm exceeds the specification needs for performing the current research.

Figure 3.7: ABB IRB 2400 robot with cold spray gun and gas heating device mounted.

3.2.2 Plasma Giken PCS-1000 Cold Spray System

A second cold spray system was brought from Plasma Giken Co., Ltd (Tokyo, Japan). It currently resides at Singapore Technologies Kinetics (Tuas, Singapore). A separate cold spray booth, measuring 6 metres (length) by 6 metres (width) by 4 metres (height) was built to house this system and it sits directly next to the STK-NTU Cold Spray Research Centre. This is shown on Figure 3.8. The system was brought in with funding support from the Civil Aviation Authority of Singapore (CAAS) Aviation Innovation Programme (Reference Number: AI/FUD/A1.1.10). The PCS-1000 system is believed to be the first industrial application-ready system in South-east Asia when it was commissioned in 2013.

Figure 3.8a: New cold spray booth (right) for the PCS-1000 system constructed next to the STK-NTU Cold Spray Research Centre.

Figure 3.8b: Spray room for new PCS-1000 cold spray system.

The PCS-1000 system is a fully automated cold spray system that comes integrated with the gas controller unit, powder feeder (0.5 litres), cold spray gun unit (Figure 3.9) and computerized control panel (Figure 3.10). The PCS-1000 system can reach gas pressure of 5 MPa and a maximum gas temperature of 1000 °C (thus the name PCS-1000). The system specifications are provided on Table 3.1.

Table 3.1: System specifications of Russian Academy of Science and Plasma Giken PCS-1000 cold spray systems.

Component	**Parameter**	**Russian Academy of Science CS System**	**Plasma Giken PCS-1000 System**
Gas Chamber	Operating Gas Pressure	**2 MPa**	**5 MPa**
	Maximum Gas Temperature	**600 ºC**	**1000 ºC**
Heater Power Source	Power Supply	**25 kW**	**70 kW**
Powder Supply Unit	Container Volume	**0.3 litres**	**0.5 litres**
Controller	Operation Method	**Manual switches with analogue gauges**	**Touch Panel**
Gas Control Unit		**Compressed air, N_2 or He gas**	**Either N_2 or He gas**
Gas Pressure Control		**Manual**	**Automatic or manual**
Gas Temperature Control		**Manual**	**Automatic**

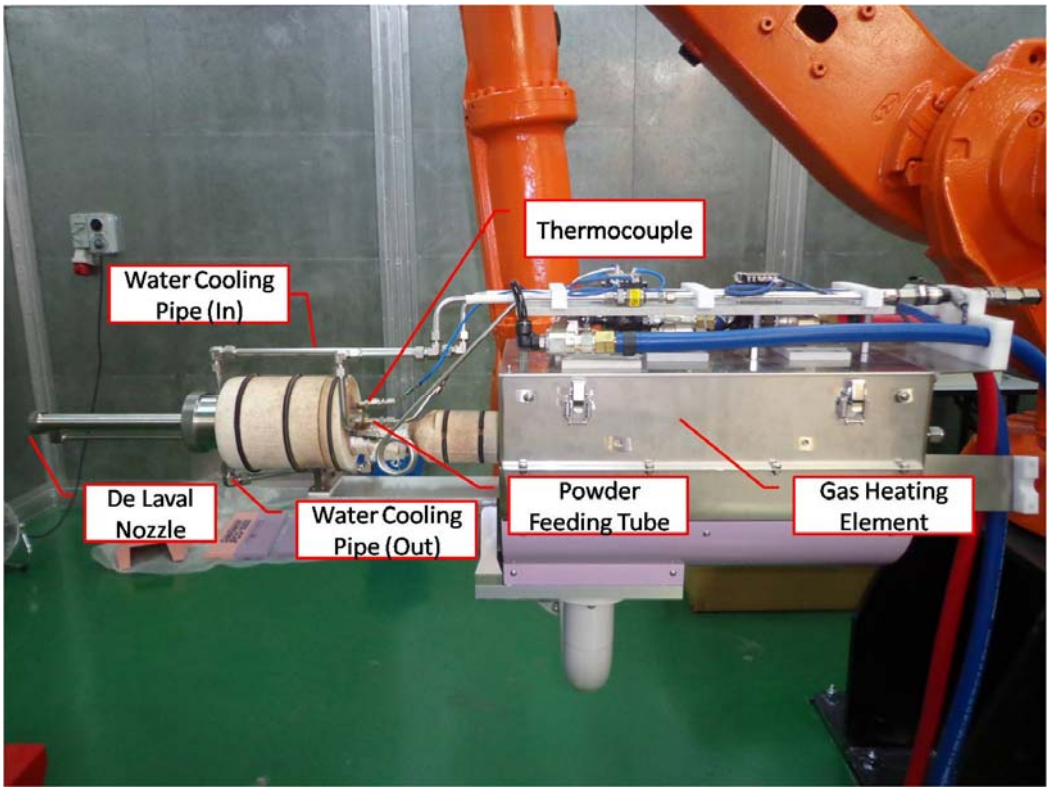

Figure 3.9: Components in the PCS-1000 cold spray gun unit.

Figure 3.10: PCS-1000 computerized control unit.

The PCS-1000 system was selected based on its versatility as well as its ability to cold spray heavier powders such as Inconel with nitrogen as a carrier gas. Economically, this is more viable than other commercially available systems that would require helium as the carrier gas for coating such powders.

A new robotic arm was employed for the PCS-1000 system. The ABB IRB 6640 (Zurich, Switzerland) 6-axis robot was selected based on its ability to handle a load of up to 130 kg and its maximum reach of 3.2 metres with an maximum rotation speed of 90° per second on all 6-axes. This would allow it to carry the PCS-1000 cold spray gun unit which weighs 51 kg and have the capacity to reach large aerospace components such as fan cases. Figure 3.8b shows the PCS-1000 cold spray gun unit mounted on the IRB 6640.

3.3 Control Parameters of Cold Spray System

The main difference in the formation of coating between cold spray and conventional thermal spray is that the process takes place in the solid state instead of a molten liquefied condition. This implies that the cold spray process takes place at a much lower temperature compared to thermal spray and a relatively higher particle velocity. As such, the parameters that affect the coating quality are generally different. To better realise the full capabilities of the cold spray system, it is crucial to understand the parameters that can impact the coating quality.

3.3.1 Gas Composition/Type of Carrier Gas

The carrier gases that are commonly used in the cold spray system are compressed air, nitrogen and helium. Compressed air, though being the most economical option, has the limitation of not being about to reach the desired particle velocities for some heavier material. Nitrogen and helium are viable alternatives because they are relatively inert and do not promote oxidation when used to spray most materials. Typically, compressed air and nitrogen are used for cold spraying mono ductile powders such as aluminium and copper as they are generally more economical than helium and yet still able to achieve the minimum gas velocity required for coating to form. Helium, being comparative lighter, is usually used in instances where the gas velocity produced by compressed air or nitrogen is insufficient to create efficient deposition or good quality coating.

3.3.2 Carrier Gas Pressure

The carrier gas pressure has a direct and positive effect on the velocity of the carrier gas. This inevitably will have a positive impact on the particle velocity exiting the cold spray nozzle and thus the quality of the coatings.

The working pressure for the Russian Academy of Science cold spray system is up to 2 MPa for compressed air and 1.5 MPa for nitrogen and helium. The critical velocity of most of the mono ductile particles can be achieved and the deposition rate can be optimised within this range of working gas pressure.

The working gas pressure for the Plasma Giken PCS-1000 can be 5 MPa for nitrogen and helium. This allows many types of high density materials, such as Inconel and tungsten carbide to be easily coated using this system.

3.3.3 Gas Temperature/Temperature of Gas Jet

Heating the carrier gas jet in the cold spray system has two noticeable benefits. Firstly, and more importantly, it minimises the effect of adiabatic cooling of the carrier gas as it expands through the converging-diverging nozzle. This prevents the nozzle from clogging by ensuring that the particles remain moisture free. Secondly, increasing the carrier gas temperature also increases the average kinetic energy of the particles and this directly increases the velocity of the particles needed for coating. It is important to emphasise that heating of the gas is not to melt the particles in the gas stream but to allow the increase in the velocity of the gas, thus assist in the deformation of the particles upon impact to substrate.

The gas temperature for the Russian Academy of Science system can be varied up to 600 °C while that for the PCS-1000 system can go up to 1000 ºC. The temperature of the carrier gas first system is controlled by adjusting the electrical power to the heat coil while the gas carrier temperature for the PCS-1000 system is pre-set at the start of every experiment by inputting the value via the computerised control panel.

3.3.4 Powder Feed Rate

The amount of powder introduced into the carrier gas jet for coating depends on the powder feed rate. A thicker coating per pass is usually obtained with a faster powder feed rate, assuming all other factors remain the same. However, the amount of powder that should be introduced into the gas stream should also be controlled. Thus, in coating conditions where there is a high powder feed rate and low carrier gas pressure, the amount of kinetic energy from the carrier gas may not be ample to accelerate the greater number of particles to their critical velocity; thereby, drastically affecting the coating deposition efficiency, which is defined as the ratio of the spray material that actually adheres to the substrate to the spray material that leaves the nozzle, in the process.

The powder feed rate of the Russian Academy of Science cold spray system is measured by controlling the rotating speed of the feeder drum in the powder feeder. The range of the feed rate for the aluminium powder was determined by 2 sources. Firstly, according to the author and inventor of the Russian Academy of Science cold spray system, Dr. Anatolii Papyrin in his book Cold Spray Technology [Papyrin, 2006], the flow rate of the powder for the system can be changed from 0 to 5 $gsec^{-1}$, or up to 300 $gmin^{-1}$ for stainless steel powder. In addition, a simple experiment was conducted with the cold spray system to measure the aluminium powder flow rate. The measurement of powder

feed rate at normal operating pressure of between 10 to 15 MPa is challenging as the powders exit from the nozzles at very high velocity and is extremely difficult to contain and collect for measurement. Thus, the measurement was carried out using the lowest powder feeder pressure possible (1.5 MPa) and with drum rotating setting at 60 Hz. The amount of aluminium powder collected was 20 $gmin^{-1}$. Extrapolating this data linearly to an operating pressure of 15 MPa, the flow rate would equate to about 200 $gmin^{-1}$ at 15 MPa powder feeder pressure. From the range of flow rate provided for stainless steel powder by Dr. Papyrin, the inventor of the system, it is deduced that the flow rate of the aluminium powder is between 0 to 250 $gmin^{-1}$ as the density of aluminium is less than half of stainless steel and would flow less easily within the drum-type powder feeder. Similarly, for the Plasma Giken PCS-1000, the powder feed rate is controlled by adjusting the rotating speed of the powder feeder cylinder and the powder feed rate can go up to 750 $gmin^{-1}$ [Dennehy, 2014].

3.3.5 Spray Distance/Standoff Distance

The standoff distance is the distance between the nozzle exit and the top surface of the substrate. It is a parameter that needs to be optimised for each powder and thermal spray system, being it cold or conventional as the particles of different process and material behave differently as it exits the thermal spray nozzle.

For the cold spray process, the standoff distance represents the distance that the particles can accelerate towards the substrate before impact. Obtaining the optimal standoff distance is crucial as setting it too short will not provide enough space for the particles to accelerate to its maximum speed. On the other hand, an excessively long

standoff distance can result in a reduction in particle velocity and adversely impact the coating deposition efficiency.

Another factor to consider when setting the standoff distance is the transverse size of the carrier gas jet. This is with relation to the compressed shock layer of the carrier gas as it hits the substrate. The particle velocity at impact will be higher if the gas jet, and thus the compressed shock layer, is thinner. In addition, for the particle to reach maximum equilibrium speed, it should cover a smaller distance after exiting the nozzle than during its travel in the nozzle. Therefore, the gas parameters inside the compressed layer are close to the stagnation values; whereas the gas inside the nozzle is less dense.

Once an optimal standoff distance is established for a certain material and set parameters, it is usually pre-set with the use of a measuring ruler before the start of the experiment.

3.3.6 Nozzle Traversing Speed

The traversing speed of the nozzle during the cold spray process has a direct impact on the coating deposition efficiency. Generally, the higher the transverse speed, the lower the deposition rate of the powder per pass as there are fewer particles impacting a specific area of the substrate.

With the exception of thin coatings, every cold spray process can be broadly considered as consisting of two stages: the first stage in each the first layer of particles is deposited onto the substrate followed by the second stage in which there is a build-up of the coating on the initial layer. The interaction between the particles and the substrate during the first stage governs the quality of the interface and thus the adhesion strength.

Inevitably the nozzle traversing speed has a direct effect on the quality of the coating adhesion strength.The transverse speed of the nozzle can be controlled by the linear motion of the robotic arm which has a range of linear speed of up to 2000 mm per second.

3.3.7 Particle Size and Properties

Similar to all conventional thermal spray processes, the coating quality and deposition efficiency of the cold spray process is directly affected by the particle size, morphology and properties. Van Steenkiste et al., [2002] found that with all other conditions being the same, the pressure required for cold spraying larger (100 μm) aluminium particles is significantly less when compared to spraying smaller (50 μm) aluminium particles. Larger agglomerated particle size was also found to require a lower critical velocity to form a coating when compared to smaller agglomerated particle size [Morgan *et al*., 2004]. Samareh et al. [2007] attributed this to the higher velocity required to perforate the Bow shock that is formed at a distance from the substrate surface due to the supersonic velocity gas jet. Particles with small diameter and low density which do not carry enough kinetic energy are unable to penetrate through the Bow shock and are thus forced to go around the Bow shock. These particles take on a trajectory which turns around the vortex in the direction directly opposite of the main gas stream. In such cases, the particles never reach the substrate and a coating is never formed.

3.4 SprayWatch In-flight Diagnostic System

The SprayWatch-2i in-flight diagnostics system (Oseir Ltd, Tampere, Finland) is used to measure the particle velocities. The SprayWatch-2i system includes a computer

controlled, motor driven focus distance and aperture adjustment which adjusts the aperture automatically according to the signal level of the process measured. The focus distance can be adjusted through the software whenever there is a need to change the working distance or measurement volume. It can range from 185 to 400 millimeters. Definition of the measurement volume and explanation of the various terms are given in Figure 3.11.

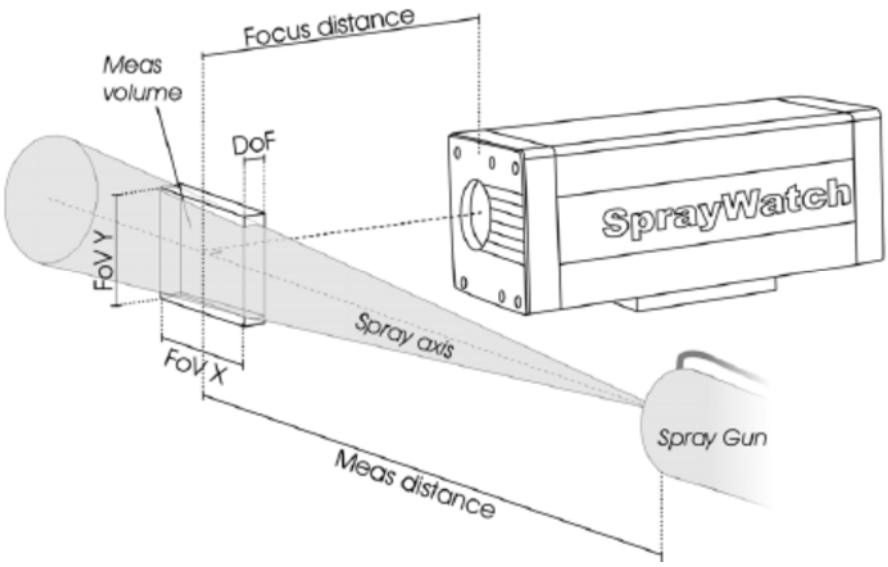

Figure 3.11: Definition of SprayWatch measurement volume.

Table 3.2 shows the correlation between the focus distance and the width and height of the measurement volume.

Table 3.2: Focus distance vs measurement volume.

Focus Distance (mm)	FOV X (mm)	FOV Y (mm)
185	18.7	14.0
250	25.1	18.8
400	39.2	29.4

Depth of the measurement volume (DoF = Depth of Field) depends on the aperture of the imaging optics. The aperture is automatically selected on the basis of the signal level or brightness of the process. A typical aperture value for hot and bright processes (plasma, wire arc) is 1-50 and for processes with lower temperatures (HVOF, flame, cold spray), between 80 and 100. The relation between the depth of the measurement volume and these aperture values is shown on Figure 3.12. Typical DoF values in plasma spray ranges from 25 to 50 mm and 6 to 10 mm for HVOF and cold spray.

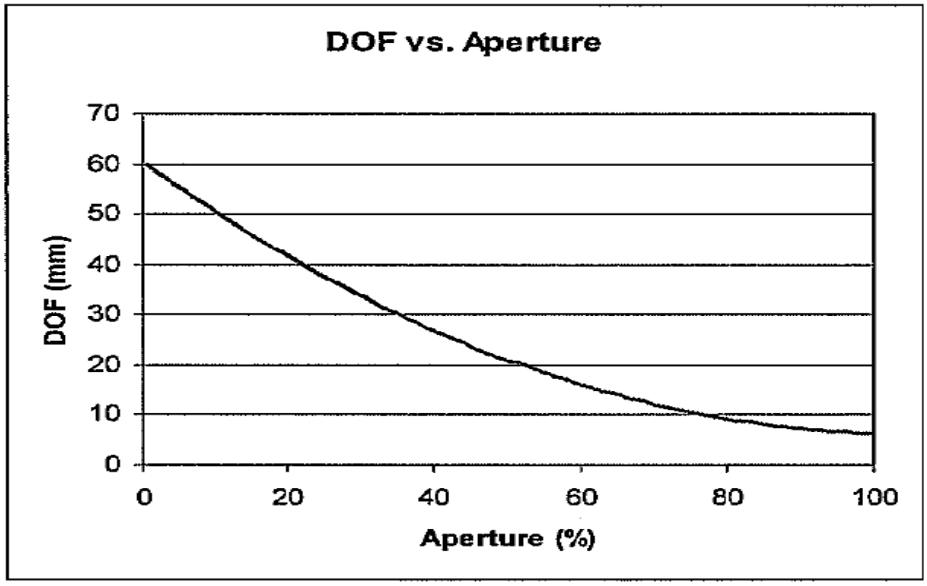

Figure 3.12: DoF versus Aperture for SprayWatch-2i System.

To assist in the illumination of the cold sprayed particles, the system was complemented by the HiWatch Laser System, a high-power diode laser stroboscope. Specifications of the HiWatch Laser System is shown on Table 3.3.

Table 3.3: HiWatch Laser System Specifications.

Parameter	Value	Remarks
Emission Wavelength	808 ± 5 nm	
Output Geometry	30 x 1 mm	10º horizontal fan angle
Emission Power	180 Watts	Peak power
Single Pulse Length	0.1 – 2 μs	
Maximum Pulse Frequency	5 MHz	
Maximum Pulse Energy	0.5 mJ	
Laser Head Weight	1.1 kg	
Laser Head Dimensions	132 (l) x 100 (w) x 67 (h) mm	50 mm clearance at back required for connectors
Maximum Operating Temperature	30 ºC	Software protects system from overheating
Cooling	Filtered dry compressed air	
Laser Safety Class	3B	Conforming to IEC 60125-A1+A2

In order to capture the particle, SprayWatch uses a high-quality, fast shutter charged-coupled device (CCD) camera to generate digital images of the spray. Instead of using just one or two photodetectors looking at a point-like measurement volume, the system has an array of hundreds of thousands small photodetetctors covering a measurement volume of about 34 x 27 x 25 mm. Digital images taken with short exposure times to capture the high-speed particles are processed by the OEM software algorithms to give the measurement data. The algorithm measures the direction, position and velocity of individual particles by identifying them in the images.

The velocity of each particle is calculated by first capturing the length of the particle traces on the CCD detector measured by the image processing algorithm. This length is then divided by the known camera shutter time to give the particle velocity. This measurement is termed the time-of-flight method. The accuracy of the velocity measurement is between 0.1 to 1 m/sec, depending on the velocity range.

Particle velocities were measured using the in-flight diagnostic system Spray Watch-2i system (Oseir Ltd., Tampere, Finland) integrated with the HiWatch laser unit (808 nm, 108 W) which illuminates the measurement volume (Figure 3.13). The velocity measurements were taken at various locations from the spray nozzle exit to better understand the in-flight characteristics. The particle velocity measurements were carried out with the absence of a substrate at the spray nozzle exit. This is to avoid the possibility of particles building up and rebounding and in the process affecting the sensor field of view. In addition, the radial distribution of the particle velocity was not considered as the velocity measurements were taken along the centerline of the nozzle. Data collected represents the average particle velocity at the nozzle centerline.

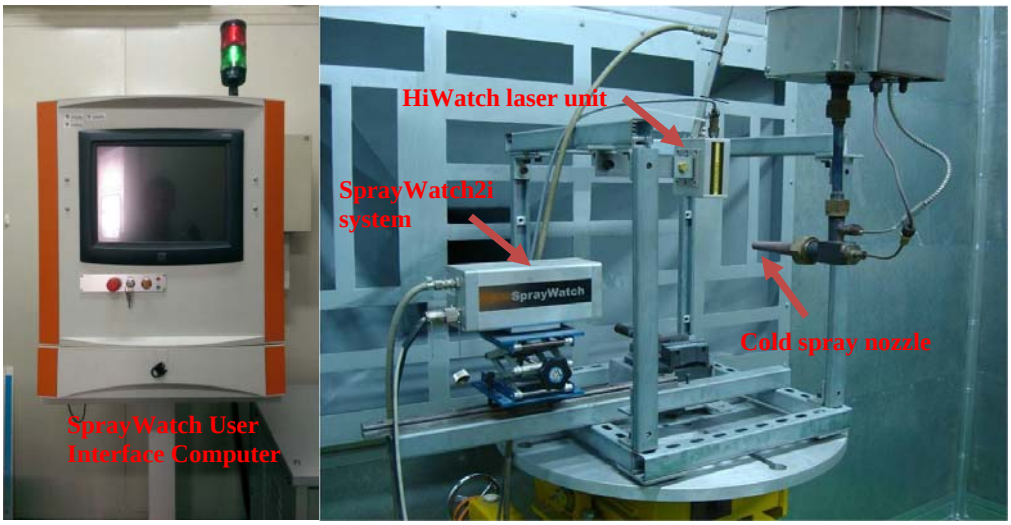

Figure 3.13: Spray Watch-2i system with integrated HiWatch laser unit.

3.5 Feedstock Powder

The powder used in this study was commercially purchased Al-6061 powder prepared by gas atomization. Image of a typical powder taken using a scanning electron microscope indicates that the powder particles are spherical in shape as shown on Figure 3.14a. Figure 3.14b shows the particle size distribution of the aluminium feedstock powder. The powder has a lognormal distribution with an average diameter 45 ± 2 μm. 90% of the particles are below 95 μm in diameter.

The powder size distribution of the aluminium powder was measured using the Malvern (Worcestershire, UK) Mastersizer MS2000 laser diffraction particle size analyser.

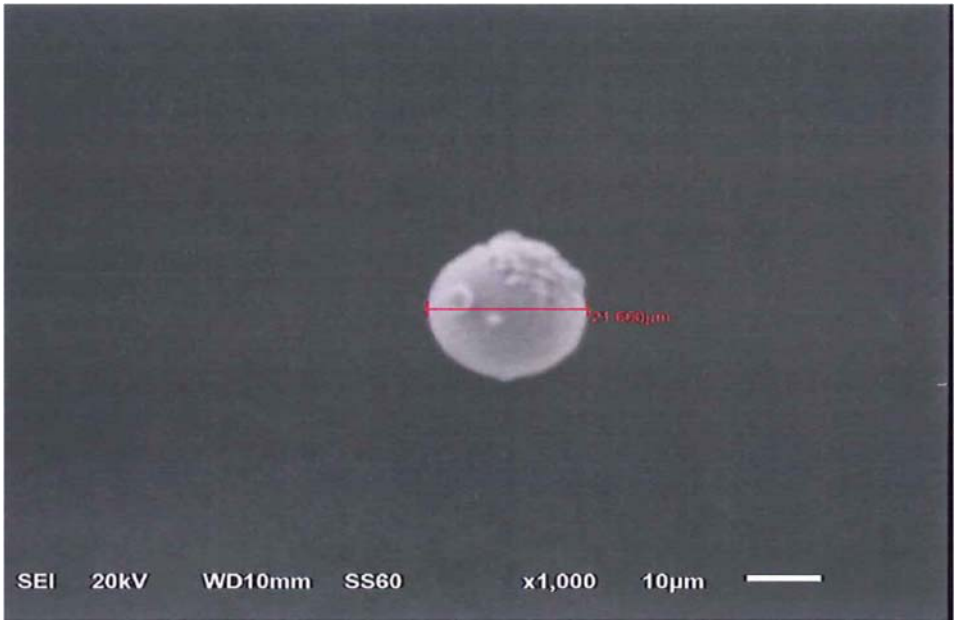

Figure 3.14a: SEM image of feedstock aluminium powder at 1000x magnification.

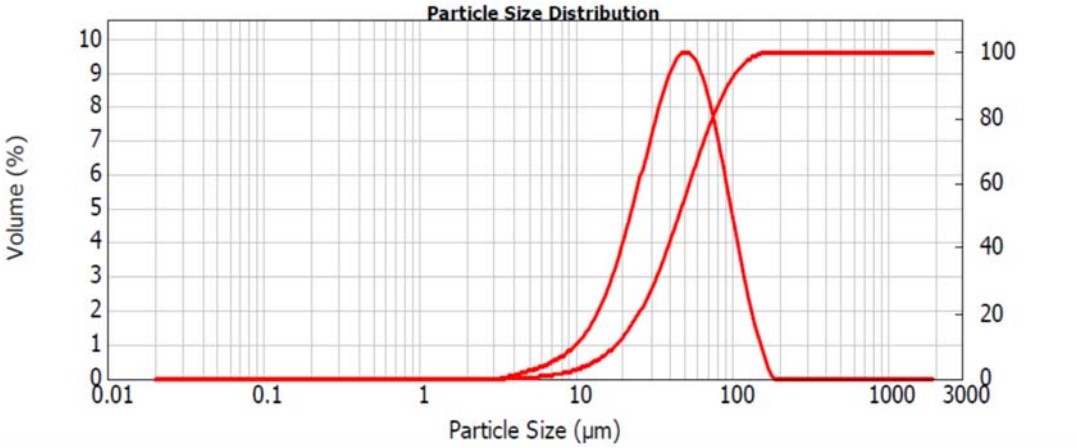

Figure 3.14b: Feedstock aluminium powder size distribution.

3.6 Effect of Carrier Gas Temperature

Aluminium powder was cold sprayed at carrier gas temperature of 100 ºC, 200 ºC, 300 ºC and 400 ºC and the particle velocity measurements downstream from the nozzle exit for the varying carrier gas temperature was taken using the Spray Watch-2i system. A total of 8 downstream measurements starting at 5mm from the exit of the nozzle and at 5 mm interval were taken. Compressed air was used as the carrier gas and the pressure was set at 5 bar and the powder feed rate was set at 60 Hz (150 g/min). The results are shown in Figure 3.15. The accuracy of the velocity data is ± 1 m/s.

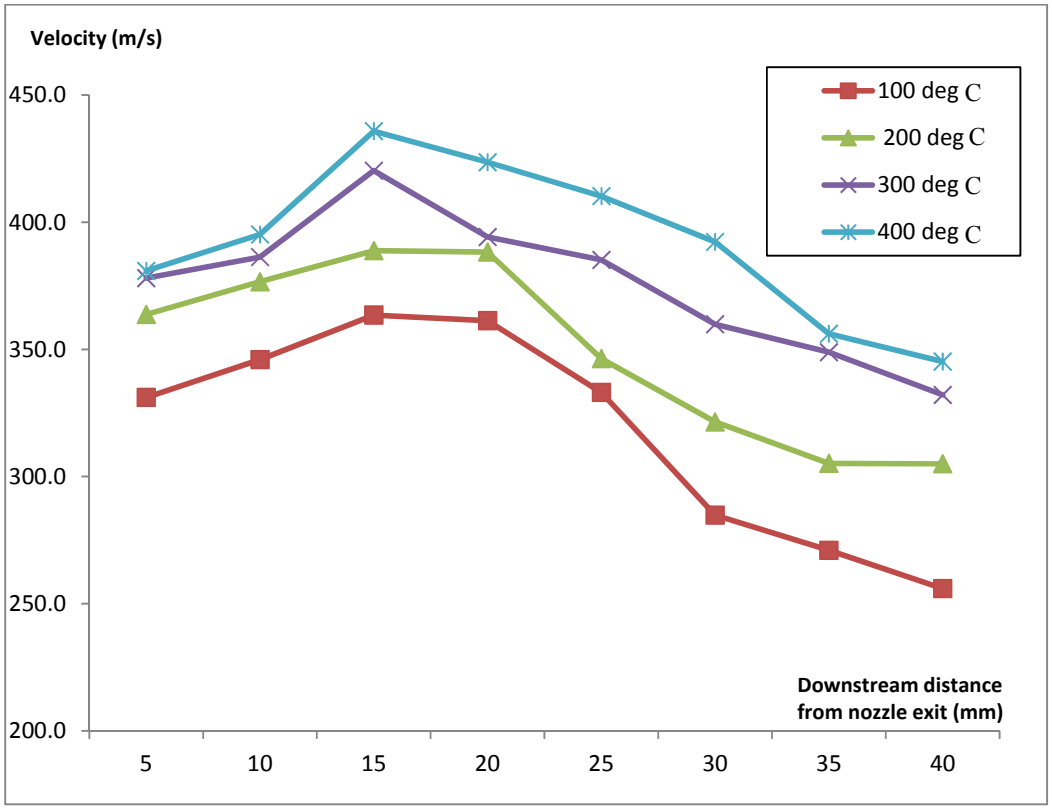

Figure 3.15: Velocity data of Aluminium powder particles at gas pressure of 5 bar and varying carrier gas temperature. The measurement of velocity has a defined error of ± 1.0 m/s.

The results suggested that the mean particle velocity increases with temperature. At carrier gas pressure of 5 bars, increasing the gas temperature from 100 ^{O}C to 400 ^{O}C resulted in an increase of about 15% in mean velocity at the immediate nozzle exit location (5 mm). According to Shapiro [1953], the gas stagnation temperature has a direct and positive effect of the gas velocity throughout the nozzle. This is because the gas velocity at any location in the nozzle is a function of the local Mach number which is determined by the nozzle geometry and local speed of sound. This in turn, is determined by the gas static pressure. Thus, a higher gas stagnation temperature will accelerate the particles to higher velocities due to the enhanced momentum transfer caused by the higher gas velocity.

In all varying carrier gas temperature conditions, there is also a trend of the particles accelerating as they leave the nozzle exit and achieving their maximum velocity before decelerating further downstream. The maximum velocity is reached at between 15 mm and 20 mm from the nozzle exit in all cases. As the particles lose their kinetic energy, the velocity decreases significantly beyond a distance of 25 mm from the nozzle exit. These results suggest that the optimum stand-off distance for the particular system should be between 15 to 20 mm from the nozzle exit.

The data also indicated that the increase in mean particle velocity becomes incremental beyond 300 ^{O}C, implying that the additional increase in temperature and thus heat energy may have limited impact on particle kinetic energy. However, there was also a previous study conducted by Lima et al [Lima *et al*., 2002] to investigate the effect of particle temperature on its critical velocity. It was found that the critical velocity decreases with an increase in the particle temperature. The decrease was approximated

to be about 14 ms^{-1} per 100 ^{O}C increase in particle temperature and the effect was attributed to thermal softening effect. This suggests that though the particle velocity may not increase with increasing carrier gas temperature, the coating deposition efficiency may continue to increase with the decreasing critical velocity of the powder particle due to the thermal softening effect.

3.7 Effect of Gas Pressure

To study the effect of gas pressure on particle velocity, aluminium powder was cold sprayed at three different pressures of 5 bar, 10 bar and 15 bar and the particle velocity with respect to the distance from the nozzle exit was measured. The carrier gas temperature was set at 100 ^{O}C and the powder feed rate was set at 60 Hz. The velocity measurements for varying carrier gas pressure are shown in Figure 3.16.

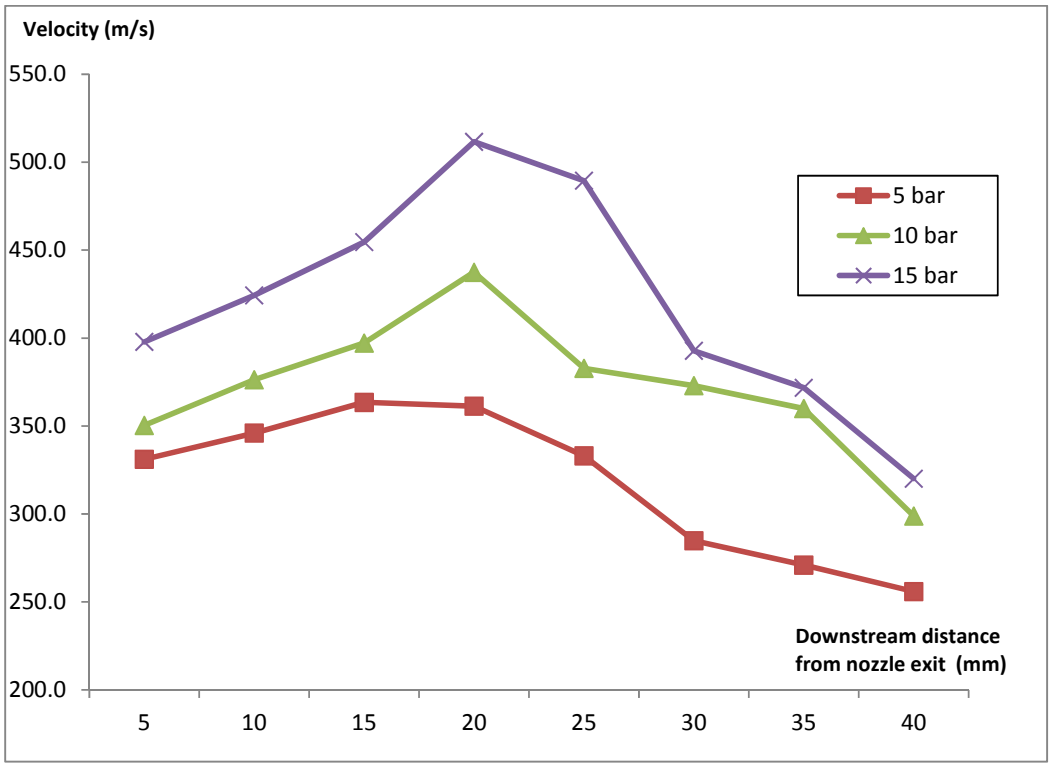

Figure 3.16: Velocity data of Aluminium powder particles at gas temperature of 100 ^{O}C and varying carrier gas pressure. The measurement of velocity has a defined error of ± 1.0 m/s.

Figure 3.16 represents the particle velocity data at different carrier gas pressures. Results indicated a positive effect on the velocity with increasing pressure. At the carrier gas temperature of 100 ^{O}C, increasing the gas pressure from 5 bar to 15 bar resulted in an increase of about 20% in mean particle velocity at 5 mm from the nozzle exit.

The graphs also suggested that as the carrier gas pressure increased, the point where the maximum particle velocity is reached increased as well. Maximum particle velocity for

both 10 and 15 bard was at 20 mm from the nozzle exit compared to 15 mm for the particles sprayed at 5 bar of gas pressure.

3.8 Effect of Powder Feed Rate

To study the effect of the powder feed rate on the mean particle velocity, three different feed rates (50 Hz, 60 Hz and 70 Hz, corresponding to 200, 240 and 280 $gmin^{-1}$ respectively) were investigated. The powder particles were cold sprayed at 18 bars and 400 ^{O}C. Particle velocity data was captured at one single location 20 mm from the nozzle exit and mean values are presented on Figure 3.17.

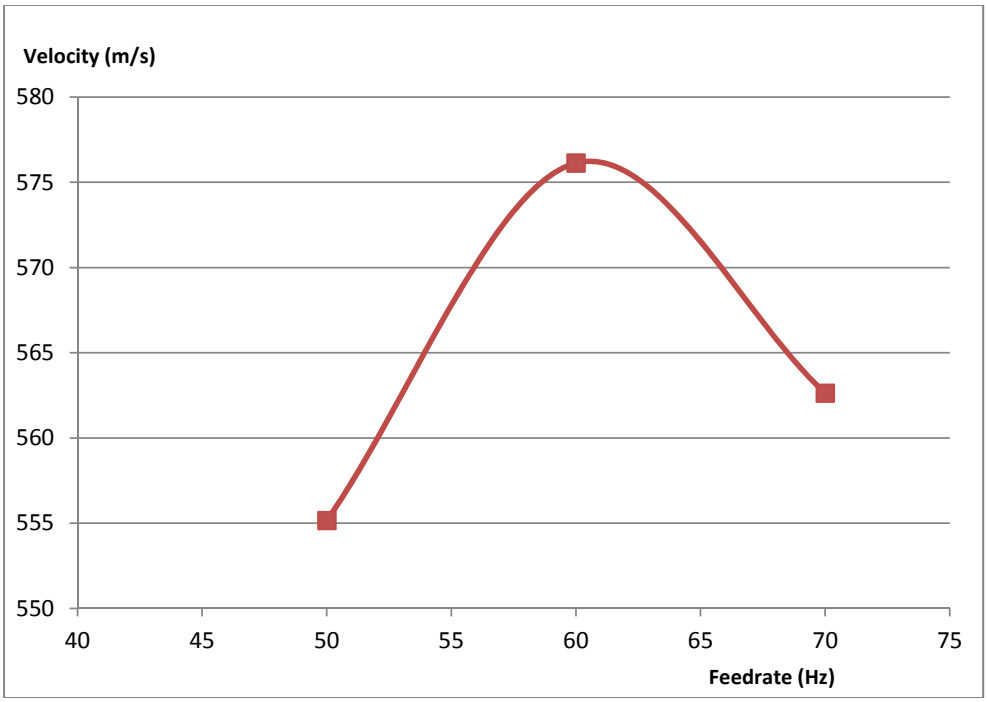

Figure 3.17: Velocity data of Aluminium powder particles at gas pressure of 18 bars and temperature of 400 ^{O}C and varying powder feed rate. The measurement of velocity has a defined error of ± 1.0 m/s.

The data suggested that increasing the feed rate from 50 to 60 Hz increased the particle velocity by about 4%. Subsequently, a 2.4% decrease in mean velocity was observed as the feed rate was further increased by 10 Hz. These changes however are fairly small relative to the absolute velocity of the particles. The impact of the powder feed rate on particle velocity does not seem substantial. Based on the data, a feed rate of between 50 Hz and 70 Hz would be acceptable for this cold spray system.

3.9 Conclusion

A parametric study of three spraying parameters, carrier gas temperature, carrier gas pressure and powder feed rate using compressed air was carried out to examine the effects they have on the in-flight velocity. It was found that a direct positive relationship exists between the carrier gas pressure and temperature with respect to the in-flight particle velocity. The relationship between the powder feed rate and the particle velocity however seems less direct, with the powder feed rate having little effect on the absolute particle velocity. The distance from the nozzle exit at which the maximum particle velocity was reached was also established. The results from the study carried out will form the basis for establishing the optimum coating parameters for subsequent experiments. The optimum coating parameters for aluminium powder are summarised in Table 3.4.

Table 3.4: Optimum coating parameters for cold spraying of aluminium powder using compressed air as carrier gas.

Optimum Parameters	
Carrier Gas Temperature (ºC)	400
Carrier Gas Pressure (bar)	15
Powder Feed Rate (Hz)	60
Stand-off Distance (mm)	15 to 20

CHAPTER 4

EFFECT OF GRIT BLASTING AND HEAT TREATMENT ON COATING MECHANICAL PROPERTIES

4.1 Introduction

In conventional thermal spray processes, the inclusion of certain pre- and post- coating processes such as grit blasting and heat treatment has significant impact on the eventual quality of the coatings. This chapter describes the experiments carried out to study the effects of pre-coating substrate preparation in the form of grit blasting and post-coating processing in the form of heat treatment of the coating on the cold sprayed coating properties. Microhardness assessment, tensile adhesion strength test and microstructure evaluation were carried out on the coatings prepared under various pre- and post- cold spray conditions. The intent is to evaluate the effects of such processes on the quality of the coatings and appraise their necessity in an industrial cold spray application.

4.2. Effects of Pre-coat Grit Blasting on Coating Properties

In traditional thermal spray processes, roughening of the substrate surface in the form of grit blasting is considered one of the most important steps in preparing the surface to accept the sprayed coating. Properly roughened surfaces provide the critical interface for the first layer of impacting coating particles by significantly increasing the surface area for particle-to-substrate contact and thus increasing the atomic and metallurgical interaction. However, little is known of the effect of grit blasting on the coating

properties for cold spray process. As such, an experiment to understand the effect of grit blasting on the mechanical properties and microstructures of the cold sprayed coating was carried out.

4.2.1 Microhardness Test

The effect of pre-coat grit blasting of the substrate on the microhardness of the coatings was investigated. Two aluminium Al-6061 substrate samples 30 mm x 30 mm x 10 mm (length x width x thickness) were used. These samples were machined from a commercially available (Metal Establishment Pte Ltd, Singapore) Al-6061 square tube of same cross-sectional area. The first was grit blasted with alumina grits (#150, average size 75 µm) at 4 MPa and standoff distance of about 25 mm using a custom built grit blasting machine (Abrasive Engineering Pte Ltd, Singapore) for 2 minutes. The second was not and the substrate surface condition was as-machined. The grit blasted and as-machined substrates are shown in Figure 4.1. The Taylor Hobson (Leicester, UK) Surtronic Duo Surface Roughness Tester was used to measure the mean arithmetic surface roughness of the grit blasted and as-machined surfaces and the results were Ra 2.51 µm and Ra 0.10 µm respectively. Both samples were subsequently cleaned with acetone prior to the cold spray process.

(a) **(b)**

Figure 4.1: Al-6061 substrate samples which was (a) grit blasted and (b) as-machined.

The cold spray process was carried out using the PCS-1000 cold spray system (Plasma Giken Co. Ltd., Japan). Nitrogen was used as the carrier gas and the flow rate was set at 250 standard litre per minute (SLM). The gas pressure was set at 4 MPa and the temperature at 400 ºC. The speed of the traversing robot was 200 mms^{-1} with a 1 mm step. The standoff distance was set at 25 mm and a total of two passes were made. Commercially available gas atomized Al-6061 powder (Valimet Inc., USA) was used for the experiment. The cold spray parameters used in this experiment are shown in Table 4.1.

Table 4.1: Cold spray operating parameters for specimen to be evaluated for microhardness.

Parameter	Value
Carrier gas	Nitrogen
Carrier gas pressure	4 MPa
Carrier gas temperature	400 ºC
Carrier gas flow rate	250 SLM
Robot traversing speed	200 mms^{-1}
Robot step	1 mm
Stand-off distance	25 mm
Number of passes	2

Figure 4.2 shows the scanning electron microscope (SEM) images of the Al-6061 feedstock powder. The particles are mainly spherical in shape and the diameter of the particles ranges from 5 µm to 50 µm with the average diameter measured at 28 µm.

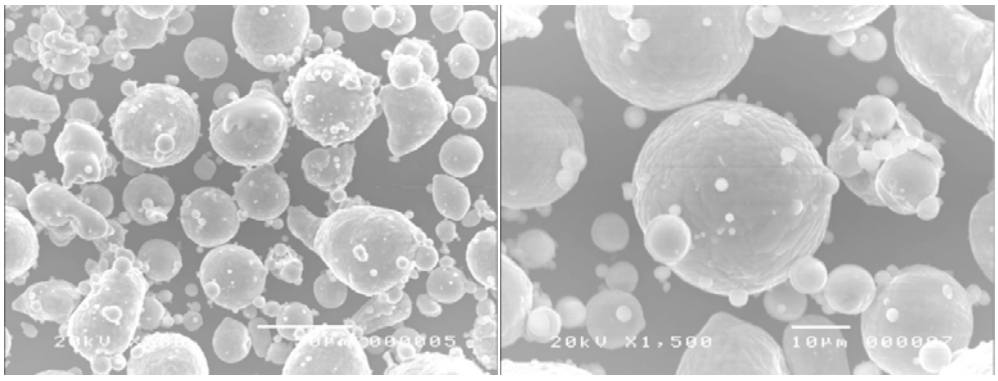

Figure 4.2: SEM images of the Al-6061 feedstock powder at (a) 500X and (b) 1500X

The coating obtained for the non-grit blasted substrate was about 380 µm in thickness while that obtained on the grit blasted substrate was about 250 µm. The coated samples were sectioned, mounted and polished. The microhardness measurements were subsequently made using the Matsuzawa (Akita, Japan) MMT-X7 tester. Five indentation measurements were taken from each sample using a 100 grams load (HV_{100g}) with a dwell time of 15 seconds along the mid-plane of the polished transverse section which is approximately 150 µm from the substrate coating interface (Figure 4.3). The results are presented on Table 4.2.

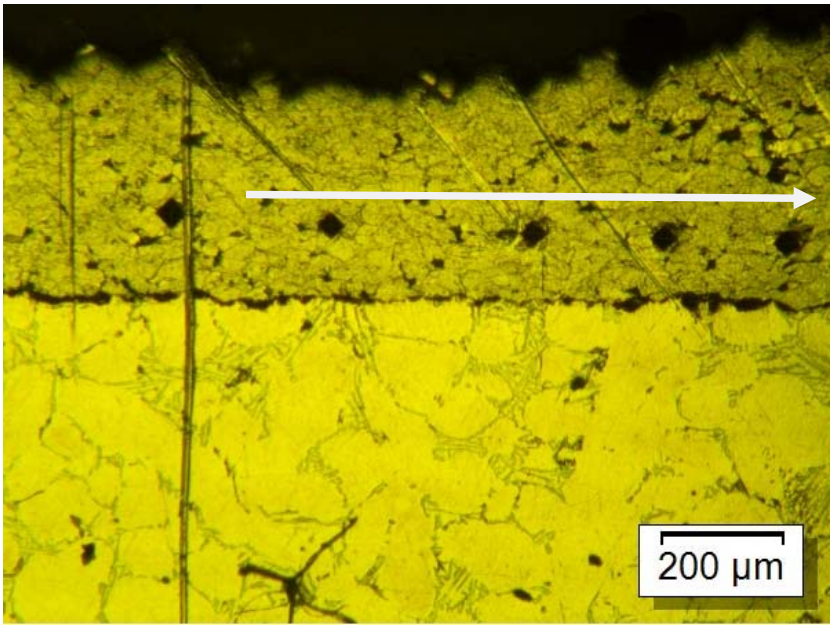

Figure 4.3a: Microhardness indentation measurements taken transversely along Al-6061 coating as indicated by the arrow. Magnification 100x.

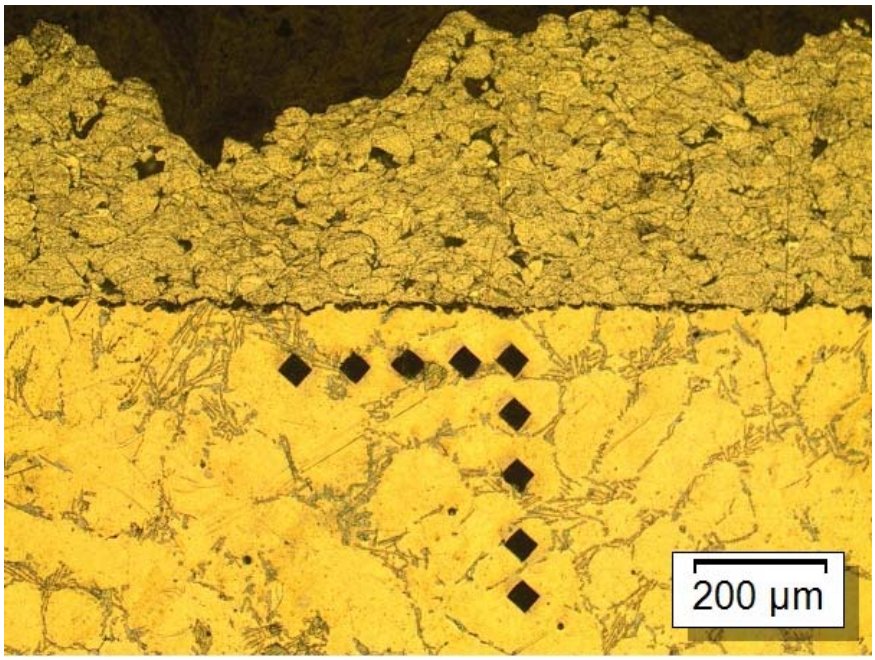

Figure 4.3b: Microhardness indentation measurements taken transversely and vertically along Al-6061 substrate. Magnification 100x.

Table 4.2: Microhardness measurement of cold sprayed Al-6061 coating on grit-blasted and non-grit blasted substrates.

	Specimen which was grit blasted (HV_{100g})		**Specimen which was not grit blasted (HV_{100g})**	
Measurement	Coating	Substrate	Coating	Substrate
1	102.8	91.4	95.1	97.1
2	104.6	100.1	98.4	96.2
3	100.2	104.1	116.0	102.1
4	94.6	97.8	95.3	108.8
5	97.0	103.8	100.2	92.0
Average	**99.8 ± 4.1**	**99.4 ± 5.2**	**101.0 ± 8.7**	**99.2 ± 6.4**

From Table 4.2, the average microhardness value for the coating with grit blasted substrate surface was 99.8 ± 4.1 while the measurement for the coating on the non-grit blasted substrate was 101.0 ± 8.7. The results indicate that the average microhardness values of both samples and standard deviation were relatively small. The results show the uniformity of the coating. In addition, the effect of grit blasted surfaces on the microhardness of the coating is minimal. Incidentally, the mean microhardness value for the aluminum Al-6061 substrate material was measured to be 99.4 HV_{100} and 99.2 HV_{100} for the grit blasted and non-grit blasted substrates respectively. The measurements were taken transversely as shown in Figure 4.6b. The microhardness measurement of the substrate showed little changes in both the transverse and vertical directions. The results indicate little deviation in microhardness characteristics between both as-sprayed coating and the substrate. The constant and repeated impact of the impinging cold sprayed particle causes a gradual compaction of the coatings, thus resulting in such relatively high microhardness values.

The variation in microhardness of the coating in the vertical direction was also investigated for coatings on both grit blasted and non-grit blasted substrates. A total of five indentation measurements spread evenly were taken along the vertical direction from the top of the coating to the substrate-coating interface of each sample as illustrated in Figure 4.4. The total coating thickness was approximately 250 μm for the coating on grit blasted substrate and 380 μm for the coating on the non-grit blasted substrate. The distance in between microhardness measurements was computed from the middle of the indentation to the same point on the following indentation as shown in Figure 4.5. The results of the microhardness value of the Al-6061 coatings along the vertical direction are shown on Figure 4.6. The measurements taken on the substrate in

the vertical direction showed little variation from the mean value of 99.4 HV_{100} and 99.2 HV_{100} for the grit blasted and non-grit blasted substrates respectively.

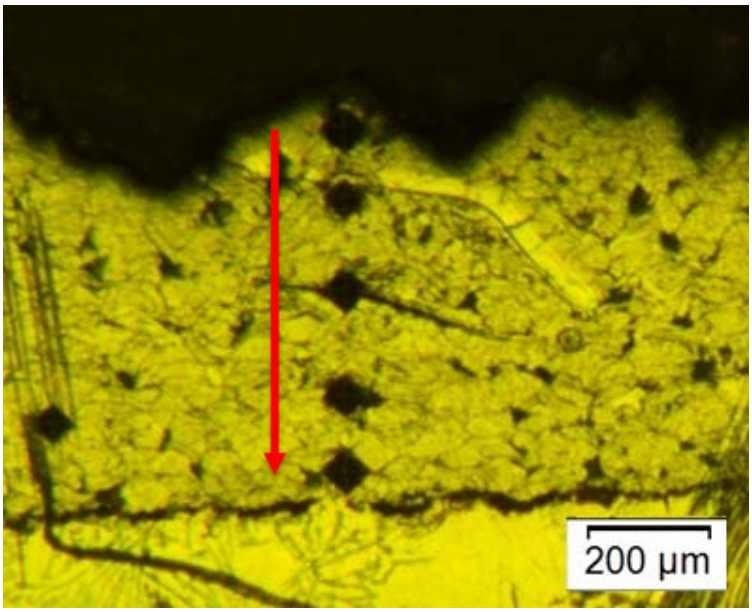

Figure 4.4: Microhardness indentation measurements taken vertically from the top of the Al-6061 coating to coating-substrate interface as indicated by the arrow.

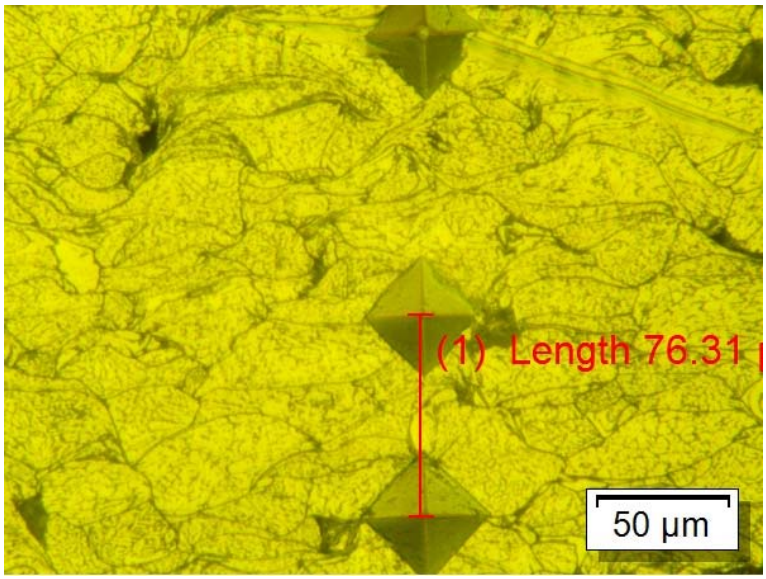

Figure 4.5: Measurement of vertical distance between two microhardness indentation measurements.

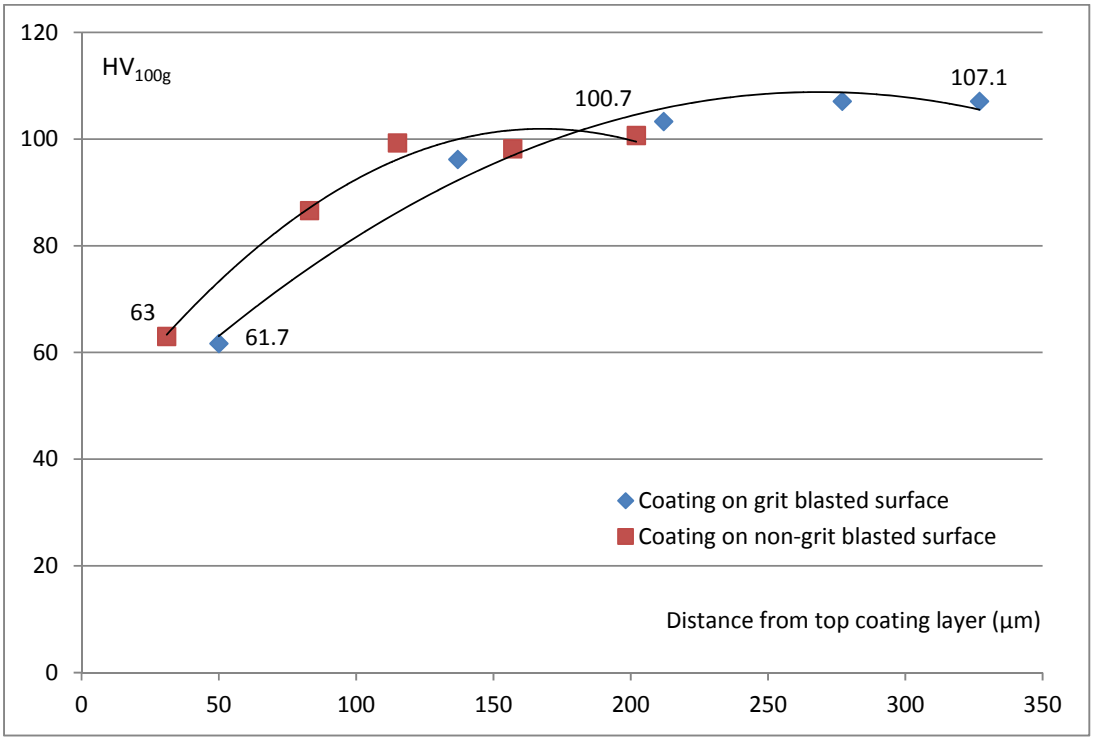

Figure 4.6: Microhardness value of Al-6061 coating along the vertical direction from the top surface of the coating.

The graph on Figure 4.6 suggests very little variation in the microhardness of the top layer of the coating between the 2 sets of samples. The maximum microhardness achieved for both samples was also almost identical at slightly more than 100 HV_{100}. This again demonstrated the minimal impact of pre-coating grit blast process on microhardness properties of the cold spray coating. In both cases, the result also indicates a progressive increase in microhardness of the coating from the top layer to the coating-substrate interface for both coatings. This is likely due to the continuing compaction of the sprayed layer as more impinging particles impact on top of the previous layer. The result also shows that the microhardness will reach a maximum value about 200 to 250 µm from the top coating layer before tapering off to the maximum value of about 100 HV_{100}. This suggests that any further compacting of the sprayed particles will have little effect on the microhardness of the underlying coating.

The variation in microhardness was calculated to be approximately 15 HV_{100} per 100 µm of coating. This implies that additional post coating heat treatment may have to be applied if coating microhardness uniformity is desired.

4.2.2 Tensile Adhesion Strength Test

The effect of pre-coat grit blasting of the substrate on the tensile adhesion strength was investigated. Two sets of experimental data each consisting of five samples was collected in accordance to the ASTM C633-01 standards (Standard Test Method for Adhesion or Cohesion Strength of Thermal Spray Coatings). The first set of substrates were grit blasted whereas the second set of substrates were left in their as-machined condition. The two set of substrates are shown in Figure 4.7. The mean arithmetic

surface roughness of the grit blasted and as-machined substrate surfaces prior to the cold spray process was measured to be Ra 2.21 µm and 0.18 µm respectively using the Taylor Hobson Surtronic Duo Surface Roughness Tester. The samples were subsequently cleaned with acetone and cold sprayed with Al-6061 powder (Valimet Inc., USA), identical to those used in Section 4.2.1. The cold spray process was carried out using the PCS-1000 cold spray system (Plasma Giken Co. Ltd., Japan). Nitrogen was used as the carrier gas and the flow rate was set at 250 standard litre per minute (SLM). The gas pressure was set at 4 MPa and the temperature at 400 ºC. The speed of the transversing robot was 200 mms^{-1} with a 1 mm step. The standoff distance was set at 25 mm and a total of two passes were made.

The samples were glued together using epoxy glue Klebbi (Oerlikon Metco, Winterthur, Switzerland) and cured at 200 °C for 2 hours. The tensile adhesion strength of the specimens was tested using the MTS/SINTECH 65/G Universal Testing Machine with crosshead speed at 1 $mmsec^{-1}$. The test specimens are shown in Figure 4.8. The results of the tensile adhesion strength test are presented on Table 5.3.

(a)

(b)

Figure 4.7: Tensile adhesion test specimens which (a) have been grit blasted and (b) are as-machined prior to cold spray coating.

Figure 4.8a: Adhesion strength test specimen with coating cold sprayed on grit blasted substrates.

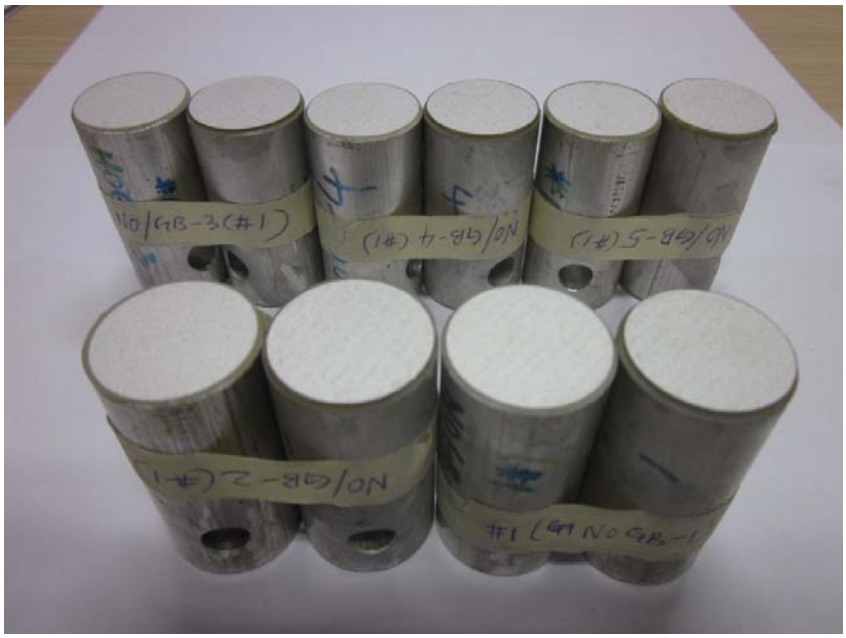

Figure 4.8b: Adhesion strength test specimen with coating cold sprayed on non-grit blasted substrates.

Table 4.3: Tensile adhesion test results for cold sprayed Al-6061 coating on grit blasted and non-grit blasted Al-6061 substrates.

	Coating with substrate grit blasted (MPa)	Failure Mode	Coating with substrate not grit blasted (MPa)	Failure Mode
1	10.36	Failure at coating/base metal interface.	36.43	Failure at coating/base metal interface.
2	13.97		39.33	
3	7.695		45.99	
4	19.10		40.14	
5	7.715		38.55	
Average	**11.77 ± 4.84**		**40.09 ± 3.58**	

From Table 4.3, the average tensile bond strength of the Al-6061 coating on the grit blasted and non-grit blasted substrates were 11.77 ± 4.84 MPa and 40.09 ± 3.58 MPa respectively. The failure mode for all the tests was at the coating and base material interface.

The results show that the tensile adhesion strength of the Al-6061 coating on the non-grit blasted substrate is significantly higher than the coating on the grit blasted substrates. This deviated from similar tests on conventional thermal spray coatings (plasma, HVOF, arc, etc) where the contrary is usually true. The results also seem to suggest that a pre-coating grit blast process may not be beneficial in enhancing the tensile adhesion strength of the coating. The results from this work suggest that grit blasting the substrate may actually be detrimental. In order to investigate further the cause for this anomalous result, the microstructure of the interface between the substrate and the coating for both specimens with and without grit blasting treatment were examined by SEM.

4.2.3 Microstructure Evaluation

The microstructure of the coatings was examined using a field emission scanning electron microscope (FESEM). The coating samples were sectioned, mounted, etched and prepared according to ASTM E3-11 standard. The samples with coating on grit blasted and non-grit blasted substrates are shown on Figure 4.9. The samples were then examined under different magnifications and the results were analysed according to ASTM E487-85 standard. Figures 4.10 and 4.11 show the SEM photos of the coatings on grit blasted and non-grit blasted surfaces at 50, 200 and 500 magnifications respectively.

Figure 4.9: Coating samples on grit blasted and non-grit blasted substrates which have been sectioned and etched for microstructure evaluation.

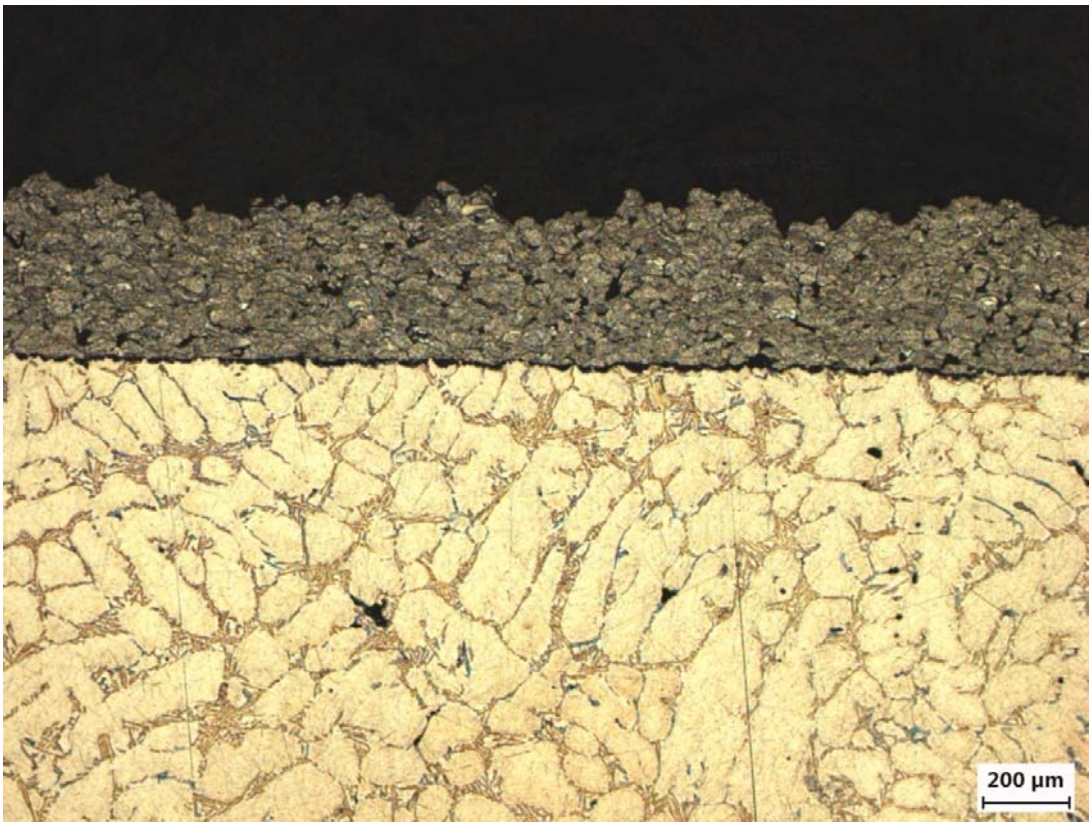

Figure 4.10a: SEM of Al-6061 coating on grit blasted substrate at 50x magnification.

Figure 4.10b: SEM of Al-6061 coating on grit blasted substrate at 200x magnification.

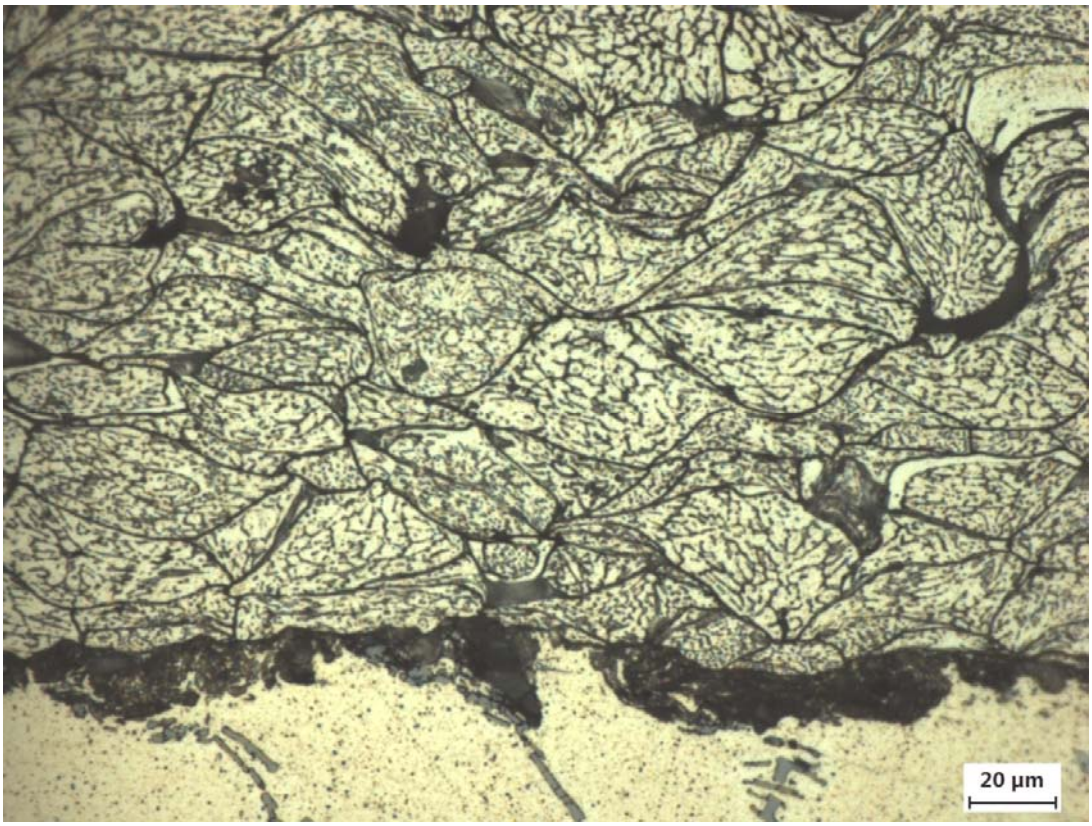

Figure 4.10c: SEM of Al-6061 coating on grit blasted substrate at 500x magnification.

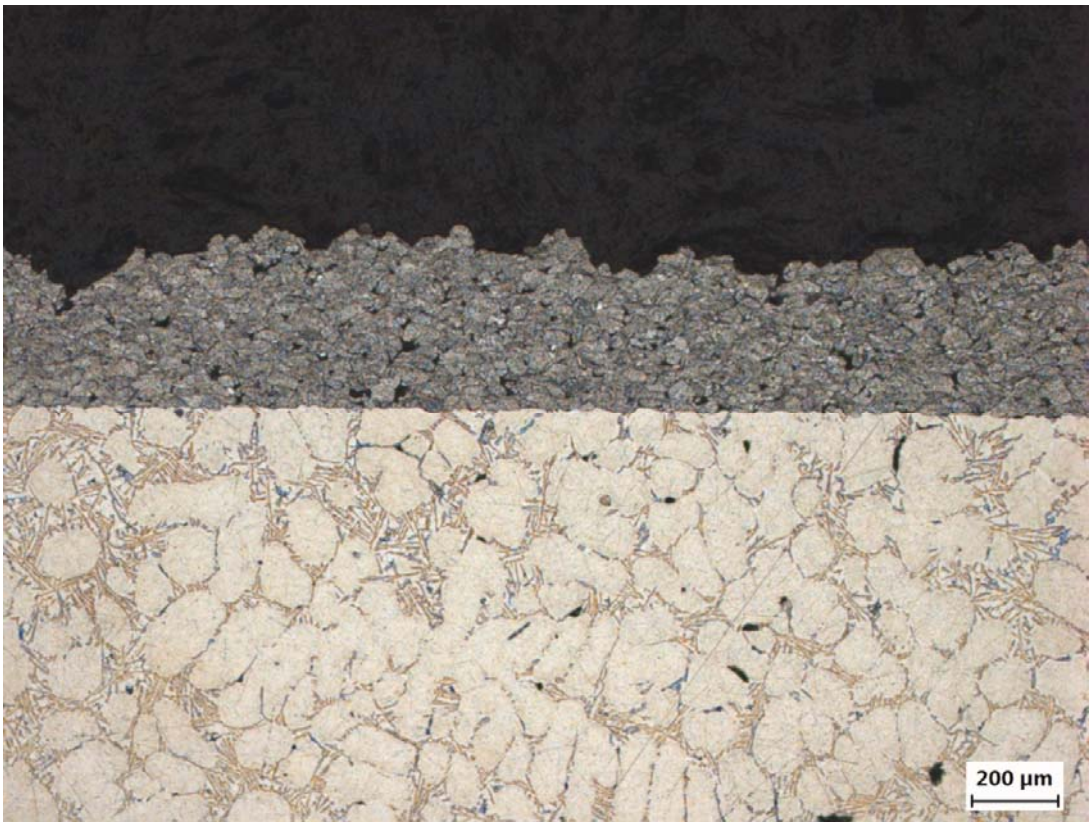

Figure 4.11a: SEM of Al-6061 coating on non-grit blasted substrate at 50x magnification.

Figure 4.11b: SEM of Al-6061 coating on non-grit blasted substrate at 200x magnification.

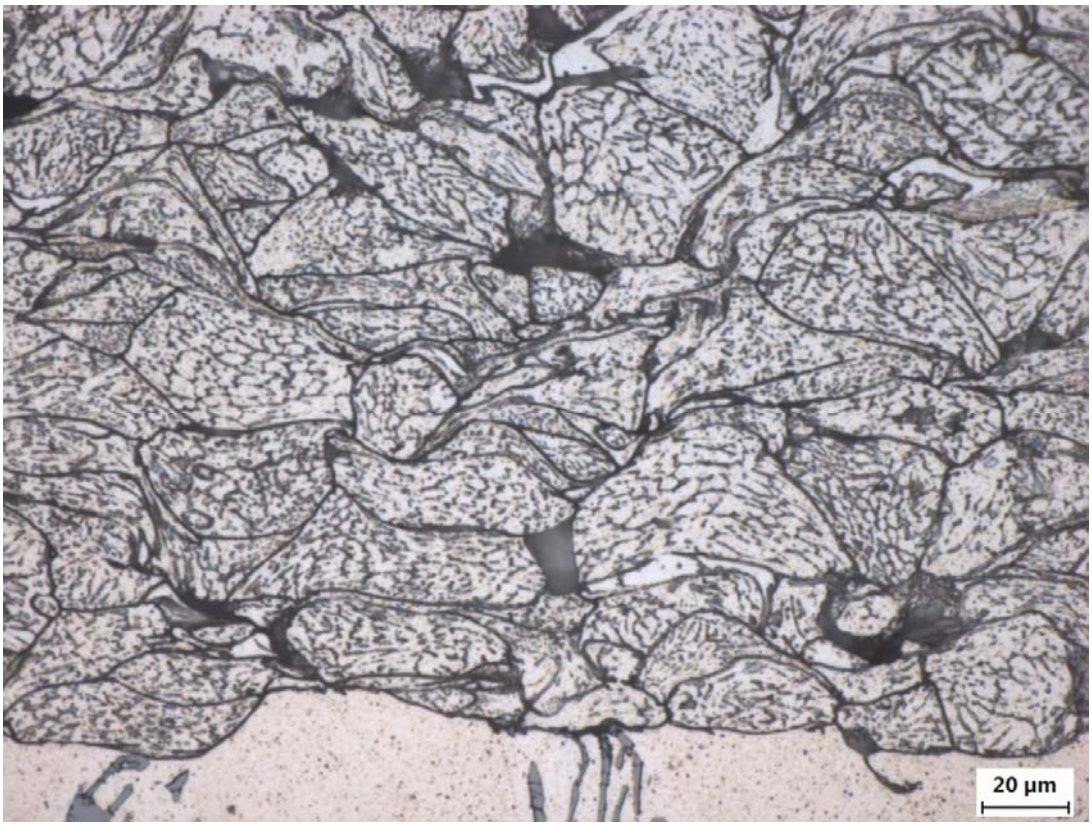

Figure 4.11c: SEM of Al-6061 coating on non-grit blasted substrate at 500x magnification.

The SEM micrographs show that the coatings prepared on different substrates have similar properties except for a few layers which are deposited initially. From Figures 4.10 and 4.11, we can observe that the geometry of the particles are relatively elongated, indicating the compressing effect of the particles as they are deposited layer by layer. Plastic deformation of the overlying particles ensures that surface irregularities are completely filled, minimising inter-particle porosity. Furthermore, the high velocity impinging particles have a peening effect on the previously deposited underlying material. This action closes any gaps or small pores in the primary material. Porosity in the coating was found to be quantitatively similar for coatings prepared on grit blasted and non-grit blasted substrates. The distribution of such defects is also almost identical.

The difference between the two coatings can be seen in the interface between the coating and the substrate. Figures 4.10a to 4.10c suggest that the presence of a layer of impurities between the substrate and the coating on the grit blasted surface. This is the most probable explanation for the significantly reduced tensile adhesion strength for the coating on grit blasted substrate compared to the coating on non-grit blasted substrate presented on Table 4.2. Figure 4.10c shows that the grit blasting process has created a layer of contamination that prevents the larger cold sprayed particles from plastically deforming into the substrate. To identify the content in that layer, energy dispersive X-ray spectroscopy (EDX) was performed at four locations between the substrate and coating interface for the grit blasted specimen. The results are shown in Table 4.4.

Table 4.4: EDX results showing elements in the layer between the coating and substrate for the grit blasted specimen.

Element	Location 1 (%)	Location 2 (%)	Location 3 (%)	Location 4 (%)
Al	86.66	33.66	4.47	58.2
Ti	6.29			
Fe	1.63		95.53	
Zr	1.61			
K	1.24			7.13
Si	1.19	1.62		2.91
Mg	0.79			4.35
Ca	0.59	64.47		
S				10.62
F				14.37
Na				2.06
Total (%)	**100**	**99.75**	**100**	**99.64**

The EDX results showed that besides aluminium (Al), high percentage of iron (Fe), Calcium (Ca), Sulphur (S) and Fluorine (F) were detected in the layer between the coating and substrate. This is a clear indication of contamination on the substrate surface due to the grit blasting process. These foreign materials are likely to be from the grit blasting machine which was used to process other industrial components.

For effective adhesion to take place, substrate surfaces should be clean and subjected to high contact pressure. This condition is enhanced by the adiabatic shear instability and the associated localization of the plastic flow into the interfacial jets. The angular contact surfaces on the substrate may have also prevented the formation of bonds due to hydrodynamic flow instability of the adiabatic shear instability. The most likely cause of the substrate jagged surface is the alumina grit material as shown in Figure

4.12 (average size 75 µm). When blasted against the substrate, these angular particles, which are much harder than the substrate, chipped away the surfaces, leaving sharp, pointed finishes. Such surface finishes seem to prevent the cold spray particles from bonding onto the substrate and forming a well-defined interface between the coating and substrate. Furthermore, the presence of impurities, likely from the alumina grit may have contributed to the decreased in tensile adhesion strength of the coating as well.

Figure 4.12: Alumina grit blasting material (size #150) at 130x magnification

In the case of the coating formed on the non-grit blasted substrate, Figures 4.11a to 4.11c show a well-defined interface between the coating particles and the substrate. There were no impurities, porosities or voids observed between the coating and substrate. As shown in Figure 4.11b, the surface of the substrate is not perfectly flat and seems to have deformed to about the same size as the impinged coating particles. The cold spray particles can be seen to plastically deform and tightly bond into the substrate,

forming a good adhesion. The tensile adhesion strength test results presented in Table 4.3 validates the observation.

The cold spray process can be described as a three-in-one or triplex process, in which the grit blasting, spray coating and shot peening are all carried out in a single pass. The in-process grit blasting in this case seem to be more effective than the one using alumina grit because the grit material in the form of the cold sprayed particles is essentially of identical size and shape. This ensures that the substrate surface which is inherently roughen are indented to similar shape and diameter to the particles, unlike the case where the angular alumina grit materials leave a jagged indentation instead. As such, upon impact, the impinging particles will adhere tightly to the roughened substrate as the surface area for contact between the substrate and the particle is maximized. This is consistent with the individual particle deposition characterization study done by Kumar *et al.* [2009] which advocated that substrate surface which is roughened with crest size the same as the particle size creates better bonding. Further discussion on this phenomenon will be discussed in Chapter 7.

4.3 Effects of Heat Treatment on Coating Properties

In order to avoid some of the detrimental effects of conventional thermal spray, coatings are often treated after spraying to improve or change the coating microstructures. Heat treatment is one of the most common methods. Heat treatment is usually carried out at elevated temperatures which is well below the melting point of the coating. The intent for heat treating conventional thermal spray coating includes [Longo, 2004]:

- Enhancement of bond strength due to diffusion between substrate and sprayed coating. Diffusion is the mixing of atoms at high temperature which creates metallurgical bonding and higher strength. Micro porosity may also be reduced in the process.

- Release of residual stresses and thus increasing inter-particle cohesion. Reduction in hardness with corresponding improved ductility and impact resistance as well as fracture toughness and modulus of elasticity may be observed.

- Enhancement of mechanical properties due to recrystallisation and grain growth via sintering. The process may efface laminar particle shapes and create new microstructural textures.

- Under hydrogen or vacuum environments, heat treatment may reduce oxides and induce phase and structural changes. Toughness may be enhanced.

Experiments were carried out to study the impact of heat treatment on cold sprayed coatings. The intent is to investigate if identical benefits from heat treating conventional thermal spray coatings can be derived from heat treating cold spray coatings.

4.3.1 Microhardness Test

Two sets of Al-6061 substrates (30 mm x 30 mm x 10 mm) were machined from a commercially available (Metal Establishment Pte Ltd, Singapore) Al-6061 square tube. Both samples were grit blasted with alumina grits (#150, average size 75 µm) using a custom built grit blasting machine (Abrasive Engineering Pte Ltd, Singapore) for 2 minutes. The mean arithmetic surface roughness of the substrates were measured using the Taylor Hobson (Leicester, UK) Surtronic Duo Surface Roughness Tester and the results were Ra 2.40 µm and Ra 2.55 µm respectively. The samples were subsequently cleaned with acetone prior to the cold spray process.

The cold spray process was carried out using the PCS-1000 cold spray system (Plasma Giken Co. Ltd., Japan). Nitrogen was used as the carrier gas and the flow rate was set at 250 standard litre per minute (SLM). The gas pressure was set at 4 MPa and the temperature at 400 ºC. The speed of the traversing robot was 200 mms^{-1} with a 1 mm step. The standoff distance was set at 25 mm and a total of two passes were made. Commercially available gas atomized Al-6061 powder (Valimet Inc., USA) was used for the experiment. Figure 4.2 shows the scanning electron microscope (SEM) images of the Al-6061 feedstock powder. The particles are mainly spherical in shape and the diameter of the particles ranges from 5 µm to 50 µm with the average diameter measured at 28 µm.

The coatings were subsequently subjected to the following heat treatment processes:

- Stress relief: First set was subjected to 150 ºC of heat treatment in an air furnace for 2 hours and air-cooled to room temperature.
- Full annealing: Second set of samples was subjected to 535 ºC for 2 hours followed by 177 ºC for 8 hours before air-cooled to room temperature.

The samples which have gone through the heat treatment processes are shown in Figure 4.13.

Figure 4.13: Al-6061 cold spray coated specimen which has undergone (a) stress relief and (b) full annealing.

Samples with coating thickness of about 400 µm were polished and tested for their microhardness using the Matsuzawa MMT-X7 tester. Five indentation measurements were taken from each sample along the mid-plane of the polished transverse section which is approximately 200 µm from the substrate coating interface. A 100 grams load

(HV_{100g}) with a dwell time of 15 seconds was used for the test. The results are presented on Table 4.5.

Table 4.5: Microhardness measurement of cold sprayed Al-6061 coatings which have undergone stress relief and annealing compared with untreated specimen.

Measurement	Coating with substrate grit blasted and stress relieved 150 deg C, 2 hours (HV_{100g})	Coating with substrate grit blasted and annealed 535 deg C, 2 hours & 177 deg C, 8 hours (HV_{100g})	Coating with substrate grit blasted and not subjected to any heat treatment. (HV_{100g})
1	84.8	83.6	102.8
2	85.8	88.5	104.6
3	88.5	89.5	100.2
4	86.2	86.4	94.6
5	90.2	89.9	97.0
Average	**87.1 ± 2.2**	**87.6 ± 2.6**	**99.8 ± 4.1**

The average microhardness of the two samples was identical. This implies that the different heat treatment for the coatings had identical effect on the microhardness of the coatings. When compared to the microhardness values of the coating which did not go through the heat treatment process (Table 4.2), the heat treated microhardness value was lower by about 20%. This shows that the heat treatment reduced the hardness of the coating and increased its ductility. The reason for this reduction in hardness with corresponding improved ductility is the release of residual stresses in the coating and increasing inter-particle cohesion. The variation in microhardness of both coatings in the vertical direction was also investigated. Five indentation measurements spread fairly evenly were taken along the vertical direction from the top of the coating to the substrate-coating interface of each sample. The results, together with the data from the non-heat treated samples are presented in Figure 4.14.

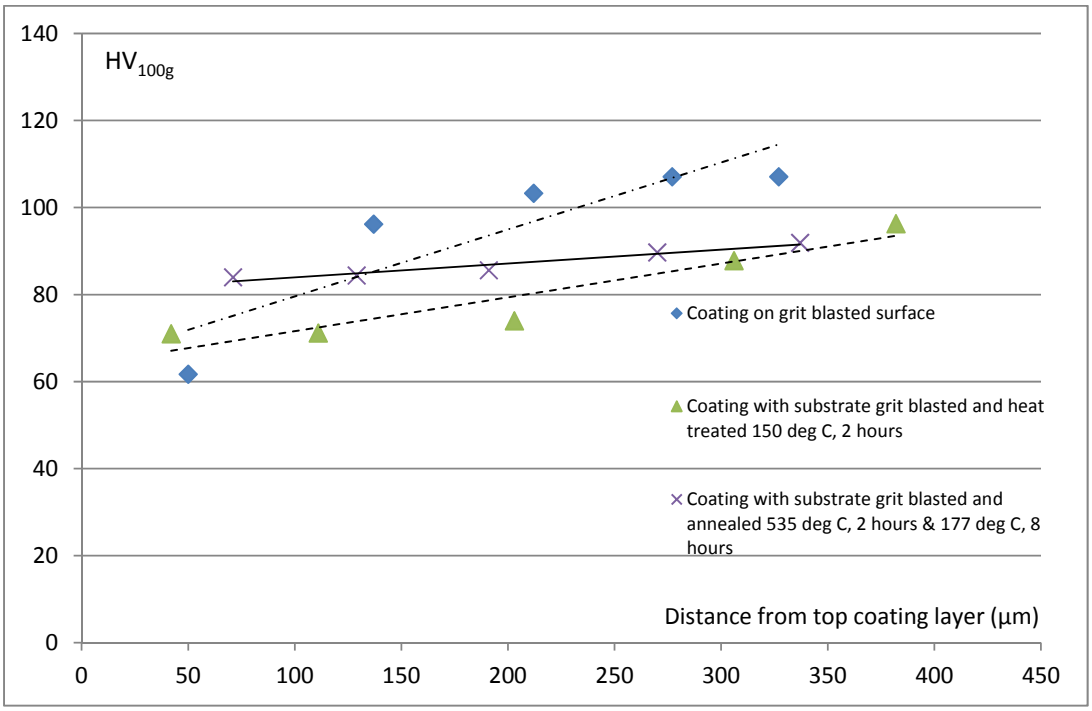

Figure 4.14: Microhardness value of Al-6061 coating along the vertical direction from the top surface of the coating.

The results from Figure 4.14 indicate that the heat treatment process had a homogenizing effect on the microhardness of the coating. The change in the microhardness for the coating subjected to two hours of heat treatment at 150 degrees Celsius was relatively small, with the change measured at about 7.8% from the top surface of the coating to about 400 µm of coating thickness. The change was even smaller for the coating which was subjected to full annealing, with the change measured at 3.2% from the top surface to 350 µm of the coating. This is relatively small compared to the 15% change for the non-heat treated coating. Thus, uniformity of the microhardness of the coatings can be achieved with the heat treatment processes, with variation in microhardness decreasing with increasing temperature and duration which the coating is subjected to. A reason behind this phenomenon is the release of the

residual stresses across the whole cross-section of the coating will the prolonged heat treatment process. This ensures uniformity of the hardness across the whole coating.

4.3.2 Tensile Adhesion Strength Test

The effect of post coating heat treatment on the adhesion strength of the coating was investigated. Four sets of experimental data each consisting of five samples was collected in accordance to the ASTM C633-01 standards (Standard Test Method for Adhesion or Cohesion Strength of Thermal Spray Coatings). Two set of samples were first grit blasted and the mean arithmetic surface roughness of the surfaces prior to the cold spray process was measured to be Ra 2.31 µm and 2.28 µm respectively using the Taylor Hobson Surtronic Duo Surface Roughness Tester. The other two set of samples were not grit blasted and the mean arithmetic surface roughness of the surfaces prior to the cold spray process was measured to be Ra 0.15 and 0.17 respectively. All samples were subsequently cleaned with acetone and cold sprayed with Al-6061 powder (Valimet Inc., USA), identical to those used in Section 4.2.1. The cold spray process was carried out using the PCS-1000 cold spray system (Plasma Giken Co. Ltd., Japan). Nitrogen was used as the carrier gas and the flow rate was set at 250 standard litre per minute (SLM). The gas pressure was set at 4 MPa and the temperature at 400 ºC. The speed of the traversing robot was 200 mms^{-1} with a 1 mm step for complete coating coverage of the substrates. The standoff distance was set at 25 mm and a total of two passes were made.

Two set of samples, one coated on the grit blasted substrates and the other on the non-grit blasted substrates were subsequently subjected to stress relief at 150 ºC in an air furnace for 2 hours and air-cooled to room temperature. The remaining two set of

samples were subjected to full annealing at 535 ºC for 2 hours followed by 177 ºC for 8 hours before air-cooled. They were all subsequently tested in accordance to the ASTM C633-01 standards (Standard Test Method for Adhesion or Cohesion Strength of Thermal Spray Coatings). The tensile adhesion test of the specimens was tested using the MTS/SINTECH 65/G Universal Testing Machine with crosshead speed at 1 $mmsec^{-1}$. The test specimens are shown in Figure 4.15. The results of the tensile adhesion strength test are presented on Figure 4.16 and Table 4.6.

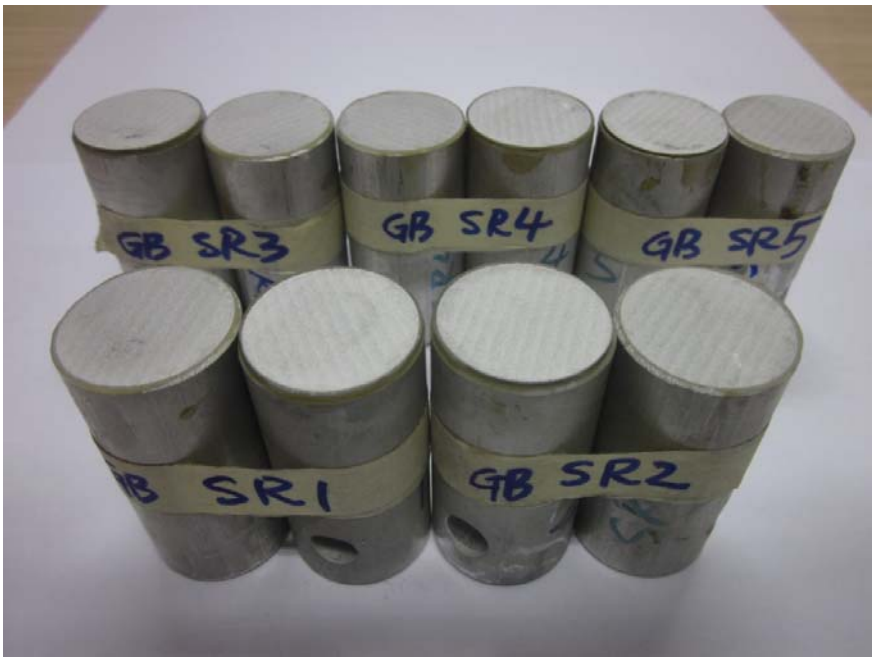

Figure 4.15a: Adhesion strength test specimen with cold sprayed coating which has undergone stress relief.

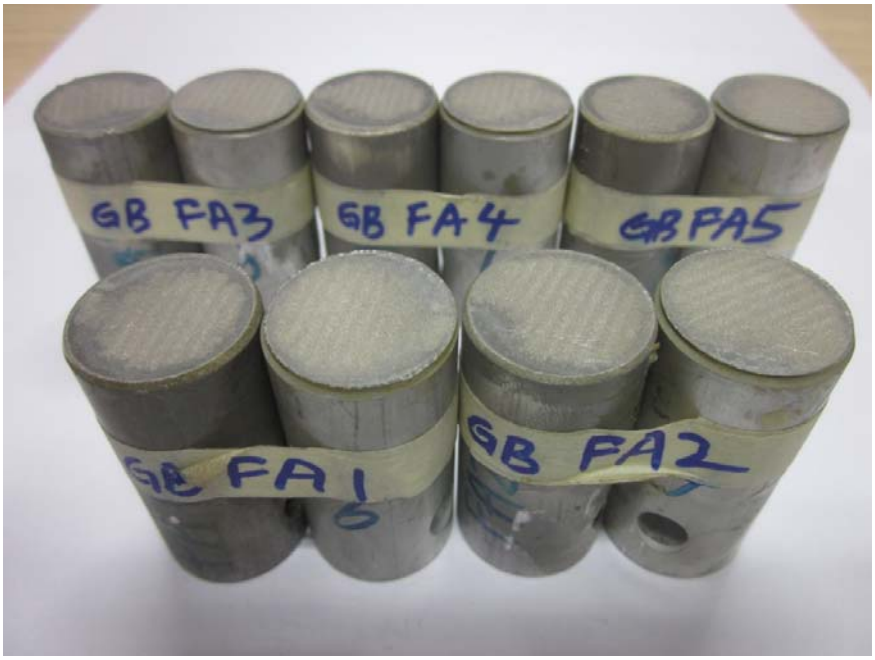

Figure 4.15b: Adhesion strength test specimen with cold sprayed coating which has undergone annealing.

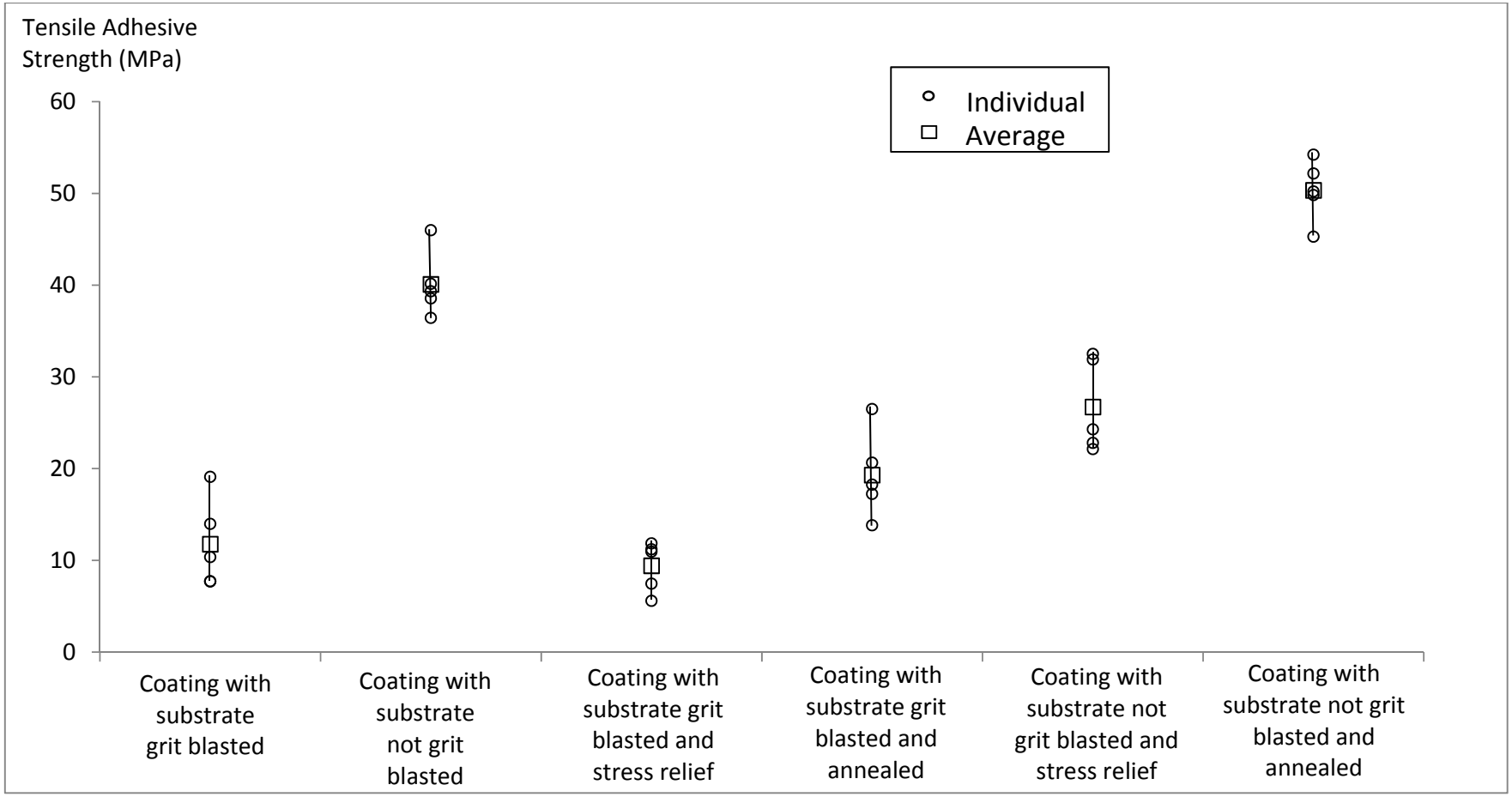

Figure 4.16: Tensile adhesion strength test results for cold sprayed Al-6061 coatings with and without post coating heat treatment.

Table 4.6: Tensile adhesion test results for cold sprayed Al-6061 coating with and without post coating heat treatment on non-grit blasted Al-6061 substrates.

	Coating with substrate not grit blasted (MPa)	Failure Mode	Coating with substrate not grit blasted and stress relief (MPa)	Failure Mode	Coating with substrate not grit blasted and annealed (MPa)	Failure Mode
1	36.43	Failure at coating/ base material	31.90	Failure at coating	50.21	Failure at coating
2	39.33		22.800		49.82	
3	45.99		22.13		52.17	
4	40.14		24.28		45.28	
5	38.55		32.500		54.22	
Ave	**40.09 ± 3.58**		**26.72 ± 5.07**		**50.34 ± 3.33**	

From Figure 4.16, the tensile adhesion strength for the coatings sprayed on grit blasted substrates which had undergone stress relief was not significantly better than those which did not. In fact the average tensile adhesion strength was actually lower, where the mean value of the 5 readings for non-heat treated and heat treated coatings were 11.77 MPa and 9.41 MPa respectively. This result is consistent with the data collected for the coatings which were cold sprayed on non-grit blasted substrates as presented in Table 4.6. The average tensile adhesion strength for the heat treated coatings was 26.72 MPa compared to 40.09 MPa for the non-heat treated samples. Both set of results indicated that unlike conventional thermal spray processes, post coating stress relief does not improve the adhesion strength of the cold spray coating. The reason could be that cold spray, being a solid state coating process, does not introduce much thermal residual stresses that may affect inter-particle cohesion. In addition, the lack of porosity in the cold spray coating may also imply minimal impact of heat treatment on enhancement of bond strength.

From Figure 4.16, the result for the coating sprayed on grit blasted substrates which has undergone full annealing however, did suggest a significant improvement in the tensile adhesion strength. The average value of the 5 readings was 19.29 MPa, a 64% increase as compared to the coating which did not undergo any heat treatment. Similarly, for the coating sprayed on non-grit blasted substrates which has undergone full annealing, the mean tensile adhesion strength was 50.34 MPa, a 26% increase as compared to the coating which did not undergo any heat treatment. Both sets of results suggest that full annealing of the cold spray coatings contribute to the strengthening of the tensile adhesion strength of the coatings.

4.3.3 Microstructure Evaluation

The microstructure of the heat treated coatings was examined using a field emission scanning electron microscope (SEM). The coating samples were sectioned, mounted, etched and prepared according to ASTM E3-11 standard (Figure 4.17). The samples were then examined under different magnifications and the rest were analysed according to ASTM E487-85 standard. Figures 4.18 and 4.19 show the SEM of the stress relief and full annealed coatings at various magnifications respectively.

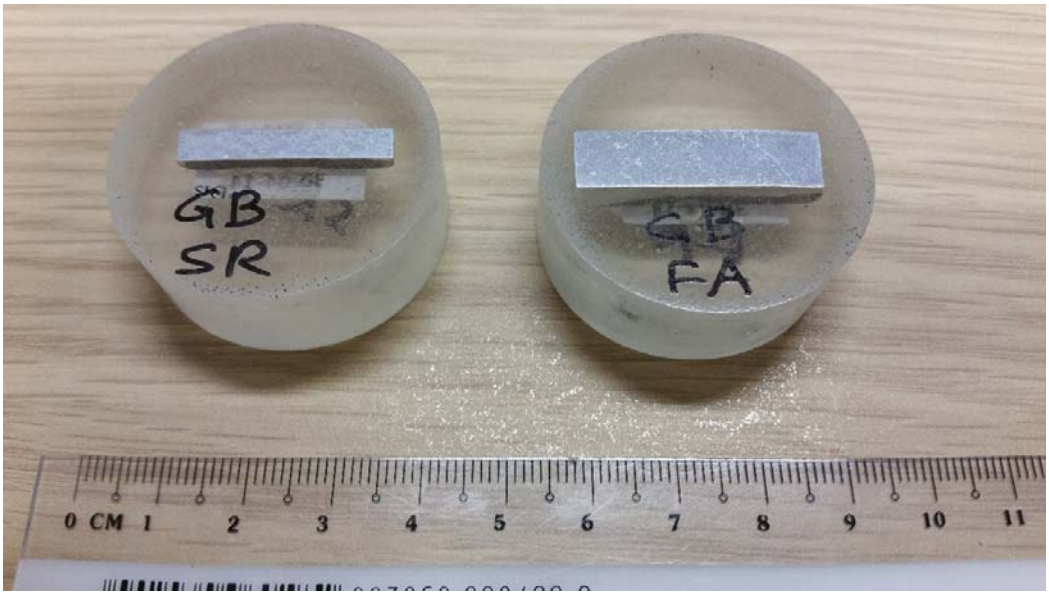

Figure 4.17: Cold sprayed coating samples which have undergone stress relief and full annealing sectioned and etched for microstructure evaluation.

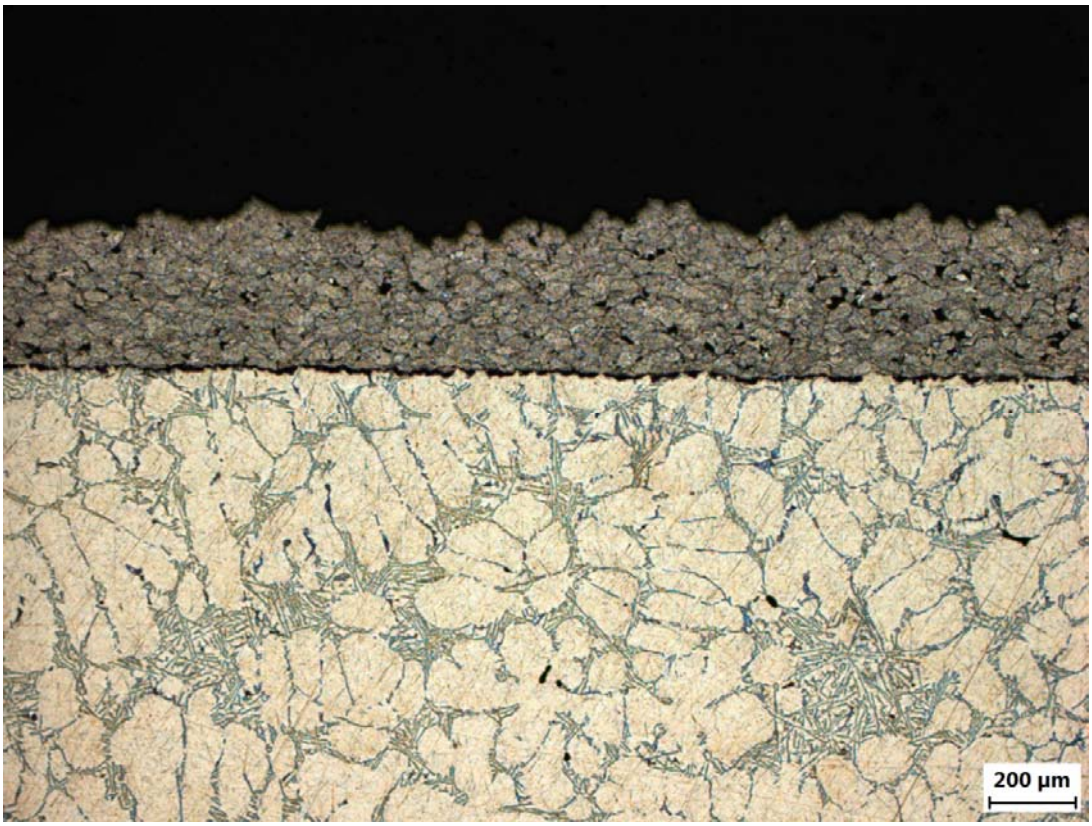

Figure 4.18a: SEM of Al-6061 coating which has been subjected to stress relief at 150 °C for 2 hours (50x magnification).

Figure 4.18b: SEM of Al-6061 coating which has been subjected to stress relief at 150 °C for 2 hours (200x magnification).

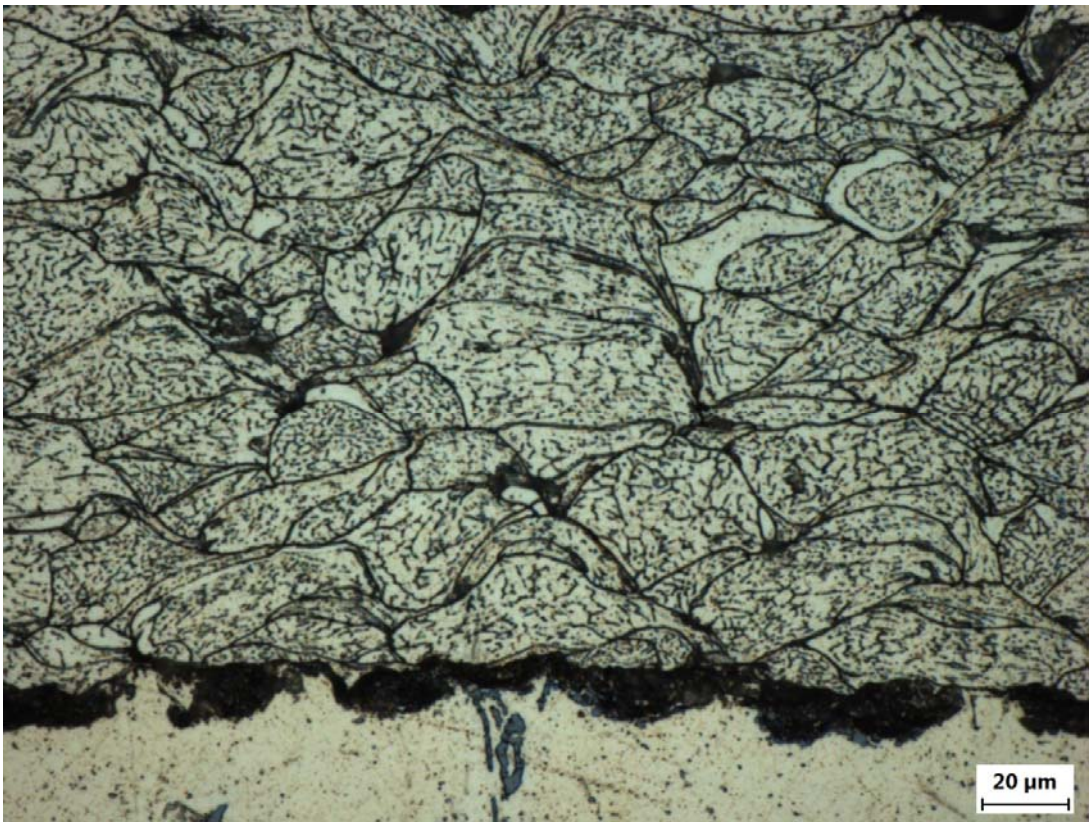

Figure 4.18c: SEM of Al-6061 coating which has been subjected to stress relief at 150 °C for 2 hours (500x magnification).

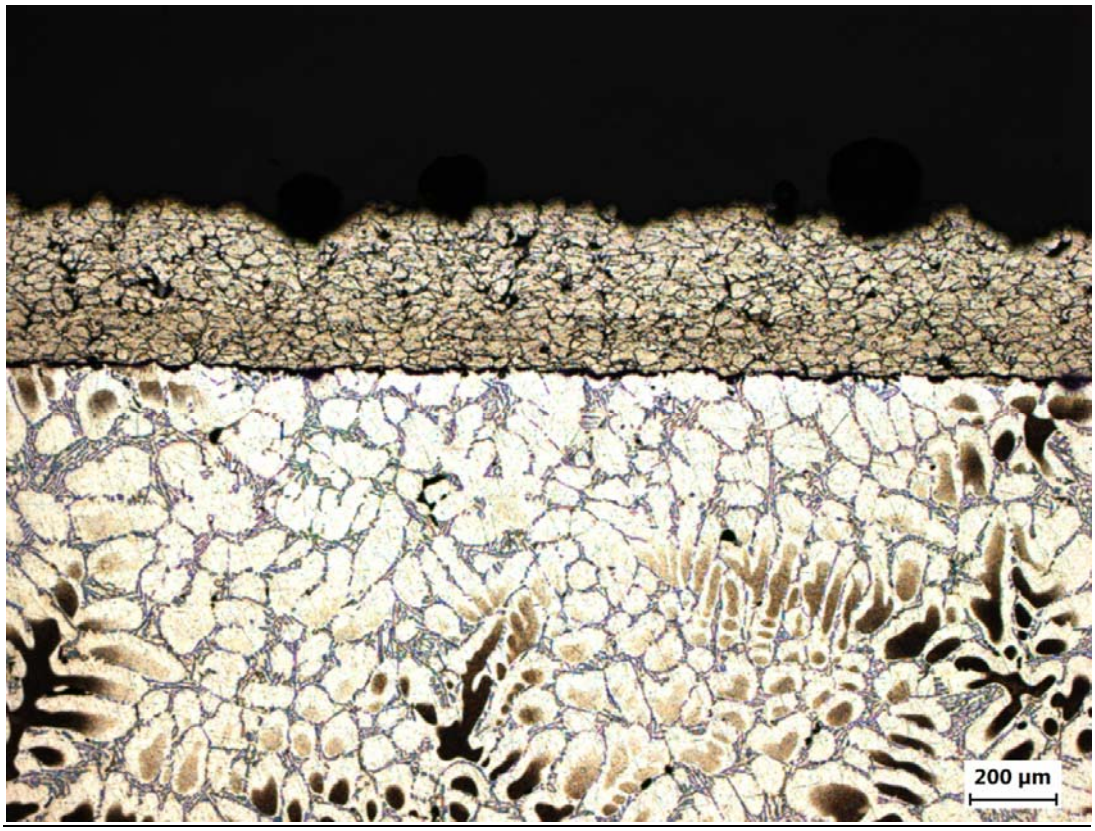

Figure 4.19a: SEM of Al-6061 coating which has been subjected to annealing at 535 °C for 2 hours followed by 177 °C for 8 hours (50x magnification).

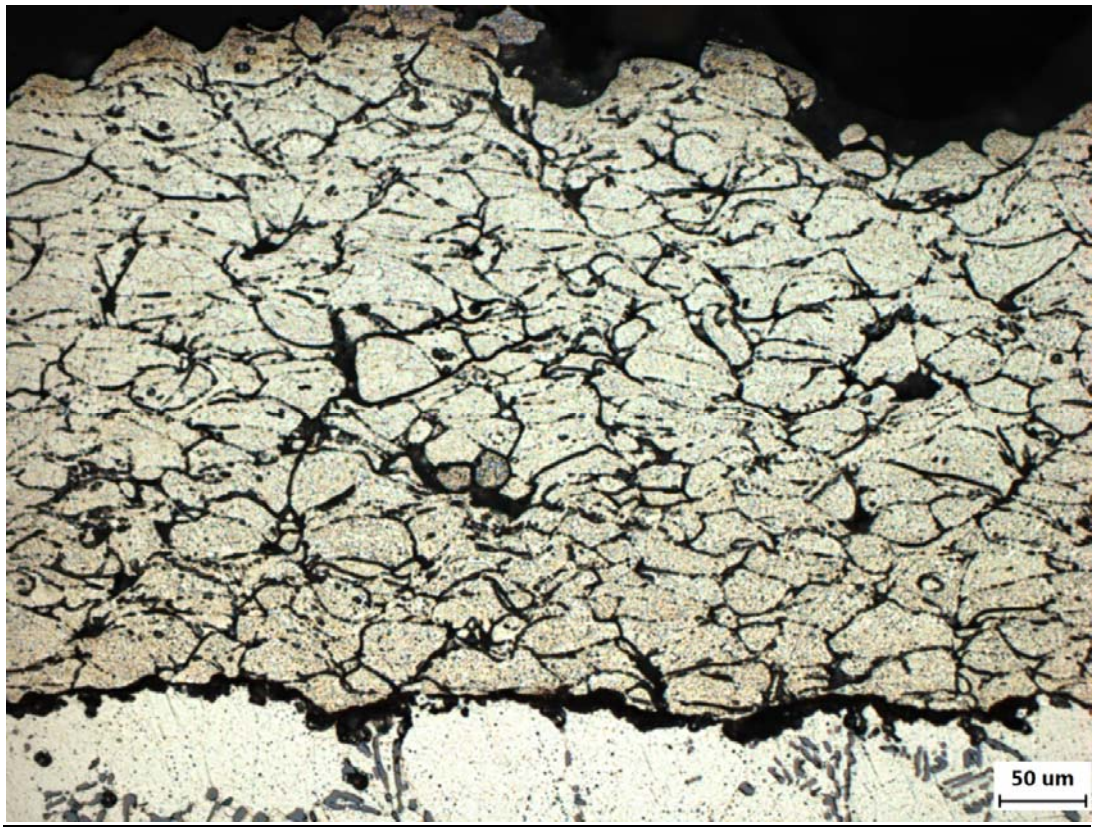

Figure 4.19b: SEM of Al-6061 coating which has been subjected to annealing at 535 °C for 2 hours followed by 177 °C for 8 hours (200x magnification).

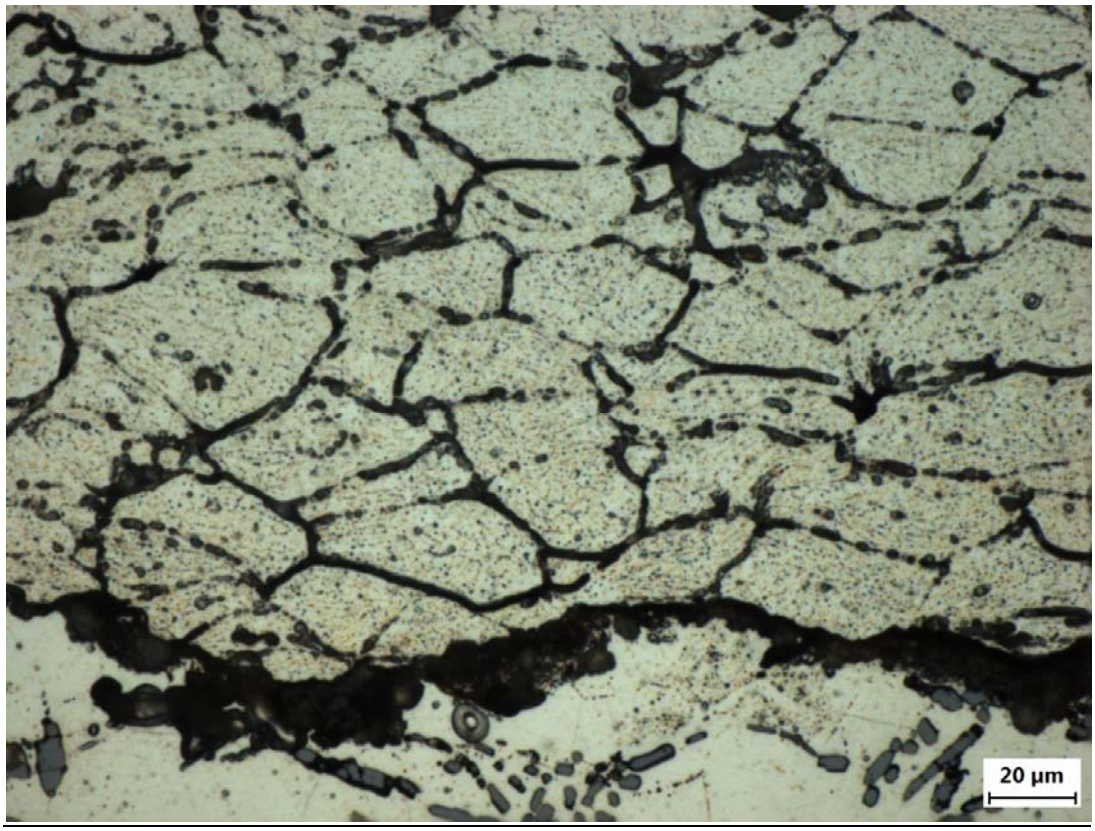

Figure 4.19c: SEM of Al-6061 coating which has been subjected to annealing at 535 °C for 2 hours followed by 177 °C for 8 hours (500x magnification).

Comparative examination of the microstructures of the coating which has undergone stress relief (Figures 4.18a to 4.18c) and that which has not (Figures 4.13a to 4.13c) does not reveal significant difference in grain structures or defects (voids, porosity etc) between the 2 coatings. There is also little difference observed at the substrate-coating interface for both sets of coatings. This observation is consistent with the similar tensile adhesion test results for both test coatings.

Analysis of the microstructures of the coating which has undergone full annealing (Figures 4.19a to 4.19c) reveals signs that recrystallisation and grain growth have taken place. In particular, the laminar particle shape of the coating in Figure 4.19c indicates that diffusion and fusion of the coating particles occurred under the elevated temperature environment. The uniformity of the change across the span of the coating also explains the fairly uniform microhardness results shown on Figure 4.14 where the change in microhardness from the top of the coating to the substrate coating interface was less than 4%.

4.4 Conclusion

In this chapter, the effect of pre-coating substrate preparation in the form of surface roughening by grit blasting on the coating microhardness was first examined. The comparative results suggested that grit blasting of the substrate has minimal impact on the microhardness of the coating. In addition, it was also observed that the microhardness increases progressively in the vertical direction from the top of the coating to the substrate-coating interface, reaching a maximum value of about 100 HV_{100g} at between 200 µm to 250 µm from the top coating layer. The maximum microhardness value of the coating was almost identical to the microhardness of the substrate. This is attributed to the gradual compaction of the coatings as the high velocity impinging particles constantly and repeatedly impact on the previously deposited underlying coating. The cumulative effect on that process is a coating with a microhardness which is equivalent to the substrate.

The effect of grit blasting of the substrates on the coating tensile adhesion strength was also investigated. The results suggest that the tensile adhesion strength of the coating on the non-grit blasted substrate is significantly higher than that on the grit blasted substrate. Microstructure evaluation of the coating on the grit blasted substrate indicates the presence of a layer of porosity or voids between the substrate and the coating which is likely due to the grit blasting process. It is believed that the micro-voids created by the angular alumina grit could have prevented the larger cold sprayed particles from plastically deforming into the substrates as well as prevented the formation of bonds due to hydrodynamic flow instability of the adiabatic shear instability. The presence of impurities from the alumina grit may have contributed to the decrease in tensile adhesion strength as well. As for the coating formed on the non-grit blasted substrate,

the microstructure evaluation suggests that the enhanced tensile adhesion strength of the coating could be the result of an inherent triplex characteristic of the cold spray process, in which the grit blasting, spray coating and shot peening are all carried out in a single pass. It can be seen that the surface of the substrate had deformed to about the same size as the impinged cold spray particles which seem to have plastically deformed and bonded tightly into the substrate. This observation will be further investigated in Chapter 6.

The effect of heat treatment on the mechanical properties of the cold sprayed coatings was investigated. The average microhardness of the coatings which have undergone stress relief and full annealing was almost identical. They are however, significantly lower compared to the coating which had not undergone any heat treatment, implying that heat treatment does have an effect of increasing the ductility of the cold spray coating. The uniformity of the coating microhardness in the vertical direction from the top of the coating to the substrate-coating interface was also investigated. The results indicate that heat treatment has a homogenizing effect on the microhardness of the coating.

The effect of heat treatment on the coating tensile adhesion strength was also studied. The results suggest that stress relief has little impact on the tensile adhesion strength compared to the coating which has not undergone any heat treatment. However, there was a significant improvement for coatings which has undergone full annealing. Microstructure evaluation of the latter reveals signs that recrystallization have taken place.

CHAPTER 5

EFFECT OF SPRAY ANGLE ON COATING MECHANICAL PROPERTIES

5.1 Introduction

In an ideal cold spray set-up, the cold spray nozzle will be positioned normally to the substrate throughout the spraying process to ensure the consistent and quality of the coating. However, this condition is not always possible as components are usually complex in geometry and sizes. Thus it is crucial to understand the effect of spray angle on the coating properties. This chapter describes the experiments which were carried out to study the effect of the spray angle (θ) of the cold spray nozzle on the mechanical properties of the cold spray coating. Microstructure evaluation of single splat coating formed at various spray angles was first performed. Subsequently, microhardness assessment, tensile adhesion strength test and microstructure evaluation of the coating formed at various spray angles were carried out. The relative coating deposition efficiency at various spray angles was also studied to understand the relationship between the two. The intent is to understand the impact of spray angle on the effectiveness of the coating process and assess the possible detrimental effect of cold spraying a component at high off-normal angles.

5.2 Single Splat Experiment

Circular Al-6061 substrates with diameter of 32 mm and 10 mm in thickness were machined from an Al-6061 bar stock of the same diameter. The substrates were polished using the Struers (Ballerup, Denmark) polisher model TegraPol-25 as shown in Figure 5.1. Grit paper of increasing finer grades, in order of 400, 800 and 1000 were used. The Surtronic Duo Surface Roughness Tester (Taylor Hobson, UK) was subsequently used to measure the mean arithmetic surface roughness of the polished substrates and the average result recorded was 0.7 Ra. The substrates were subsequently kept in a desiccant chamber until they were ready to be cold sprayed to prevent oxidation on the surfaces.

Gas atomized Al-6061 powder (Valimet Inc., USA) similar to those used in Section 4.2 was used for the experiment. The particles are spherical in shape. The diameter of the particles ranges from 5 μm to 50 μm with the average diameter measured at 28 μm. The scanning electron microscope (SEM) images of the Al-6061 feedstock powder are shown in Figure 4.4.

The experiment was carried out using the PCS-1000 cold spray system (Plasma Giken CO. Ltd., Japan), similar to the system used in Section 4.2. Nitrogen was used as the carrier gas and the flow rate was set at 250 standard litres per minute (SLM). The gas pressure was set at 4 MPa and the temperature at 400 ºC. The splats were sprayed by a line movement robot programme with a traversing speed of 1000 mm/s. This fairly rapid speed was chosen to allow individual splats to be segregated from each other and yet when compared to the velocity of the impacting particles which are in the

magnitudes of 400 to 500 m/s, have a negligible impact on the overall direction of the impacting particles. The standoff distance was set at 25 mm and only a single pass was made to avoid overlapping the splats. The parameters used in this experiment are shown in Table 5.1.

Figure 5.1: Struers Polisher model TegraPol-25.

Table 5.1: Cold spray parameters for single splat experiment.

Parameter	Value
Carrier gas	Nitrogen
Carrier gas pressure	4 MPa
Carrier gas temperature	400 ºC
Carrier gas flow rate	250 SLM
Robot traversing speed	1000 mms^{-1}
Robot step	N.A.
Stand-off distance	25 mm
Number of passes	1

The spray angle is defined as the angle between the centerline of the spray nozzle and substrate surface as shown in Figure 5.2.

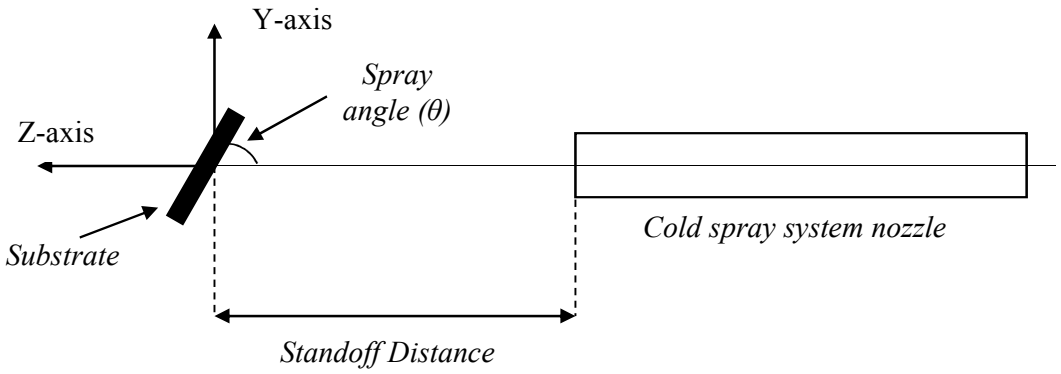

Figure 5.2: Schematic diagram of experimental set-up for spray angle investigation.

The variation in spray angle was adjusted by using the tilting mechanism of the turn table which the substrate was mounted on as shown in Figure 5.3. By turning the tilting wheel, the turn table can be inclined forward to vary the angle of spray while holding the cold spray nozzle horizontally straight. The angle of inclination of the turn table is measured with the help of the Compass application on an iPhone 4 (Apple Inc., California, USA) smartphone which has an accuracy of ± 0.1°.

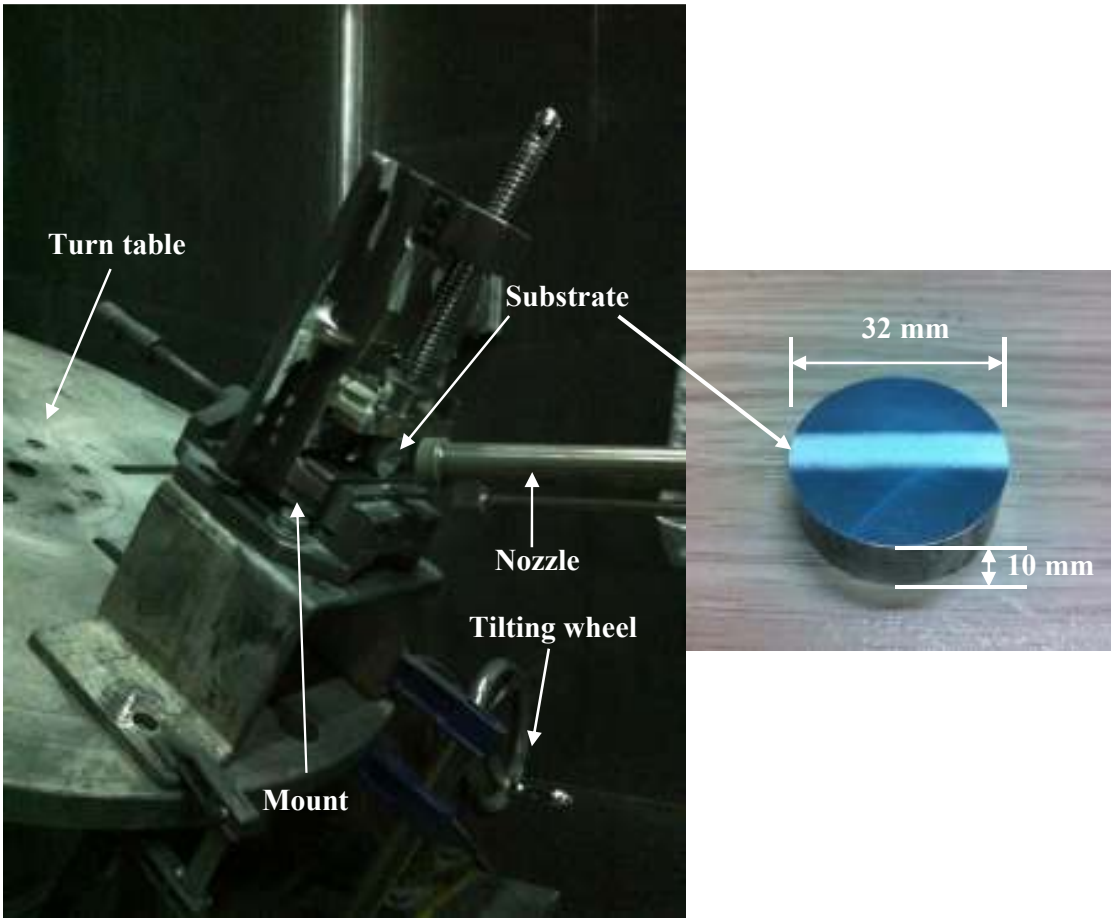

Figure 5.3: (a) Experimental set-up for varying spray angle single splat investigation and (b) 32 mm diameter circular Al-6061 substrate with Al-6061 coating.

In the current investigation, spray angles ranging from 90º to 40º at intervals of 10º were evaluated. This is illustrated on Figure 5.4. A total of 6 coated samples were obtained with one substrate sprayed for each spray angle. The samples were then examined under a microscope and the results are shown in Figures 5.5 to 5.10.

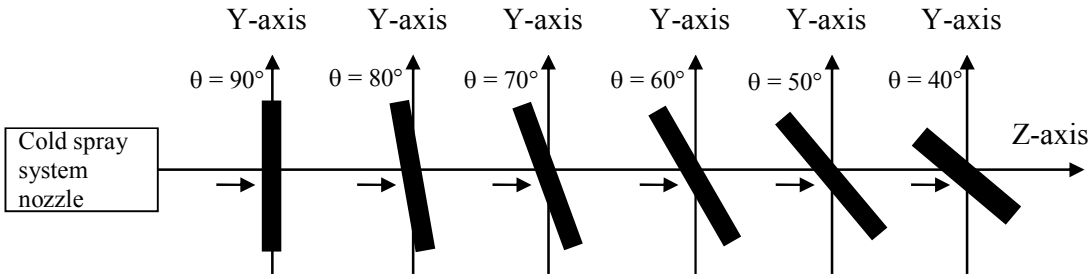

Figure 5.4: Schematic diagram for 6 spray angles conducted in the experiment.

Figures 5.5 to 5.10 each shows images of single splat of Al-6061 particles embedded on the Al-6061 substrate when sprayed at various spray angles. For each of the six spray angles, two images which are representative of the single splat particle are presented.

In Figure 5.5 in which the particles were sprayed at spray angle θ = 90°, the morphology of the Al-6061 particles remains circular in shape while the diameter of the embedded particles is within the feedstock powder particle size of between 5 to 50 μm. What can be seen on the peripheral of the embedded particle is an area characterized by a lighter shade. In a computational analysis work done by Grujicic et al (2003) to study the collision between a single aluminium particle with a copper substrate, the simulation results show the formation of a interfacial jet composing of materials from the substrate

and particle at the substrate-particle interface contact surface as the particle decelerates upon impact. This jet points away from the flattened particle as it reaches the free surface and the area is commonly termed jet explusion. When viewed from the top, this interfacial jet explusion appears as a lighter shade area circular ring around the embedded particle which was sprayed normally into the substrate.

As the spray angle decreases and become more off-normal, the impact splats as seen from Figures 5.6 to 5.10 become more and more elliptic when viewed from the top. This is a result of two factors; (1) the skip mark created as the particle decelerates across the substrate surface before coming to a complete stop by embedding itself to the substrate and (2) the more pronounced spreading effect of the particle as the tangential kinetic energy increases. As shown in Figure 5.11, when particles are sprayed at an angle which is off-normal to the substrate surface, the particle velocity (V_p) can be broken down into the normal (V_n) and tangential (V_t) components. The relationship is defined as follows:

$$V_n = V_p sin\theta$$

Eq. 5.1

$$V_t = V_p cos\theta$$

Eq. 5.2

When the spray angle θ = 90°, the normal component of the particle velocity will be equal to the particle velocity itself, i.e. $V_p = V_n$. While the tangential component would be equal to zero, $V_t = 0$.

As the spray angle decreases and the particles are hitting the substrate at a higher off-normal angle, the normal component of the particle velocity will decrease. Conversely, the tangential component will increase as the spray angle decreases. As the particle hits the substrate, the kinetic energy in the tangential direction is being converted to the particle spreading energy. The increase in the tangential kinetic energy as the spray angle decreases results in a more pronounced spreading effect of the particle and thus a more elliptic splat. In addition, a longer substrate surface distance is required to stop the particle and thus a more elongated elliptic impact splat is created as the spray angle θ decreases. This phenomenon is demonstrated in Figures 5.6 to 5.11.

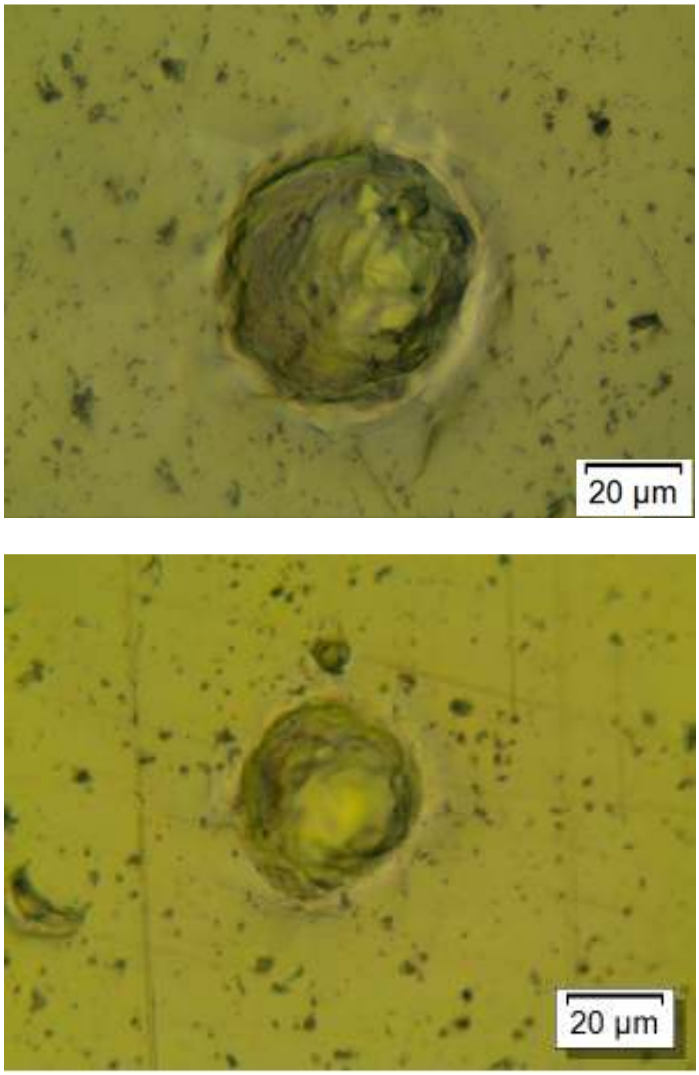

Figure 5.5a: Microscopic images of a single splat Al-6061 cold spray particle formed at spray angle θ = 90° at 1000x magnification.

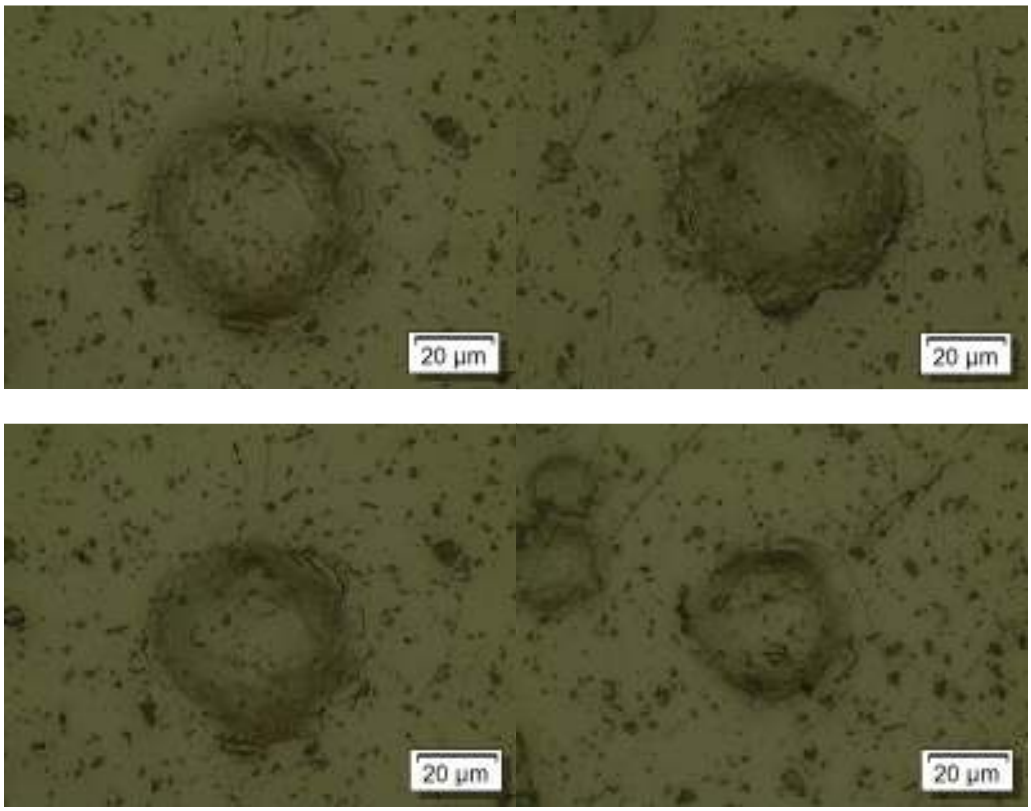

Figure 5.5b: Microscopic images of a single splat Al-6061 cold spray particle formed at spray angle θ = 90° at 1000x magnification using layered images.

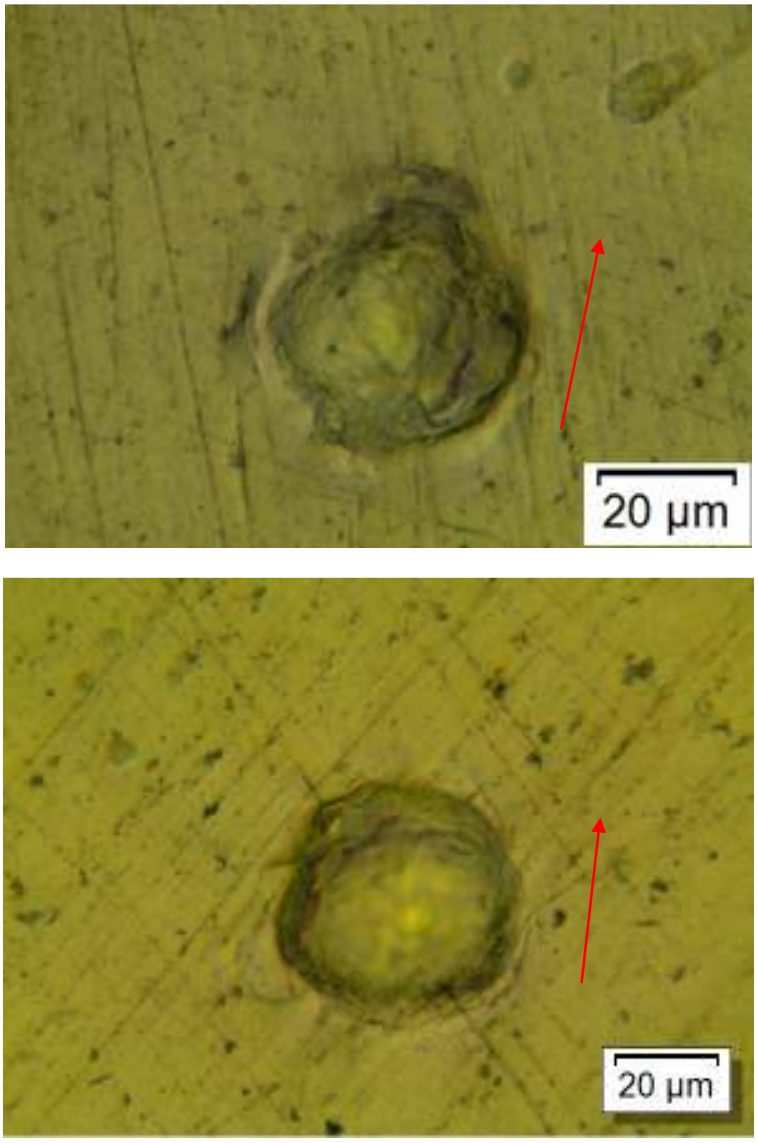

Figure 5.6a: Microscopic images of a single splat Al-6061 cold spray particle formed at spray angle θ = 80° at 1000x magnification. Arrows indicate the directions of the incoming particles.

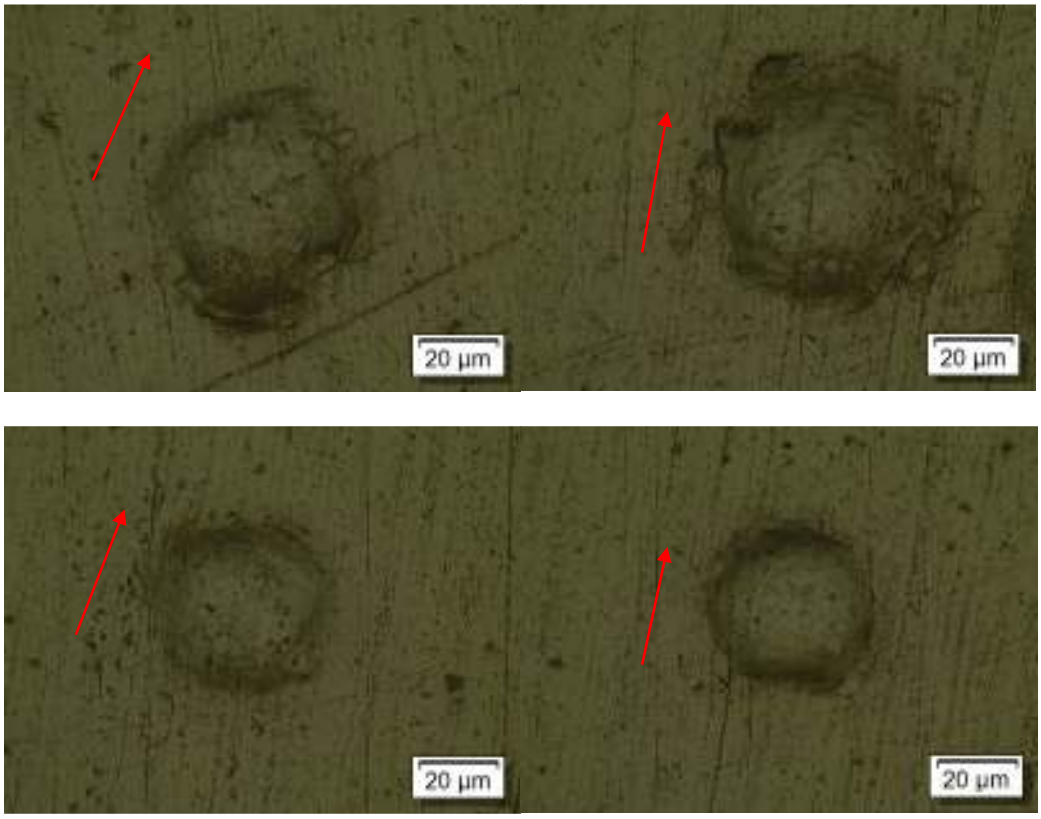

Figure 5.6b: Microscopic images of a single splat Al-6061 cold spray particle formed at spray angle θ = 80° at 1000x magnification using layered images. Arrows indicate the directions of the incoming particles.

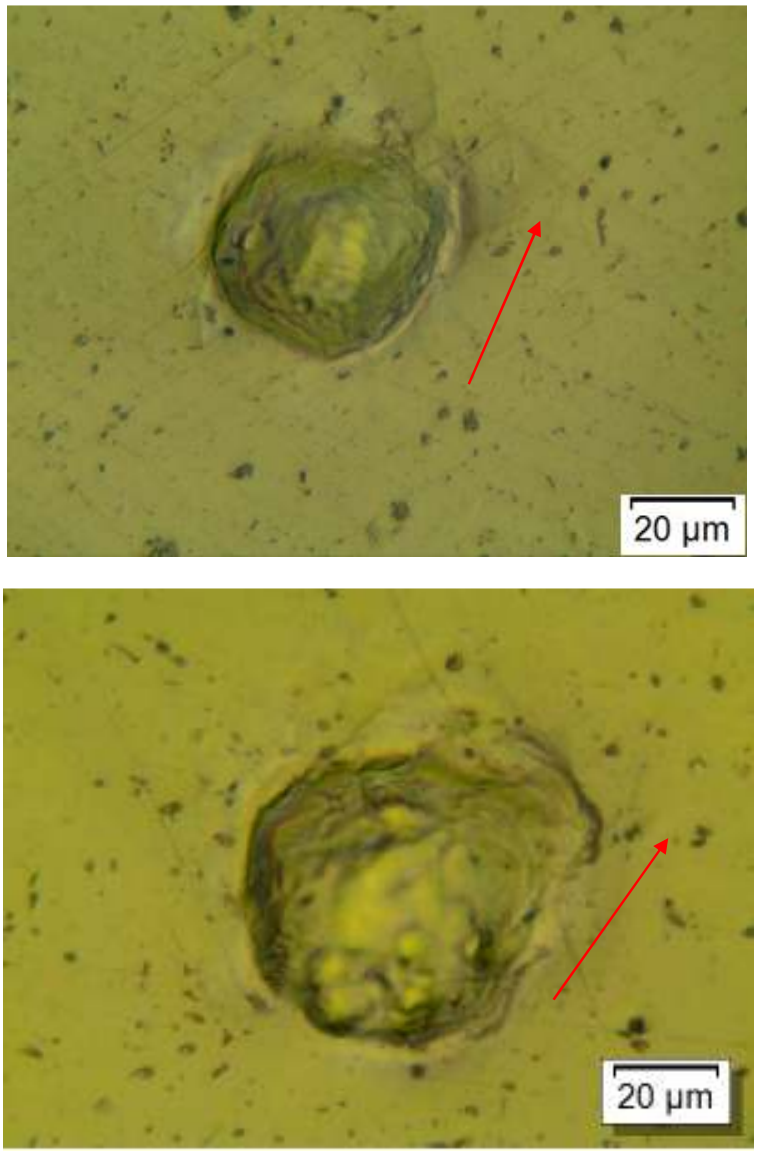

Figure 5.7a: Microscopic images of a single splat Al-6061 cold spray particle formed at spray angle θ = 70° at 1000x magnification. Arrows indicate the directions of the incoming particles.

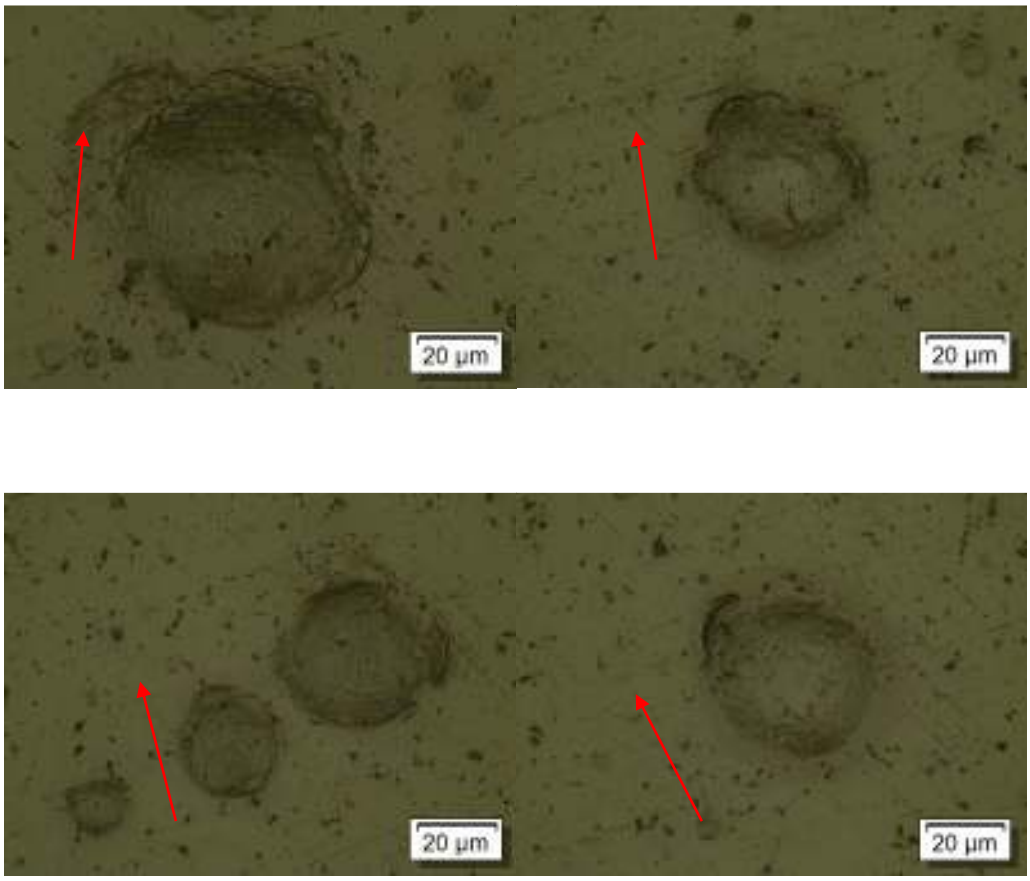

Figure 5.7b: Microscopic images of a single splat Al-6061 cold spray particle formed at spray angle θ = 70° at 1000x magnification using layered images. Arrows indicate the directions of the incoming particles.

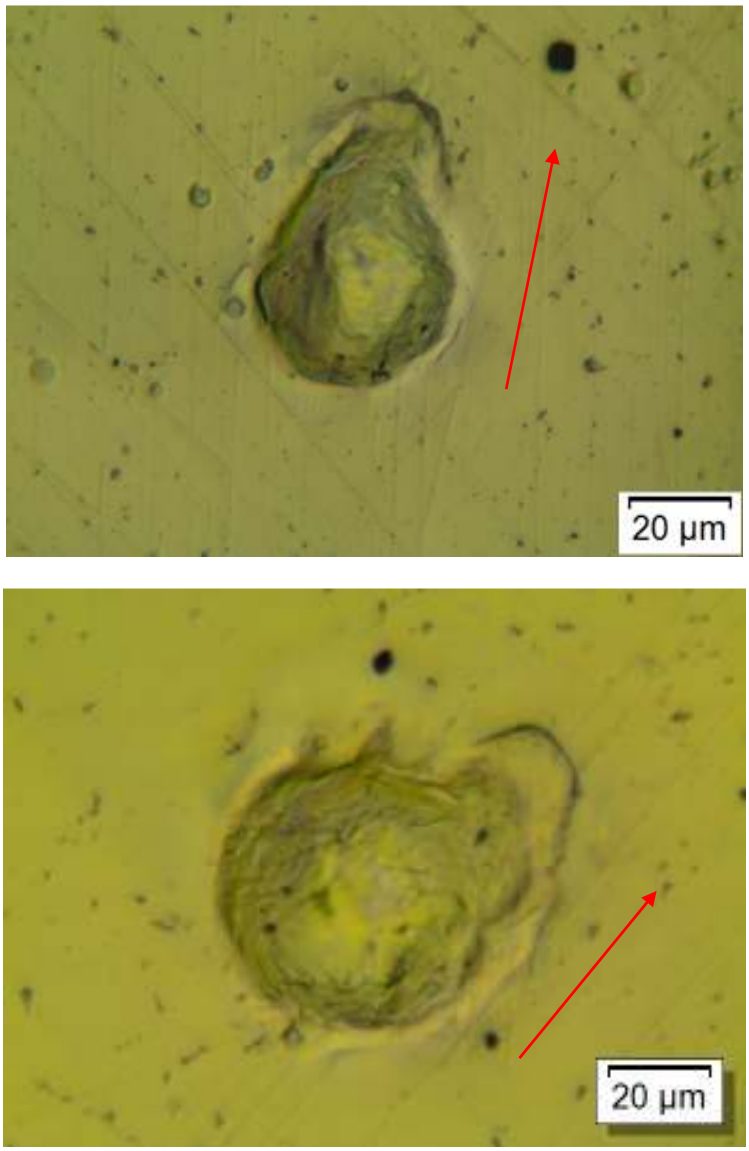

Figure 5.8a: Microscopic images of a single splat Al-6061 cold spray particle formed at spray angle θ = 60° at 1000x magnification. Arrows indicate the directions of the incoming particles.

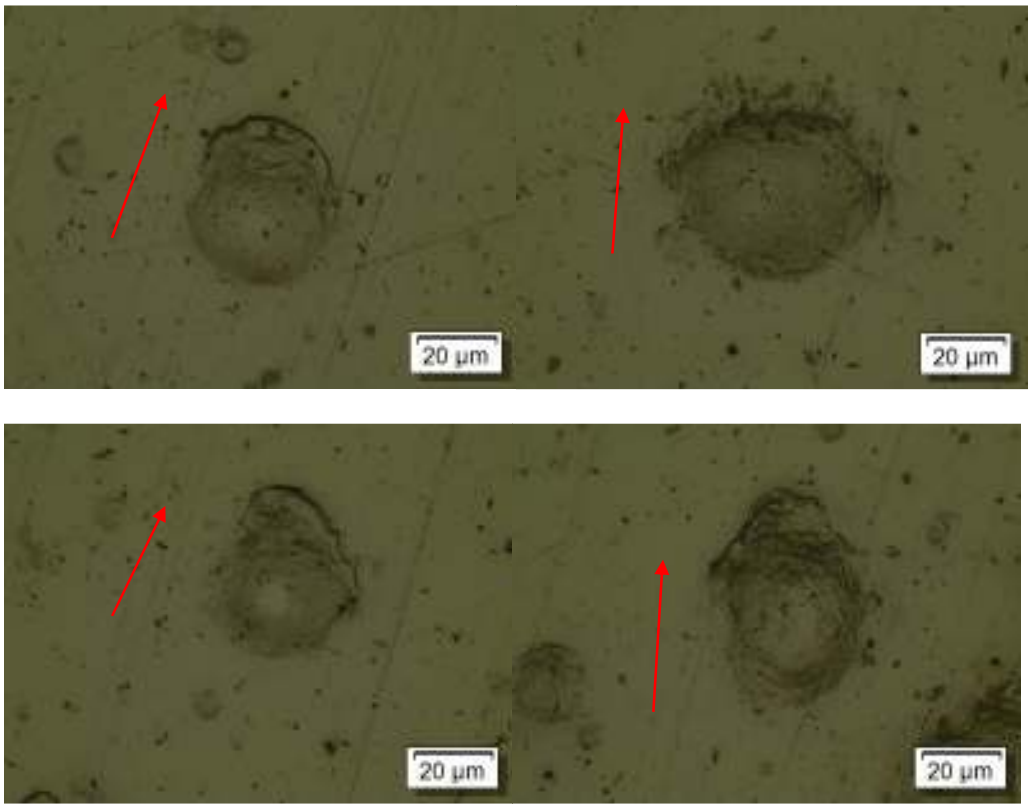

Figure 5.8b: Microscopic images of a single splat Al-6061 cold spray particle formed at spray angle θ = 60° at 1000x magnification using layered images. Arrows indicate the directions of the incoming particles.

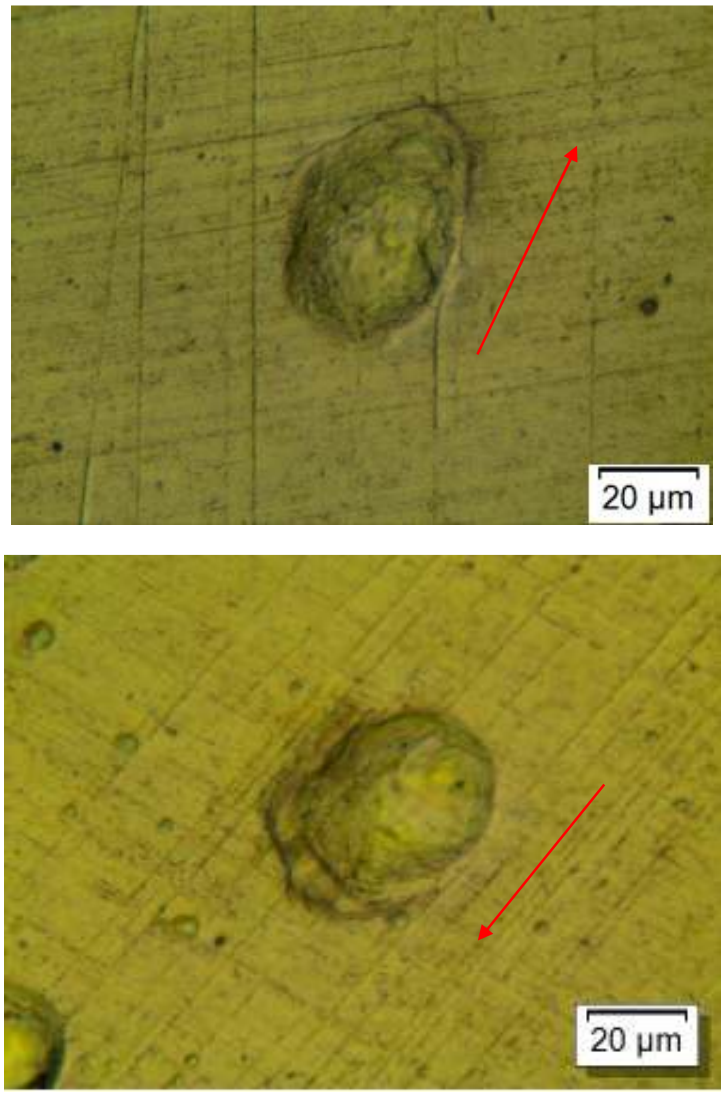

Figure 5.9a: Microscopic images of a single splat Al-6061 cold spray particle formed at spray angle θ = 50° at 1000x magnification. Arrows indicate the directions of the incoming particles.

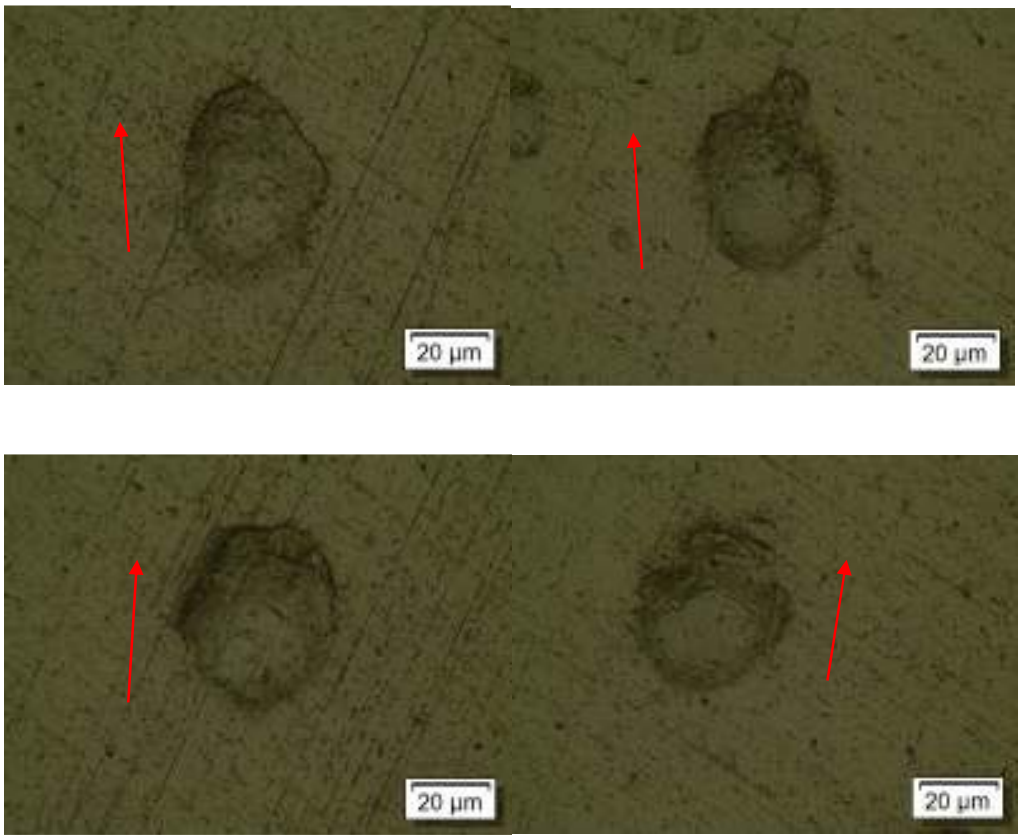

Figure 5.9b: Microscopic images of a single splat Al-6061 cold spray particle formed at spray angle θ = 50° at 1000x magnification using layered images. Arrows indicate the directions of the incoming particles.

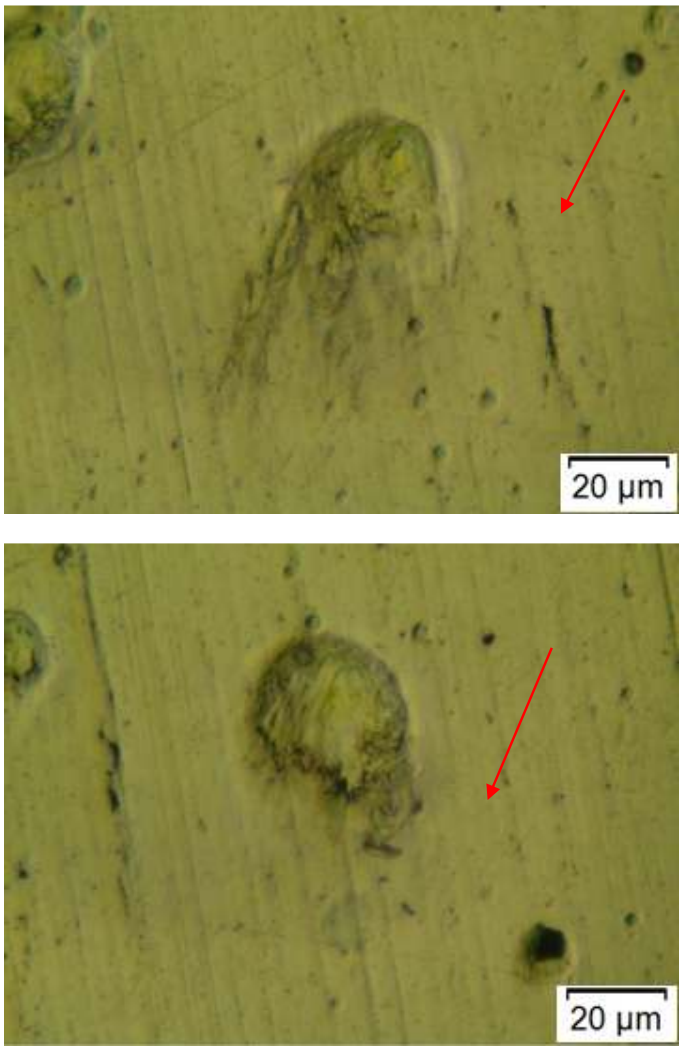

Figure 5.10a: Microscopic images of a single splat Al-6061 cold spray particle formed at spray angle θ = 40° at 1000x magnification. Arrows indicate the directions of the incoming particles.

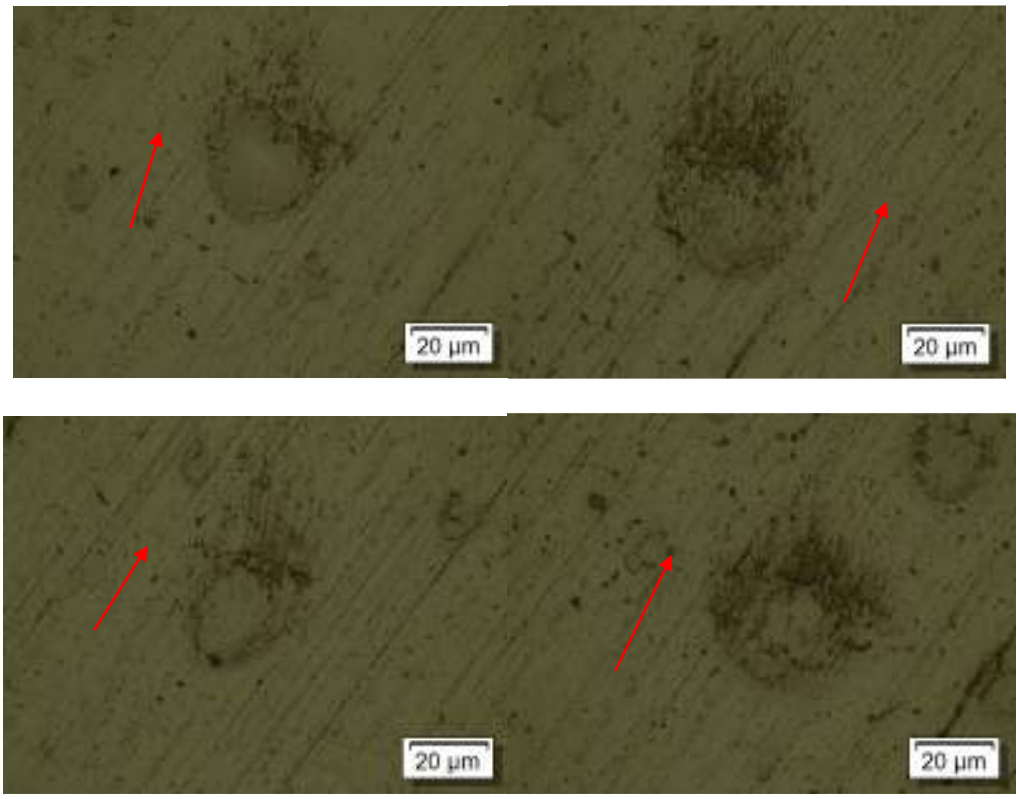

Figure 5.10b: Microscopic images of a single splat Al-6061 cold spray particle formed at spray angle θ = 40° at 1000x magnification using layered images. Arrows indicate the directions of the incoming particles.

5.3 Microhardness Test

The effect of the angle of incidence of the cold spray nozzle on the microhardness of the cold spray coating was investigated. Gas atomized Al-6061 powder (Valimet Inc, USA), identical to the ones used in Section 4.2.2 was used for the experiment. The cold spray process was carried out using the PCS-1000 cold spray system (Plasma Giken Co. Ltd., Japan). Five sets of experimental data each consisting of one sample were collected. The five sets of Al-6061 substrates were cleaned with acetone and cold sprayed without any grit blast. The powder was cold sprayed at 6 different angles of incidence of 90°, 80°, 70°, 60°, 50°, and 40° respectively. Nitrogen was used as the carrier gas and the flow rate was set at 250 standard litre per minute (SLM). The gas pressure was set at 4 MPa and the temperature at 400 ºC. The speed of the transversing robot was 200 mms^{-1} with a 1 mm step. The standoff distance was set at 25 mm and a total of two passes were made.

The coating samples were sectioned, mounted and polished. The mounted samples are shown in Figure 5.11. The average thickness of the coatings obtained was between 214 μm ($\theta = 40°$) to 991 μm ($\theta = 90°$). The microhardness measurements were subsequently made using the Matsuzawa MMT-X7 tester as shown in Figure 4.5. Five indentation measurements were taken from each sample using a 100 grams load (HV_{100g}) with a dwell time of 15 seconds along the transverse section which is approximately 150 μm from the substrate coating interface. The results are presented on Table 5.2.

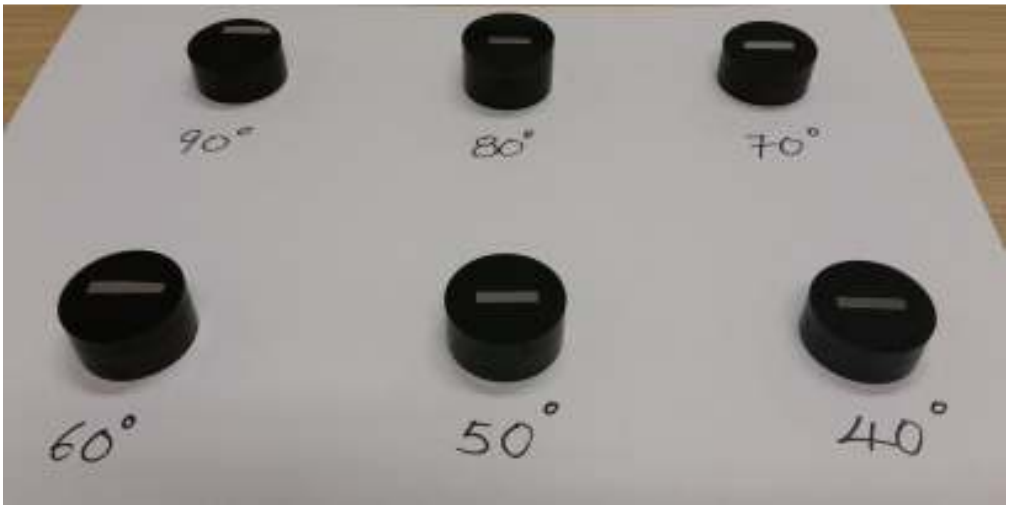

Figure 5.11: Samples of coatings obtained at various spray angles mounted for microhardness test.

Table 5.2: Microhardness measurement of cold sprayed Al-6061 coating obtained at various angle of incidence.

Spray angle	90° (HV_{100g})	80° (HV_{100g})	70° (HV_{100g})	60° (HV_{100g})	50° (HV_{100g})	40° (HV_{100g})
1	97.9	89.8	90.7	102.8	116.3	116.5
2	92.4	91.5	87.4	92.4	107.0	117.5
3	94.2	95.1	98.8	92.4	110.6	109.2
4	91.5	91.5	90.7	91.5	105.9	110.3
5	96.0	89.0	96.0	108.1	116.3	116.8
Average	**94.4 ± 2.6**	**91.4 ± 2.3**	**92.7 ± 4.6**	**97.4 ± 7.6**	**111.2 ± 5.0**	**114.1 ± 4.0**

From Table 5.2, the average microhardness values for the coatings obtained at spray angles of 90°, 80° and 70° were 94.4 HV_{100g}, 91.4 HV_{100g} and 92.7 HV_{100g} respectively. The values were fairly consistent and comparable to the microhardness value obtained previously in section 4.2.1. However, as the spray angle of incidence decreases from 60° to 40°, the average microhardness values increases from 97.4 HV_{100g} to 114.1

HV_{100g}. The increase in the average microhardness was as high as 20.9% when compared between the coating obtained at $\theta = 40°$ and $\theta = 90°$. There appears to be an incremental increase in average microhardness values as the spray angle of incidence decreases, suggesting an inversely proportional relationship between the microhardness of the coating and the spray angles. In fact, the highest microhardness value of 116.8 HV_{100g} was recorded at spray angle of incidence of 40°. This value is actually higher than the mean microhardness value for the Al-6061 substrate which was measured to be 107 HV_{100g}.

The possible reason for the increase in coating microhardness values as the spray angle decreases is the increase in plastic deformation of the feedstock particles as they collided onto the substrate with decreasing spray angle. The increase in plastic deformation promotes the dislocation within the crystal structure of the impinging particles, thus cold working the coating as it builds up. This in terms increases the microhardness of the coating. The resulting effect is the increase in microhardness of the coating as validated with the measured data.

5.4 Tensile Adhesion Strength Test

The effect of the angle of incidence of the cold spray nozzle on the tensile adhesion strength of the cold spray coating was investigated. Five sets of experimental data each consisting of three samples were collected in accordance to the ASTM C633-01 standards. The five sets of Al-6061 substrates were cleaned with acetone and cold sprayed without any grit blast. Gas atomized Al-6061 powder (Valimet Inc, USA), identical to the ones used in Section 4.2.1 was used for the experiment. The cold spray process was carried out using the PCS-1000 cold spray system (Plasma Giken Co. Ltd., Japan) and the cold spray conditions and parameters used were identical to those described in section 5.3.The coated samples are shown in Figure 5.12.

The samples were glued together using epoxy glue Klebbi (Oerlikon Metco, Winterthur, Switzerland) and cured at 200 °C for 2 hours. The tensile adhesion test of the specimens was tested using the MTS/SINTECH 65/G Universal Testing Machine with crosshead speed at 1 mms^{-1}. The test specimens after the adhesion strength test are shown in Figure 5.13. The results of the tensile adhesion strength test are presented on Table 5.3 and Figure 5.14. Tensile adhesion test data collected previously from Chapter 4.2.2 for spray angle of incidence of 90º at using identical cold spray parameters was also captured for our comparative analysis.

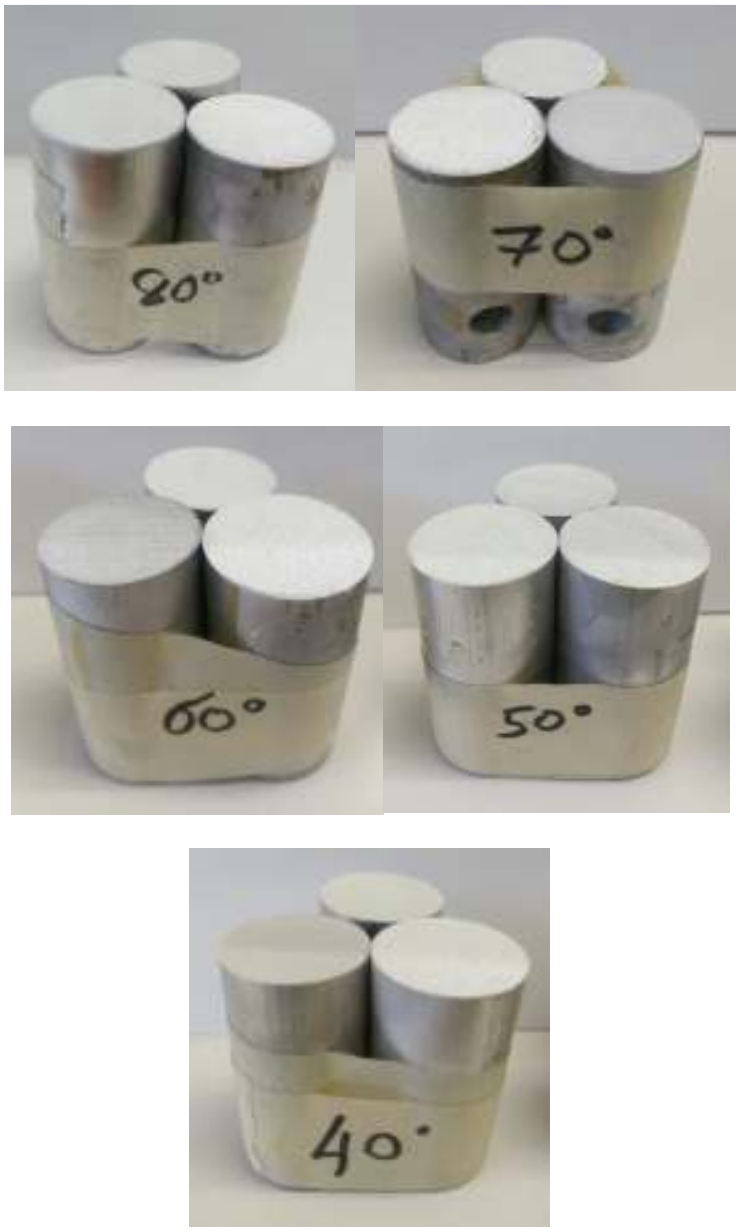

Figure 5.12: Tensile adhesion strength test specimen with coatings cold sprayed at angle of incidence of 80°, 70°, 60°, 50° and 40° respectively.

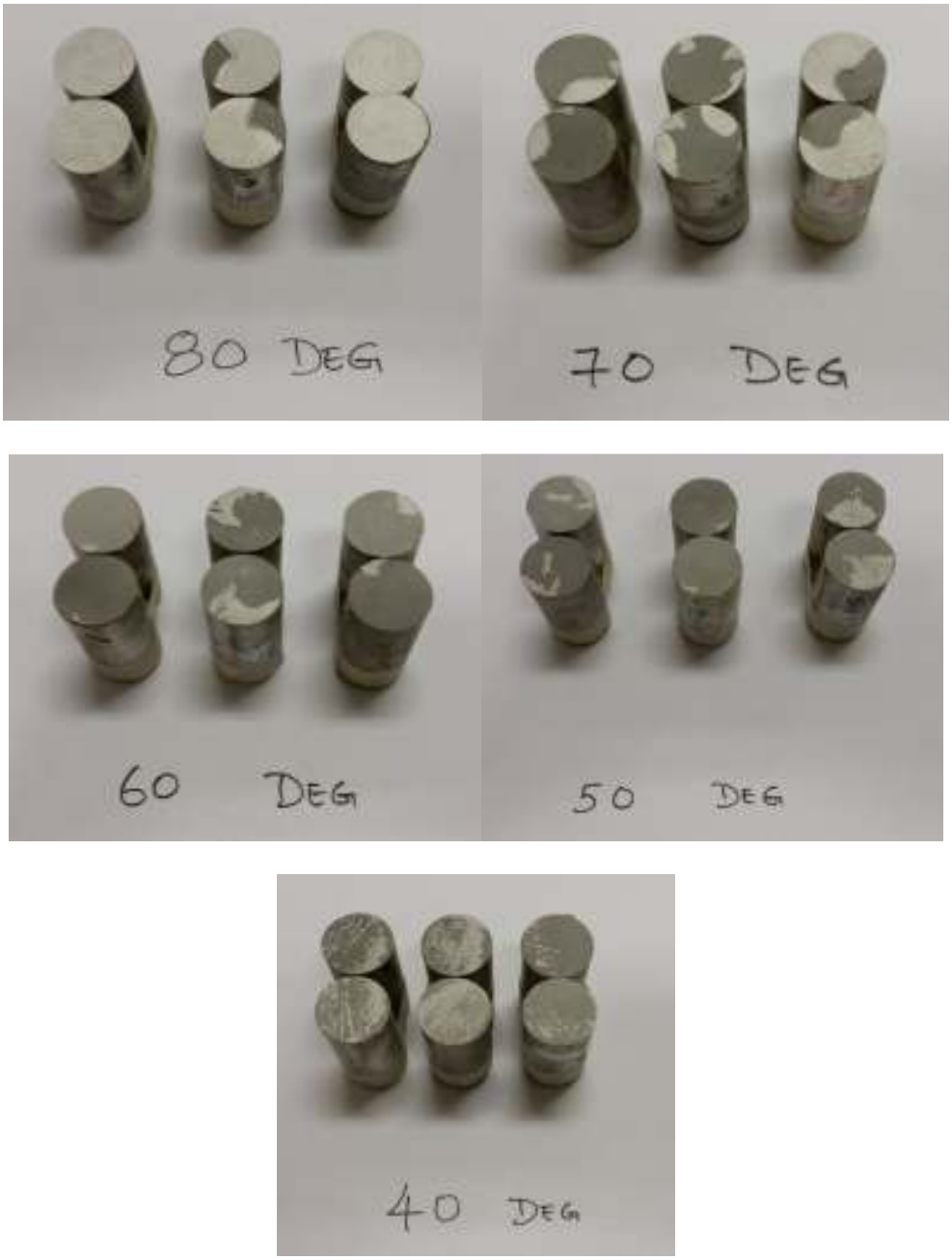

Figure 5.13: Specimen of coatings obtained at various spray angles after tensile adhesion strength test.

Table 5.3: Tensile adhesion test results for cold sprayed Al-6061 coating sprayed at various angle of incidence.

	Coating at 40 deg (MPa)	Failure Mode	Coating at 50 deg (MPa)	Failure Mode	Coating at 60 deg (MPa)	Failure Mode	Coating at 70 deg (MPa)	Failure Mode	Coating at 80 deg (MPa)	Failure Mode
1	46.93	Failure at coating/ substrate material interface	45.750	Failure at coating/ substrate material interface	54.43	Failure at coating/ substrate material interface	40.32	Failure at coating/ substrate material interface	47.11	Failure at coating/ substrate material interface
2	53.48		58.56		59.76		58.76		49.56	
3	58.83		68.35		60.86		68.77		62.22	
Ave	**53.08**		**57.55**		**58.35**		**55.95**		**52.96**	
±	**5.96**		**11.33**		**3.44**		**14.43**		**8.11**	

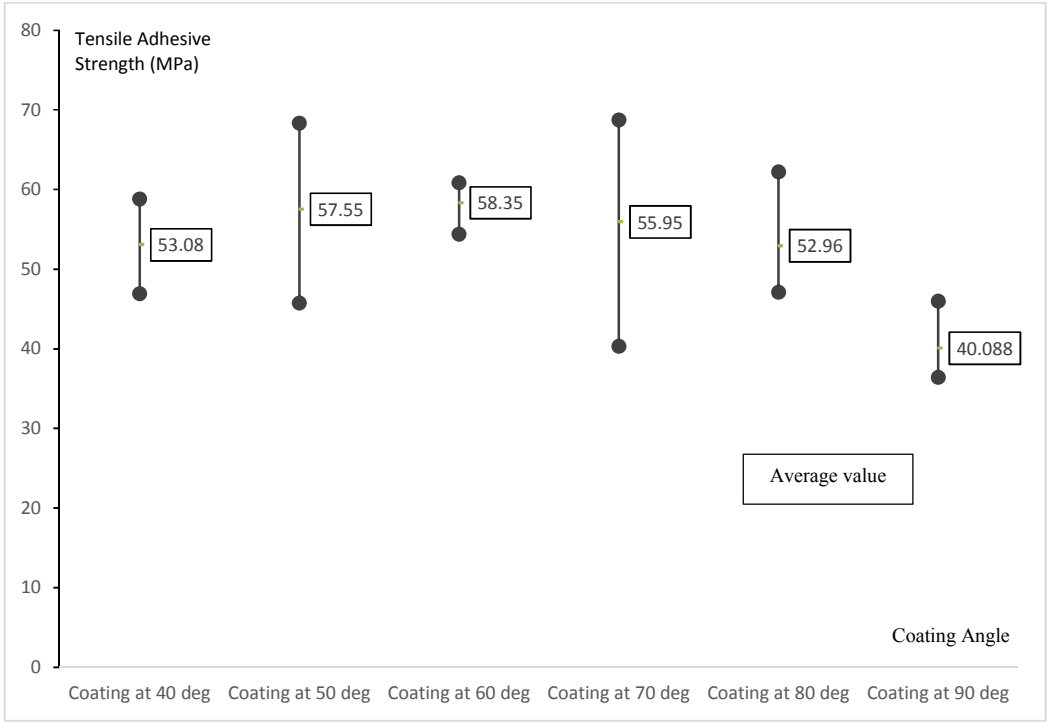

Figure 5.14: Tensile adhesion test results for cold sprayed Al-6061 coatings obtained at various spray angles.

From Figure 5.14, the average mean tensile adhesion strength for the coatings obtained at various angle of incidence seem to vary very little from 40° to 80° spray angles. The highest mean tensile adhesion strength was 58.35 MPa obtained with a spray angle of 60° compared with the lowest value of 52.96 MPa obtained with a spray angle of 80°. This was a reduction of only 9.2%. The tensile adhesion strength test results seem to suggest that the spray angle has minimal impact on the tensile adhesion of the coatings. In fact, when the results were compared with the coating which was sprayed directly perpendicular to the substrate surface, the mean tensile adhesion strength of coatings obtained from 40° to 80° were all marginally higher.

The results of the tensile adhesion strength test suggests that once the particle hits a certain critical velocity and forms a coating, the adhesion between the particle and the substrate will remain within a certain value. This is regardless of the angle at which the particle hits the substrate. There seems to be little or no relationship between the tensile adhesion strength and the spray angles once a coating is formed.

5.5 Microstructure Evaluation

The microstructure of the coatings obtained at various spray angles was examined using a microscope. The coating samples were sectioned, mounted, etched and prepared according to ASTM E3-11 standard. The samples were subsequently examined under different magnifications and the results are shown in Figures 5.15 to 5.20.

The microscopic images of all the coatings show very well defined coating-substrate interface, with very close coating-substrate interaction. There was practically no visible

gaps or voids between the coating and the substrate in all the coatings obtained at all spray angles, including $\theta = 40°$. In terms of porosity within the coatings, the images do not show profound differences in porosity among all the coatings obtained.

The major difference in terms of coating microstructure observed among the images shown in Figures 5.15 to 5.20 is the cross-sectional geometry of the impinged particles, especially those embedded on the substrates. In Figure 5.15(c), the cross-sectional image of the coating obtained at spray angle $\theta = 90°$ shows the particles which are embedded on the substrate are relatively oval in shape and retain certain geometrical characteristics. However, as θ decreases, it was observed that the particles take on a more irregular geometry. At $\theta = 40°$, as shown in Figure 5.20, the splats at the coating-substrate interface take on the shape of the contour of the substrate surface, hugging the peaks and valleys as the particles embedded onto the substrate. This validates the higher coating microhardness value obtained at lower spray angles ($\theta \leq 60°$) which was postulated to be due to the higher plastic deformation of the particles and cold working effect on the particles.

The images also provided us with insights on the reason why the tensile adhesion strength was not affected by the decreasing spray angle. The overall strength of the coating-substrate adhesion bond is dependent on the magnitude of the contact surface area between the particle and the substrate. Based on the images of the cross-sectional areas of all the coatings, the contact surface area was not affected even as the spray angle decreases. All the particles adhere closely to the substrate surface. This explains why the tensile adhesion strength for all the spray angles were almost identical.

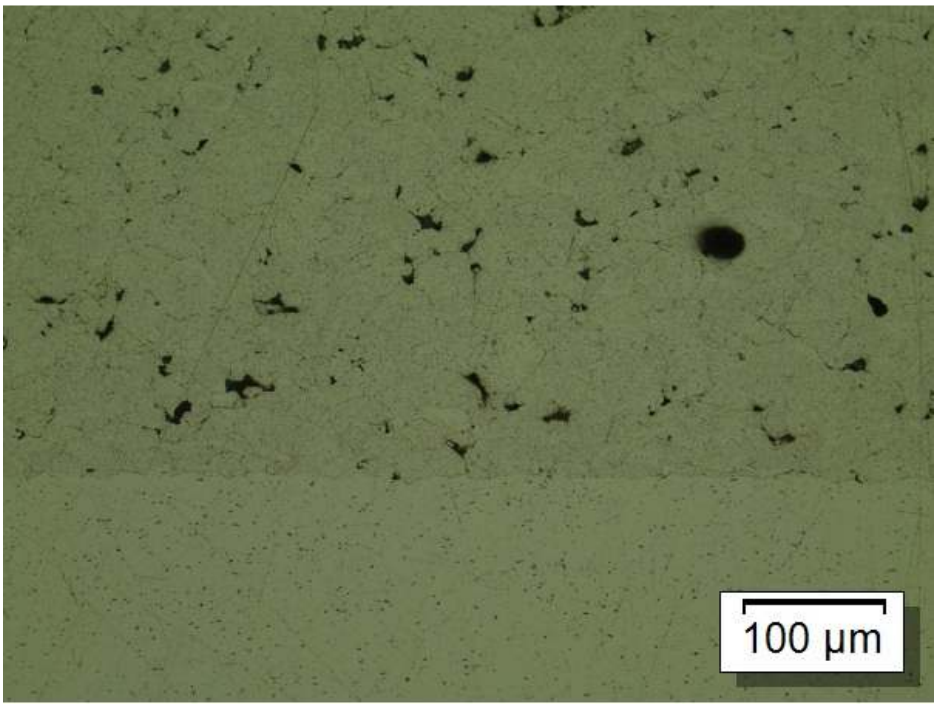

Figure 5.15a: Microscopic images of Al-6061 coating obtained at spray angle 90° (200x magnification).

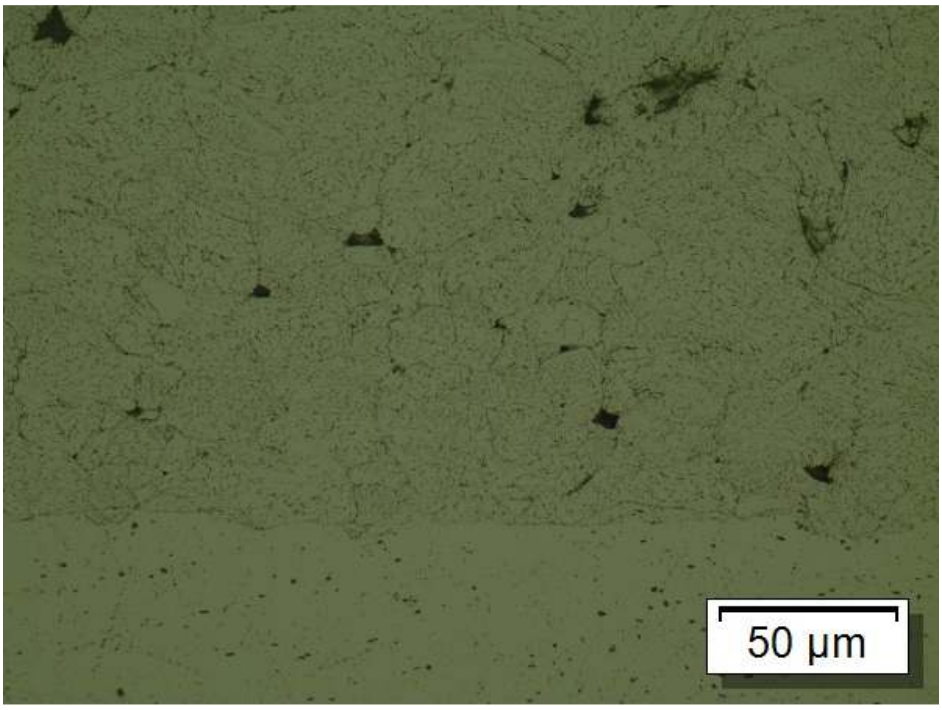

Figure 5.15b: Microscopic images of Al-6061 coating obtained at spray angle 90° (500x magnification).

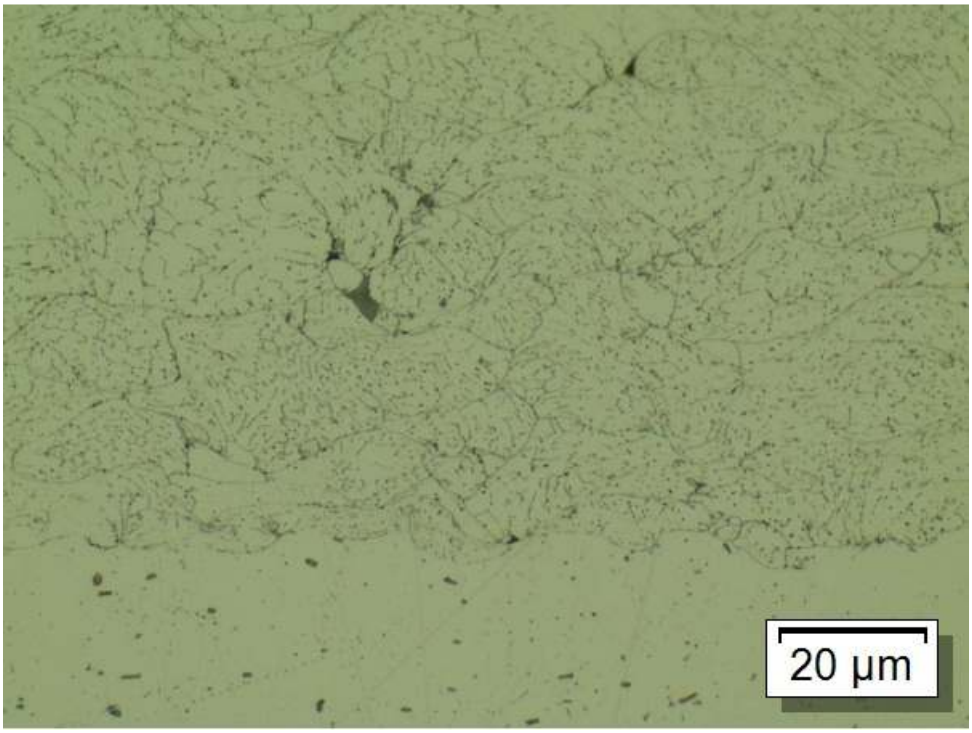

Figure 5.15c: Microscopic images of Al-6061 coating obtained at spray angle 90° (1000x magnification).

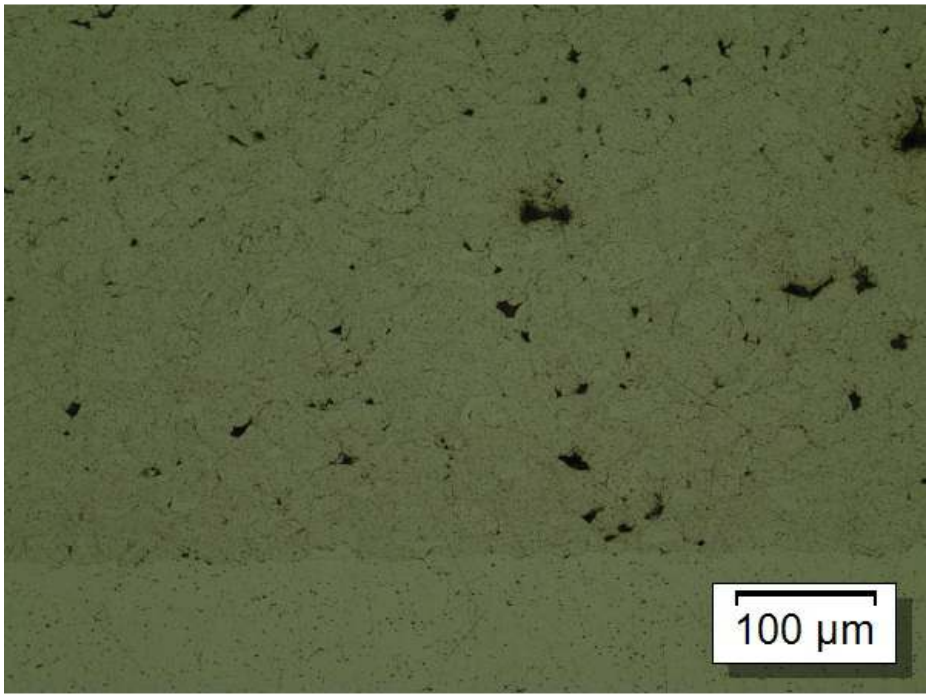

Figure 5.16a: Microscopic images of Al-6061 coating obtained at spray angle 80° (200x magnification).

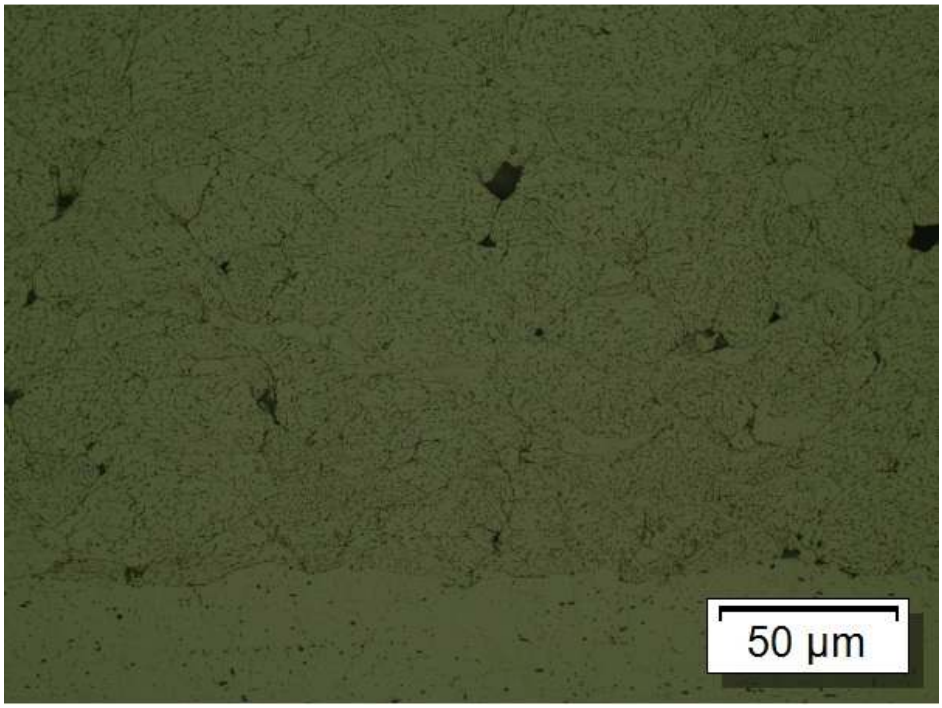

Figure 5.16b: Microscopic images of Al-6061 coating obtained at spray angle 80° (500x magnification).

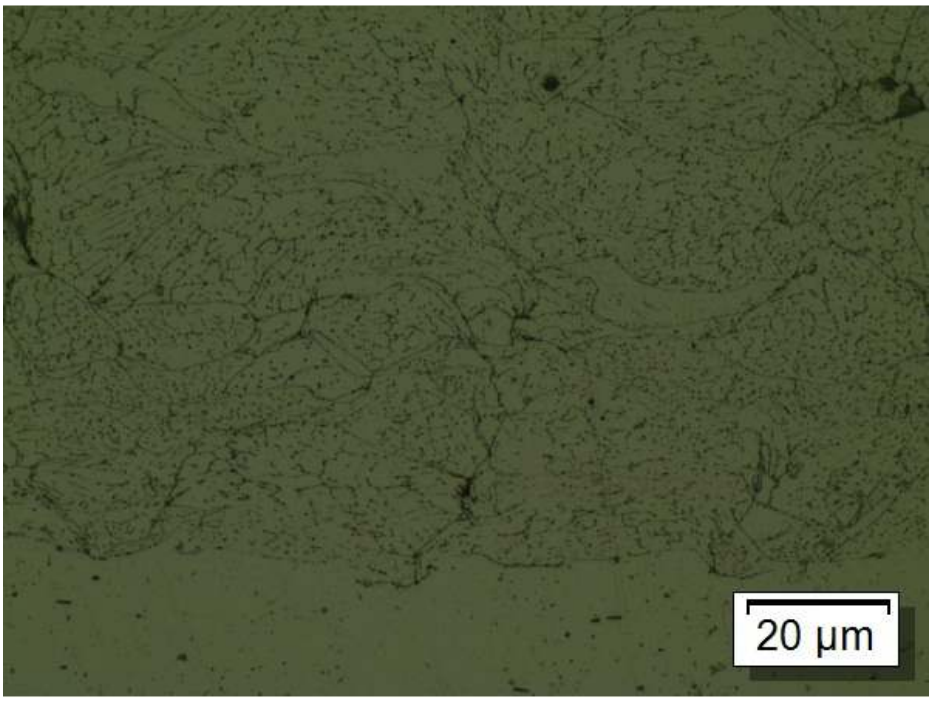

Figure 5.16c: Microscopic images of Al-6061 coating obtained at spray angle 80° (1000x magnification).

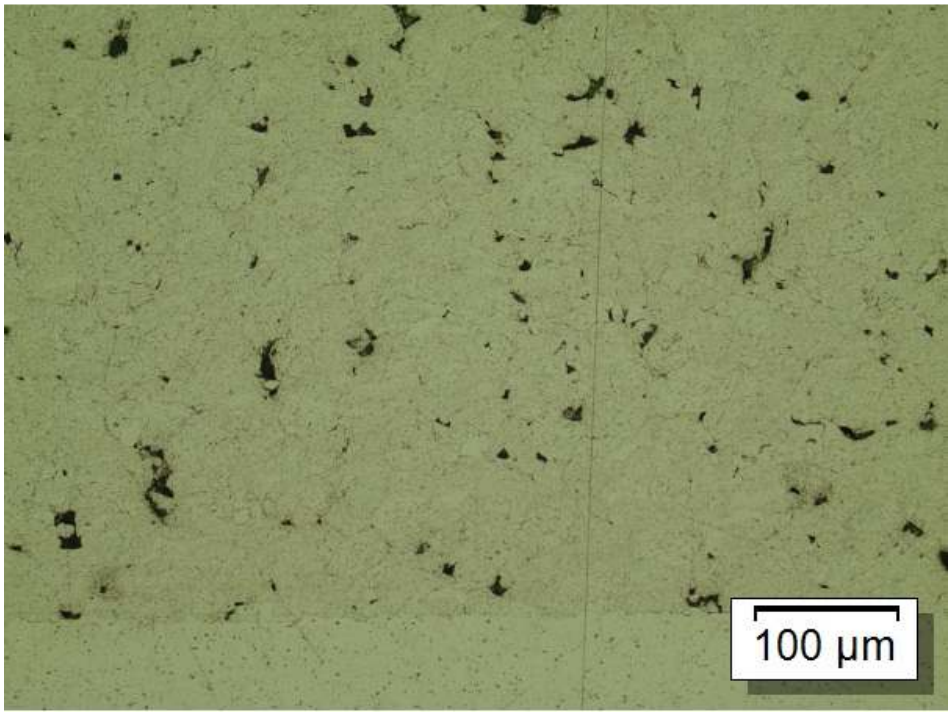

Figure 5.17a: Microscopic images of Al-6061 coating obtained at spray angle 70° (200x magnification).

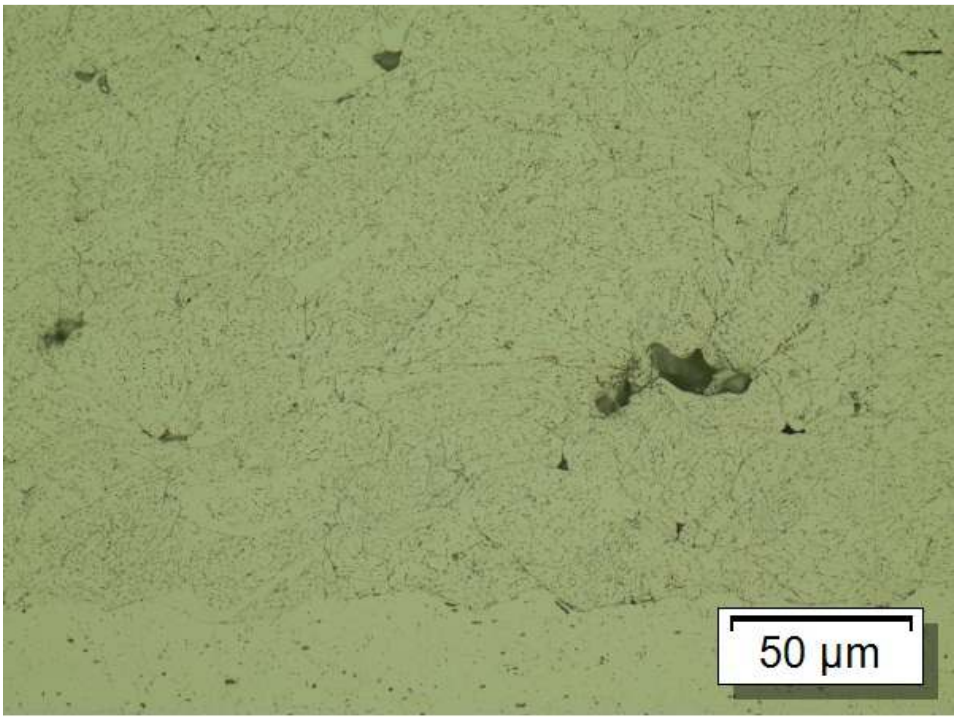

Figure 5.17b: Microscopic images of Al-6061 coating obtained at spray angle 70° (500x magnification).

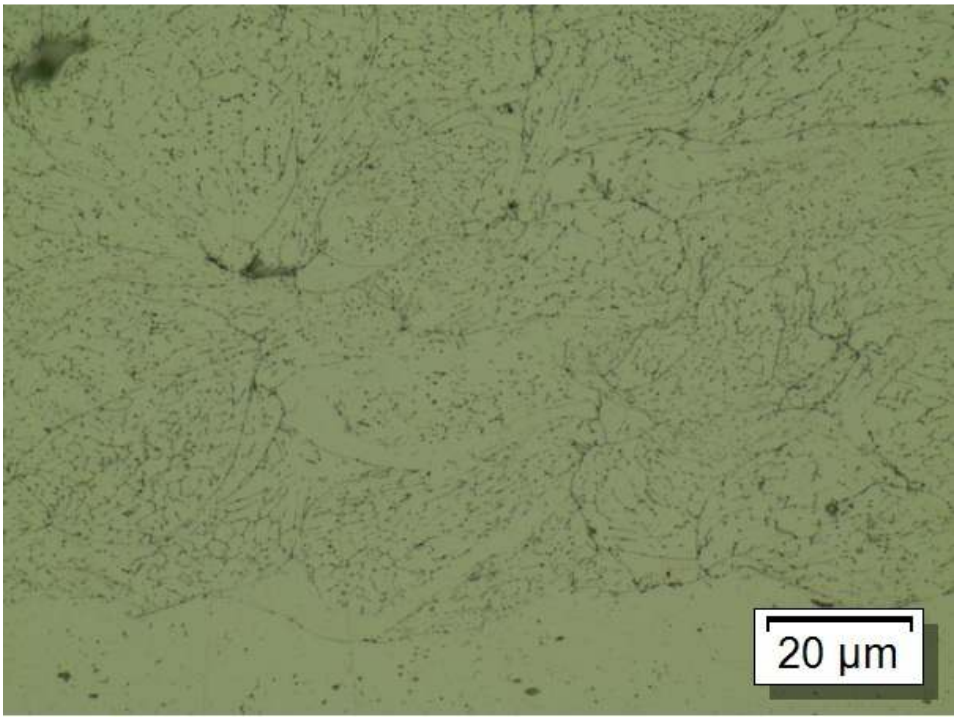

Figure 5.17c: Microscopic images of Al-6061 coating obtained at spray angle 70° (1000x magnification).

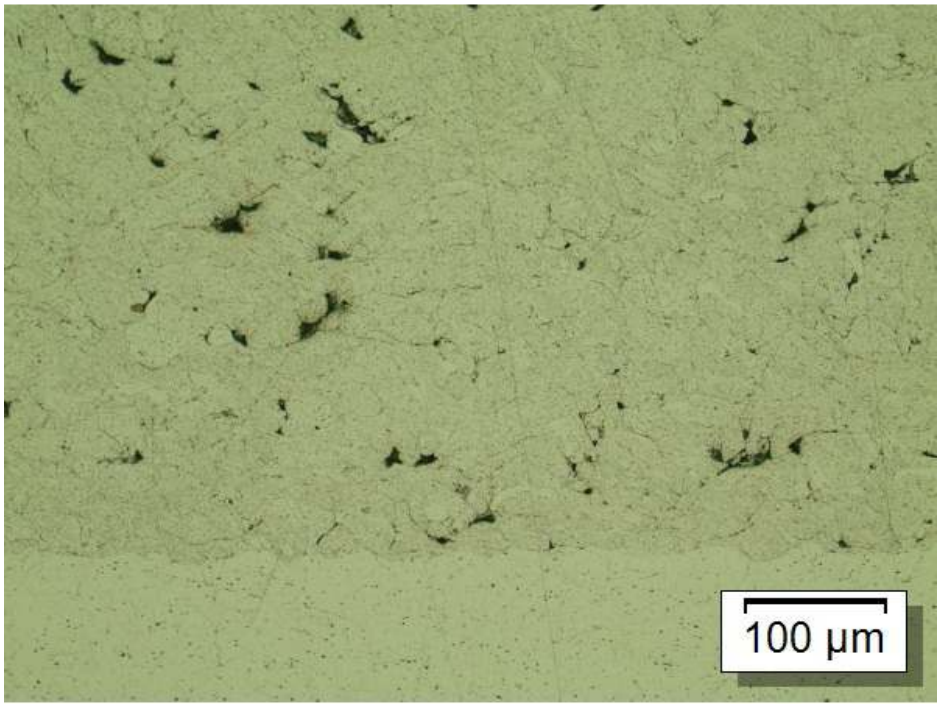

Figure 5.18a: Microscopic images of Al-6061 coating obtained at spray angle 60° (200x magnification).

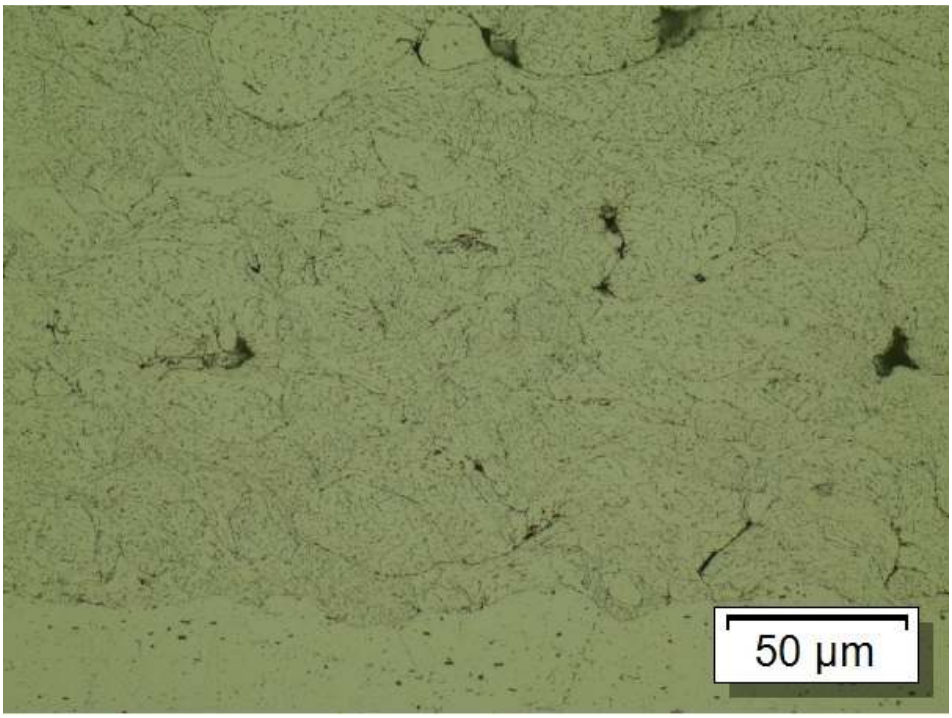

Figure 5.18b: Microscopic images of Al-6061 coating obtained at spray angle 60° (500x magnification).

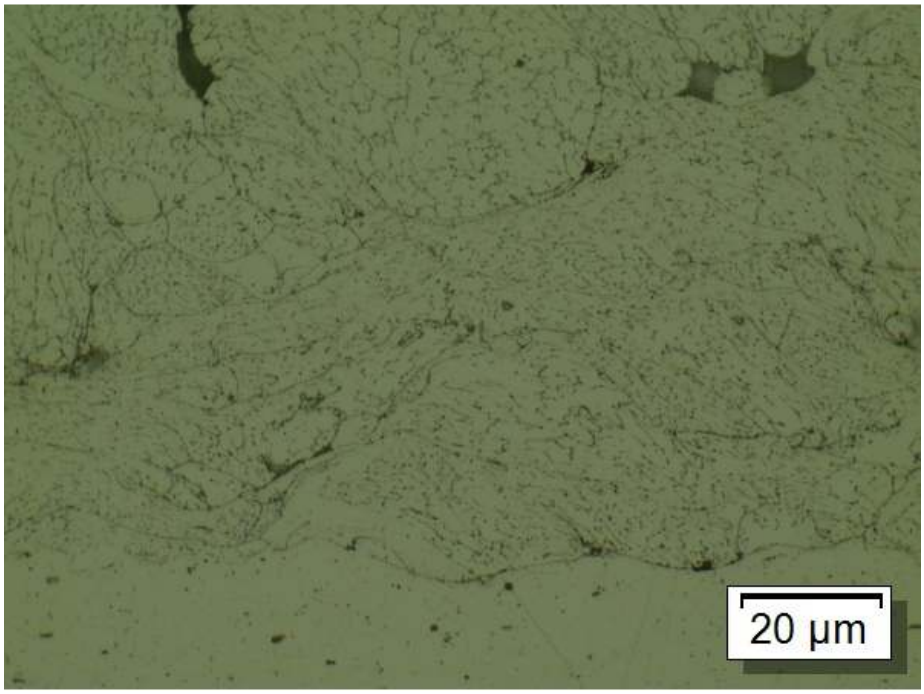

Figure 5.18c: Microscopic images of Al-6061 coating obtained at spray angle 60° (1000x magnification).

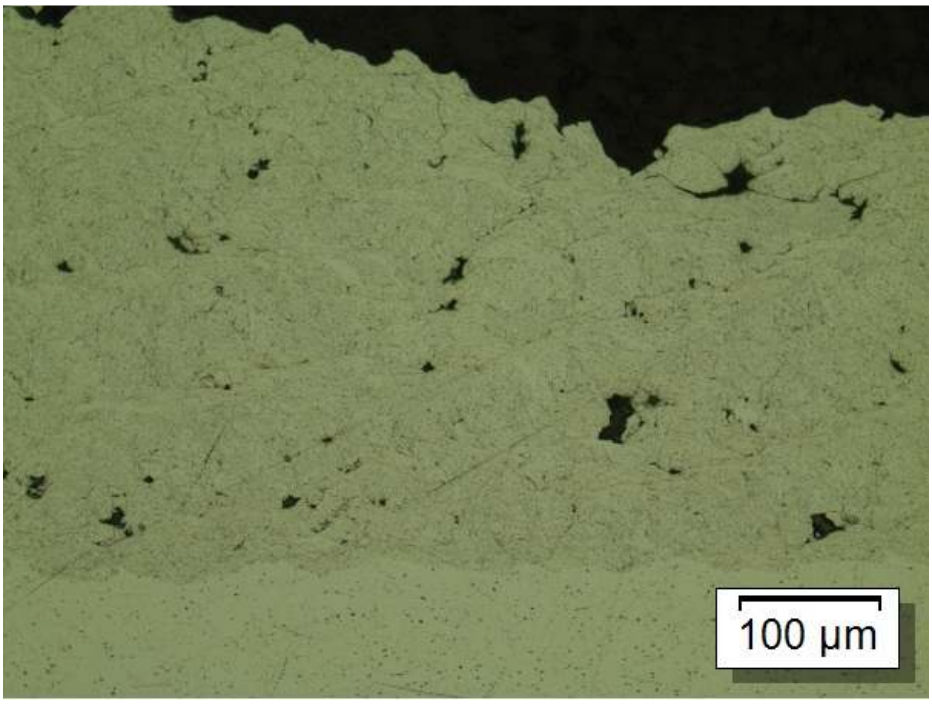

Figure 5.19a: Microscopic images of Al-6061 coating obtained at spray angle 50° (200x magnification).

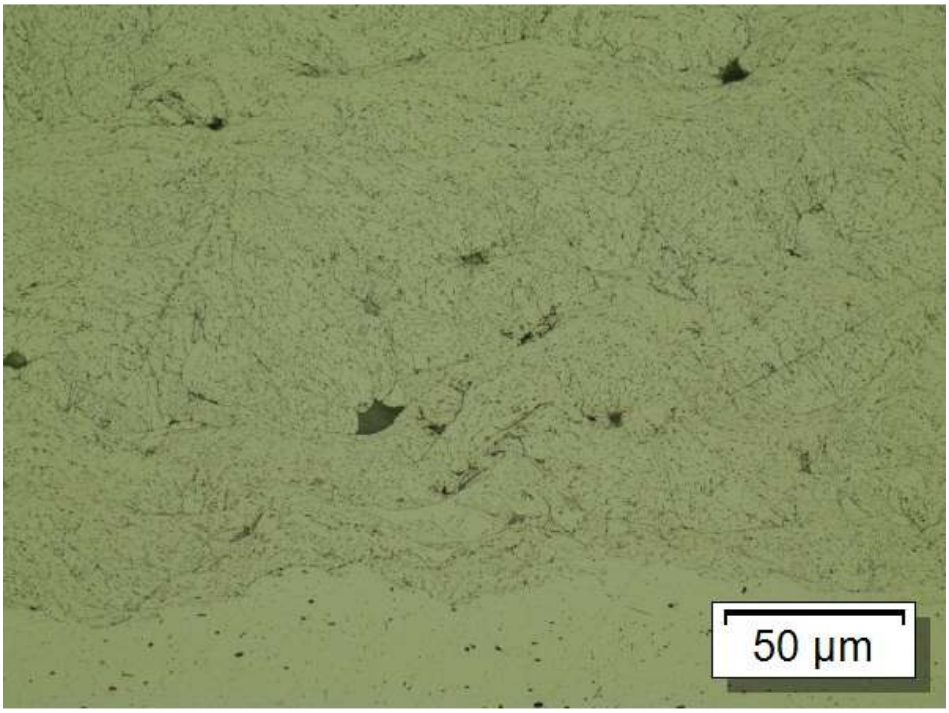

Figure 5.19b: Microscopic images of Al-6061 coating obtained at spray angle 50° (500x magnification).

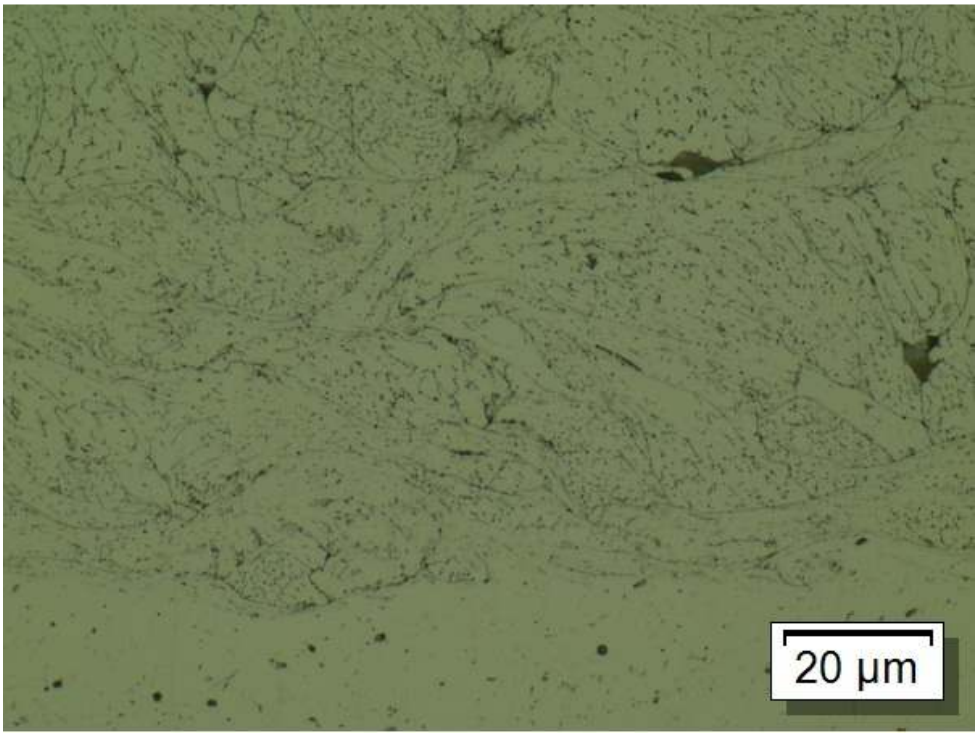

Figure 5.19c: Microscopic images of Al-6061 coating obtained at spray angle 50° (1000x magnification).

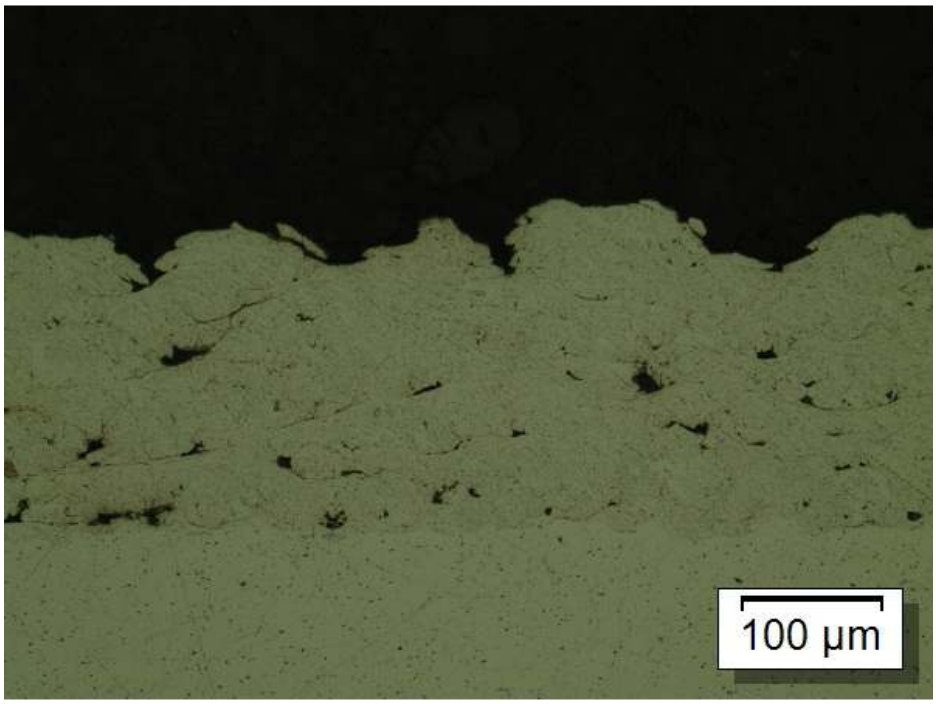

Figure 5.20a: Microscopic images of Al-6061 coating obtained at spray angle 40° (200x magnification).

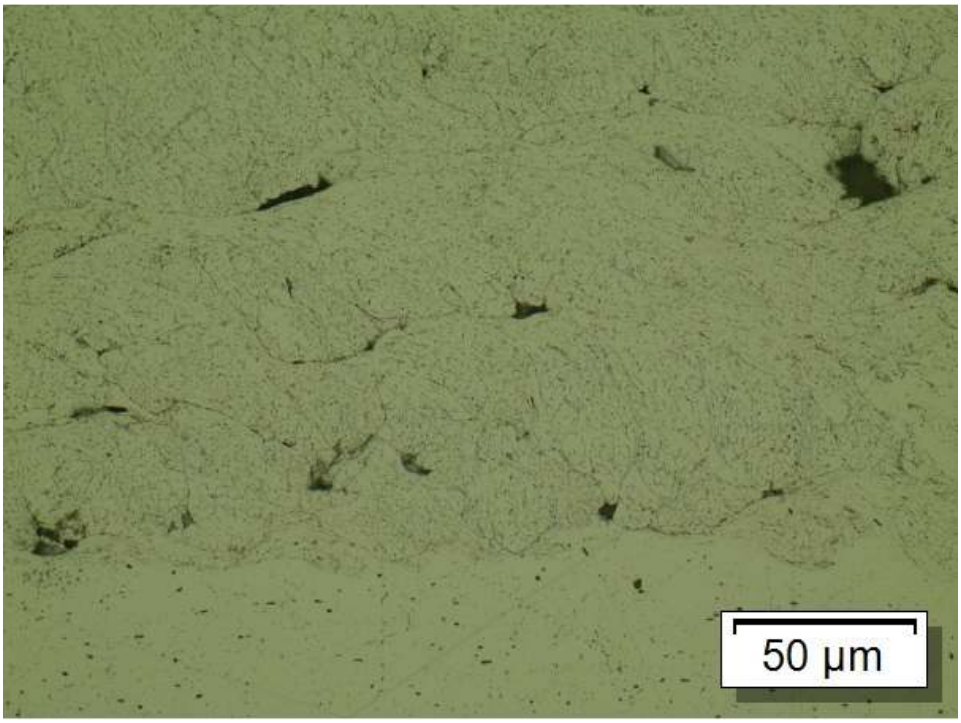

Figure 5.20b: Microscopic images of Al-6061 coating obtained at spray angle 40° (500x magnification).

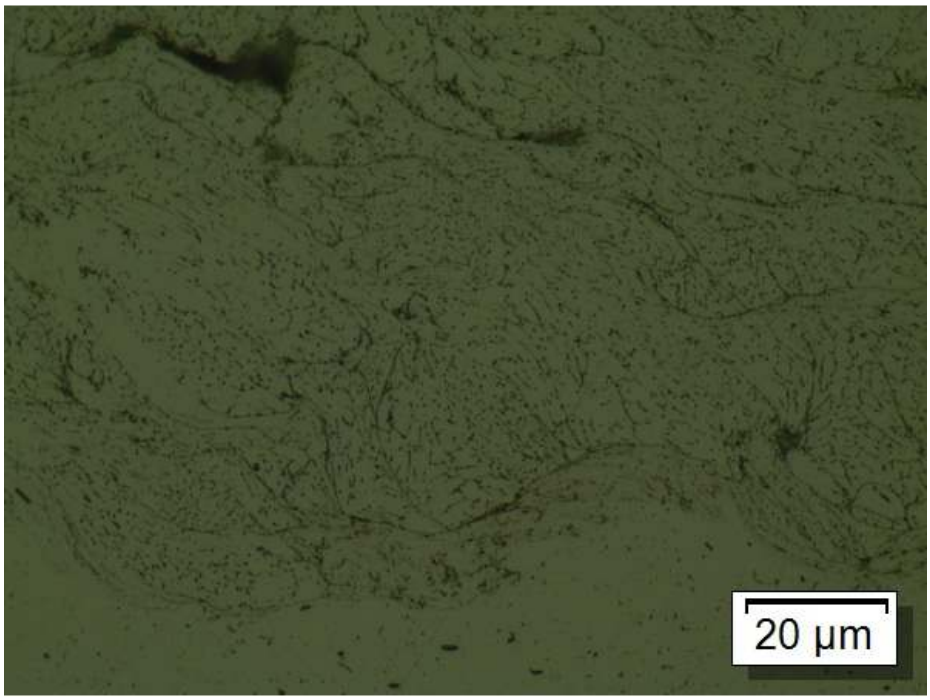

Figure 5.20c: Microscopic images of Al-6061 coating obtained at spray angle 40° (1000x magnification).

5.6 Relative Coating Deposition Efficiency Evaluation

The effect of the angle of incidence of the cold spray nozzle on the relative coating deposition efficiency was also investigated. Five sets of Al-6061 substrates (100 mm x 50 mm x 3 mm) were cleaned with acetone and cold sprayed without grit blast. Gas atomized Al-6061 powder (Valimet Inc., USA), identical to the ones used in Section 4.2.1 was used for the experiment. The cold spray process was carried out using the PCS-1000 cold spray system (Plasma Giken Co. Ltd, Japan). Nitrogen was used as the carrier gas and the flow rate was set at 250 standard litre per minute (SLM). The gas pressure was set at 4 MPa and the temperature at 400 °C. The powder was cold sprayed at 6 different angles of incidence of 90°, 80°, 70°, 60°, 50° and 40° respectively. The speed of the traversing robot was 200 mms^{-1} with a 1 mm step. A total of 8 steps were made for each pass and 2 passes were made for each spray angle. The standoff distance was set at 25 mm. An area of approximately 50 mm x 17 mm was coated for each sample.

To evaluate the relative coating deposition efficiency at various spray angles, the weight of the substrates before and after the cold spray process was measured and the weight gained was calculated. The area which was cold spray coated was almost identical for the various spray angle and the weight gained can be equated to the weight of the coating obtained. The weight of the samples were measured using the Sartorius CP224S (Goettingen, Germany) weighing scale with an accuracy of ±0.1 mg. The comparative results of the weight gained is shown in Table 5.4.

Table 5.4: Weight of Al-6061 cold spray coating obtained at various spray angles.

Spray Angle	**90°**	**80°**	**70°**	**60°**	**50°**	**40°**
Dimension of Substrate (mm)	100 x 50 x 3					
Weight of Substrate (grams)	41.25	41.75	40.75	40.65	41.34	40.49
Weight of Substrate and Coating (grams)	43.38	43.73	42.38	42.25	42.24	40.99
Weight of Coating (grams)	**2.13**	**1.98**	**1.63**	**1.6**	**0.9**	**0.5**

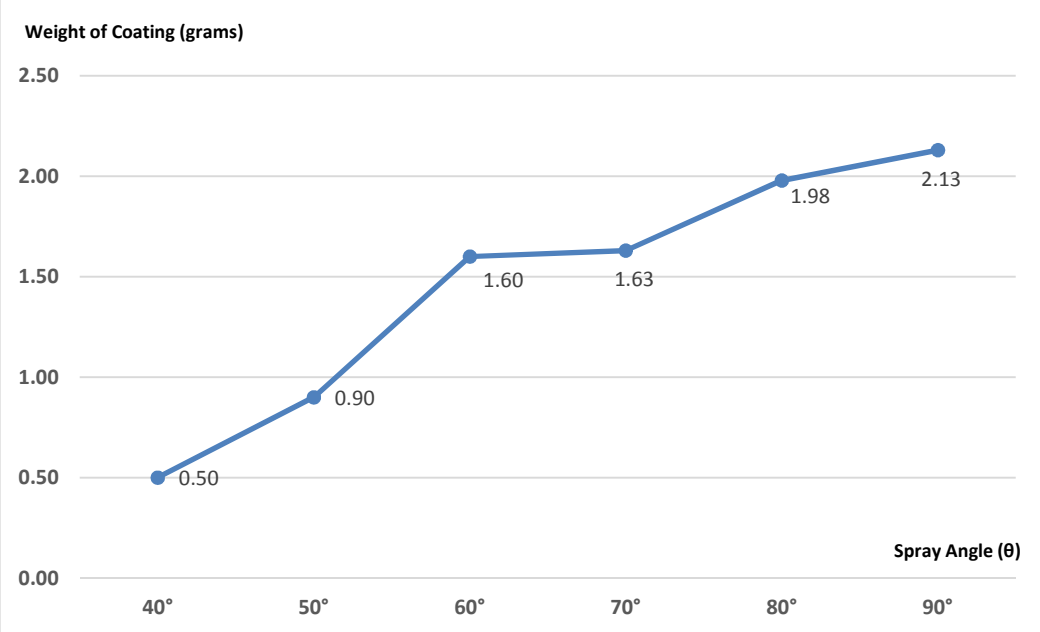

Figure 5.21: Weight of coating obtained at various spray angle (θ).

The results on Table 5.4 and Figure 5.21 show a steady decline in the weight of the coating as the angle of incidence of the cold spray nozzle decreases from 90° to 40°. The decrease in the weight of the coating was as high as 76.5% from 90° to 40°. This is an indication that as the angle of spray becomes more off-normal, the amount of coating deposited on the substrate decreases. The spray angle has a direct effect on the coating deposition efficiency.

In addition, the coating deposition efficiency was also determined based on the coating thickness obtained under the same cold spray conditions and parameters. The coating samples were first sectioned, mounted and polished for microscopic evaluation. The coating thickness was subsequently measured using the microscopic photos captured at 50x magnification for the coating obtained at spray angles of 90°, 80°, 70°, 60°, 50° and 40°. The photos are shown in Figure 5.22. A total of 4 coating thickness measurements were taken for each coating and the average thickness was calculated and tabulated in Table 5.5.

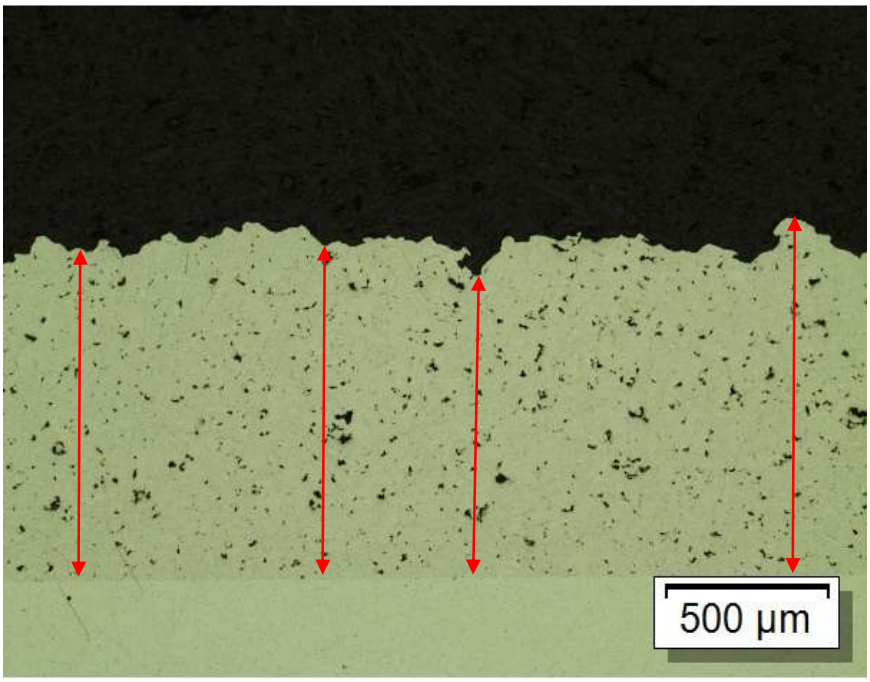

Figure 5.22a: Microscopic images of Al-6061 coating obtained at spray angle 90° (50x magnification).

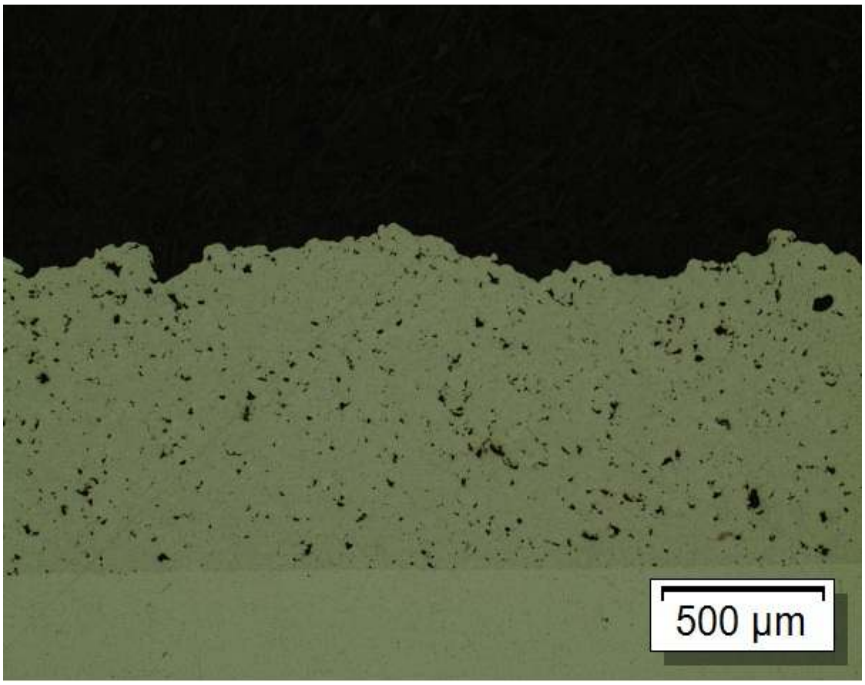

Figure 5.22b: Microscopic images of Al-6061 coating obtained at spray angle 80° (50x magnification).

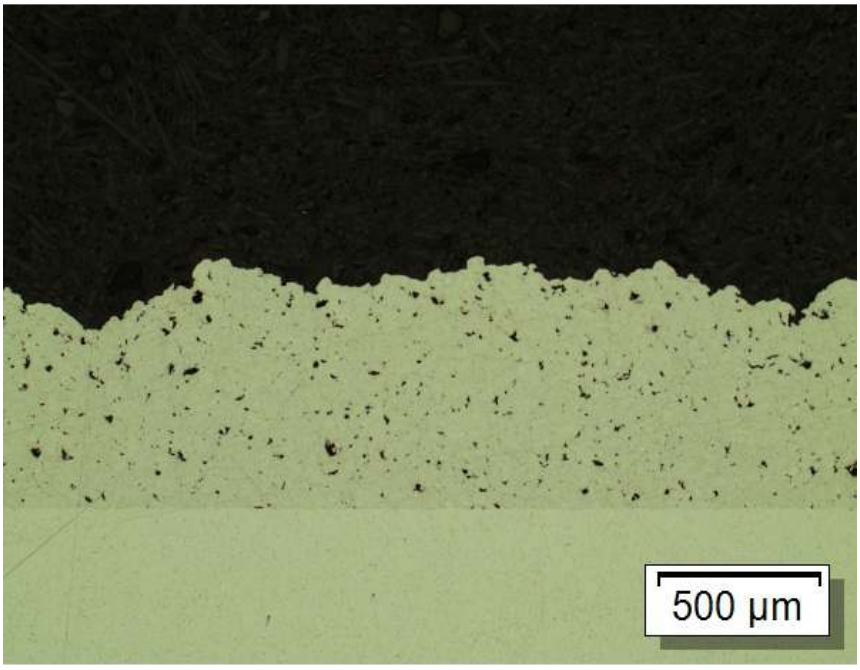

Figure 5.22c: Microscopic images of Al-6061 coating obtained at spray angle 70° (50x magnification).

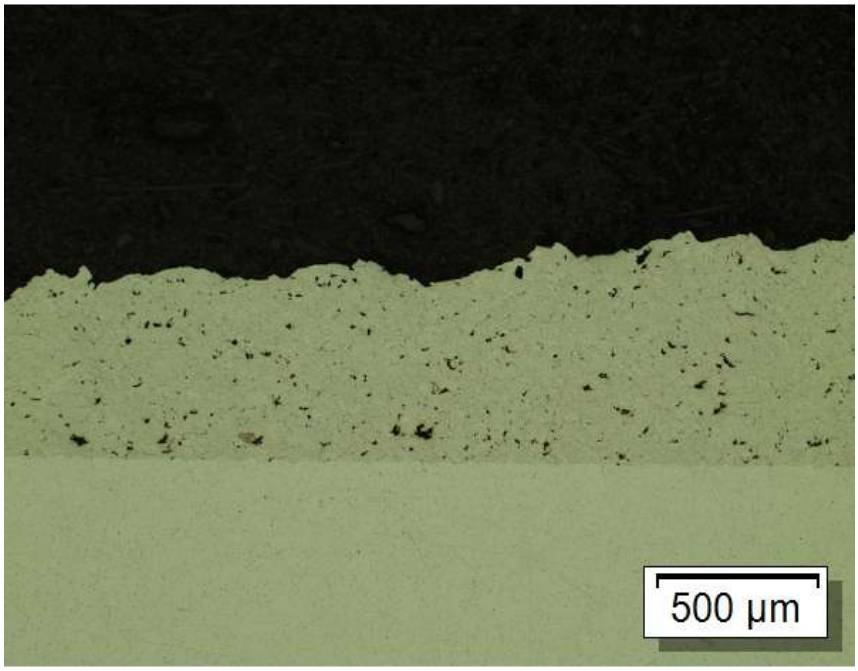

Figure 5.22d: Microscopic images of Al-6061 coating obtained at spray angle 60° (50x magnification).

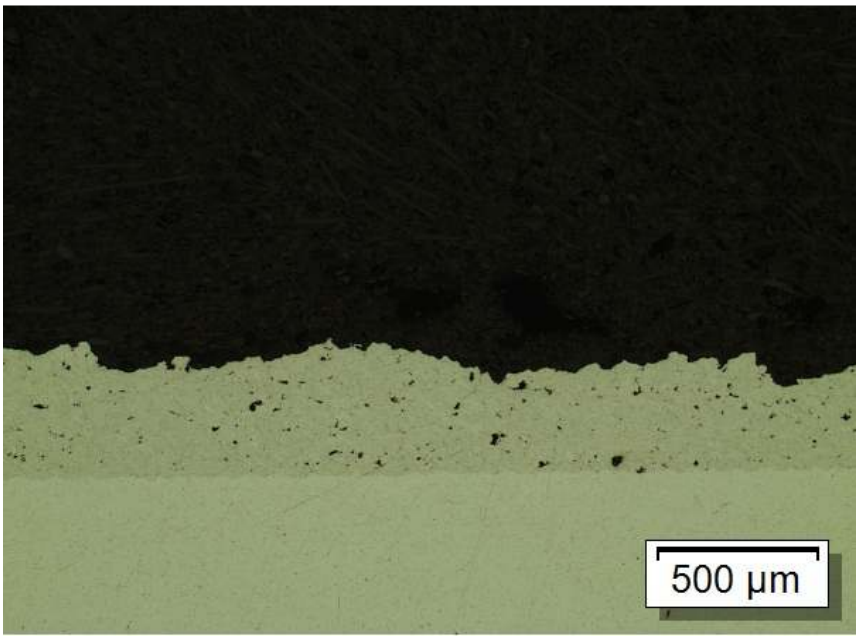

Figure 5.22e: Microscopic images of Al-6061 coating obtained at spray angle 50° (50x magnification).

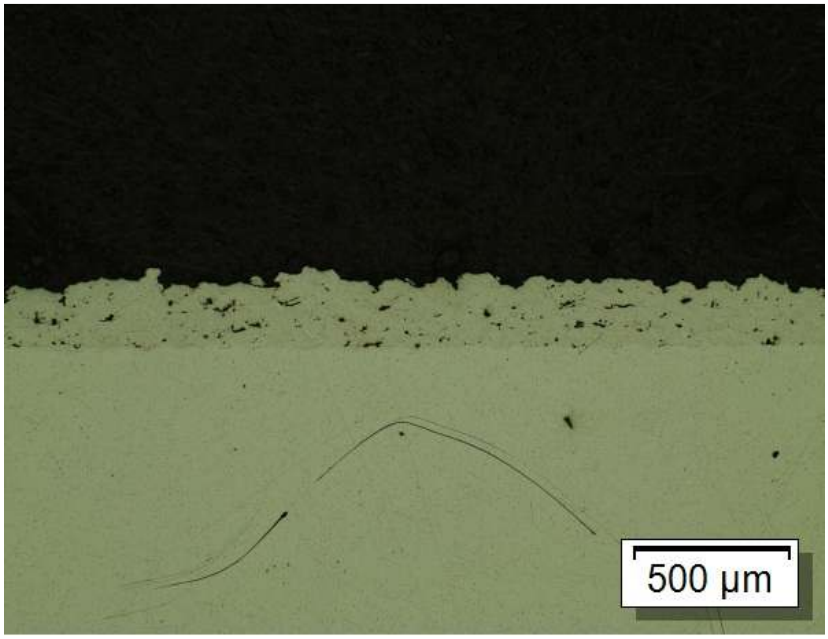

Figure 5.22f: Microscopic images of Al-6061 coating obtained at spray angle 40° (50x magnification).

Table 5.5: Average coating thickness of Al-6061 cold spray coating obtained at various spray angles.

Spray Angle	90°	80°	70°	60°	50°	40°
Average Coating Thickness (µm)	991	929	696	607	339	214

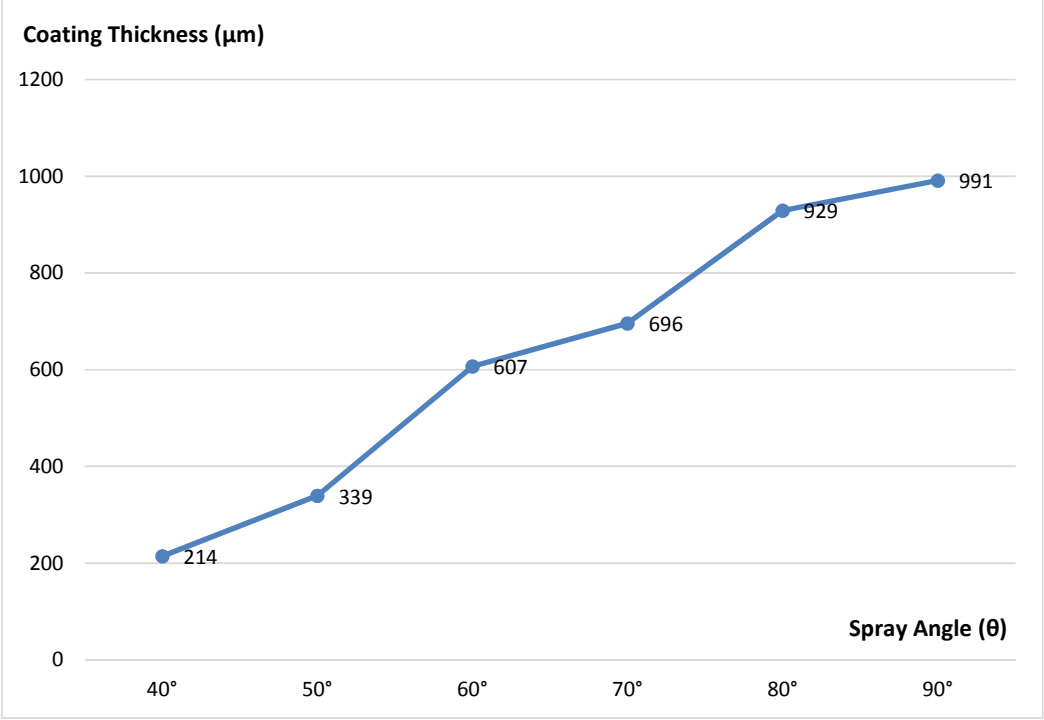

Figure 5.23: Coating thickness obtained at various spray angle (θ).

The results shown on Table 5.5 and Figure 5.23 indicate that the coating thickness obtained when the cold spray nozzle was placed at normal to the substrate was closed to 1000 μm with 2 passes of the cold spray nozzle. The coating thickness decreases as the spray angle decreases from 90° to 80° and more significantly as the spray angle becomes even more off-normal. The percentage decrease in coating thickness for spray angle $\theta = 40°$ when compared to $\theta = 90°$ is as high as 78.4%. This percentage decrease is almost identical to the percentage decrease in weight of the coating when the spray angle θ decreases from 90° to 40°.

The relative weight and thickness of the coatings obtained at various spray angles are presented on Figures 5.21 and 5.23 respectively. The two graphs show similarity in terms of the rate of increase in coating weight and coating thickness. As the spray angle increases from $\theta = 60°$ to $\theta = 90°$, the percentage rate of increase in both coating weight and thickness is fairly small, measured at approximately 1% per $\Delta\theta$. This rate of increase however increases significantly to about 2 to 2.5% per $\Delta\theta$ as the spray angle changes from 40° to 60° for both coating weight and coating thickness. This is an indication that the coating deposition efficiency could be significantly decreased if the spray angle is smaller than 60°.

5.7 Conclusion

In this chapter, the effect of the spray angle of a cold spray nozzle on the mechanical properties of the coating was investigated.

The effect of the spray angle on the average microhardness of the coating was found to be negligible as the spray angle decreases from 90° to 70°. However, with a further decrease in spray angle from 70° to 40°, the average coating microhardness actually increases. This increase was as high as 20.9% for the coating obtained at $\theta = 40°$ when compared to the coating obtained at $\theta = 90°$. The highest coating microhardness value was recorded at 116.8 Hv_{100g} which was obtained at spray angle $\theta = 40°$.

The possible reason for the increase in the coating microhardness is the increase in the plastic deformation of the cold sprayed particles as they collided onto the substrate and impinge onto each other with decreasing spray angle. The increase in plastic deformation enhances the dislocation within the crystal structure of the impinging particles, thus cold working the coating as it builds up and in the process, increasing its microhardness.

The effect of the spray angle on the coating tensile adhesion strength was also investigated. The spray angle of the cold spray nozzle with respect to the substrate was found to have minimal impact on the tensile adhesion strength of the coatings. This is due to the fact that when the particles embed themselves onto the substrate surface, there is little or no gap between the particles and substrate. Thus, the tensile adhesion bond strength which is dependent on the magnitude of the contact surface area, is not

affected. The microscopic images taken of the coating cross-section support this observation.

The effect of the spray angle on the relative coating deposition efficiency was also evaluated. It was found that the relative coating deposition efficiency decreases as the spray angle becomes more off-normal. This is measured in terms of the weight of the coating and coating thickness obtained with identical cold spray parameters and robotic manipulation sequence. It was also found that a more profound and drastic decrease takes place as the spray angle decreases from 60° to 50°, suggesting that spray angle smaller than 60° should be avoided if coating deposition efficiency is a key consideration in the cold spray process.

However, the results do suggest that for hard-to-reach areas in which a cold spray nozzle cannot be placed normally to the substrate, a spray angle as small as 40° is still acceptable as the mechanical properties of the coating in terms of coating microhardness and tensile adhesion strength were not in any way affected.

CHAPTER 6

EXPERIMENTAL STUDY OF STATIONARY NOZZLE DEPOSITION

6.1 Introduction

As cold spray is a relatively low temperature process compared to conventional thermal spray, the build-up of thermal residual stresses is comparative lower. This presents the possibility of an effective and quick build-up of a cold spray coating at a localised position by holding the cold spray nozzle stationary. However, the effect on the coating quality is not well understood. In addition, the relatively high tensile adhesion strength for the coating obtained on the non-grit blasted surface as shown in Chapter 4 of this thesis runs contrary to the results we normally experience with conventional thermal spray coatings. An experimental study was conducted to observe the coating as it is built-up with the cold spray nozzle held stationary at various dwell time to address the following:

1. The effect on the cold spray coating quality when it is built-up quickly by holding the cold spray nozzle stationary.
2. To better understand the possible reason(s) for the relatively high tensile adhesion strength for the coating obtained on the non-grit blasted substrate.

6.2 Stationary Nozzle Experiment

An experiment was carried out to study the effect of a stationary cold spray deposition process on the surfaces of the substrate. The nozzle of the PCS-1000 cold spray system was placed 25 mm from the Al-6061 substrate (100 mm x 100 mm x 5 mm) which was cleaned but not grit blasted. The Al-6061 powder was sprayed using Nitrogen as the carrier gas set at flow rate of 250 SLM, pressure of 4 MPa and temperature of 400 ºC. The coating process lasted for 5 seconds before the gun nozzle was moved away from the substrate. During the cold spray process, a conical shaped Al-6061 coating was built up on the substrate as shown in Figure 6.1. The conical shaped coating was about 5 mm in diameter and 5 mm in height.

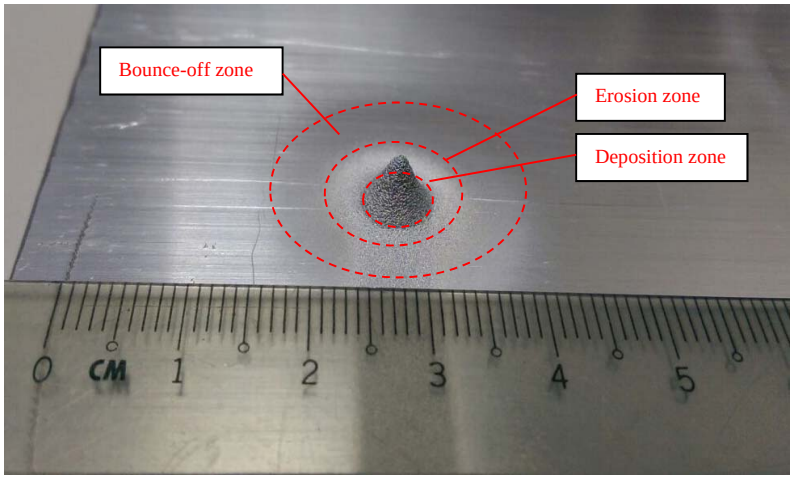

Figure 6.1: Conical shaped Al-6061 coating with three distinct zones created by a stationary cold spray deposition process.

As can be seen from Figure 6.1, there are 3 distinct zones which can be identified on the substrate from the coating process. Right in the middle from the centerline of the cold spray nozzle is the deposition zone. The area is about 5 mm in diameter and can be identified by the conical shaped coating deposition on top. This is the area where the velocity of the cold spray particles exceeds the critical velocity and the particles plastically deform and adhere to the substrate. The coating build-up is due to the impinging particles impacting on top of the previous layer as the cold spray nozzle stayed stationary in position for five seconds. Immediately beyond the deposition zone is the erosion zone, a circular area between 2.5 mm and 7.5 mm from the centre of the conical deposition zone. The area is easily distinguished by the matt surface finish on the substrate. This is likely due to the effect of the cold spray powder eroding the substrate surfaces as they do not have sufficient energy to embed onto the substrate. Beyond the erosion zone and extending to a radius of about 10.5 mm from the centre is the bounce-off region. Particles hitting this region do not have sufficient energy to erode or embed onto the substrate surface and simply bounces off due to its relatively low velocity.

The coating was subsequently sectioned, etched and polished as shown in Figure 6.2. The sample was then examined under a microscope and the results are shown in Figure 6.3.

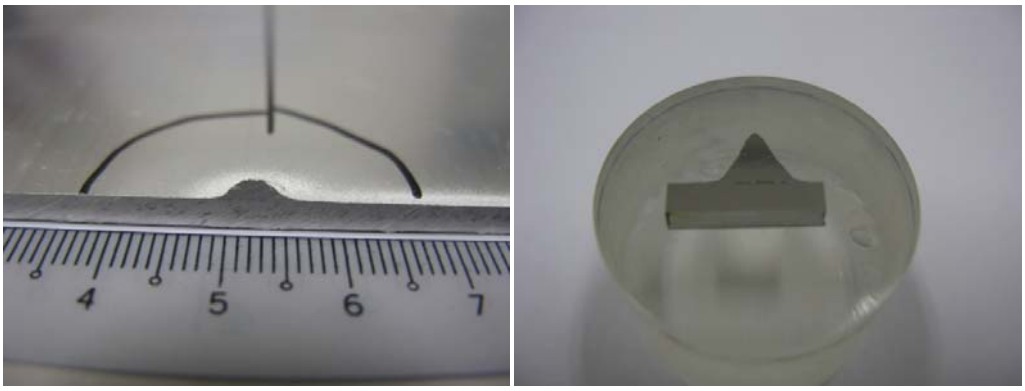

Figure 6.2: Conical shaped Al-6061 coating was sectioned, mounted and polished for microscopic examination.

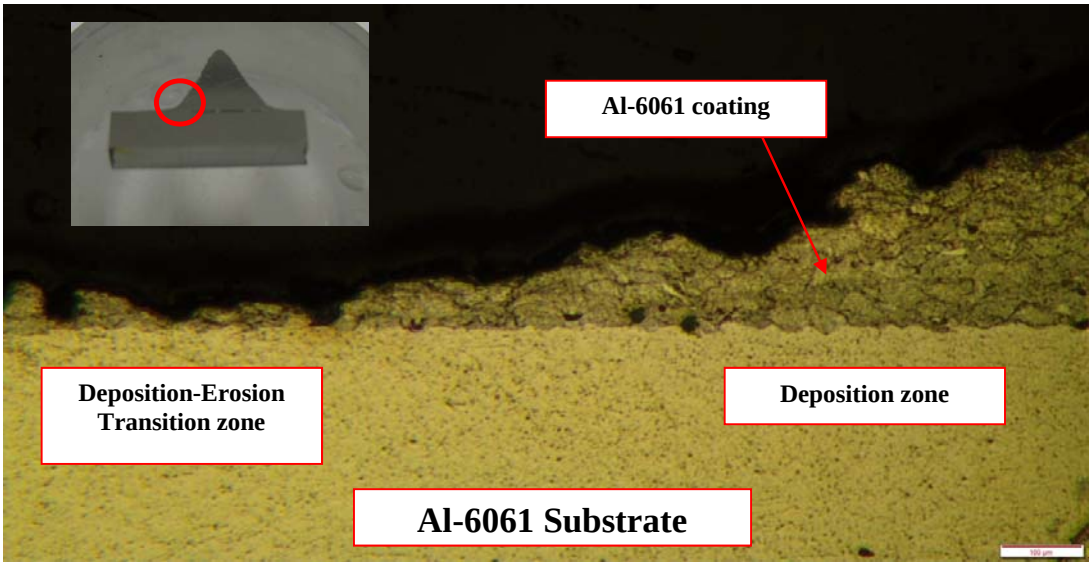

Figure 6.3a: Microscopic image of coating-substrate interface at the deposition and deposition-erosion zones deposited with a stationary cold spray process (200x magnification). Inserted photo indicating where micrograph is taken.

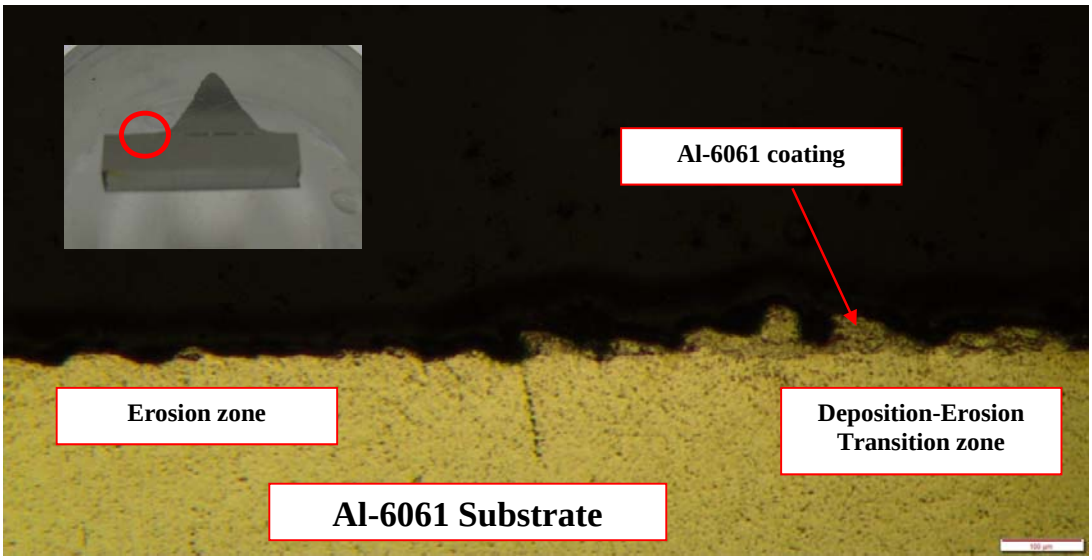

Figure 6.3b: Microscopic image of coating-substrate interface at the deposition-erosion and erosion zones deposited with a stationary cold spray process (200x magnification). Inserted photo indicating where micrograph is taken.

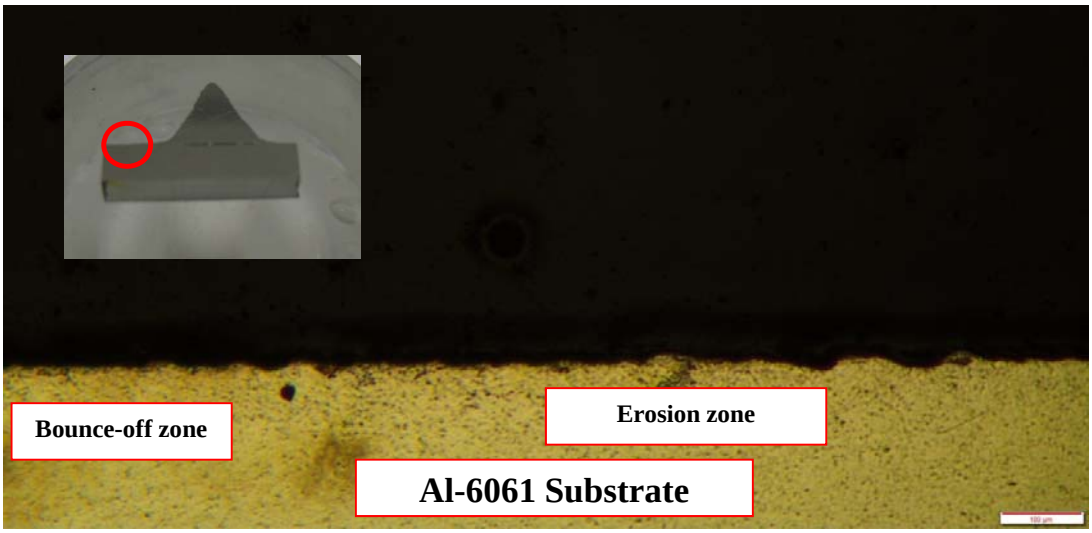

Figure 6.3c: Microscopic image of coating-substrate interface at the erosion and bounce-off zones deposited with a stationary cold spray process (200x magnification). Inserted photo indicating where micrograph is taken.

Figure 6.3a shows the image of the Al-6061 substrate from the deposition zone and the transition zone between the deposition and erosion processes. The thickness of the Al-6061 coating decreases as we move further away from the spray centerline. In the deposition-erosion transition zone, the Al-6061 coating is sparse and in some areas, only a single layer of coating is observed.

In Figure 6.3b, Al-6061 coating can be seen to be deposited along the deposition-erosion transition zone. As we transit towards the erosion zone, little or no coating can be seen on the substrate surface. In addition, the surface of the substrate appears roughened. This observation seem to validate the grit blasting effect caused by the impinging powders which have velocity lower than the critical velocity and do not have sufficient kinetic energy to embed onto the substrate.

Figure 6.3c captures the erosion and bounce-off zones. No Al-6061 coating was observed on the substrates and the surface roughness decreases significantly in the bounce-off zone as the particles hitting onto the substrates do not have sufficient energy to erode the surfaces.

6.3 Short Term Effect of Stationary Nozzle

To further verify the grit blasting effect of the cold spray process, another experiment was carried out to observe the short term effect of a stationary cold spray deposition process on the surface of the substrate. The cold spray nozzle was first positioned 200 mm from the edge of the Al-6061 substrate. The cold spray system was then started and

the Al-6061 powder was sprayed into the atmosphere using Nitrogen as the carrier gas set at flow rate of 250 SLM, pressure of 4 MPa and temperature of 400 °C. The cold spray nozzle was then moved horizontally at 200 $mmsec^{-1}$ towards the centre of the 100 mm by 100 mm substrate and held in position for one second at a standoff distance of 25 mm. The cold spray nozzle was subsequently moved back to the start position via the same path and traversing speed. The coating produced is shown on Figure 6.4a.

The coating was sectioned, mounted, etched and polished as shown in Figure 6.4b. The sample was then examined under a microscope and the results are shown in Figure 6.4c and 6.4d.

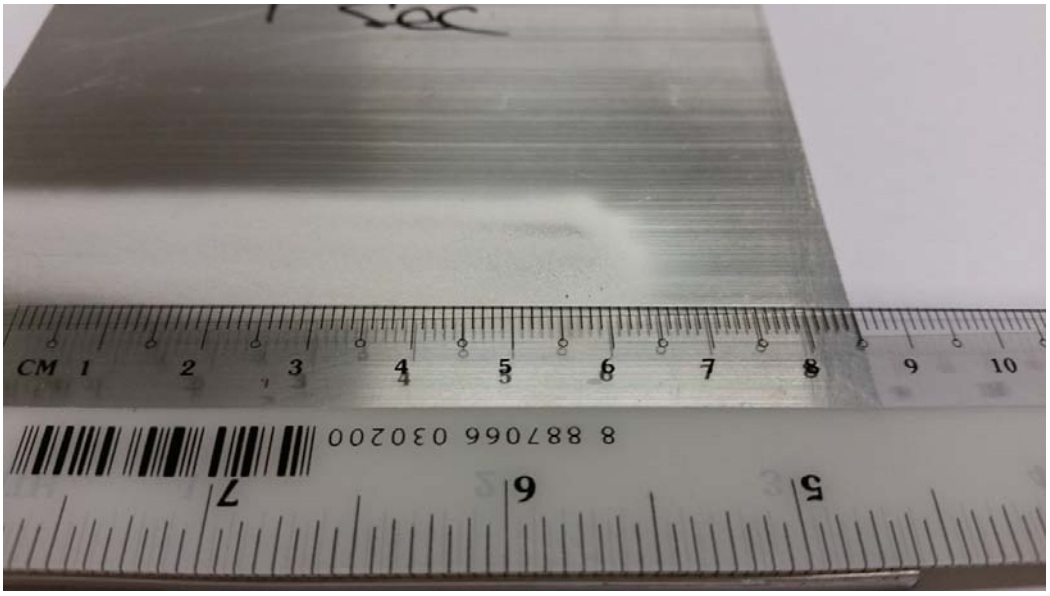

Figure 6.4a: Al-6061 cold spray coating formed with a nozzle held stationary for one second.

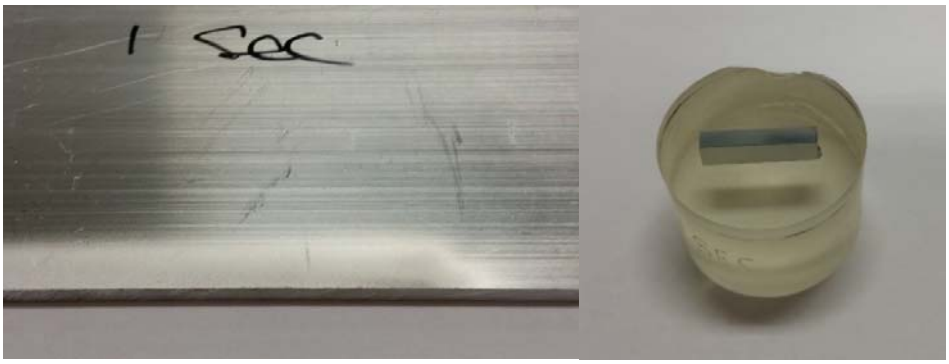

Figure 6.4b: Al-6061 cold spray coating obtained with the nozzle held stationary for one second was sectioned, mounted, etched and polished for microscopic evaluation.

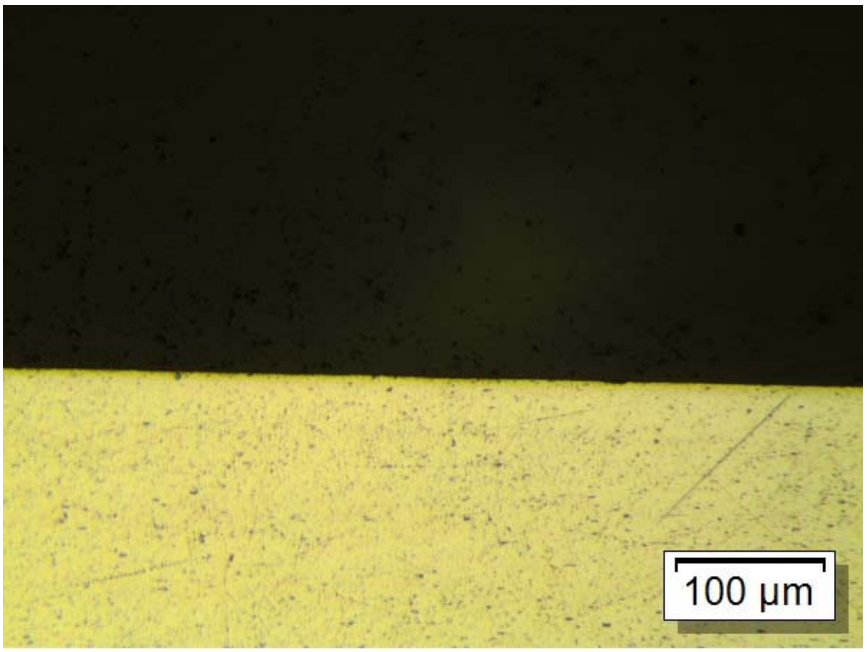

Figure 6.4c: Microscopic image of substrate surface which was not within the deposition process (200x magnification).

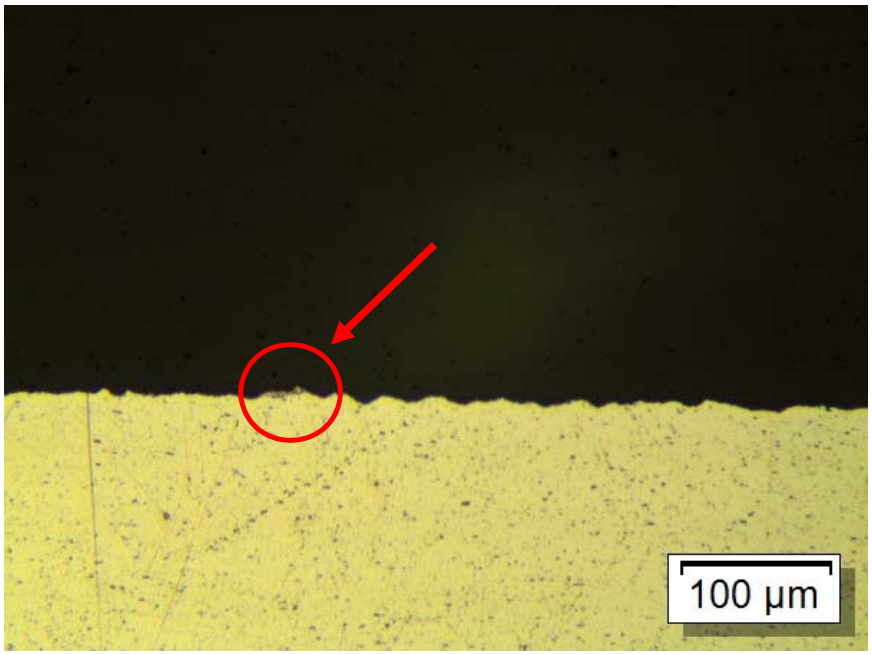

Figure 6.4d: Microscopic image of substrate surface which was subjected to one second of stationary cold spray deposition process (200x magnification). Arrow indicating cold spray deposition.

Figure 6.4c shows the surface of a substrate that was not within the deposition process. The substrate surface appears smooth with no jagged edges. In Figure 6.4d, the substrate surface appears serrated, demonstrating the roughening effect of the cold sprayed Al-6061 powder on the substrate surface before a coating is formed. Figure 6.4d also shows traces of the Al-6061 powder adhering to the substrate and forming an initiate layer of coating. This result validates the hypothesis that cold spray in itself has a surface roughening effect on the substrate and does not require a pre-coat grit blasting process prior to coating.

6.4 Additional Study on Effect of Stationary Nozzle

One other observation that was seen from the experiment when the cold spray nozzle was held stationary for five seconds was the presence of a non-adhesion zone in the middle of the coating as shown in Figures 6.5a and 6.5b. This area is approximately 2 mm in radius from the centerline of the coating. The microscopic image shown in Figure 6.5c suggests that the coating has delaminated from the substrate as the impinging particles built up a coating on top of the initial layer.

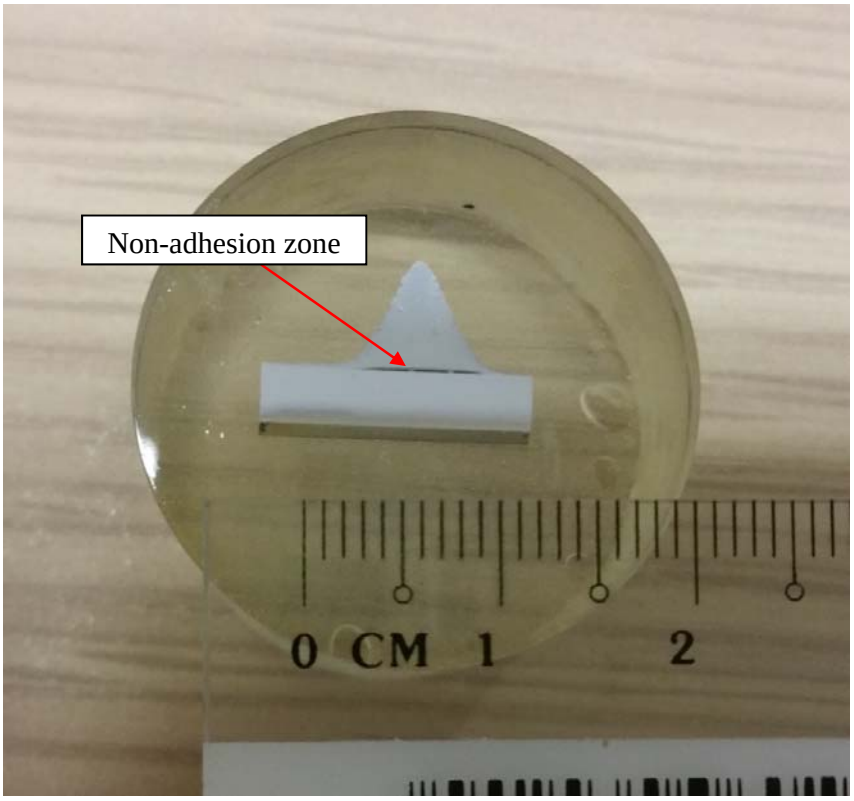

Figure 6.5a: Al-6061 cold spray coating formed with a stationary nozzle showing a non-adhesion zone.

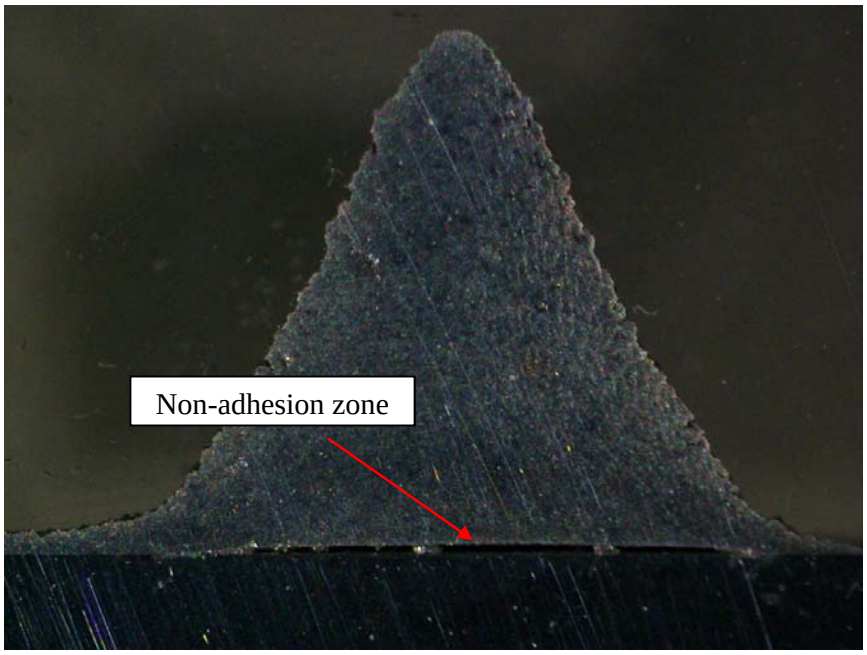

Figure 6.5b: Microscopic images of Al-6061 cold spray coating formed with a stationary nozzle showing a non-adhesion zone (10x magnification).

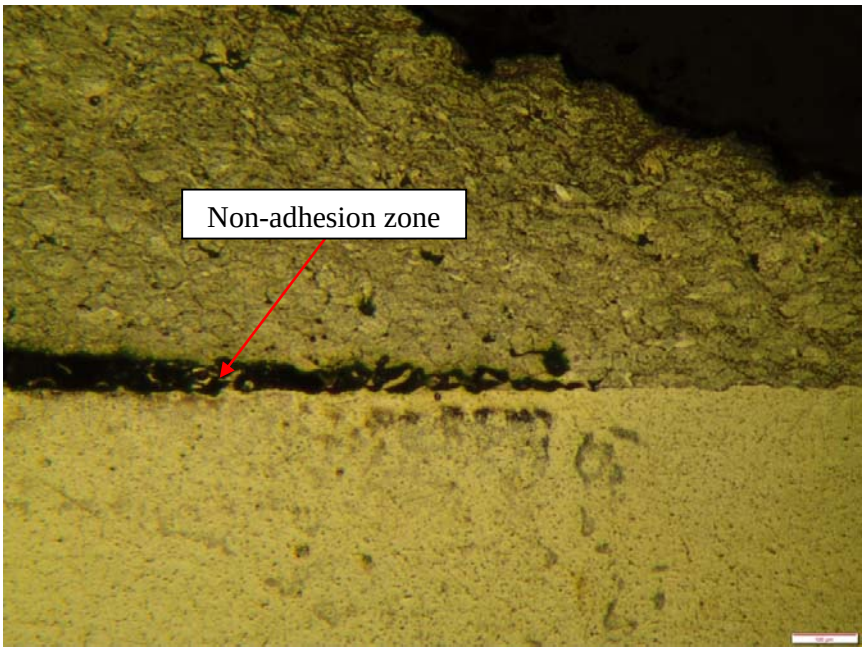

Figure 6.5c: Microscopic images of Al-6061 cold spray coating formed with a stationary nozzle showing a non-adhesion zone (200x magnification).

To further study into the delamination phenomenon, a series of cold spray coatings was carried out to observe the possible causes for the formation of such a distinct non-adhesion zone. Different Al-6061 coatings were obtained with the cold spray nozzle positioned at a stationary location for a duration of one, two, three, four and five seconds respectively. To obtain the coatings, the cold spray nozzle was first positioned 200 mm from the edge of the Al-6061 substrate. The cold spray system was then started and the Al-6061 powder was sprayed into the atmosphere using Nitrogen as the carrier gas set at flow rate of 250 SLM, pressure of 4 MPa and temperature of 400 °C. The cold spray nozzle which is mounted on a six-axis ABB robot was then moved horizontally at 200 $mmsec^{-1}$ towards the centre of the 100 mm by 100 mm substrate and held in position for the required duration (one, two, three, four or five seconds) at a standoff distance of 25 mm. The cold spray nozzle was subsequently moved back to the start position via the same path and traversing speed. The five different coatings produced are shown on Figure 6.6.

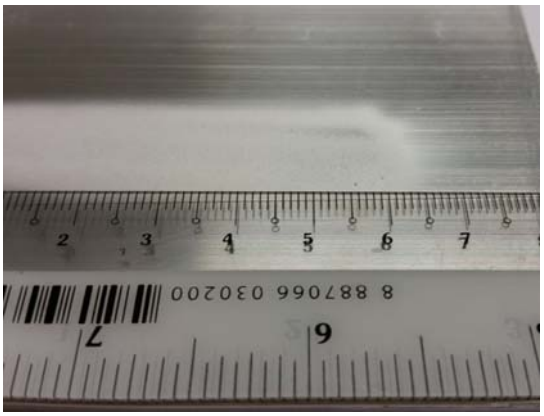

(a)

(b)

(c)

Figure 6.6: Al-6061 cold spray coating formed with a nozzle held stationary for (a) one, (b) two, (c) three, (d) four and (e) five seconds respectively.

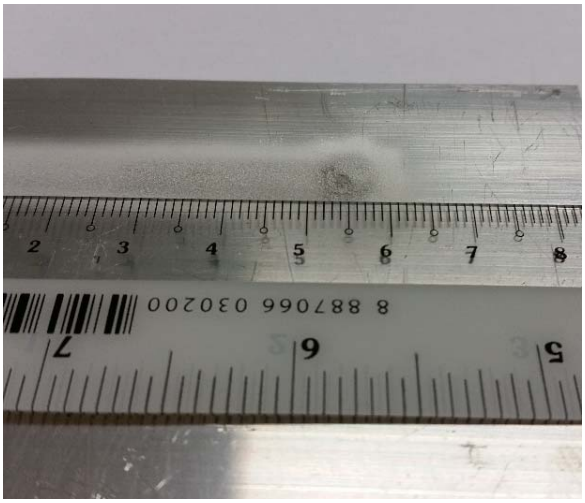

(d)

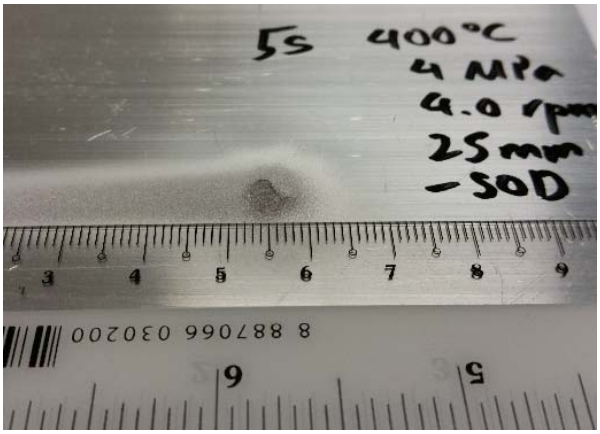

(e)

Figure 6.6: Al-6061 cold spray coating formed with a nozzle held stationary for (a) one, (b) two, (c) three, (d) four and (e) five seconds respectively.

The coatings were sectioned, mounted, etched and polished as shown in Figure 6.7. The samples were then examined under a microscope and the results are shown in Figures 6.8 to 6.11.

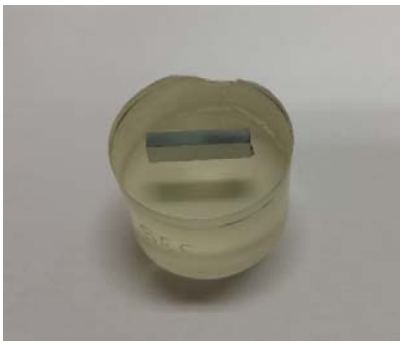

(a)

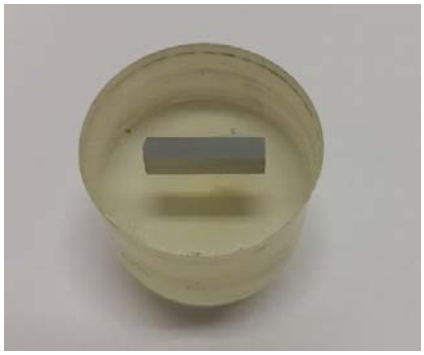

(b)

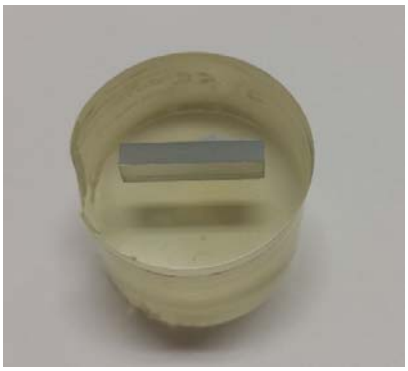

(c)

Figure 6.7: Al-6061 cold spray coatings obtained with the nozzle held stationary for (a) one, (b) two, (c) three, (d) four and (e) five seconds respectively were sectioned, mounted, etched and polished for microscopic evaluation.

(d)

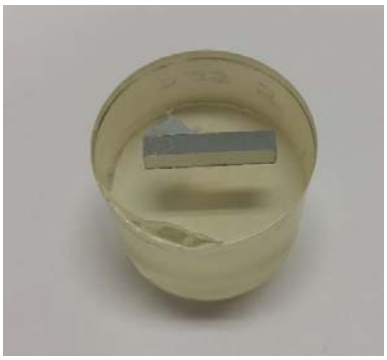

(e)

Figure 6.7: Al-6061 cold spray coatings obtained with the nozzle held stationary for (a) one, (b) two, (c) three, (d) four and (e) five seconds respectively were sectioned, mounted, etched and polished for microscopic evaluation.

(a)

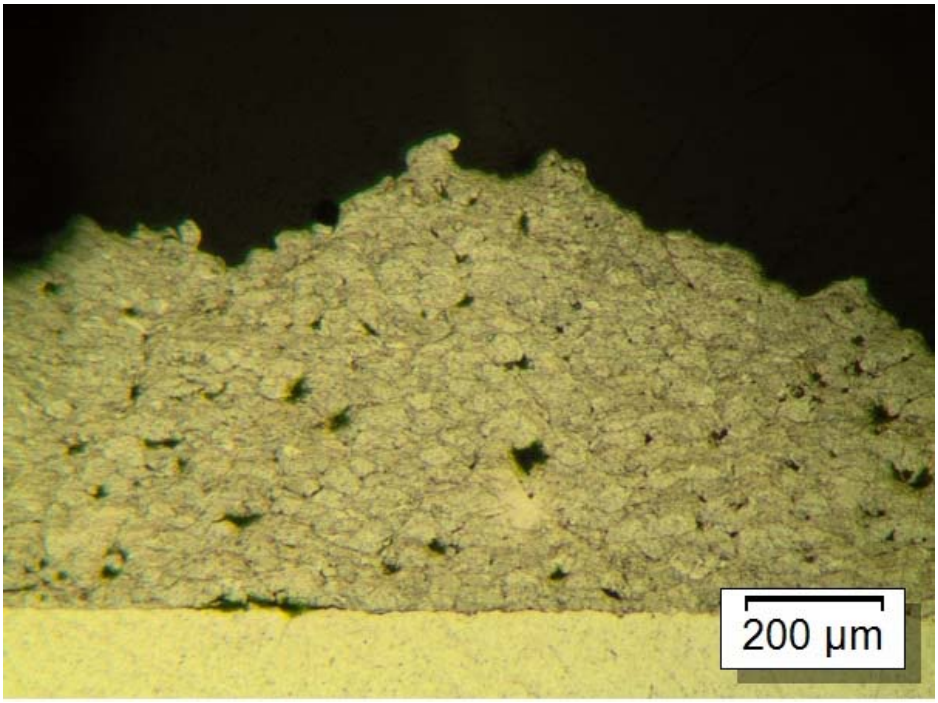

(b)

Figure 6.8: Microscopic images of Al-6061 cold spray coating formed with a nozzle placed stationary for two seconds at (a) 10x and (b) 100x magnification.

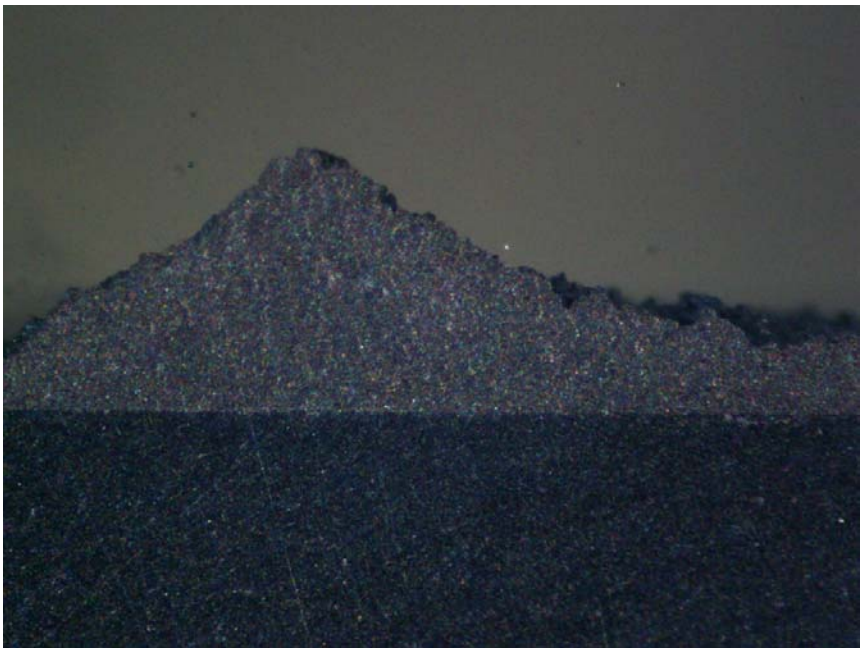

(a)

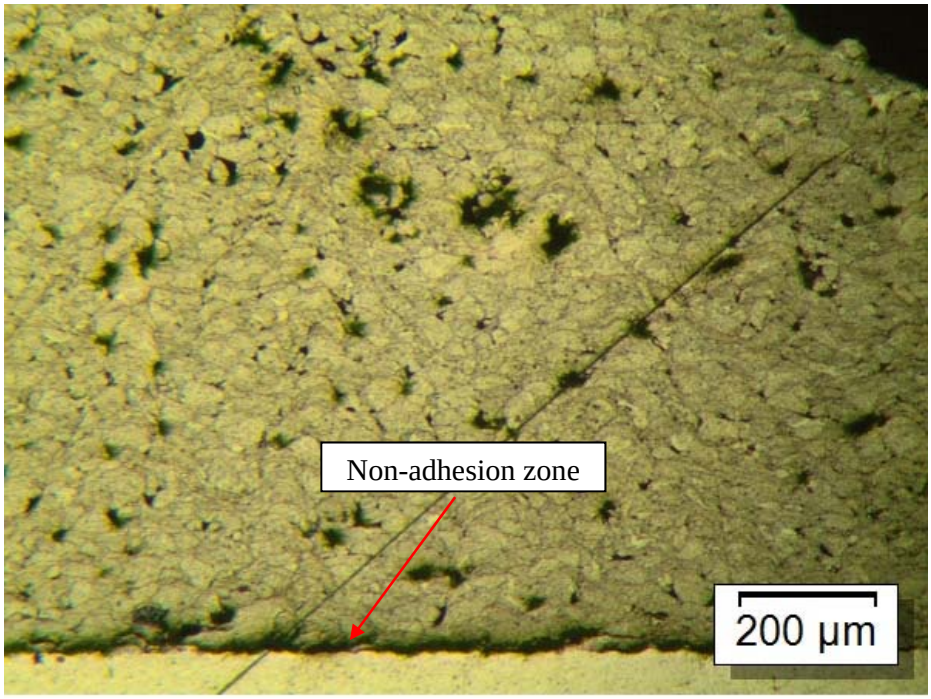

(b)

Figure 6.9: Microscopic images of Al-6061 cold spray coating formed with a nozzle placed stationary for three seconds at (a) 10x and (b) 100x magnification.

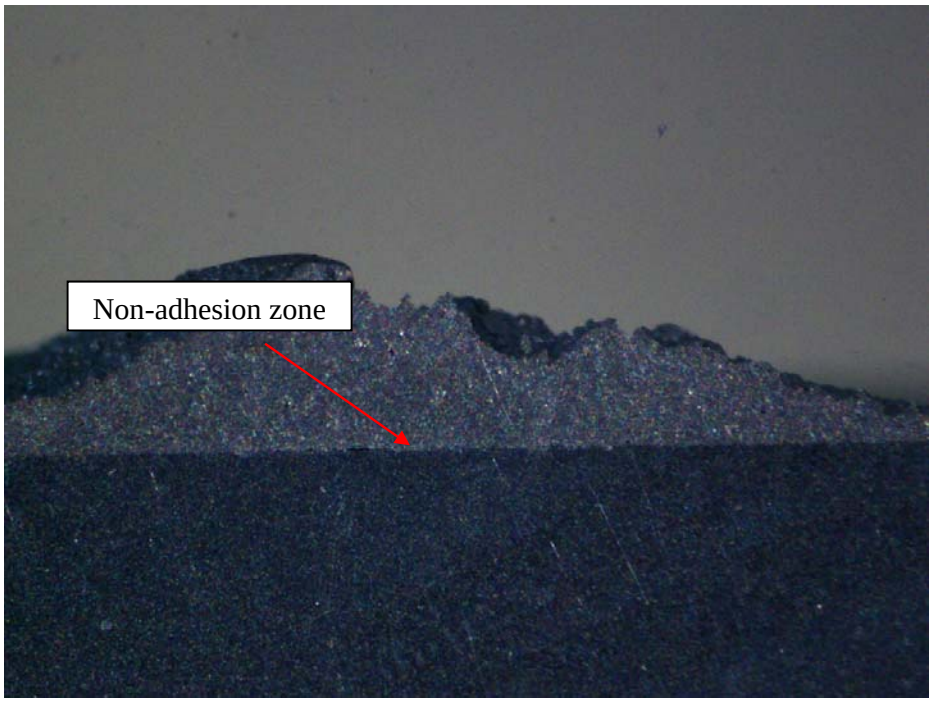

(a)

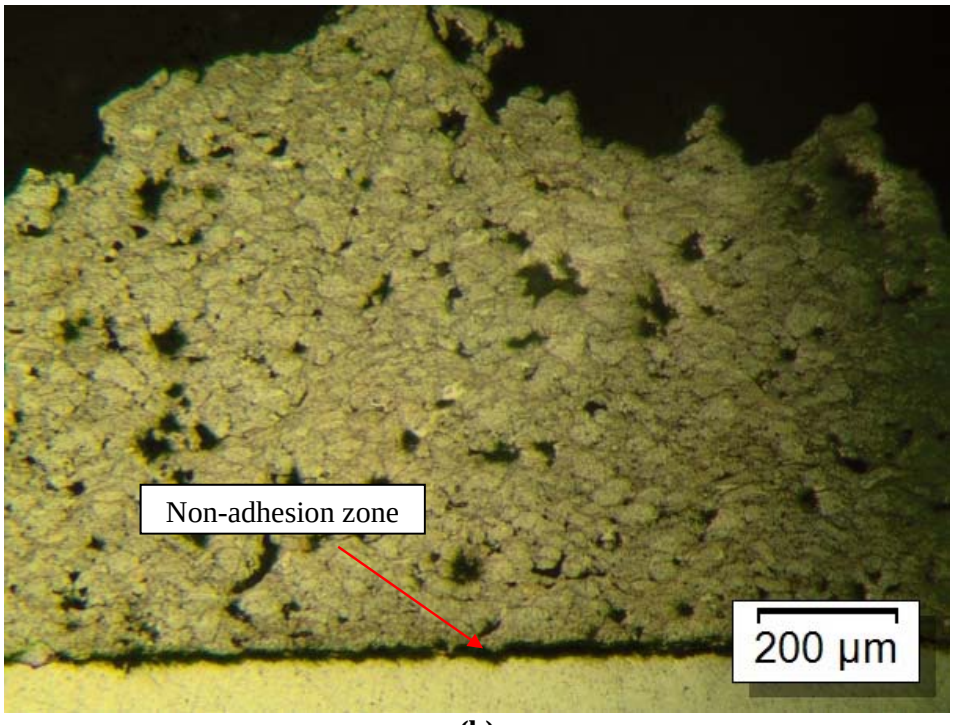

(b)

Figure 6.10: Microscopic images of Al-6061 cold spray coating formed with a nozzle placed stationary for four seconds at (a) 10x and (b) 100x magnification.

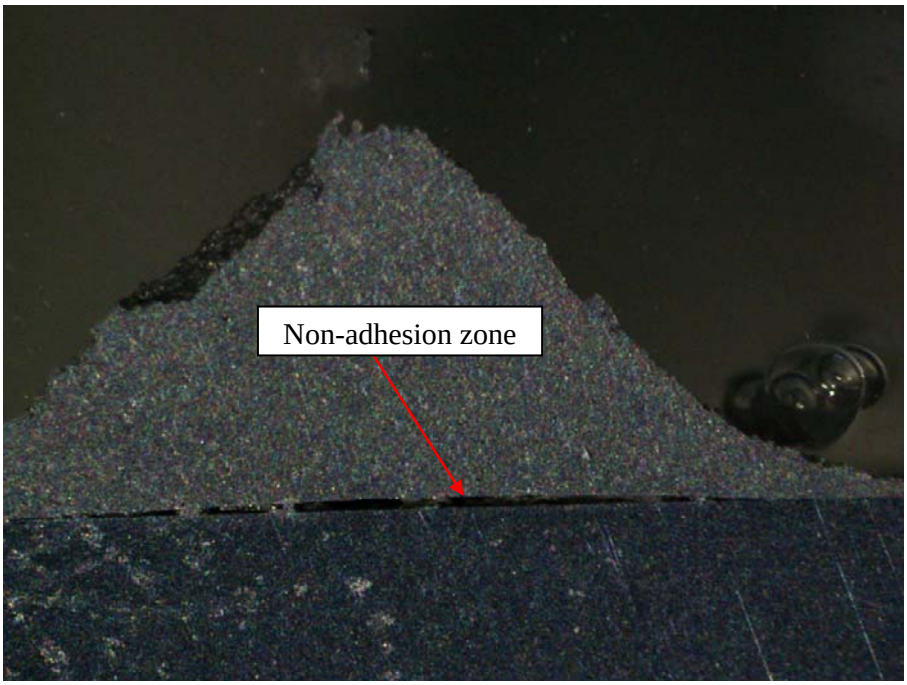

(a)

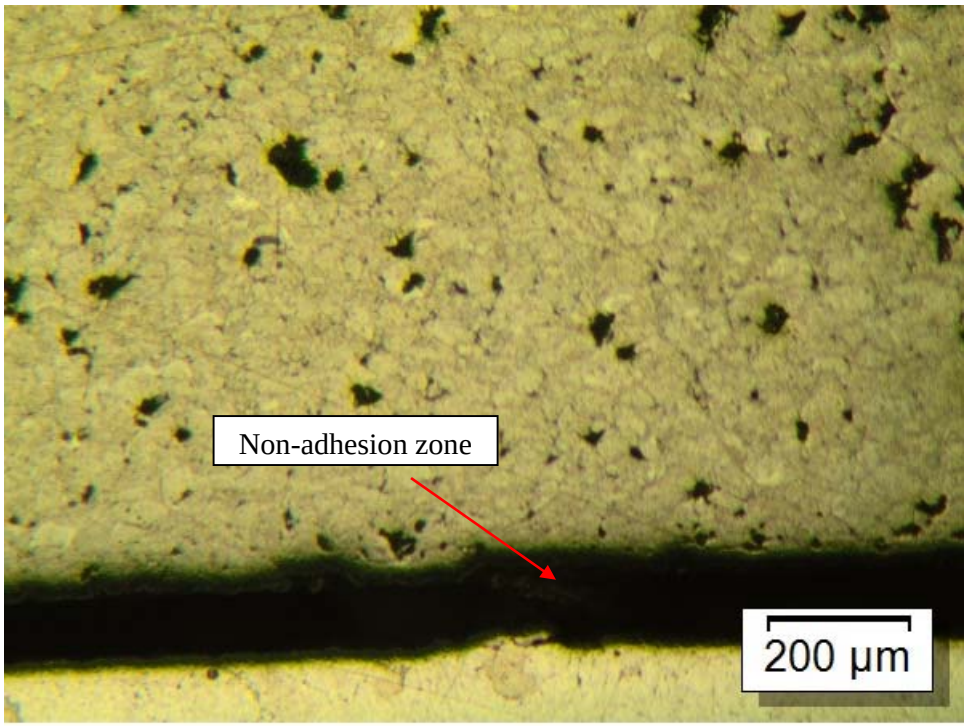

(b)

Figure 6.11: Microscopic images of Al-6061 cold spray coating formed with a nozzle placed stationary for five seconds at (a) 10x and (b) 100x magnification.

Figures 6.8 to 6.11 show the build-up of the Al-6061 coating as the cold spray nozzle was placed stationary above the Al-6061 substrate for two, three, four and five seconds respectively.

As the Al-6061 coating built-up within two seconds of stationary spraying, a well-defined interface between the coating and substrate can be seen, as shown in Figure 6.8. The cold spray particles were embedding themselves onto the roughened substrate surface and the impinging particles were building a layer of coating on top of the initial layer. There was no evidence of the coating delaminating from the substrate.

However, as the coating duration increases to three seconds, signs of delamination between the coating and the substrate started appearing as shown in Figure 6.9. The delamination appears to start from the middle and propagates towards the edges of the coating. As the duration of the stationary nozzle increases to four and five seconds, the delamination condition worsen, with the gap width and affected area increasing. A gap as wide as 150 μm can be seen between the coating and the substrate for the coating produced with the nozzle placed stationary for up to 5 seconds.

The progressive delamination of the Al-6061 coating from the substrate is likely due to the gradual build-up of both thermal and compressive residual stresses as the powder particles impinge on the substrate and subsequently on top of each layer. The cumulative residual stresses increases to the point where the top of the substrate plastically deform, causing the curvature of the substrate. The force created exceeded the tensile adhesion bond strength between the coating and the substrate and the delamination of the coating from the substrate occurs at the interface. As the cold spray

nozzle is stationary during the coating process, the cumulative residual stress should be highest at the centerline of the cold spray nozzle and decreases radially outwards. This probably explains the reason that the delamination starts from the centre of the coating where the widest gap is being observed and propagates outwards. In addition, as the magnitude of the temperature variation between the substrate and the impinging particles is relative small, the build-up of compressive residual stress is significantly higher than the thermal residual stress. This phenomenon will be further discussed in Chapter 7.

6.5 Measurement of Substrate Temperature during Cold Spray Process

An experiment to measure the substrate temperature during the cold spray process was carried out. A square Al-6061 substrate measuring 300 mm x 300 mm and 20 mm thick was used for this study. Prior to the start of the experiment, the substrate was marked with measurement points at 20 mm intervals from the centerline of the substrate where the cold spray nozzle will be directed, as shown in Figure 6.12. This is to facilitate the measurement of the temperature at various points radially away from the centerline of the cold spray location. The substrate surface temperature was measured using the Fluke 62 Mini Infra-red Thermometer. The thermometer works on the principle that every form of matter with a temperature above absolute zero emits infrared radiation (generically termed characteristic radiation) according to its temperature. The internal mechanical movement of molecules causes this and its intensity depends on the temperature of the object. And since the molecule movement represents charge displacement, electromagnetic radiation (photon particles) is emitted. These photons which operates in the 0.7 to 1000 μm wavelength spectrum, travel at the speed of light

and are detected by the photon sensors in the thermometer. This in term is processed and displayed as a digital reading on the thermometer interface display. The Fluke (Washington, USA) 62 Mini Infra-red thermometer can measure temperatures ranging from -30 °C to 500 °C and has an accuracy of ± 1.5 °C or ± 1.5% of the reading, whichever is higher. It can be used to measure a target up to 2 m and has a response time of less than 500 msec.

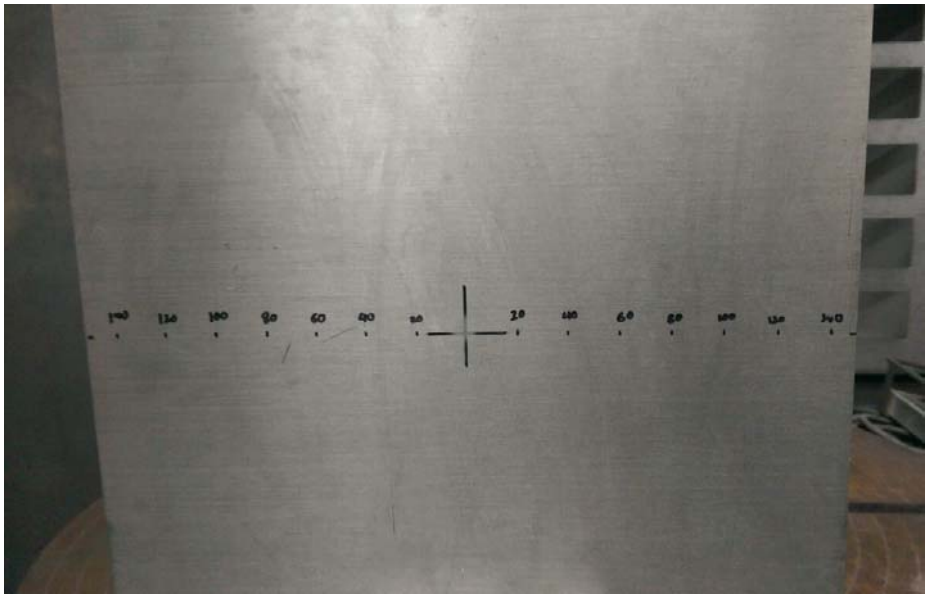

Figure 6.12: Al-6061 substrate used for measurement of temperature as the cold spray nozzle was held stationary.

At the start of the experiment, the cold spray system was turned on with Nitrogen as the carrier gas set at flow rate of 250 SLM, pressure of 4 MPA and temperature of 400 °C. No powder was introduced into the cold spray nozzle. The nozzle was subsequently moved to the centrepoint of the substrate and held stationary in that position as shown in Figure 6.13. Temperature of the substrate at the centerline was measured over 40 seconds and presented in Figure 6.14.

As shown in Figure 6.14, the temperature of the substrate at its center rises from room temperature (27 °C) at the start of the cold spray process. It reaches a steady state of about 41 °C from 30 seconds onwards. Similar increase in temperature was measured at the point 40 mm from the centre of the substrate. The steady state temperature reached was 38.4 °C after 30 seconds.

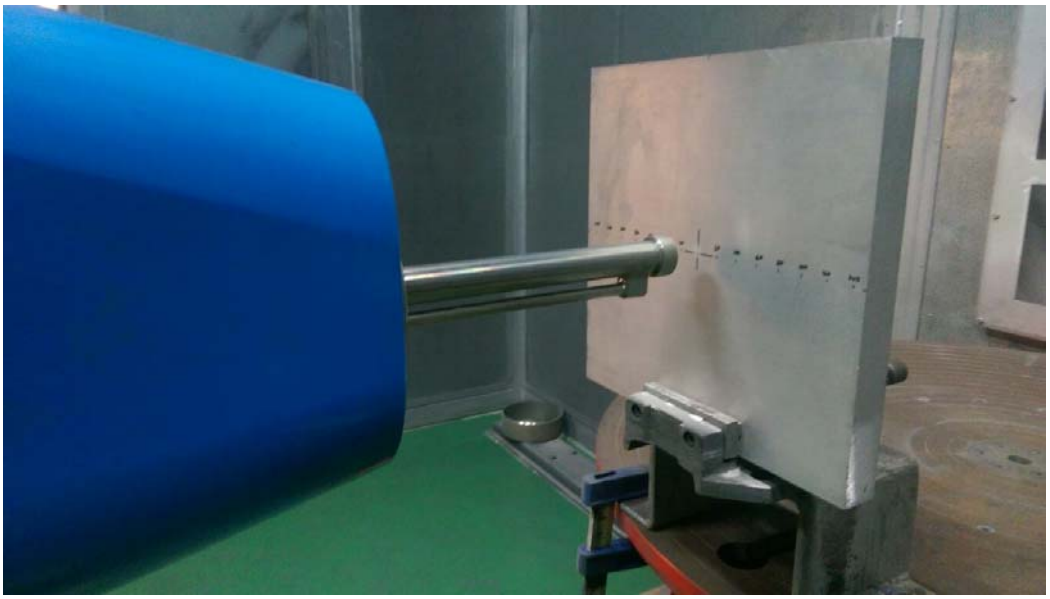

Figure 6.13: Position of cold spray nozzle during the substrate temperature measurement experiment.

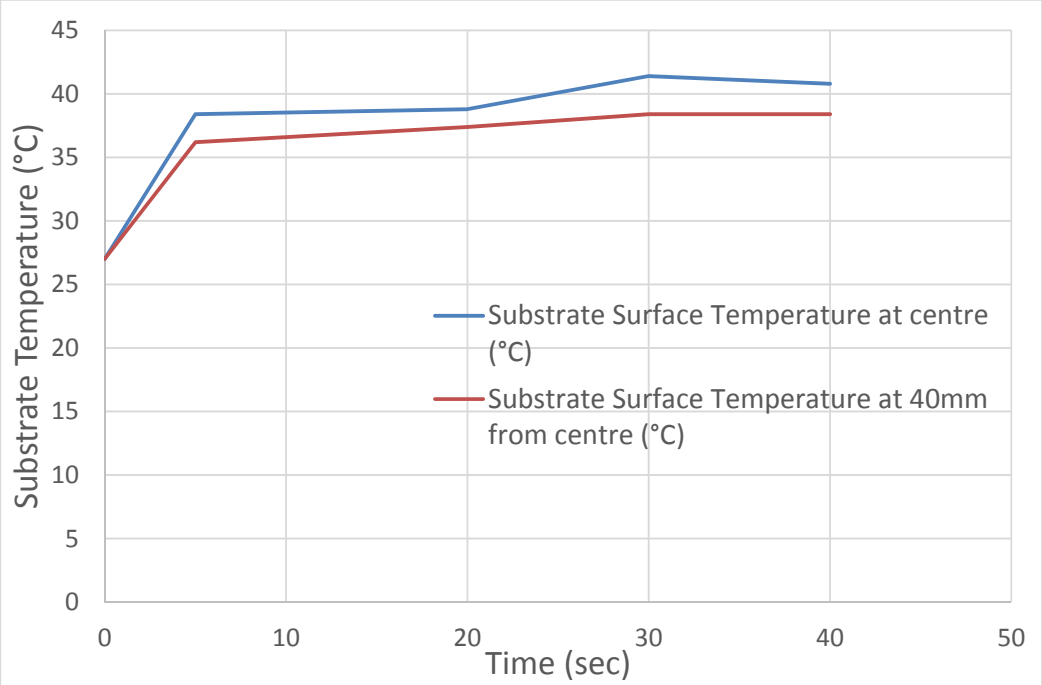

Figure 6.14: Temperature variation on the Al-6061 substrate during the cold spray of Nitrogen carrier gas at 400 °C, 4 MPa.

6.6 Conclusion

An experimental study was conducted to observe the cold spray coating as it is built-up with the nozzle held stationary. The intent is to understand and validate the cold spray as a multiple functional process. Microstructure analysis of the cross-sectional area of the cold spray coatings obtained at nozzle dwell time of one, two, three, four and five seconds respectively was performed. The results show that the cold spray process itself has a pre-coat surface roughening effect on the substrate. This suggests that a pre-coat grit blasting process which is typically employed in a conventional thermal spray process may not be necessary in a cold spray process. The coating microstructure results also indicated a delamination of the coating as the nozzle dwell time increases to three

seconds and beyond. The delamination appears to start from the centre of the conical shaped coating and propagates outwards towards the edges. The surface profile of the substrate and the coating at the substrate-coating interface suggests that the delamination occurs after the particles have previously embedded to the substrate. A residue stress larger than the adhesion strength seems to have forced the coating to delaminate from the substrate.

An experimental work to investigate the substrate temperature during the cold spray process was also carried out. The cold spray nozzle was placed stationary in the middle of an Al-6061 substrate and turned on without the powder. Nitrogen carrier gas at 400 °C and 4 MPa was expelled continuously from the nozzle onto the substrate and the temperature at 2 locations were measured periodically. It was found that the temperature at the centre of the substrate increases from room temperature (27 °C) to a steady-state of 41 °C from 30 seconds onwards. For a second measurement point 40 mm from the centre of the substrate, the steady-state temperature reached was 38.4 °C after 30 seconds.

The observation and measurements obtained in this chapter will be discussed further in Chapter 7.

CHAPTER 7

DISCUSSION AND CONCLUSIONS

7.1 Discussion

This chapter discusses the results and observations obtained from the experimental study in chapters 4, 5 and 6. The intent is to understand the effect of pre-coat substrate surface grit blasting, post-coat heat treatment and nozzle spray angle on the cold spray coating properties. The delamination phenomenon of the coating as the cold spray nozzle was held stationary will also be discussed in detail.

7.1.1 Effect of Pre-coat Grit Blasting

In the first study, the effect of surface roughening on the pre-coated substrate on the coating microhardness was investigated. It was found that pre-spray grit blasting has minimal impact on the microhardness of the cold sprayed coatings. The maximum microhardness value of the coating was also found to be almost identical to the microhardness of the substrate. This is attributed to the gradual compaction of the coatings which is a result of the constant and repeated impact of the cold sprayed impinging particles. The effect is so pronounced that the microhardness of the coating is almost equivalent to that of the substrate.

A second study to evaluate the effect of pre-coating substrate surface grit blasting on the coating tensile adhesion strength was also carried out. The results suggest that grit blasting the substrate may not have any positive effect on the coating adhesion strength.

This is contrary to the effect surface roughening has on the tensile adhesion strength of conventional thermal spray coatings. Microstructure evaluation of the coating formed on the non-grit blasted substrate suggests that the cold spray could be an intrinsic triplex process, in which the grit blasting, spray coating and shot peening are all carried out in a single pass. The grit blasting effect of the cold spray process was validated when a separate experiment was conducted to understand the short term effect of a stationary cold spray nozzle on the substrate surface. When the cold spray nozzle was held stationary for 1 second and allowed to spray on a substrate, the substrate surface appeared pitted, demonstrating the roughening effect of the cold spray process. This validates the hypothesis that cold spray in itself has a surface roughening effect on the substrate and does not require a pre-coat grit blasting prior to the process.

The high tensile adhesion strength obtained for the cold spray coating which was sprayed on non-grit blasted substrates is likely due to the unique feature of cold spray as a three-stage process. As cold spray deposition process occurs at temperatures well lower than the melting point of the feedstock materials, the adhesion mechanism differs from that of conventional thermal spray process. It is believed that the adhesion is based on severe plastic deformation or shear instability between solid plastic flow of particle and substrate materials. The interface reaction due to high velocity impact is believed to result in mechanical anchorage, physical adhesion and metallic interactions. As a result, the general understanding is that the rougher substrate surface will result in higher mechanical anchorage as the impacting particles get deformed more severely on roughened surface, enhancing their mechanical interlocking. However, for a cold spray process, the velocity distribution across the spray beam is typically Gaussian as shown in Figure 7.1. The velocity of the particles near the centerline will be higher than the

critical velocity while the particles at the rim will have velocities lower than the critical velocity when the cold spray system is operating at optimized parameters. As the spray beam travels transversely across the substrate, its surface is being impacted by the leading edge particles with less than the critical deposition velocity. This results in the erosion of the surface by the solid particles, creating an in-situ grit blasting effect. As the spray beam continues with its travel, the particles in the core with higher than the critical velocity, plastically deform over the freshly cleaned rough surface upon impact and in the process, form a coating. The process completes with the trailing edge particles hitting the substrates at lower than critical velocity. These particles will remove any loose particles and in the process shot peen the freshly formed coating. Thus cold spray can be considered as a three-in-one process, in which the grit blasting, spray coating and shot peening are all carried out in a single pass.

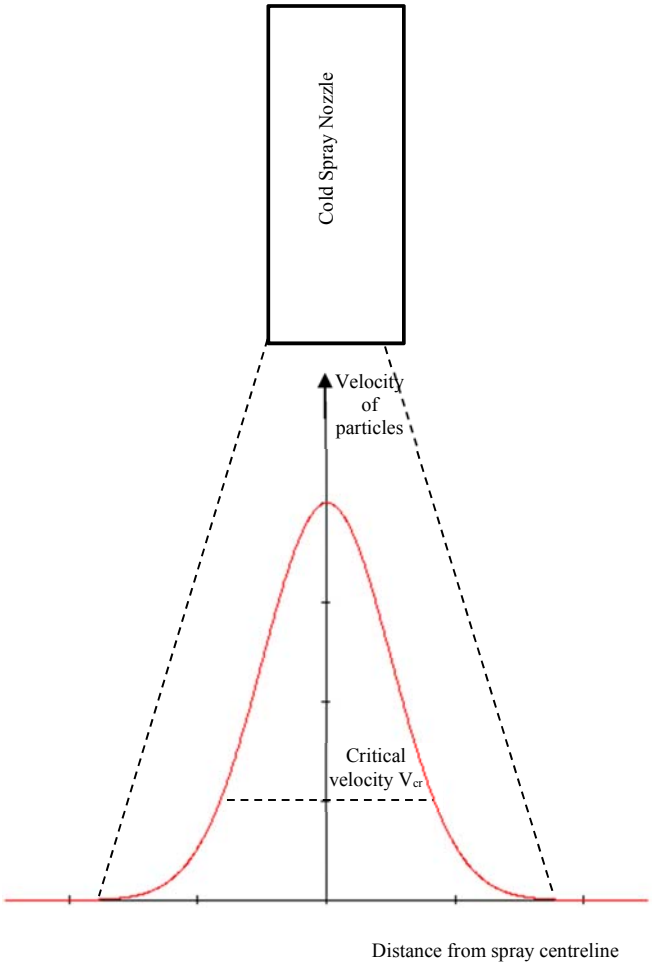

Figure 7.1: Gaussian distribution of particle velocity in cold spray process.

The results of these two experimental studies suggest that cold spray may require minimal surface preparation prior to coating. If grit blasting is eliminated from the pre-coating procedure, it will facilitate a more economical coating process.

7.1.2 Effect of Post-coat Heat Treatment

The effect of heat treatment heat treatment on the mechanical properties of the cold spray coatings was subsequently investigated. The intent is to find out if such post coating treatment will have a positive effect on the microhardness and tensile adhesion strength of the coatings. The results of the experimental study suggests that microhardness of the coatings was significantly lower after undergoing either stress relief or full annealing when compared to the coating which had not undergone any post treatment. The relative microhardness of the coatings which had undergone stress relief and full annealing were almost identical. The uniformity of the microhardness after undergoing stress relief or full annealing was also investigated. The results indicate that the heat treatment has a homogeneous effect on the microhardness of the coating.

A similar study to investigate the effect of post coating heat treatment on the coating tensile adhesion strength was also carried out. The results suggest that stress relief has little impact on the tensile adhesion strength of the coating when compared to the coating which had not undergone any heat treatment. However, for the coatings which had undergone full annealing, the tensile adhesion strength was significantly higher. Microstructure evaluation of the fully annealed coatings revealed signs that recrystallization and grain growth has taken place. It is believed that diffusion and fusion of coating particles at elevated temperature have contributed to the improved tensile adhesion strength of the coating.

The implication of the study is that both stress relief and heat treatment processes have the effect of increasing the ductility of the coating as well as homogenizing it. Stress relief however, has little impact on the tensile adhesion strength whereas for the coating

which was annealed, significant improvement was observed. Depending on the eventual desired properties of the coating, both heat treatment processes can be prescribed accordingly.

7.1.3 Effect of Spray Angle

In an ideal cold spray process set-up, the cold spray nozzle will be positioned normally (at 90 degrees) to the substrate throughout the spraying process. Unfortunately, this condition is not always possible as components are usually complex in their shape. In reality, off-normal coating is more commonly practiced and it is paramount to understand its effect on the coating quality. An experimental study was thus carried out to evaluate the effect of off-normal cold spray spraying on the mechanical properties of the coating. In the first study, the microhardness of the coatings obtained at spray angles of 90° (normal spray angle), 80º, 70°, 60º, 50° and 40º was evaluated. It was found that the average microhardness of the coatings was relatively similar for spray angles from 90° to 70º. However, as the spray angle decreased from 70° to 40º, the average microhardness of the coatings actually increased. The highest microhardness value was recorded at 116.8 Hv_{100g}, which was obtained at spray angle of 40°. The likely cause of the increase in coating microhardness as the spray angle decreased was the increase in plastic deformation of the cold sprayed particles as they collided onto the substrate and impinged onto each other. The increase in plastic deformation enhanced the dislocation within the crystal structure of the impinging particles, thus cold working the coating as it builds up. The result is an increase in the microhardness of the coating.

In the second study, the effect of the spray angle on the coating tensile adhesion strength was evaluated. The experimental results suggested that the spray angle had minimal impact on the tensile adhesion strength of the coatings. The cross-sectional microstructure images of the coatings showed that at all spray angles, the particles embedded themselves onto the substrate surface, leaving little or no gap between the particles and the substrate. As tensile adhesion strength was dependent on the magnitude of the contact surface area, its value was not affected in all the spray angles.

In the third study, the effect of the spray angle on the relative coating deposition rate was investigated. The results suggested that there was a detrimental effect on the relative coating deposition rate as the spray angle became more off-normal. It was also found that a more pronounced decrease in relative coating rate took place as the spray angle decreased from 60º to 50° and even more significantly at 40º.

The implication of the above studies is that for hard-to-reach areas, a spray angle as small as 40° is still acceptable as the mechanical properties of the coating in terms of microhardness and tensile adhesion strength will not be affected. However, the results also suggest that if coating deposition rate is a key consideration, spray angle smaller than 60° should be avoided.

7.1.4 Delamination of Coating with Stationary Cold Spray Nozzle

In Chapter 6, an experimental study was carried out to observe the coating build-up phenomenon as the cold spray nozzle was held stationary for up to five seconds. One

of the observations was the delamination of the coating from the substrate in the middle of the coating. This was shown in Figures 6.5a and 6.5b.

What we have also observed in this experimental study was the formation of the coating on top of the high pressure region which suggested that as the initial particles decelerate, the subsequent particles continue to impinge on the initial particles, forming the coating. Over time, a non-adhesion zone was formed around the high pressure region as the coating continued to build up.

One possible explanation for the observation could be the presence of a bow shock near the substrate as was reported by Samareh et al. [27]. The three-dimensional numerical analysis suggested the formation of a strong Bow shock formed on the substrate with a high stagnation point created near the plate. This high pressure region causes the particles to decelerate and impact the substrate in an off-normal angle. The numerical study shows that some particles do not impact the substrate and are removed by the gas flow instead as the deviation of particle trajectories from the centreline can be excessively strong.

However, as we look at the interface between the coating and substrate surface, the profile on the delaminated surfaces matches. This showed that the particles did adhere to the substrate before being pulled apart. This observation, together with the absence of delamination of the coating at early time phase (up to two seconds) suggested that the b ow shock proposed by Samareh *et al*. [27] is unlikely to be the cause of the delamination.

In an elastic deformation condition, a material may deform and subsequently return to its original state after the release of the applied load or temperature. The behaviour is governed by Hooke's Law. During the deposition process when the cold spray nozzle is held stationary, the stresses which the substrate is subjected to is likely to go beyond the elastic limit and deform plastically. Plastic deformation is not a reversible process and unlike elastic deformation, is dependent on the initial and final states of the loading as well as the loading history path by which the final state is achieved. Using the Mróz [1967] model, the material behaviour of Bauschinger effect with kinematic hardening rule is adopted to describe the plastic deformation. This is shown in Figure 7.2 where the uniaxial tensile stress test is taken beyond the yield point and into the inelastic regime and subsequently unloaded to zero strain. At the zero strain state, there exist a stress that is compressive in nature which is termed the residual stress.

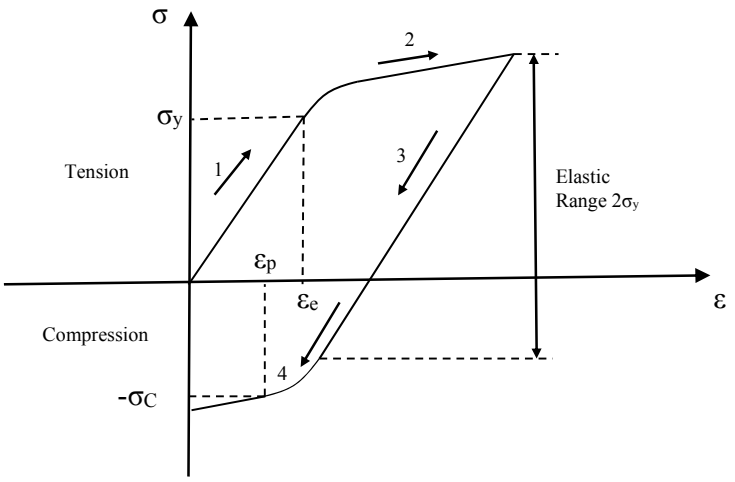

Figure 7.2: Mróz model illustrating Bauschinger effect with kinematic hardening rule.

In order to understand the stress-strain behaviour in the case where the cold spray nozzle was placed stationary, we reverse the plot in Figure 7.2 where the initial stress direction is compressive as shown in Figure 7.3.

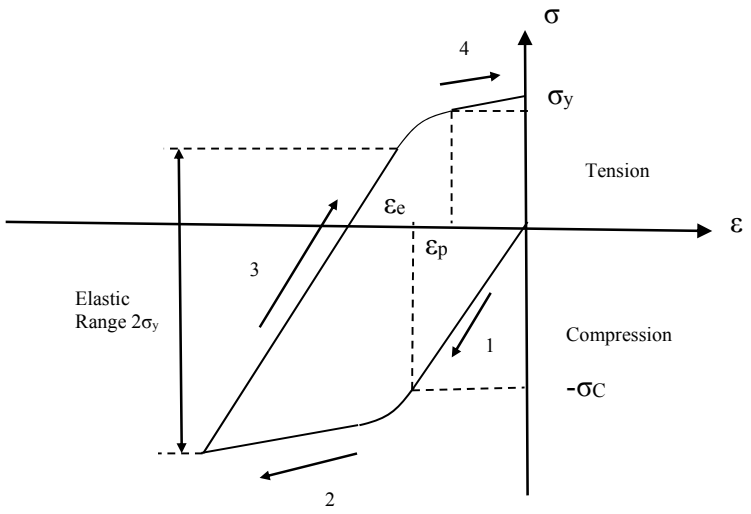

Figure 7.3: Reversed compressively loaded stress strain curve.

When the cold spray nozzle was placed stationary and ignited, the substrate and the coating deposited on it were subjected to stresses beyond the elastic yield stress in the compressive state (path 1) and was plastically deformed (path 2). As the cold spray deposition stopped, the compressive stresses was released and the substrate tries to return to its original state (path 3 to 4), giving rise to the tensile residual stress. However, the residual tensile stresses which has build-up over that duration was sufficient enough to cause the coating to delaminate from the substrate. This residual tensile stress would have to be greater than the tensile adhesion strength obtained in Chapter 4, i.e., greater than 40 MPa for the non-grit blasted coating.

The effect of temperature on the substrate in the whole process is considered negligible as the experiment conducted in Section 6.5 suggests that the change in temperature on the substrate is small (approximately 13 °C).

The implication from the results of the above experimental study is that holding a cold spray nozzle stationary for an effective and quick build-up of coating at a localized area is not encouraged. The build-up of compressive residual stresses is likely to result in delamination of the coating from the substrate, leading to premature coating failure.

7.2 Conclusions

Cold spray technology has demonstrated its potential as a viable alternative coating method to address abrasion, wear and corrosion issues in various industries. To further explore its versatility, this research work specifically looked into the use of cold sprayed Al-6061 coating as a possible repair for corroded gas turbine engine fan cases. Though preliminary results showed its technical viability as an alternate repair method, there was still a need to better understand the effect of pre and post spraying conditions on the properties of the coatings. In addition, as most components are complex in their shapes, it was also crucial to evaluate the effect of varying spray angle on the coating properties.

This work started with the study on the effects of three spraying parameters; carrier gas temperature, carrier gas pressure and powder feed rate on the cold spray particle in-flight velocity. Using commercially available Aluminium powder, it was found that a direct positive relationship exists between the carrier gas pressure and temperature with respect to the in-flight particle velocity. The relationship between the powder feed rate and the particle velocity however seems insignificant. The distance from the nozzle exit at which the maximum particle velocity was reached was also established. The results from the study carried out were used to form the basis for establishing the optimum coating parameters for subsequent experiments.

Experimental studies were subsequently carried out to evaluate the effect of pre and post cold spray conditions on the coating mechanical properties. This was done with the intent to understand the effects of such processes on the quality of the coatings and appraise their necessity in an industrial cold spray application.

Experiments were first carried out to evaluate the effect of pre-coating substrate surface roughening in the form of grit blasting on the coating microhardness and tensile adhesion strength. The results show that grit blasting of the substrate has minimal impact on the coating microhardness. The results from the tensile adhesion strength test indicated that grit blasting on the substrate surface can have a detrimental effect on the coating adhesion strength. The presence of micro-voids created by the angular alumina grit which prevented the formation of bonds due to adiabatic shear instability as well as impurities from the alumina grit are believed to be the two contributing factors to the decreased tensile adhesion strength. In addition, the inherent triplex characteristic of cold spray process, in which the grit blasting, spray coating and shot peening are all carried out in a single pass resulted in coating with non-grit blasted substrate obtaining enhanced tensile adhesion strength. The results further validated the elimination of grit blasting as a pre-coating process, contrary to conventional thermal spray processes. This finding will further optimize the operating processes required for cold spray in an industrial application.

The effect of post coating heat treatment on the microhardness and tensile adhesion strength of the cold sprayed coatings was also evaluated. The results indicated that both stress relief and annealing processes reduces as well as homogenizes the microhardness of the coatings. The tensile adhesion strength of the coating was found to be unaffected by stress relief but improved significantly when subjected to annealing. The results show that both stress relief and annealing can be utilized if either uniformity of microhardness and/or an increase in tensile adhesion strength is desired in an actual cold spray industrial application.

The effect of nozzle spray angle on the microhardness and tensile adhesion strength was also studied. The results showed that the effect of spray angle as small as 40° on the coating microhardness and tensile adhesion strength is minimal. However, the relative deposition efficiency is severely affected for spray angle smaller than 60°. As off-normal cold spraying is inevitable in industrial application, this is a trade-off which has to be managed.

The effect of a stationary cold spray nozzle on the coating deposition was also studied. Experimental results showed that when the cold spray nozzle is held stationary for up to three seconds, the coating formed will start to delaminate from the substrate. This is due to the build-up of compressive residual stresses which exceeds the tensile adhesion strength of the coating. From an application perspective, the results indicate that holding the cold spray nozzle in a stationary position is not an ideal method to build-up cold spray deposition.

In summary, the work carried out in this report serves to contribute to the cold spray technology body of knowledge in the following ways:

1. A literature review that is focused in the area of cold spray technology and guides the interested readers to main sources of information which is related to this work. The review done is also critical and directly associated to the intended motivation of the thesis.
2. Diagnostic and measurement techniques that provides engineering and scientific feedback were use such that the quality of the cold spray coatings can be directly related to the processing environment.

3. The results of the experimental studies carried out in this work serve as a comprehensive guide in terms of the implementation of this relatively new coating technology in an industrial setting, specifically the repair and remanufacturing of an aluminium gas turbine engine fan case.
4. A thorough and unique quantitative analysis of spray angle effects in relation to cold spray technology. This has important implications concerning the efficiency and implementation of these coatings into actual production as most components have complex geometry.

7.3 Recommendations for Future Work

The following are suggested areas for future work:

1. A numerical simulation to investigate the build-up of thermal and mechanical residual stresses on the coating-substrate interface during a stationary nozzle deposition process should be conducted to investigate the cause of the delamination. This would provide better insights into the mechanism that contributed to the coating delamination. It is believed that the impact dynamics of the particles on the substrate resulted in the built-up of residual stresses which causes the delamination. A programme with a detailed finite element analysis of the deposition at various dwell times and heights should be carried out.

2. Additional numerical study can be carried out to simulate in-flight behaviour of cold spray powder in supersonic flow. This will help to provide better understanding on the flight trajectory, powder velocity and density just before impact. And compliment the experimental results which have been obtained from the current work.

3. As this study was started with a specific industrial application, optimization of the process can be further enhanced. A study with variation in cold spray parameters in terms of carrier gas pressure and temperature combine with varying spray angles can be carried out to better characterize the process. This would serve to improve the coating quality and coating deposition efficiency.

4. In an industrial application, the cold spray coating requires additional machining to obtain the desired surface finish. The need for post coating

finishing is often resource consuming. Further work can be performed to understand how to better control the surface finishing of a cold spray coating. This could be in the form of using a nozzle with a smaller diameter, finer powder or different spray nozzle traversing speed. Such a study would further enhance the effectiveness of cold spray technology as a viable remanufacturing process.

5. Parameters used for grit blasting of the substrates as well as the methods for cleaning can be further investigated to understand their impact on the mechanical properties of the coating. Similar study of different materials and substrate combination using identical cold spray parameters would also provide better insight on the bonding mechanism between the particles and substrate.

6. In addition, cold spray has established itself as a promising coating process which overcomes the deficiencies of conventional thermal spray methods that employs melting of feedstock as the main process. Its prospect lies in its application in very selective conditions which require high purities and superior mechanical properties. Key challenges for the technology remain but if these are overcome it could open up new range of applications not achievable with existing materials and practices. Specifically, with the establishment of the capability and potential of cold spray system in coating 2 types or conglomerated powder, research work can focus on the search and the ultimate discovery of the existence of an ideal ductile/brittle composition for optimal coating deposition efficiency with the aid of in-flight diagnostic devices. The impact of ductile and brittle powder particle sizes (nano versus micro) as well as particle morphology on coating deposition efficiency should also be studied.

References

Ajdelsztajn L., Jodoin B., Kim G.E., Schoenung J.M. and Mondoux J., 2005, *Cold Spray Deposition of Nanocrystalline Aluminium Alloys*, Metall., Mater. Trans. A, 36, p657-666.

Ajdelsztajn L., Tang F., Kim G.E., Provenzano V. and Schoenung J.M., 2005, *Synthesis and Oxidation Behaviour of Nanocrystalline McrAlY Bond Coatings*, J. Thermal Spray Technol., 14 (1), p23-30.

Al-Mangour B., Vo P., Mongrain R., Irissou E. and Yue S., 2014, *Effect of Heat Treatment on the Microstructure and Mechanical Properties of Stainless Steel 316L Coatings Produced by Cold Spray for Biomedical Applications*, J. Thermal Spray Technol., 24 (4), p188-192.

Alkhimov A.P., Gudilov A.I., Kosarev V.F. and Nesterovich N.I., 2000, *Specific Features of Microparticle Deformation Upon Impact on a Rigid Barrier*, J. Appl. Mech. Tech. Phys., 41(1), p188-192.

Alkhimov A.P., Kosarev V.F. and Klinkov S.V., 2001, *The Feature of Cold Spray Nozzle Design*, J. Thermal Spray Technology, Vol. 10 (No. 2), p375-381.

Alkhimov A.P., Papyrin A.N., Dosarev V.P., Nesterovich N.J. and Shuspanov M.M., 1994, *Gas-dynamic Spraying Method for Applying a Coating*, US Patent 5,302,414.

Ang A.S.M., Berndt C.C., Cheang P., 2011, *Deposition Effects of WC Particle Size on Cold Sprayed WC-Co Coatings*, Surface & Coatings Tech, Vol. 205 (10), p3260-3267.

Assadi H., Gartner F., Stoltenhoff T., Kreye H., 2003, *Bonding Mechanism in Cold Gas Spraying*, Acta Mater., 51, p4379-4394.

ASTM C633-01, *Standard Test Method for Adhesion or Cohesion Strength of Thermal Spray Coatings*, ASTM International, West Conshohocken, PA, 2013.

ASTM E3-01(2007)e1, *Standard Guide for Preparation of Metallographic Specimens*, ASTM International, West Conshohocken, PA, 2013.

ASTM E407-07, *Standard Practice for Microetching Metals and Alloys*, ASTM International, West Conshohocken, PA, 2013.

ASTM G44-99, *Standard Practice for Exposure of Metals and Alloys by Alternate Immersion in Neutral 3.5% Sodium Chloride Solution*, ASTM International, West Conshohocken, PA, 2013.

Bauchhage K., Schöne F., Wriedt T., and Dopheide D., 1986, *Phase Doppler Measurements Using Laser and Avalanche Photo-diodes in a Back Scattering Arrangement*, Laser Anemometry – Proceedings of the 3rd International Conference, Lisbon, Portugal, p455-468.

Birtch W., Russell G. and Hale S.E., 2008, *Kinetic Spray for Corrosion Protection and Metal Part Restoration*, Commercial Technologies for Maintenance Activities (CTMA) Symposium, Baltimore, Maryland, USA.

Bisson J.F., Moreau C., Dorfman M., Dambra C., and Mallon J., 2003, *Behavior and Characterization of Two 7-8wt% Yttria-Stabilized Zirconia Powders and Coatings Produced Using Plasma Spray Deposition*, Thermal Spray 2003: Advancing the Science & Applying the Technology, (Ed.) Moreau C. and Marple B., Published by ASM International, Materials Park, Ohio, USA, p1583-1589.

Borchers C., Gartner F., Stoltenhoff T. and Kreye H., 2003, *Microstructural and Macroscopic Properties of Cold Sprayed Copper Coatings*, J. Appl. Phys., 93, p10064-10070.

Calla E., McCartney D.G. and Shipway P.H., 2006, *Effect of Deposition Conditions on the Properties and Annealing Behaviour of Cold-Sprayed Copper*, J. Thermal Spray Technol., 15 (2), p255-262.

Cetegen B.M. and Yu W., 1999, *In-Situ Particle Temperature, Velocity, and Size Measurements in DC Arc Plasma Thermal Sprays*, J Thermal Spray Technology, Vol. 8, p57-63.

Champagne V.K., 2008, *The Repair of Magnesium Rotorcraft Components by Cold Spray*, Journal of Failure Analysis and Prevention, Vol. 8, 2, p164-175.

Champagne V.K., Helfritch D., Leyman P., Lempicki R. and Grendahl S., 2005, *The Effects of Gas and Metal Characteristics on Sprayed Metal Coatings*, Modelling and Simulation in Materials Science and Engineering, Vol. 13, p1119-1128.

Champagne V.K. and Barnett B., 2012, *Cold Spray Technology for DoD Applications*, ASETS Defense 2012: Workshop on Sustainable Surface Engineering for Aerospace and Defense, San Diego, CA., USA.

Champagne V.K. and Ziegler W., 2002, *Cold Spray Technology for Military Applications*, U.S. Army Corrosion Summit, St. Petersburg, FL., USA.

Crawmer, D.E., 2013, *Thermal Spray Processes*, Thermal Spray Technology, Vol. 5A, ASM Handbook, ASM International, p3-9.

Dennehy N., 2014, *Plasma Giken: Thermal Spray Solutions since 1980*, Plasma Giken Co., Ltd.

Dykhuizen R.C., Smith M.F., Gilmore D.L., Neiser R.A., Jiang X. and Sampath S., 1999, *Impact of High Velocity Cold Spray Particles*, J. Thermal Spray Technol., 8(4), p559-564.

Fauchais P.L., Heberlein J.V.R., Boulos M.I., 2014, *Overview of Thermal Spray*, Thermal Spray Fundamentals: From Powder to Part, Springer, p17-72.

Fincke J.R., Swank W.D., Bewley R.L., Haggard D.C., Gevelber M. and Wroblewski D., 2001, *Diagnostics and Control in the Thermal Spray Process*, Surface and Coatings Technology, Vol. 146/147, p537–543.

Friis M., Persson C. and Wigren J., 2001, *Influence of Particle In-Flight Characteristics on the Microstructure of Atmospheric Plasma Sprayed Yttria Stabilized ZrO_2*, Surface and Coating Technology, Vol. 141, p115-127.

Fukanuma H. and Huang Y., 2000, *Splat Formation in Off-normal Angel Spray*, Thermal Spray: Surface Engineering via Applied Research, ASM International, OH, p767-776.

Fukanuma H., Ohno N., Sun B. and Huang R., 2006, *In-flight Particle Velocity Measurements with DPV-2000 in Cold Spray*, Surface & Coating Technology, 201, p1935-1941.

Gaffet E., Malhouroux N. and Abdellaoui M.,1993, *Far from Equilibrium Phase Transition Induced by Solid State Reaction in the Fe-Si System*, J. Alloys Compd., 194, p339-360.

Gartner F., Stoltenhoff T., Schmidt T. and Kreye H., 2006, *The Cold Spray Process and Its Potential for Industrial Applications*, J. Thermal Spray Technology, Vol. 15 (No. 2), p223-232.

Gauthier B., Tailleart N., Eidelman S., Book D. and Scully J.R., 2008, *Spray Applied Amorphous/Nnaocrystalline Aluminium Alloy Coatings as a Replacement for Aluminium Cladding*, The Electrochemical Society, 11(15), p59-74.

Gilmore D.L., Dykhuizen R.C., Neiser R.A., Roemer T.J. and Smith M.F., 1999, *Particle Velocity and Deposition Efficiency in the Cold Spray Process*, J. Thermal Spray Technology, Vol 8 (No. 4), p576-582.

Goldman M.E., Unlu N., Shifflet G.J. and Scully J.R., 2005, *Selected Corrosion Properties of a Novel Amorphous Al-Co-Ce Alloy System*, Electrochem. Solid State Lett., 8(2), pB1-B5.

Gougeon P. and Moreau C., 1993, *In-Flight Particle Surface Temperature Measurement: Influence of the Plasma Light Scattered by The Particles*, Journal of Thermal Spray Technology, Vol. 2 (3), p229-234.

Grasme D., 2003, *First Serial Application of Cold Spraying for Coating Heat Sinks*, 6th Colloquim "High Velocity Oxy Fuel Spraying", Erding, D, GTS e.V., p119-122.

Grujicic M., Saylor J.R., Beasley D.E., Derosset W.S. and Helfritch D., 2003, *Computational Analysis of the Interfacial Bonding between Feed Powder Particles and the Substrate in the Cold-gas Dynamic-spray Process*, Appl. Surf. Sci., 219, p211-227.

Hall A.C., Cook D.J., Neiser R.A., Roemer T.J. and Hirschfeld D.A., 2006, *The Effect of a Simple Annealing Heat Treatment on the Mechanical Properties of Cold Sprayed Aluminium*, J. Thermal Spray Technol., 15 (2), p233-238.

Haynes J. and Karthikeyan J., 2003, *Cold Spray Copper Application for Upper Stage Rocket Engine Design*, Thermal Spray: Advancing the Science and Applying the Technology (Proc. ITSC 2003), (Orlando, FL), ASM International, p117-222.

Jen T., Li L., Cui W., Chen Q. and Zhang X., 2005, *Numerical Investigations on Cold Gas Dynamic Spray Process with Nano- and Microsize Particles*, International Journal of Heat and Mass Transfer, 48, p4384-4396.

Kang C.W. and Ng H.W., 2006, *Splat Morphology and Spreading Behaviour due to Oblique Impact of Droplets onto Substrates in Plasma Spray Coating Process*, Surf. Coat. Technol., 200, p5462-5477.

Kang C.W., Ng H.W. and Yu S.C.M., 2006, *Comparative Study of Plasma Spray Flow Fields and Particle Behaviour Near to Flat Inclined Substrates*, Plasma Chemistry and Plasma Processing, 26, p149-175.

Kang C.W., Ng H.W. and Yu S.C.M., 2006, *Imaging Diagnostics Study on Obliquely Impacting Plasma-Sprayed Particles Near to the Substrate*, J. Thermal Spray Technol., 15 (1), p118-130.

Karthikeyan J., 2004, *Cold Spray Technology: International Status and USA Efforts*, ASB industries, Inc.

Klassen T. and Kreye H., 2006, The Cold Spray Process and its Optimization, poster published by Institute of materials Technology, Helmut-Schmidt University.

Klinkov S.V., Kosarev V.F. and Rein M., 2005, *Cold Spray Deposition: Significance of Particle Impact Phenomena*, Aerospace Science and Technology 9, p582-591.

Koh P.K., Loke K., Cheang P. and Lee C.T., 2012, *Cold Spray Repair of Gas Turbine Engine Fan Cases*, Singapore Aerospace Technology & Engineering Conference, Singapore.

Koh P.K., Loke K., Cheang P., Yu S.C.M. and Ang S.M., 2012, *Deposition of Amorphous Aluminium Powder Using Cold Spray*, Thermal Spray 2012: Proceedings from the International Thermal Spray Conference and Exposition, Houston, Texas, USA.

Kucuk A., Lima R.S. and Berndt C.C., 2001, *Influence of Plasma Spray Parameters on Formation and Morphology of ZrO_2-8 Wt% Y_2O_3 Deposits*, Journal of American Ceramic Society, Vol. 84 (4), p693-700.

Kumar S., Bae G. and Lee C., 2009, *Deposition Characteristics of Copper Particles on Roughened Substrates through Kinetic Spraying*, Applied Surface Science, 255, p3472-3479.

Leigh S.H. and Berndt C.C., 1997, *Evaluation of Off-angle Thermal Spray*, Surf. Coat. Technol., 89 (3), p213-224.

Lesinki J. and Boulos M.I., 1988, *Laser Doppler Anemometry under Plasma Conditions - Part I: Measurements in a D.C. Plasma Jet*, Plasma Chemistry and Plasma Processing, Vol. 8, p113-132.

Li C.J. and Li W.Y., 2003, *Deposition Characteristics of Titanium Coating in Cold Spraying*, Surf. Coat. Technol., 167, p278-283.

Li C.J., Li W.Y. and Fukanuma H., 2004, *Impact Fusion Phenomenon during Cold Spraying of Zinc*, Thermal Spray 2004: Advances in Technology and Application, ASM International, May 10-12, 2004 (Osaka, Japan), ASM International, p1129.

Li C.J., Li W.Y., Wang Y.Y. and Fukanuma H., 2003, *Effect of Spray Angle on Deposition Characteristics in Cold Spraying*, Thermal Spray 2003: Advancing the Science of Applying the Technology, ASM International, Material Parks, OH, USA, p91-96.

Li W.Y., Li C.J. and Liao H., 2006, *Effect of Annealing Treatment on Microstructure and Properties of Cold-Sprayed Cu Coating*, J. Thermal Spray Technol., 15 (2), p206-211.

Lima R.S., Karthikeyan J., Kay C.M., Lindermann J. and Berndt C.C., 2002, *Microstructural Characteristics of Cold-Sprayed Nanostructured WC-Co Coatings*, Thin Solid Films, 416, p129-135.

Lima R.S., Kucuk A., Berndt C.C., Karthikeyan J., Kay C.M. and Lindemann J., 2002, *Deposition Efficiency, Mechanical Properties and Coating Roughness in Cold-sprayed Titanium*, J. Materials Science Letters, 21, p1687-1689.

Longo F.N., 2004, *Postcoating Operations*, Handbook of Thermal Spray Technology, J.R. Davis, Ed., ASM International, p128-131.

Ma J., Yu S.C.M. and Ng H.W., 2005, *The Particle In-Flight Characteristics in Plasma Spraying Process Measured by Phase Doppler Anemometry (PDA)*, Plasma Chemistry and Plasma Processing, Volume 25 (1), p55-86.

Ma J., Yu S.C.M., Ng H.W. and Lam C.Y., 2004, *Some Observations on Particle Size and Velocity Measurements Using Phase Doppler Anemometry in Plasma Spray*, Plasma Chemistry and Plasma Processing, 24 (1), p85-115.

McCune R.C., 2003, *Potential Applications of Cold-Spray Technology in Automotive Manufacturing*, Thermal Spray 2003: Advancing the Science and Applying the Technology, C. Moreau and B. Marple, Ed., ASM International, p63–70.

McCune R.C., Papyrin A.N., Hall J.N., Riggs W.L. and Zajchowski P.H., 1995, *An Exploration of the Cold Gas-Dynamic Spray Method for Several Materials Systems*, Advances in Thermal Spray Technology (Proc. of the Eighth National Thermal Spray Conf.), C.C. Berndt and S. Sampath, Ed., ASM International, p1–6.

Military Specification, MIL-DTL-83488D, Coating, Aluminum, High Purity, revision D, DOD, 01 Apr 1999.

Mishin J., Vardelle M., Lesinski J. and Fauchais P., 1987, *Two-Colour Pyrometer for the Statistical Measurement of the Surface Temperature of Particles Under Thermal Plasma Conditions*, Journal of Physics E, Vol. 20, p620-624.

Montavon G., Sampath S., Berndt C.C., Herman H. and Coddet C., 1997, *Effect of the Spray Angle on Splat Morphology during Thermal Spraying*, Surf. Coat. Technol., 91 (1-2), p107-115.

Morelli D.T., Elmoursi A.A., Van Steenkiste T.H., Fuller B.K., Gillispie B.A. and Gorkiewicz D.W., 2006, *Kinetically Sprayed Aluminium Metal Matrix Composites for Thermal Management*, US Patent US7081376.

Moridi A., Hassani-Gangaraj S.M., Guagliano M., Dao M., 2014, *Cold Spray Coating: Review of Material Systems and Future Perspectives*, Surface Engineering, Vol. 36, No. 6, p369-395.

MOOG Aircraft Group, 2012, *Advanced Surface Repair Capabilities*, MOOG Corporate website.

Morgan R., Fox P., Pattison J., Sutcliffe C. and O'Neill W., 2004, *Analysis of Cold Gas Dynamically Sprayed Aluminium Deposits*, Mater. Lett., 58, p1317-1320.

Mroz Z., 1967, *On the Description of Anisotropic Workhardening*, J. Mech. Phys. Solids 15, p163-175.

Naqwi A. and Durst F., 1992, *Light Scattering Applied to LDA and PDA Measurements Part 2: Computational Results and their Discussion*, Particles and Particle Systems Character, Vol. 9, 1992, p66-80.

Papyrin A., 2006, *Cold Spray Equipments and Technologies*, Cold Spray Technology, Elsevier Science, p179-247.

Planche M.P., Normand B., Suzon E. and Coddet C., 2001, *The Relationships Between In-Flight Particles Characteristics and Coatings Properties under Plasma Spraying Conditions*, Thermal Spray 2001: New Surfaces for a New Millenniums, (ED.) C.C. Berndt C.C., Khor K.A., and Lugscheider E.F., Published by ASM International, Materials Park, Ohio, USA, p771-777.

Qiu H.H. and Sommerfeld M., 1992, *A Reliable Method for Determining the Measurement Volume Size and Particle Mass Fluxes Using Phase-Doppler Anemometry*, Experiments in Fluids, Vol. 13, p393-404.

Richer P., Jodoin B. and Ajdelsztajn L., 2004, *Characteristics of Cold Sprayed Coatings Using Nano-Aluminium and Nano-Nickel Powders*, 16th Canadian Materials Science Conference, Ottawa, ON, Canada.

Richer P., Jodoin B., Ajdelsztajn L. and Lavernia E.J., 2006, *Substrate Roughness and Thickness Effects on Cold Spray Nanocrystalline Al-Mg Coatings*, J. Thermal Spray Technol., 15 (2), p246-254.

Saffman M., Buchhave P. and Tanger H., 1984, *Simultaneous Measurement of Size, Concentration and Velocity of Spherical Particles by a Laser-Doppler Method*, Proceedings of 2nd. International Symposium on Application of Laser Anemometry Fluid Mechanics, p1037-1050.

Sakaki K., 2007, *The Influence of Nozzle Design in the Cold Spray Process*, The Cold Spray Materials Deposition Process, Fundamentals and Applications, Ed. V. Champagne, Woodhead Publishing Limited, p117-126.

Samareh B. and Dolatabadi A., 2007, *A Three-Dimensional Analysis of the Cold Spray Process: The Effects of Substrate Location and Shape*, J. Thermal Spray Technol., 16(5-6), p634-642.

Sansoucy E., Jodoin B. and Ajdelsztajn L., 2004, *Conventional and Nano-Structured Nickel Coatings Produced by Cold Spray Processing*, 16th Canadian Materials Science Conference, Ottawa, ON, Canada.

Sansoucy E., Kim G.E., Moran A.L. and Jodoin B., 2007, *Mechanical Characteristics of Al-Co-Ce Coatings Produced by the Cold Spray Process*, J. Thermal Spray Tech, 6(5-6), p651-660.

Schmidt T., Assadi H., Gartner F., Richter H., Stoltenhoff T., Kreye H. and Klassen T., 2009, *From Particle Acceleration to Impact and Bonding in Cold Spraying*, J. Thermal Spray Technol., 18(5-6), p794-808.

Schmidt T., Gartner F., Assadi H., Kreye H., 2006, *Development of a Generalized Parameter Window for Cold Spray Deposition,* Acta. Mater., 54, p729-742.

Shapiro A.H., 1953, *The Dynamics and Thermodynamics of Compressible Fluid Flow*, Ronald Press, New York.

Smith M.F., 2007, *Comparing Cold Spray with Thermal Spray Coating Technologies*, The Cold Spray Materials Deposition Process, Fundamentals and Applications, Ed. V. Champagne, Woodhead Publishing Limited, p43-61.

Staia M.H., Ramos E., Carrasquero A., Roman A., Lesage J., Chicot D. and Mesmacque G., 2000, *Effect of Substrate Roughness Induced by Grit Blasting upon Adhesion of WC-17%Co Thermal Sprayed Coatings*, Thin Solid Films, 377-378, p657-664.

Sundararajan G., Chavan N.M. and Kumar S., 2013, *The Elastic Modulus of Cold Spray Coatings: Influence of Inter-splat Boundary Cracking*, J. Thermal Spray Technol., 22 (8), p1348-1357.

Tucker Jr. R.C., 1994, *Thermal Spray Coatings*, Surface Engineering, Vol. 5, ASM Handbook, ASM International, p497-509.

Tucker Jr. R.C., 2013, *Introduction to Thermal Spray Technology*, Thermal Spray Technology, Vol. 5A, ASM Handbook, ASM International, p3-9.

Van Steenkiste T.H., Smith J.R. and Teets R.E., 2002, *Aluminum Coatings via Kinetic Spray with Relatively Large Powder Particles*, Surf. Coat. Technol., 154, p237-252.

Van Steenkiste T.H., Drew G.A., Gorkiewicz D.W. and Gillispie B.A., 2006, *Kinetic Sprayed Electrical Contacts on Conductive Substrates*, US Patent US7001671.

Van Steenkiste T.H., Gorkiewicz D.W., Smith J.R., Stier M. and Drew G.A., 2006, *Kinetic Spray Application of Coatings onto Covered Materials*, US Patent US7125586.

Wang P., Yu S.C.M., and Ng H.W., 2004, *Particle Velocities, Sizes and Flux Distribution in Plasma Spray with Two Powder Injection Ports*, Materials Science and Engineering A, Vol. 383, Issue 1, (10), p122-136.

Wang Y.-Y., Li C.-J. and Ohmori A., 2005, *Influence of Substrate Roughness on the Bonding Mechanisms of High Velocity Oxy-fuel Sprayed Coatings*, Thin Solid Films, 485, p141-147.

William H., Hu Y. and Frederico R., 2005, *Method for Applying Abrasive and Environment-resistant Coatings onto Turbine Components*, European Patent EP1634976A1.

Wu Y., Lin P., Xie G., Hu J. and Cao M., 2006, *Formation of Amorphous and Nanocrystalline Phases in High Velocity Oxy-Fuel Thermally-Sprayed aFe-Cr-Si-B-Mn Alloy*, Materials Science Engineering A, 430, p34-39.

Wu J., Yang J., Fang H., Yoon S. and Lee C., 2006, *The Bond Strength of Al-Si Coating on Mild Steel by Kinetic Spraying Deposition*, Applied Surface Science, 252, p7809-7814.

Yin S., Suo X., Su J., Guo Z., and Wang X., 2014, *Effects of Substrate Hardness and Spray Angle on the Deposition Behaviour of Cold Sprayed Ti Particles*, J. Thermal Spray Technol., 23 (1-2), p76-83.

Zheng W., Derushie C., Lo J. and Essadigi E., 2006, *Corrosion Protection of Joining Areas in Magnesium Die Cast and Sheet Products*, Materials Science Forum, 546-549, p523-528.